B06861-000

THE NIMBUS IV USER'S GUIDE

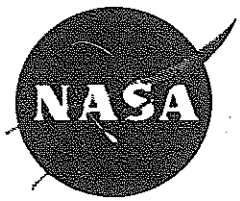

GODDARD SPACE FLIGHT CENTER

GREENBELT, MARYLAND

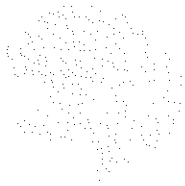

THE NIMBUS IV USER'S GUIDE

Prepared By

The NIMBUS Project
Goddard Space Flight Center
National Aeronautics and Space Administration

Edited By

Romeo R. Sabatini
Allied Research Associates, Inc.
Concord, Mass.

March 1970

TABLE OF CONTENTS

TABLE OF CONTENTS (Continued)

TABLE OF CONTENTS (Continued)

TABLE OF CONTENTS (Continued)

TABLE OF CONTENTS (Continued)

TABLE OF CONTENTS (Continued)

LIST OF FIGURES

LIST OF FIGURES (Continued)

LIST OF FIGURES (Continued)

LIST OF FIGURES (Continued)

LIST OF TABLES

LIST OF TABLES (Continued)

THE NIMBUS IV USER'S GUIDE

FOREWORD

This document has been prepared to provide potential data users with background information on the Nimbus IV spacecraft and experiments as a basis for selecting, obtaining and utilizing Nimbus IV data in research studies.

The basic spacecraft system operation and the objectives of the Nimbus IV flight are outlined, followed by a detailed discussion of each of the experiments. The format, archiving, and access to the data are also described. Finally, the contents and format of the Nimbus IV Data Catalogs are described. These catalogs will be issued at approximately monthly intervals. They will contain IDCS and THIR pictorial data obtained during each period as well as information on the collection and availability of all Nimbus IV data.

The individual sections on the meteorological experiments were prepared by the respective experimenters. The assembly and editing of this publication was accomplished by the Geophysics and Aerospace Division of Allied Research Associates, Inc. (ARA), Concord, Massachusetts under Contract No. NAS 5-10343 with the Goddard Space Flight Center, NASA, Greenbelt, Maryland.

Harry Press
Nimbus Project Manager
Goddard Space Flight Center

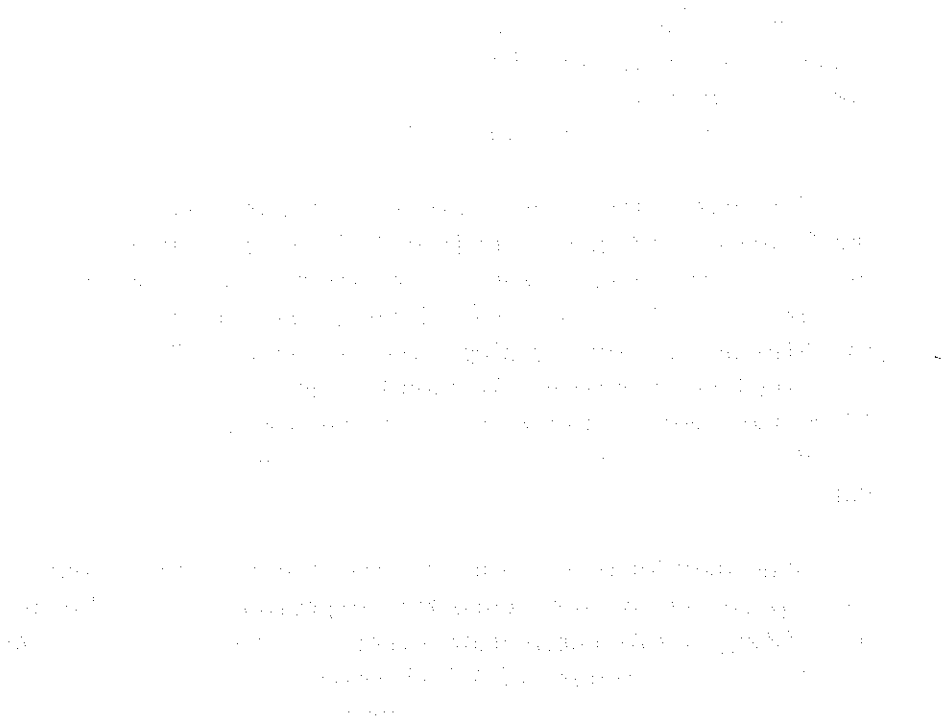

SECTION I

THE NIMBUS IV SPACECRAFT SYSTEM

by
Staff Members, Nimbus Project
National Aeronautics and Space Administration
Goddard Space Flight Center

The purpose of this section is to outline the component subsystems of the Nimbus IV spacecraft and the objectives of the Nimbus IV flight.

1.1 The Nimbus IV Objectives

The Nimbus program has developed an observatory spacecraft system which serves to support the research and development needs of the nation's atmospheric scientists and environmental science services. The Nimbus spacecraft provides daily global surveillance of the atmospheric structure from the orbit altitude.

The goal of the Nimbus IV spacecraft (Figure 1-1) is to develop and expand the capabilities to measure the atmospheric structure on a global scale. New experiments cover potentially important regions of the electromagnetic spectrum of the earth's atmosphere. These data have yet to be collected and investigated on a global scale. Updated versions of experiments of previous Nimbus flights will further develop the use of infrared techniques. The Nimbus IV experiments are listed in Table 1-1.

The experiment concepts support the world weather watch program which is designed to expand weather observational capability and promote understanding of, and ability to predict, weather processes. The specific objectives of the Nimbus IV are to:

Scientific

- Acquire a sufficient number of samples of infrared spectra from which global vertical temperature and water vapor profiles can be derived, and which will provide a basis for comparing the merits of several instrument approaches

- Provide supporting cloud cover imaging

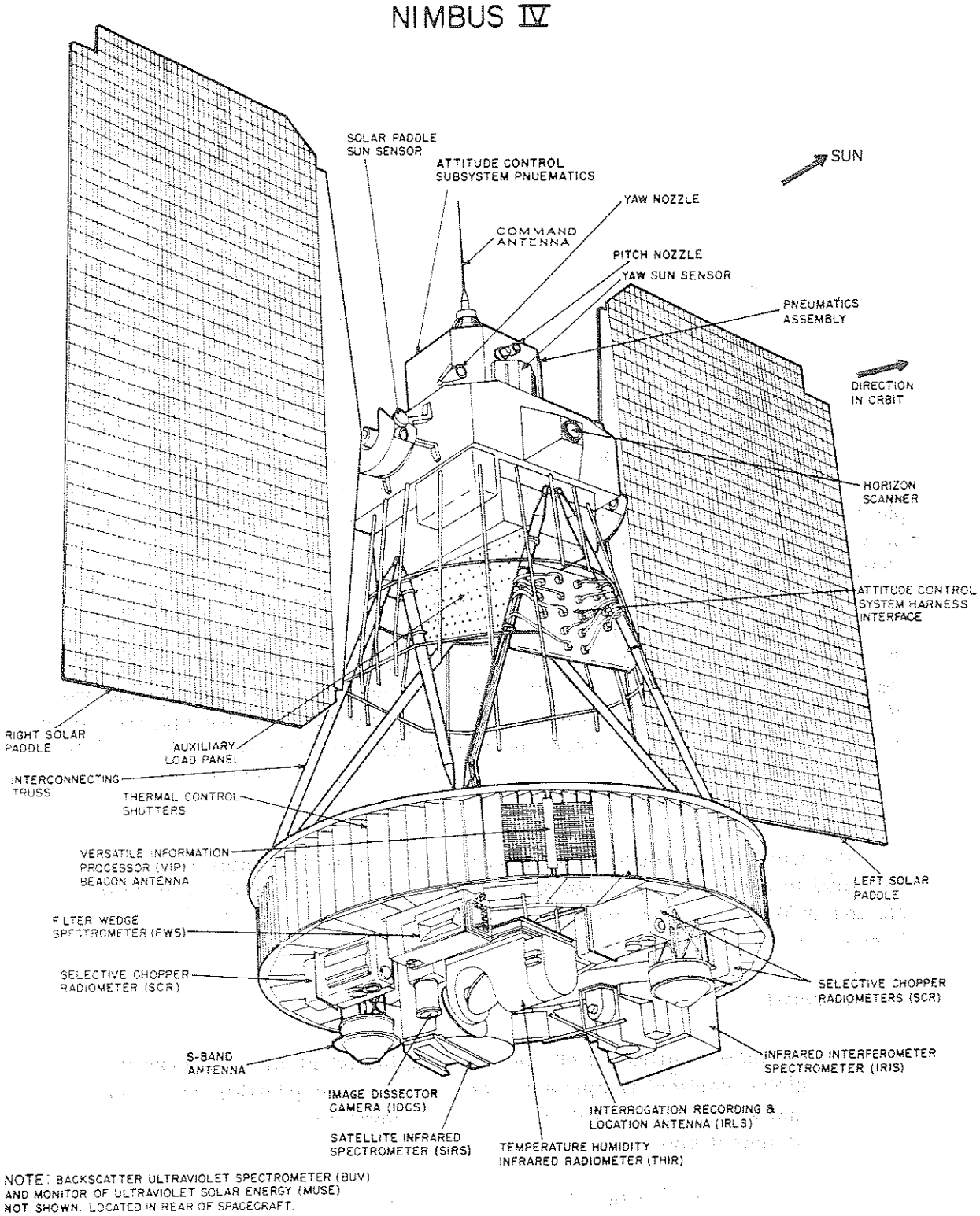

Figure 1-1. Basic Configuration of Spacecraft

Table 1-1
Nimbus IV Meteorological Experiments

Experiment	Spectral Bands Microns	Main Purpose
Temperature Humidity Infrared Radiometer (THIR)	10.5-12.5	Daytime and Nighttime Surface and Cloud Top Temperatures and Cloud Mapping
	6.5-7.0	Atmospheric Water Vapor Mapping
Infrared Interferometer Spectrometer (IRIS)	8-20	Atmospheric Temperature Profile, O_3, Water Vapor Surface Temperature and Minor Atmospheric Gases
Satellite Infrared Spectrometer (SIRS)	11	Surface and Cloud Top Temperatures
	13-15	Atmospheric Temperature Profile
	19-36	Atmospheric Humidity Profile
Monitor of Ultraviolet Solar Energy (MUSE)	0.12 0.16 0.18 0.21 0.26	Monitors Changes in Solar Radiation
Selective Chopper Radiometer (SCR)	13-15	Atmospheric Temperature Profile
Filter Wedge Spectrometer (FWS)	1.2-2.4 3.2-6.4	Atmospheric Water Vapor
Backscatter Ultraviolet Spectrometer (BUV)	0.25-0.34	Atmospheric Ozone Distribution
Image Dissector Camera System (IDCS)	0.45-0.65	Daytime Cloud Mapping
Interrogation, Recording, Location System (IRLS)	—	Data Collection from Platforms

- Demonstrate the feasibility of determining wind velocity fields by the tracking of multiple balloons

- Obtain global samples of backscattered solar ultraviolet radiation from which ozone profiles can be derived and compared with ozone profiles obtained from infrared data

Engineering

- Advanced attitude-control system with alternate stabilization modes (±1 degree, 3 axes)

- Versatile information processing system on spacecraft (ground programmable)

- Expanded spacecraft command capability (up to 512 commands)

1.2 Orbit

The Nimbus IV orbit was selected to satisfy the diverse experiment power and data retrieval requirements. Nimbus IV is intended to be placed in an orbit which is circular at 600 nautical miles, sun-synchronous, having a local high noon equator crossing, and an 81 degree retrograde inclination. Successive orbits cross the equator at 26° of longitude separation. The period for this orbit is about 107 minutes. Nimbus IV is scheduled to be launched in the second quarter of 1970 from the Western Test Range in California. The launch vehicle is a Thorad-Agena D.

1.3 Spacecraft Attitude

The Nimbus IV spacecraft system contains an improved active 3 axis stabilization system designed to maintain the spacecraft body axes earth stabilized, with the yaw axis pointing normal to the earth, and the roll axis aligned to the spacecraft velocity vector (See Figure 1-2). The improved attitude control subsystem of Nimbus IV will permit fine control to ±1 degree in all axes. In view of the high pointing accuracy and the lack of more precise orientation data, attitude corrections are not utilized in the geographic location procedures. All the data obtained are geographically located by using the orbit ephemeris data only.

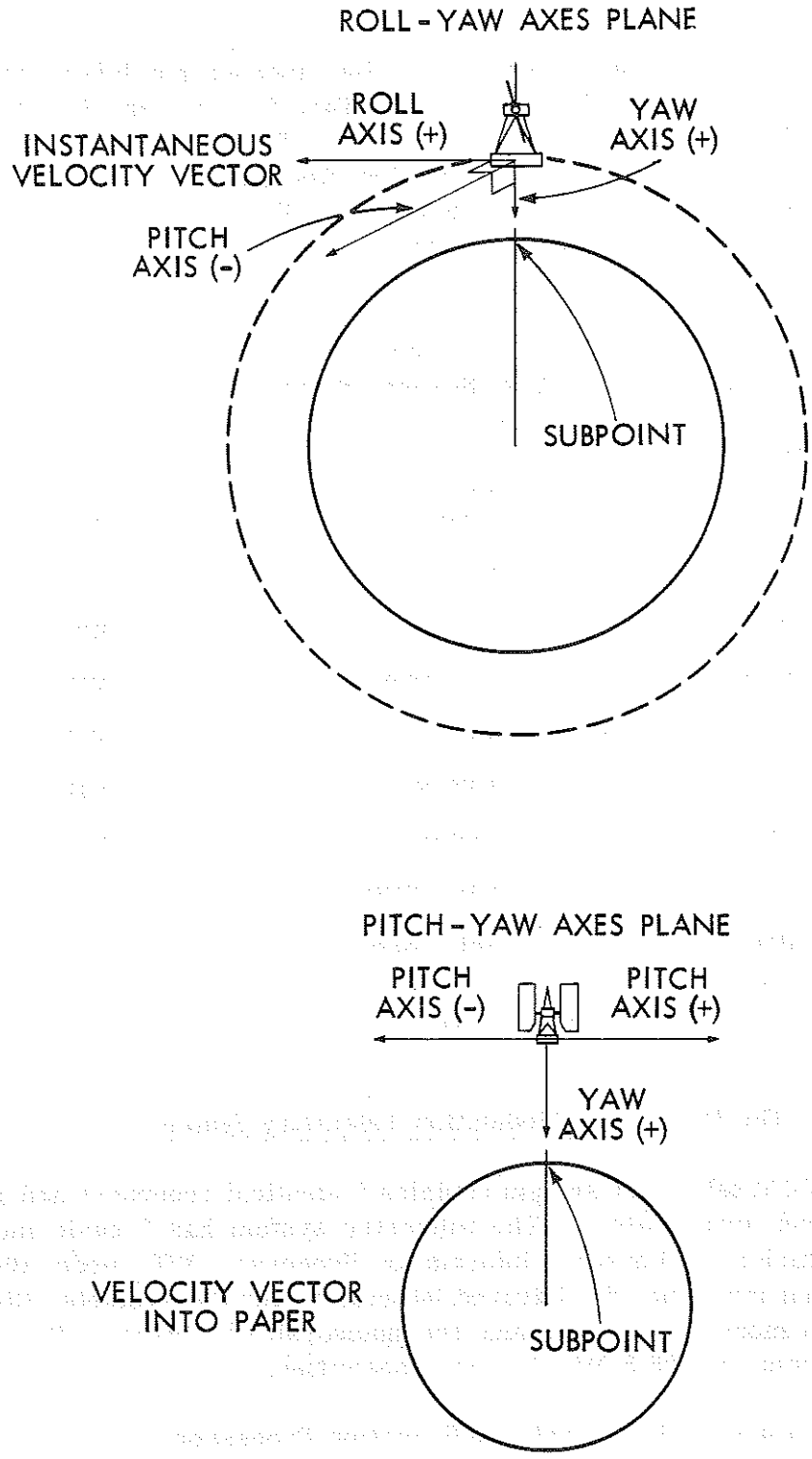

Figure 1-2. Nimbus Attitude Axes

1.4 Spacecraft Data System

Data are stored and transmitted via four independent data systems on the Nimbus IV Spacecraft. They are the High Data Rate Storage System (HDRSS), the Pulse Code Modulation Telemetry System (PCM), the Real Time Transmission System (RTTS), and the Interrogation, Recording and Location System (IRLS). The individual data systems are described below. A summary of how the meteorological experiments are handled is provided in Table 1-2.

Table 1-2
Data Systems Summary

Experiment	Data System	Backup Mode
IRIS	HDRSS	Beacon*
THIR	HDRSS	RTTS/VIP
IDCS	HDRSS	RTTS
MUSE	VIP/HDRSS	VIP Beacon
SIRS	VIP/HDRSS	VIP Beacon
BUV	VIP/HDRSS	VIP Beacon
FWS	VIP/HDRSS	VIP Beacon
SCR	VIP/HDRSS	VIP Beacon
IRLS	Self Contained	NONE

*When IRIS is on Beacon there is no VIP data.

1.4.1 The Pulse Code Modulation Telemetry System

The PCM telemetry system contains 2 identical recorders and 136.5 MHz PCM beacon transmitters. The telemetry system has 3 basic modes of operation which are: Versatile Information Processor (VIP) mode, 10-kHz time code format mode, and the Infrared Interferometer Spectrometer (IRIS) subsystem direct mode. Upon command, the spacecraft will transmit the selected output data using the 136.5 MHz beacon transmitter.

1.4.1.1 The Versatile Information Processor

The VIP samples the output of approximately 1000 sensors. The sensor data are digitized (where necessary), time multiplexed, and formatted into a

4-kbps serial bit stream. The serial bit stream can be recorded in biphase on the HDRSS tape recorder and simultaneously transmitted over the PCM 136.5 MHz beacon transmission link.

Data transmitted in the VIP mode include spacecraft subsystem and experiment housekeeping telemetry such as temperature of components, calibration signals and voltages, plus the output of five experiments: SIRS, FWS, BUV, MUSE and SCR, and selected THIR.

1.4.1.2 10-kHz Time Code Format Mode

In this mode, the standard NASA time code format data (100-bps, pulse duration modulation, least significant bit first) are substituted for the VIP data.

1.4.1.3 Infrared Interferometer Spectrometer Direct Mode

In this mode, the 3.75-kbps IRIS data are substituted for the 4-kbps VIP data.

1.4.2 High Data Rate Storage System

The High Data Rate Storage System (HDRSS) consists of a 5-channel tape recorder and the associated recording and playback electronics for collecting and storing the data from the THIR, IDCS, IRIS, and VIP subsystems and the time code. For purposes of redundancy and extending useful data capacity, there are two parallel and independent HDRSS on Nimbus IV. Each has a total capacity which will allow 134 minutes of data to be collected. The recorders can record in parallel or can be programmed to record sequentially for more complete coverage during blind orbits. Included with this subsystem is the S-Band transmitter used for sending the data to the ground. Each HDRSS operates into a 4-watt solid-state transmitter. The transmitters operate at 1702.5 MHz.

This system is used for the high data rate experiments: IDCS, IRIS, and THIR. The fifth track contains the spacecraft time code which is also used for flutter and wow compensation. PCM data from the Versatile Information Processor (VIP) subsystem are also redundantly recorded on the HDRSS.

1.4.3 Real Time Transmission System (RTTS)

The RTTS system transmits IDCS or THIR data over a 136.950 MHz, 5 watt transmitter, in real time. The IDCS data format is compatible with existing APT stations around the world; the THIR data are available to APT stations modified to receive 48 rpm THIR data.

1.4.4 Interrogation Recording and Location System

This is a data collection device that is commanded and programmed to identify, locate, interrogate, and store data from remote platforms (weather stations, buoys, or balloons). Its ranging system permits accurate platform location by triangulation techniques after two successive interrogations. Platform data are stored on the spacecraft for relay through the DAF to GSFC.

The IRLS experiment includes a UHF transmitter and antenna system to transmit data at a frequency of 401.5 MHz and to receive commands and platform data at a frequency of 466 MHz. Refer to the section on IRLS operations for more detailed information.

1.5 Ground Station Complex

Data from the HDRSS are received at the two STADAN Data Acquisition Facilities (DAF) located near Fairbanks, Alaska and Rosman, North Carolina. The HDRSS data acquired at Alaska are recorded on pass and then transmitted over a microwave link at reduced rates to the Nimbus Data Handling Facility (NDHF) at GSFC. HDRSS data acquired at Rosman are relayed directly from the Rosman DAF to GSFC over a wideband data link. PCM data acquired at either Alaska or Rosman are relayed by data link to GSFC as they are received from the spacecraft. Real Time PCM data acquired at other STADAN sites are recorded and retransmitted to GSFC at reduced rates. Data from the IRLS system are received at the Alaska DAF for relay to NDHS, and at the GSFC.

Alaska acquires the spacecraft 10 orbits each day (of the 13 to 14 orbits per day). Rosman acquires two orbits per day missed by Alaska. Other STADAN stations acquire real time PCM data for orbits missed by Rosman and Alaska.

All spacecraft data are processed in the Nimbus Data Handling Facility at GSFC. Photographic images of IDCS, and THIR data are processed through the Nimbus Data Utilization Center. Digitized magnetic tape recordings of the IRIS, THIR, FWS, BUV, and MUSE experiment data are distributed to the respective experimenters for further data reduction.

SIRS data, extracted and formatted in the NDHS, is transmitted over landline in near real time, to NESC/ESSA. SCR data, with associated housekeeping and extracted corollary THIR data, is stripped from the data stream, formatted, and transmitted by data link to the experimenter at Clarendon Laboratories, Oxford University, England.

1.6 Nimbus Data Utilization Center

The Nimbus Data Utilization Center (NDUC) performs the following functions:

1. Accountability for and distribution of all experiment data processed by the NDHF.

2. Processing and reproduction of photographic data until they have been archived.

3. Generation of periodic data catalogs in a format as outlined in Section 12 to provide information on all experimental data collection and availability.

4. Special technical services concerning data processing to the experimenters and data users, including maintenance of a complete photographic data reference file.

1.7 Archival and Dissemination of Nimbus IV Data

The nature and format of the data to be available from each experiment are explained in detail in the respective sections of this guide. The data will be archived and available as described below:

1. IDCS photographic data will be archived and available through the National Weather Records Center (NWRC), Environmental Science Services Administration, Federal Building, Asheville, North Carolina 28801.

2. THIR photographic data will be archived and available through the National Space Science Data Center (NSSDC), Goddard Space Flight Center, Code 601, Greenbelt, Maryland 20771.

3. THIR, SCR, FWS, BUV, IRIS and MUSE digital data tabulated as radiance values will be archived and available through the NSSDC.

4. SIRS digital data will be archived and available from two sources: Digital data tapes containing radiance values will be archived in the NSSDC. Digital data tapes containing temperature profiles will be archived in the NWRC.

IDCS photographic data and SIRS digital data will be available from the NWRC at cost. Limited quantities of all other data will be furnished to qualified investigators, by the NSSDC, without charge. A charge for production and

dissemination costs may be established by NSSDC if a large volume of data is requested. Whenever it is determined that a charge is required, a cost estimate will be provided to the user prior to filling his data request.

All requests from non-United States researchers for THIR, SCR, FWS, BUV, IRIS, SIRS or MUSE data, in either film (THIR only) or digital output format, archived and available through NSSDC must be specifically addressed to: Director, World Data Center A for Rockets and Satellites, Code 601, Goddard Space Flight Center, Greenbelt, Maryland, 20771, U.S.A.

B07742

SECTION 2

THE IMAGE DISSECTOR CAMERA SYSTEM (IDCS) EXPERIMENT

By
Ed Werner and Gilbert A. Branchflower
National Aeronautics and Space Administration
Goddard Space Flight Center

2.1 Introduction

The Image Dissector Camera System (IDCS) flown on Nimbus IV is essentially the same system flown on Nimbus III. Daytime pictures of the earth will be taken at intervals of 208 seconds, stored on tape and played back at the prime Nimbus Data Acquisition Facilities near Rosman, North Carolina, and Fairbanks, Alaska. The same pictures will also be transmitted in real time to APT stations worldwide. Section 11 of this Guide and the Nimbus IV Real Time Transmission System manual provide information on the IDCS Real Time Transmission mode (DRID).

The IDCS is mounted on the bottom of the sensory ring of the earth stabilized Nimbus IV satellite. The "optic axis" of the camera system is aligned with the positive yaw axis (see Figure 1-2) of the satellite. The image dissector is a shutterless electronic scan and step tube mounted behind a wide angle lens. Scanning and stepping functions occur continuously while the satellite is progressing along its orbital path, i.e., the earth scene contained in a single frame is not exposed instantaneously from a fixed location in space. The image dissector scanning and stepping cycles in conjunction with the satellite orbital motion have been designed to achieve an image with a nearly 1:1 aspect ratio for the Nimbus IV 600 nautical mile circular orbit. Successive IDCS frames are initiated at intervals of 208 seconds. An interval of 208 seconds is the complete timing cycle for an IDCS frame and associated electronic functions.

Advantages of the experimental IDCS over the more conventional vidicon camera systems are: the ability to sense a greater dynamic range (about 100:1), high signal to noise ratios, direct relationship between light flux input and electron current output, and the avoidance of a mechanical shutter.

2.2 Description

2.2.1 Optics

The optical system of the IDCS consists of a wide angle Tegea lens. The lens has a nominal focal length of 5.7 millimeters and a nominal diagonal field of view of 108 degrees. A minus blue filter in front of the lens is employed for enhancement of cloud images. The image dissector tube (sensor) is mounted directly behind the optical system.

Ground resolution obtained from the IDCS at an altitude of 600 nautical miles is approximately 2 nautical miles over most of the field of view except near the edges where it decreases to about 5 nautical miles.

2.2.2 Sensor

The image dissector tube is a non-storing, scanning detector of the photomultiplier class (see Figure 2-1). Basic components of the tube are a photocathode, an accelerating screen, a drift tube, an aperture and an electron multiplier. Excitation of the photocathode by light causes electrons to be emitted in direct proportion to the light level applied. The emitted electrons are accelerated from the photocathode and pass through a fine mesh screen into a unipotential drift space. A magnetic focus field (the focus coil is a long solenoid enclosing both the photocathode and aperture plane) is applied such that the electrons spiral, arriving at the aperture plane with the same spatial relationship as the original optical image on the photocathode. Thus, the optical image has been translated into an electron image and transferred to the single aperture plane within the image dissector tube.

At the center of the aperture plane is a small hole (the aperture). The aperture diameter is chosen to admit electrons from a selected area of the photocathode. Size and shape of the aperture may be chosen, within limits, as a function of the required sampling technique and resolution. The Nimbus IV image dissector tube has a circular aperture of 0.001 inches diameter with an S11 photocathode of 0.7 inches diameter. The effective instantaneous field of view of the sensor is 0.166 degrees.

To generate a proper scan sequence for a normal raster, it is necessary to apply a transverse magnetic field in the drift space. Deflection coils, which are similar to vidicon deflection coils, develop the transverse field which causes the complete electron image to shift orthogonal to the direction of the magnetic field. Thus, selected areas of the complete electron image can be scanned past the aperture centered in the aperture plane. Horizontal deflection generates scan lines and vertical deflection generates the scan step.

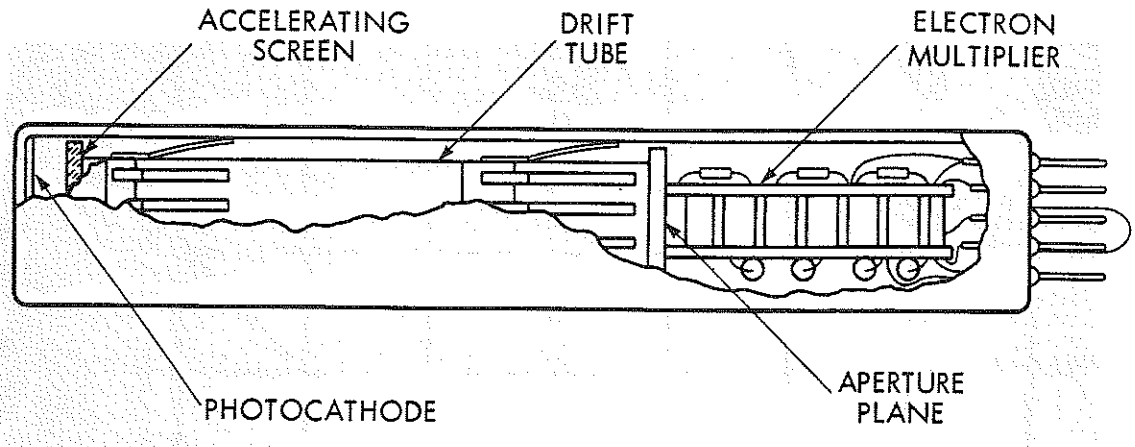

Figure 2-1. Components of Image Dissector Tube

As the electron image is moved past the aperture, that spot of information passed through the aperture is detected as an electrical signal and is multiplied over a million times by the electron multiplier assembly located behind the aperture plane. After electron multiplication, the signal current is fed to the electronic circuits that enable the signal to be transmitted directly to the ground in real time (DRID) and/or to be stored on magnetic tape for subsequent playback at the Data Acquisition Facilities.

2.2.3 Sensor Operation

An entire image dissector video frame consists of 800 scan lines and requires 200 seconds of cycling time. The elapsed time for one complete scan line is 250 milliseconds (0.25 seconds). A complete scan line is composed of two parts: a 225 millisecond active scan following a 25 millisecond blanked scan. Video data are collected during the active portion of the scan. The blanked portion of the scan occurs during scan reorientation to the new start position. A scan line corresponds to a nominal viewing angle of 98.2 degrees in the image dissector tube. The stepping cycle (800 steps), which is perpendicular to the scan line direction, corresponds to a nominal 73.6 degrees viewing angle in the image dissector tube. These angles are not the actual angles of the field of view because they do not at this point include lens distortion, blanking, or satellite movement during the 200 second picture taking time.

2.3 Calibration Results

Figure 2-2 is an IDCS calibration picture showing the field of view of the camera system including simulated satellite motion for a circular orbit at a height of 600 nautical miles.

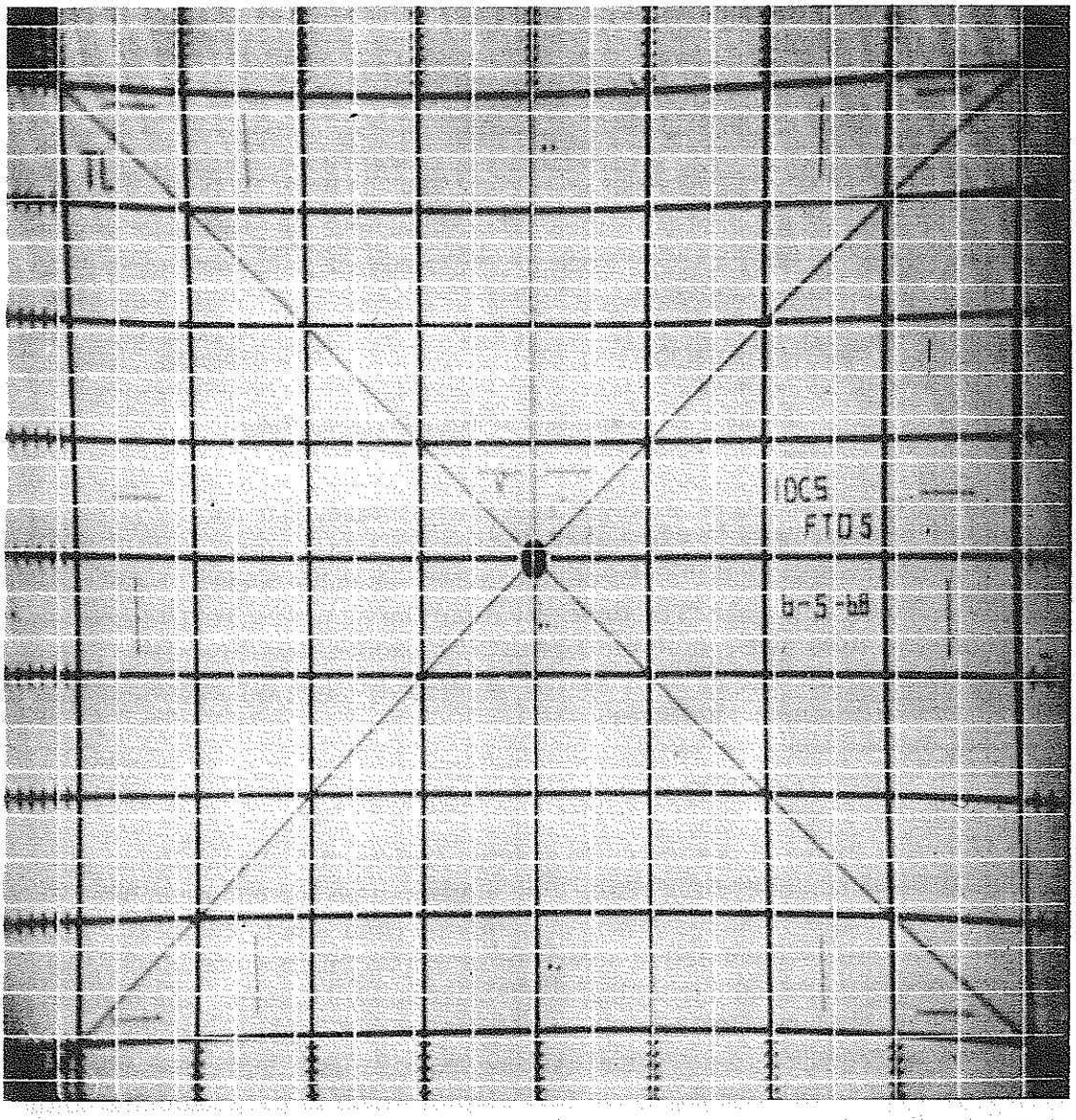

Figure 2-2. IDCS Target Calibration Picture

The black grid network shown in Figure 2-2 should theoretically consist of squares. Deviations from a square grid network represent a combination of lens distortion, internal sensor alignments, and known mechanical and electronic distortions introduced during the calibration procedures. Henceforth, the combined distortions resulting from the camera lens and the internal sensor alignments will be referred to, simply, as lens distortion.

The "pin-cushion" distortion pattern exhibited by the black grid network in the calibration picture is, however, indicative of the true camera system distortions.

2.3.1 Image Principal Point

At one instant during the scanning sequence of a complete IDCS frame the image dissector sensor will be aligned with the local vertical. The instantaneous satellite subpoint, at that time, is defined to be the object principal point. The corresponding location of this instantaneous subpoint in the final IDCS display is defined to be the image principal point.

As determined from the calibration picture (Figure 2-2) the image principal point is not located at the geometric center of the IDCS display but is offset slightly toward the right and below the center of the display.

The image principal point is located 47.9 percent of the horizontal distance from the right hand edge of the display and 50.6 percent of the vertical distance from the top of the display (step 395 from the bottom of the IDCS display) (Figure 2-3).

2.3.2 Lens Distortion

The wide angle Tegea lens coupled with the image dissector tube results in a low distortion optical system in the central portion of the field of view. Distortion effects are zero in the center of the field of view and become more noticeable near the sides and corners of the picture.

2.3.3 Field of View

The coverage presented in an IDCS frame results from a composite of the fixed scan and step modes of the image dissector tube, blanking, plus the satellite motion and lens distortion. Earth coverage measured from the image principal point to the picture boundaries are given in Table 2-1 for satellite heights at and near the nominal 600 nautical miles.

2.3.4 Shading Characteristics

When a constant light intensity impinges on the sensitized surface of the image dissector tube, the resultant output shows slight shading characteristics. Figure 2-4 is an enhanced calibration test picture which displays the shading pattern for a 10,000 foot lambert input over the full field of view of the camera. This response pattern is essentially the same for all light inputs below 10,000 foot lamberts. The arbitrary gray levels in Figure 2-4 are used only to delineate the different shading characteristics of the camera for a given input.

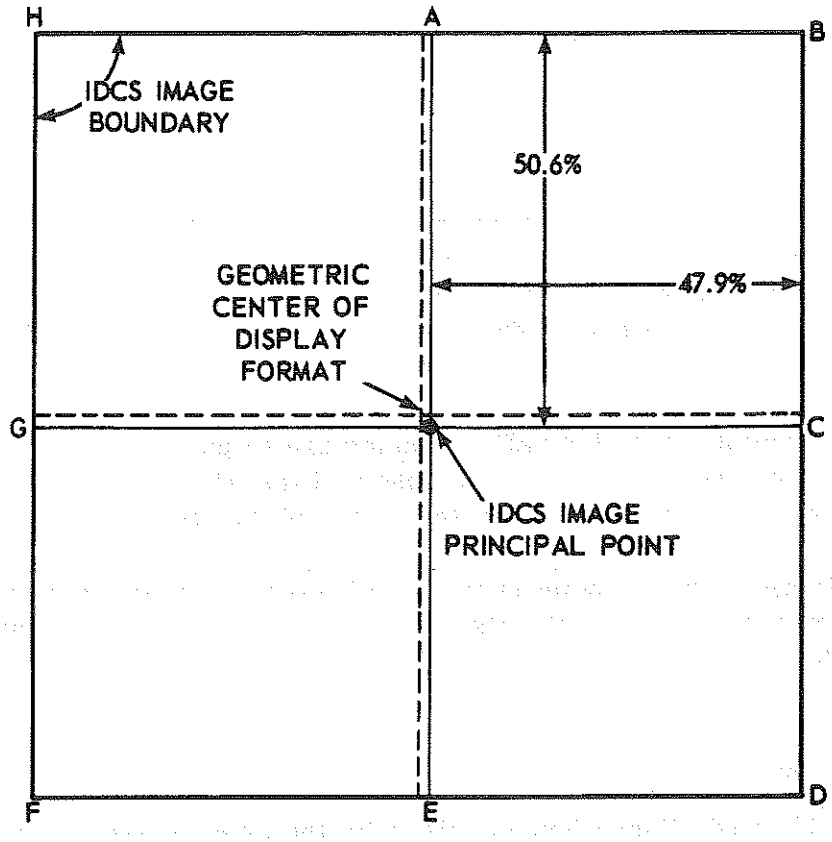

Figure 2-3. Location of Geometric Center and Image Principal Point, on IDCS Display

Correct boundaries between different shading areas are closely approximated by the contours superimposed on the calibration picture. Striated patterns within the picture result from interference in the test equipment and should be ignored.

The lower central area of the picture labeled 10,000 foot lamberts is the brightest response and is very near or at saturation. The two adjacent areas delineated and labeled 9,500 foot lamberts represent a five percent drop in camera output for the same 10,000 foot lambert input. Differences between the 10,000 and 9,500 foot lambert areas, or any two adjacent areas, may not be noticeable in the IDCS pictures played back on the ground equipment. In fact, the camera response deviation may barely be noticeable throughout the entire frame. At the four corners and near the right hand edge of the picture additional areas of camera response "fall off" are delineated and appear at 9,000, 8,500 and 8,000 foot lamberts. Interpretation of the shading phenomenon, from the user standpoint, is that he be aware that a given albedo, when observed in the lower central portion of the picture will appear slightly brighter than the identical albedo observed toward the edges or corners of the picture.

Table 2-1
IDCS Picture Coverage

Satellite Height Nautical Miles	Distances (Nautical Miles) From Image Principal Point To IDCS Image Boundary as Indicated in Figure 2-3							
	A	B	C	D	E	F	G	H
540	714	1073	558	1053	699	1199	660	1225
550	720	1090	569	1069	705	1223	674	1251
560	726	1108	581	1088	711	1248	688	1277
570	732	1126	592	1104	716	1273	703	1304
580	738	1144	604	1123	722	1299	717	1331
590	744	1163	615	1139	727	1325	731	1359
600	750	1182	627	1158	733	1352	746	1387
610	756	1202	639	1177	739	1379	761	1416
620	762	1220	650	1194	744	1407	775	1446
630	768	1241	662	1214	750	1439	790	1479
640	774	1261	674	1234	756	1475	805	1521
650	780	1282	686	1254	762	1523	821	1570

2.4 Picture Formulation

The IDCS display is a composite resulting from the fixed scan and step mode of the image dissector tube plus the contribution provided by the satellite motion during the 200 seconds picture taking cycle.

2.4.1 Scan Component

An active IDCS scan line samples data that are perpendicular to the instantaneous spatial heading of the satellite. Due to the electronic stepping, or "pitching" sequence of the sensor, the instantaneous satellite subpoint is not contained in the sampled data of a scan line, except for data sampled during scan line 395. The user should note that the scan direction is not perpendicular to the subpoint track of the satellite.

Facing the direction of motion of the satellite, an active scan is generated by observing the earth from right to left relative to the satellite location (Figure 2-5).

The field of view represented by a single active scan line, as determined from calibration data, is 90.9 degrees from side to side.

2.4.2 Step Component

During the framed picture-taking interval the electronic stepping component continuously varies the sensor look angle in the roll-yaw plane from behind the

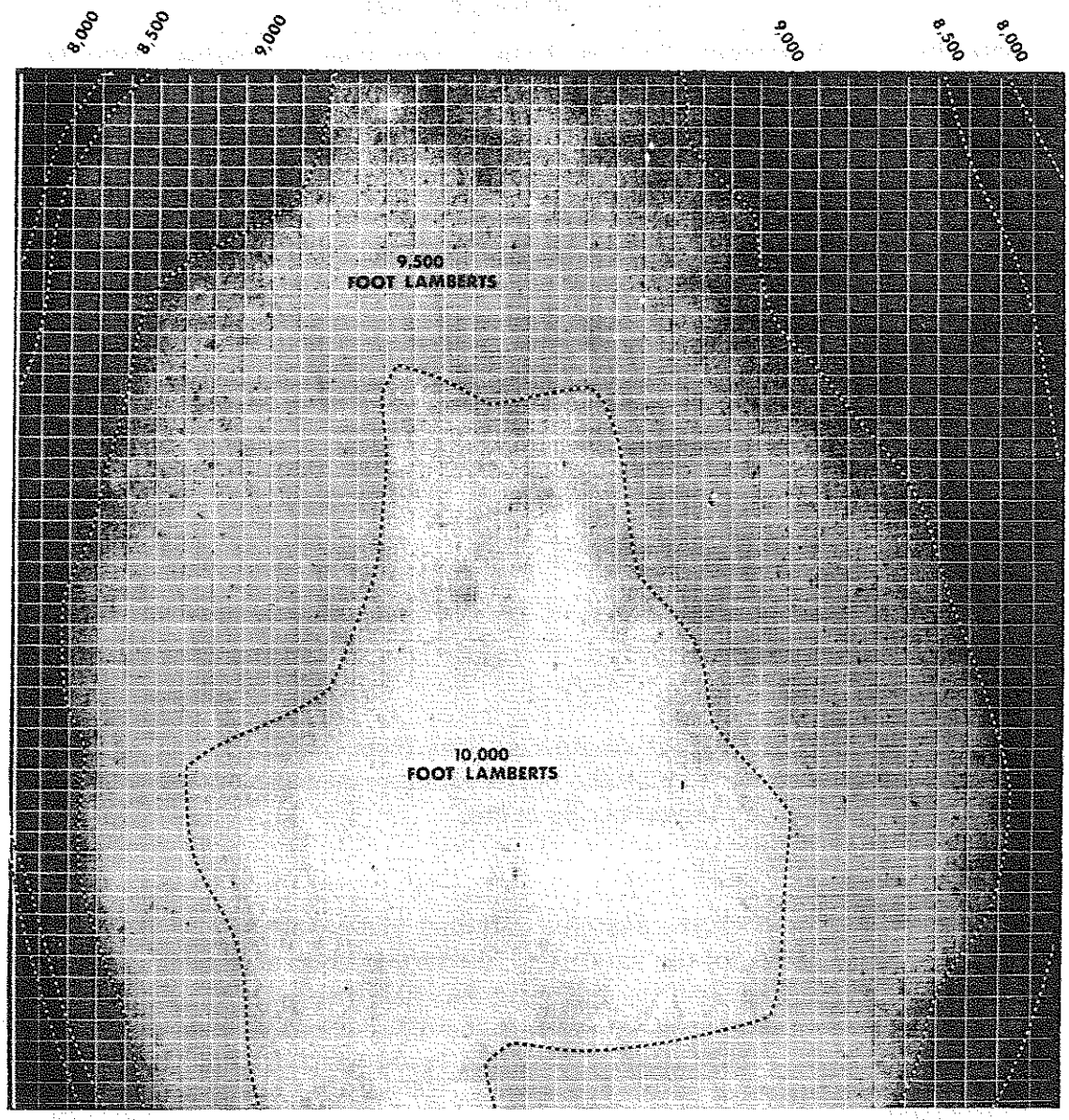

Figure 2-4. IDCS Shading Characteristics

satellite, through the yaw axis to a point ahead of the satellite. For clarity of illustration we temporarily assume that the satellite is fixed in space. Figure 2-6 shows schematically the stepping mode of the image dissector tube for one complete video frame.

At the start of the picture-taking interval the sensor look angle is 35.3 degrees behind the satellite. Approximately midway during the picture taking

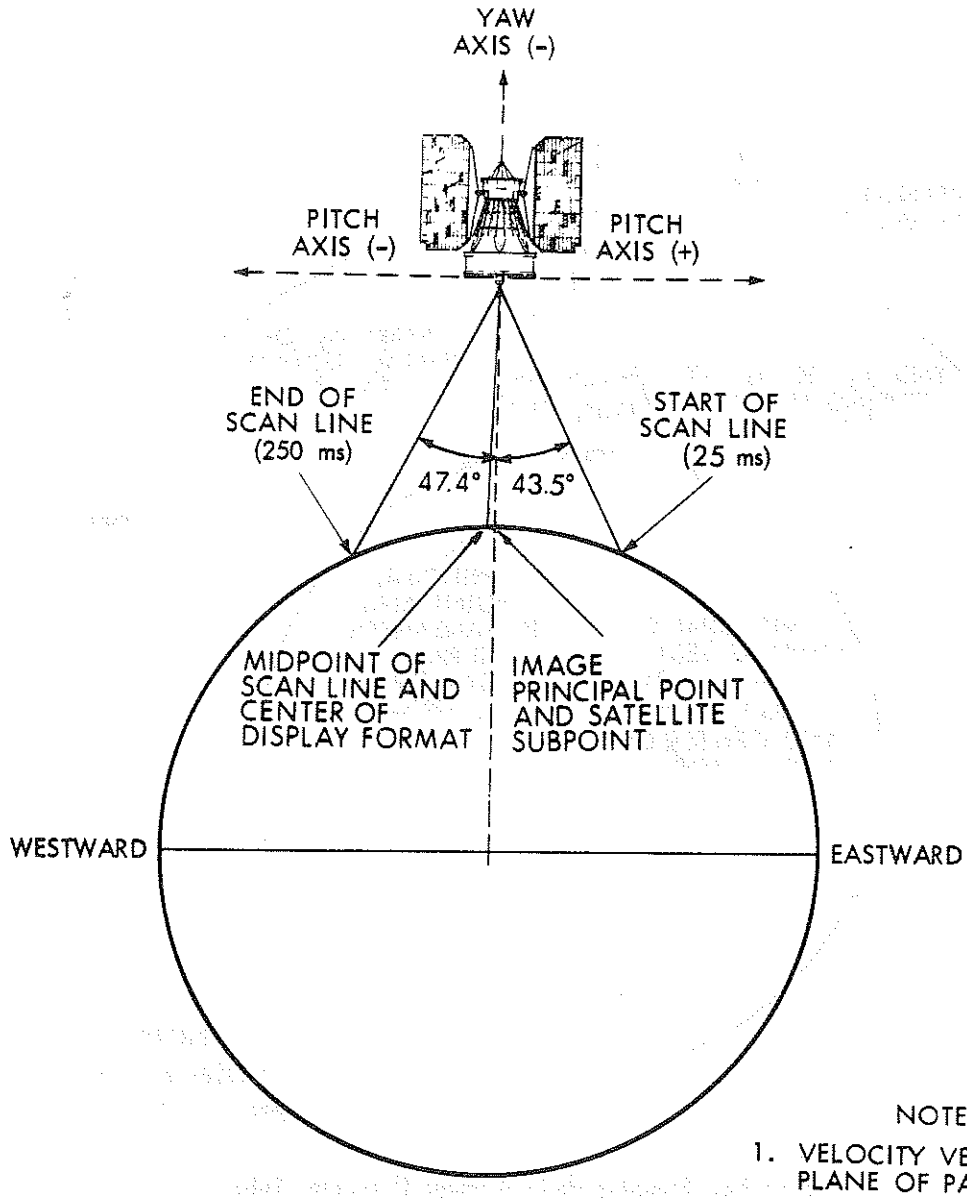

NOTES

1. VELOCITY VECTOR INTO PLANE OF PAPER
2. ZERO ATTITUDE ERROR
3. ANGLES NOT SCALED
4. ms = MILLISECONDS

Figure 2-5. IDCS Active Scan in Pitch-Yaw Plane

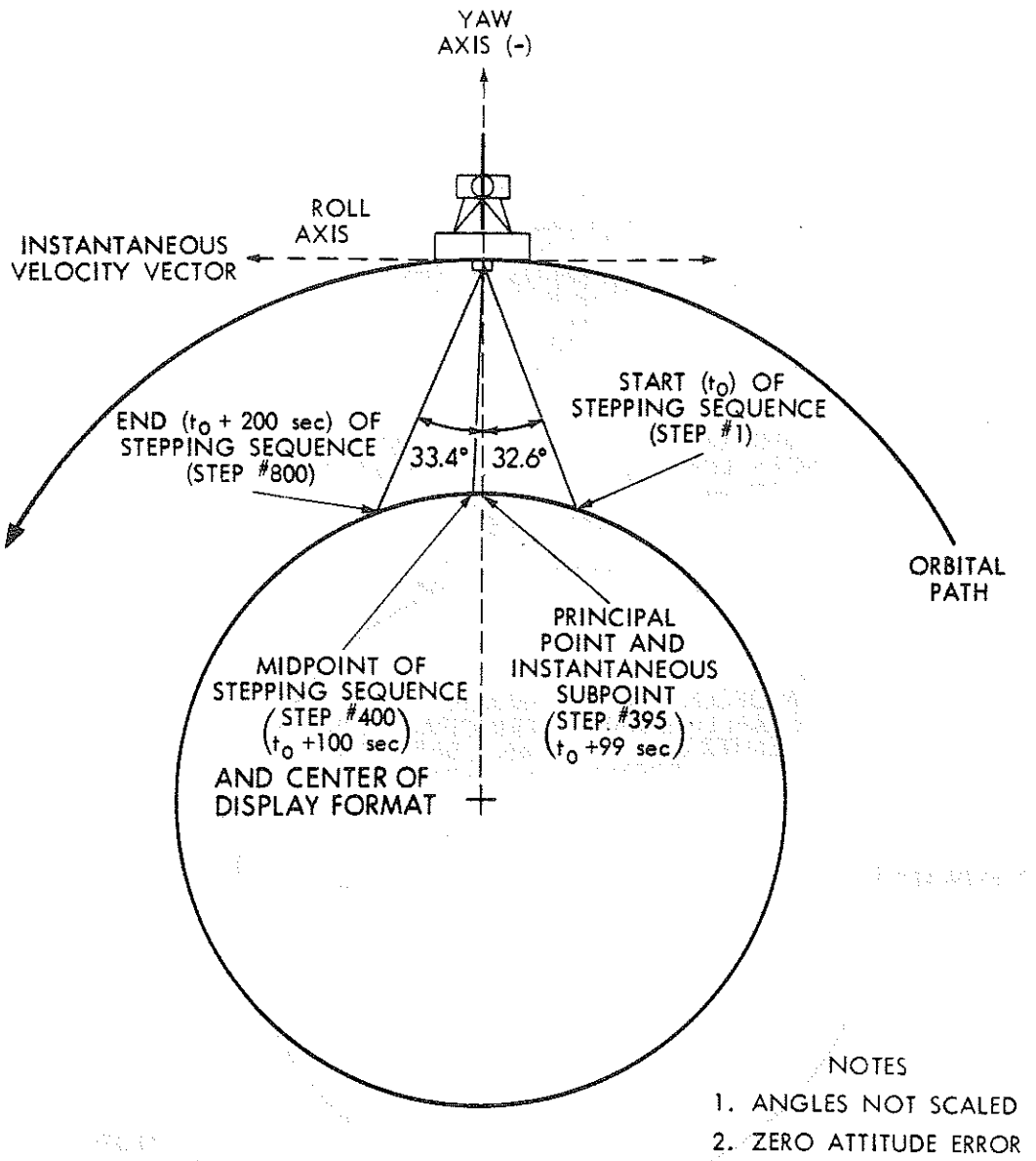

Figure 2-6. Stepping Mode of Image Dissector Tube

interval, at step number 395 the sensor look angle is aligned with the yaw axis. At the end of the picture taking interval, the sensor look angle is 33.4 degrees ahead of the satellite. Thus, the total field of view in the roll-yaw plane accounted for by the electronic stepping sequence (excluding satellite motion) is 66.0 degrees.

The sensor varies linearly through 66.0 degrees in 800 steps. A composite picture resulting from the scanning and stepping cycles requires 200 seconds for completion (800 successive steps or scan lines at 0.25 seconds per scan line).

2.4.3 Satellite Motion Component

The image dissector camera is in continuous operation for 200 seconds. During this time interval the satellite is constantly progressing along its orbit. The motion of the satellite, relative to the earth, contributes significantly to the image aspect ratio, resolution, and area viewed during the 200 second camera cycle.

Angular and timing specifications for the image dissector tube were preselected so that when integrated with the satellite motion, the resultant image would be in a nearly 1:1 aspect ratio. The most significant contribution made by the satellite motion is to expand the viewed image in the direction of motion of the satellite (along the heading line) so that the aspect ratio approaches 1:1.

A true aspect ratio of 1:1 cannot be achieved by the image dissector camera system since another variable, the rotation of the earth during the 200 second picture taking cycle, is not compensated. However, the image distortion resulting from earth rotation is a second order effect.

Figure 2-7 shows schematically the integration of the satellite motion with the limits of the stepping motion of the image dissector camera. The 600 nautical mile circular orbit causes the Nimbus IV satellite to traverse 11.11 degrees of great circle arc during the 200 seconds of the picture taking cycle.

2.5 IDCS Data Processing, Archiving and Access

2.5.1 IDCS Data Processing

The IDCS data are stored in the High Data-Rate Storage Subsystem (HDRSS) and transmitted on command to the DAF station, in reverse at 32 times the record rate.

The IDCS data are received on the S-band frequency at the DAF. The S-band signal consists of five channels of multiplexed data, four on separate subcarrier frequencies and one at the baseband. At the ALASKA DAF, the composite group of subcarriers is demultiplexed and the subcarriers are recorded on magnetic tape so that the data may be transmitted to the GSFC NDHF. The Video Data processing system for Nimbus IV generates 70 mm film negative for photographic laboratory processing.

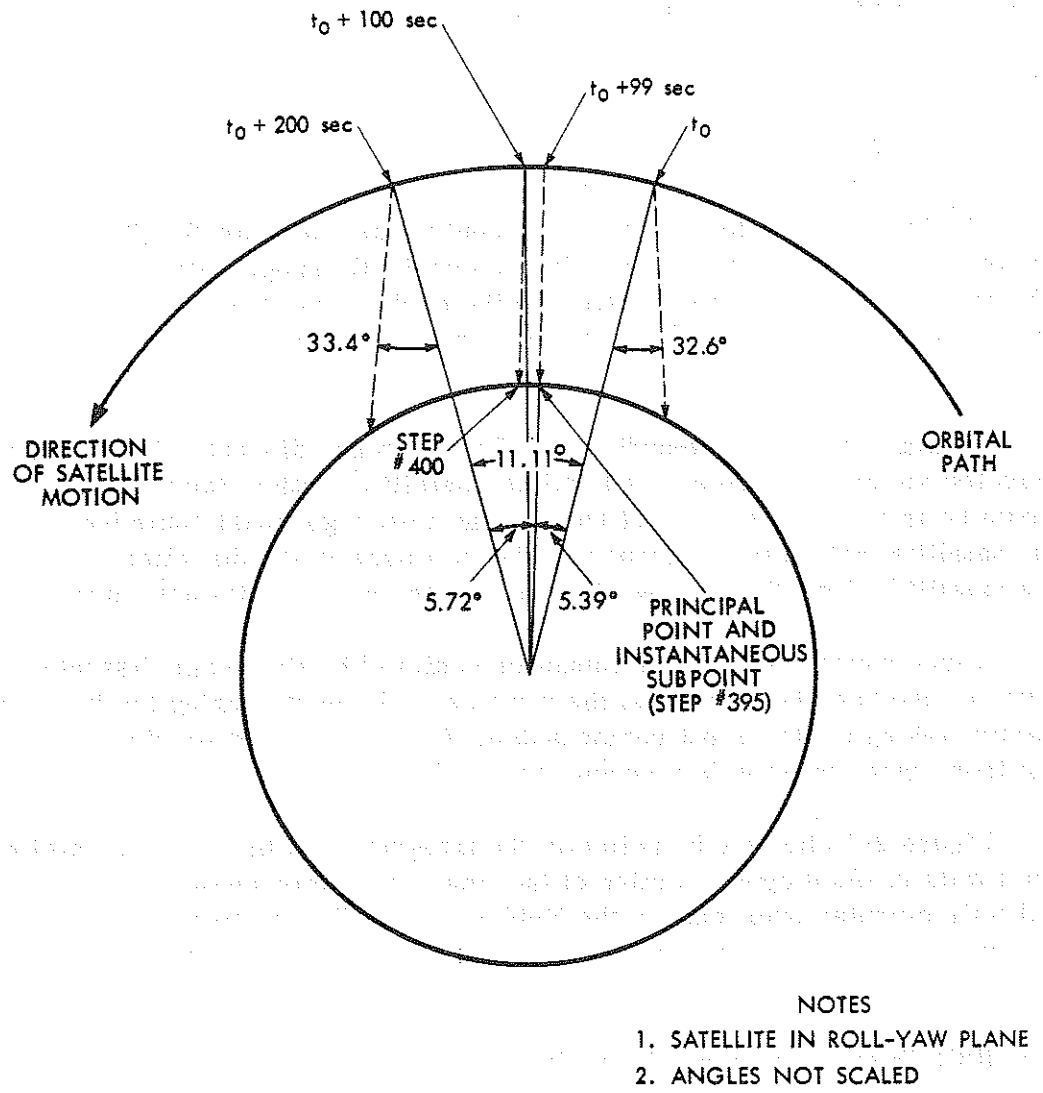

Figure 2-7. IDCS Satellite Motion Compensation

Each IDCS frame, approximately 2 × 2 inches, has a computer produced latitude-longitude grid and time of the first scan line (bottom) of the video display. Figure 2-8 is an illustrative example of the IDCS picture format with time and latitude-longitude grids.

The latitude-longitude grid points are computed by a CDC 924 computer and electronically integrated with the video signal at the ground station. The grid points form latitude grid lines at 10° intervals and are composed of grid points at two degree intervals. The longitude grid lines are formed at ten degree

intervals between 60°S to 60°N and are composed of grid points at two degree intervals. The longitude grid lines from 60°S and 60°N to the Poles are formed at 20 degree intervals and are composed of grid points at 5° intervals from 60° to 80° Colatitude.

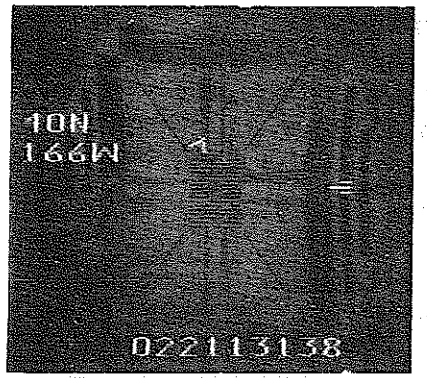

Figure 2-8. Sample IDCS Picture Format

An arrowhead pointing to the north appears in the picture at a latitude-longitude intersection. The latitude and longitude of the intersection appears at the left side of the picture. Latitude is indicated by the two upper digits followed by an "N" for north or "S" for south. Longitude is given by the three digits below followed by "E" for east or "W" for west. The longitude display does not appear at the Poles. Three tick marks are located at the center right of the picture. The longer tick mark in the middle positions the four hundredth line of the frame which is midway during the picture-taking interval. For all practical purposes this corresponds to the sensor scan through the subsatellite point. The time annotation at the bottom of the display is the time of the first scan (bottom line) of the video display. The time of the 400th scan line (defined by the longer tick mark) is obtained by adding 100 seconds to the time given at the bottom of the display. In the example shown (Figure 2-8) the arrowhead is located at 40°N and 166°W and the time (Universal) is 022 days (January 22), 11 hours, 31 minutes, 38 seconds.

2.5.2 IDCS Data Archiving and Access

The original 70 mm negatives are arranged in data orbit or swath format, i.e., sequential pictures of a single swath from pole to pole. The individual swaths, labeled by appropriate data orbit number are spliced together in orbit sequence. These negatives are reproduced under strict quality control standards

on 70 mm roll film stock as both positive and negative transparencies. The transparencies, in 500-foot reels, will be forwarded to the National Weather Records Center (NWRC) in Asheville, North Carolina, for archiving. A 500-foot reel of film will contain approximately one week's IDCS coverage. Film data can be ordered from NWRC at cost of reproduction.

Reference to the Nimbus IV monthly catalog containing daily IDCS montages and coverage will enable the user to determine his data requirements as to time and geographical location and in turn the particular swaths of data he requires. Orders and inquiries should be addressed to:

National Weather Records Center
ESSA
Federal Building
Asheville, North Carolina 28801

The following information should be included in correspondence or on orders:

1. Satellite, i.e., Nimbus IV
2. Sensor, i.e., IDCS
3. Date
4. Swath Number
5. Positive or Negative Transparency

For the interim period between launch of Nimbus IV and the issuance of the first Nimbus Monthly Catalog, the GSFC, upon request, can make available Nimbus IDCS film data in 70-mm copies on a limited and time available basis. As resources permit, limited quantities of data will be furnished to qualified investigators without charge.

Special requests for Nimbus IDCS data during the interim period should be addressed to:

National Aeronautics & Space Administration
Goddard Space Flight Center
Nimbus Project, Code 450
Greenbelt, Maryland 20771

It is sufficient to indicate the date and specific geographical area of coverage for these special interim requests. 70-mm IDCS data can be made available in the following formats by swath:

Negative Transparencies
Positive Transparencies
Positive Contact Prints

SECTION 3

THE TEMPERATURE-HUMIDITY INFRARED RADIOMETER (THIR) EXPERIMENT

By
Andrew W. McCulloch
National Aeronautics and Space Administration
Goddard Space Flight Center

3.1 Introduction

The THIR is a two channel high resolution scanning radiometer designed to perform two major functions. First, a 10.5-12.5μ window channel will provide both day and night cloud top or surface temperatures. Second, a water vapor channel at 6.7μ will give information on the moisture content of the upper troposphere and stratosphere and the location of jet streams and frontal systems. The ground resolution at the subpoint is 8 Km for the window channel and 22 Km for the water vapor channel. The window channel will operate day and night while the water vapor channel will operate mostly at night.

3.2 Instrumentation

3.2.1 Radiometer

The THIR radiometer consists of an optical scanner (shown in Figure 3-1) and an electronic module (not shown). The blackened collar seen near the scan mirror is a sun shield whose function is to prevent sunlight contamination during spacecraft sunrise and sunset. The other side of the sun shield is painted white. The end of the scanner opposite the sun shield contains the optical system and preamplifiers.

The optical system (shown in Figure 3-2) consists of a scan mirror, a telescope (comprised of primary and secondary mirrors) and a dichroic beamsplitter. The scan mirror, inclined at 45° to the optical axis, rotates at 48 rpm and scans in a plane perpendicular to the direction of the motion of the satellite. The scan mirror rotation is such that, when combined with the velocity vector of the satellite, a right-hand spiral results. Therefore, the field of view scans

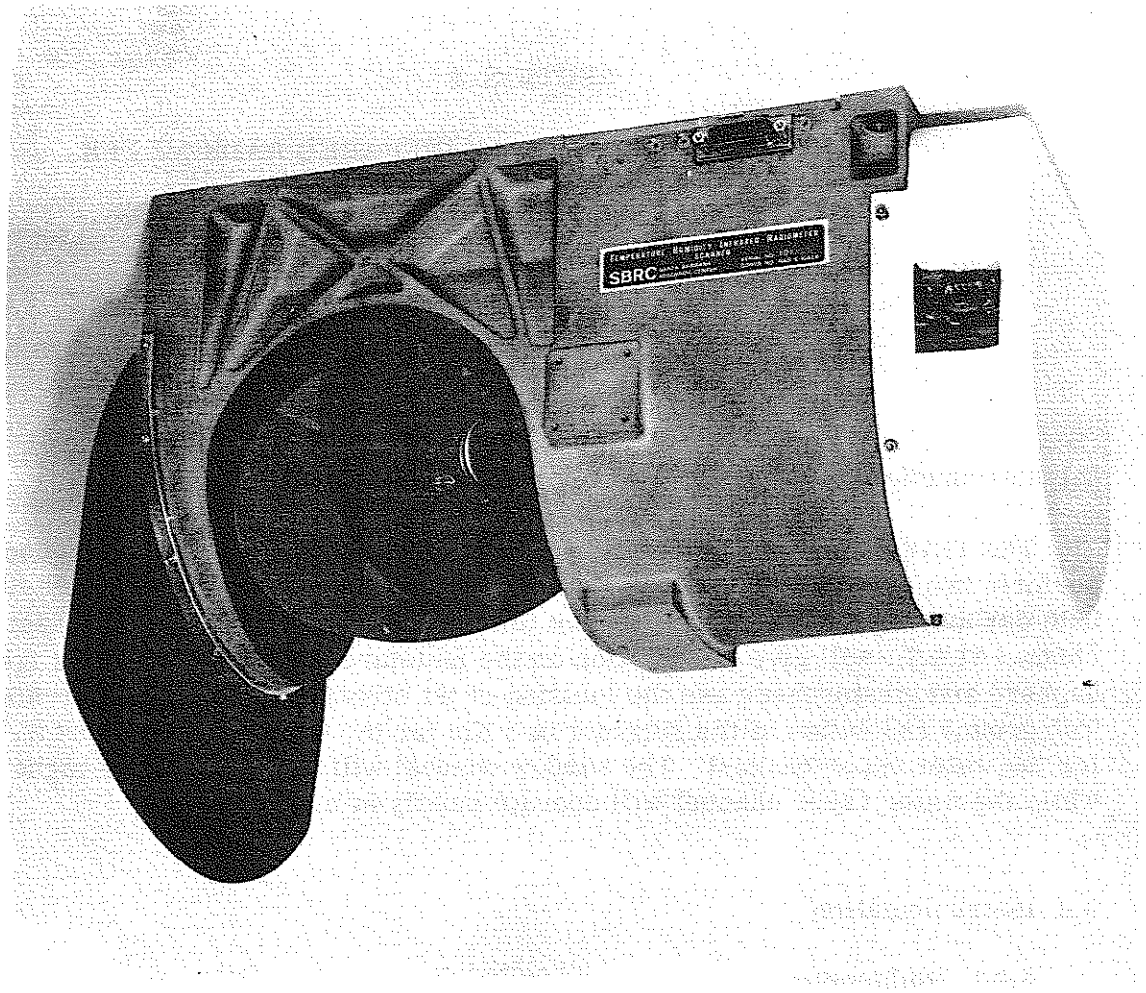

Figure 3-1. The Temperature-Humidity Infrared Radiometer

across the earth from east to west in daytime and west to east at night, when the satellite is traveling northward and southward respectively.

The telescope focuses the energy at the dichroic beamsplitter which divides the energy spectrally and spatially into two (2) channels. A 21-milliradian channel detects energy in the 6.7 micron band and consists of a passband filter, germanium relay lens, baffles, and germanium immersed thermistor bolometer. A 7.0 milliradian channel detects energy in the 10.5-12.5 micron band. It consists of a bandpass filter (transmission portion of the dichroic), an Itran-2 relay lens which also serves as a long wavelength blocking filter, a folding mirror, and a germanium immersed thermistor bolometer.

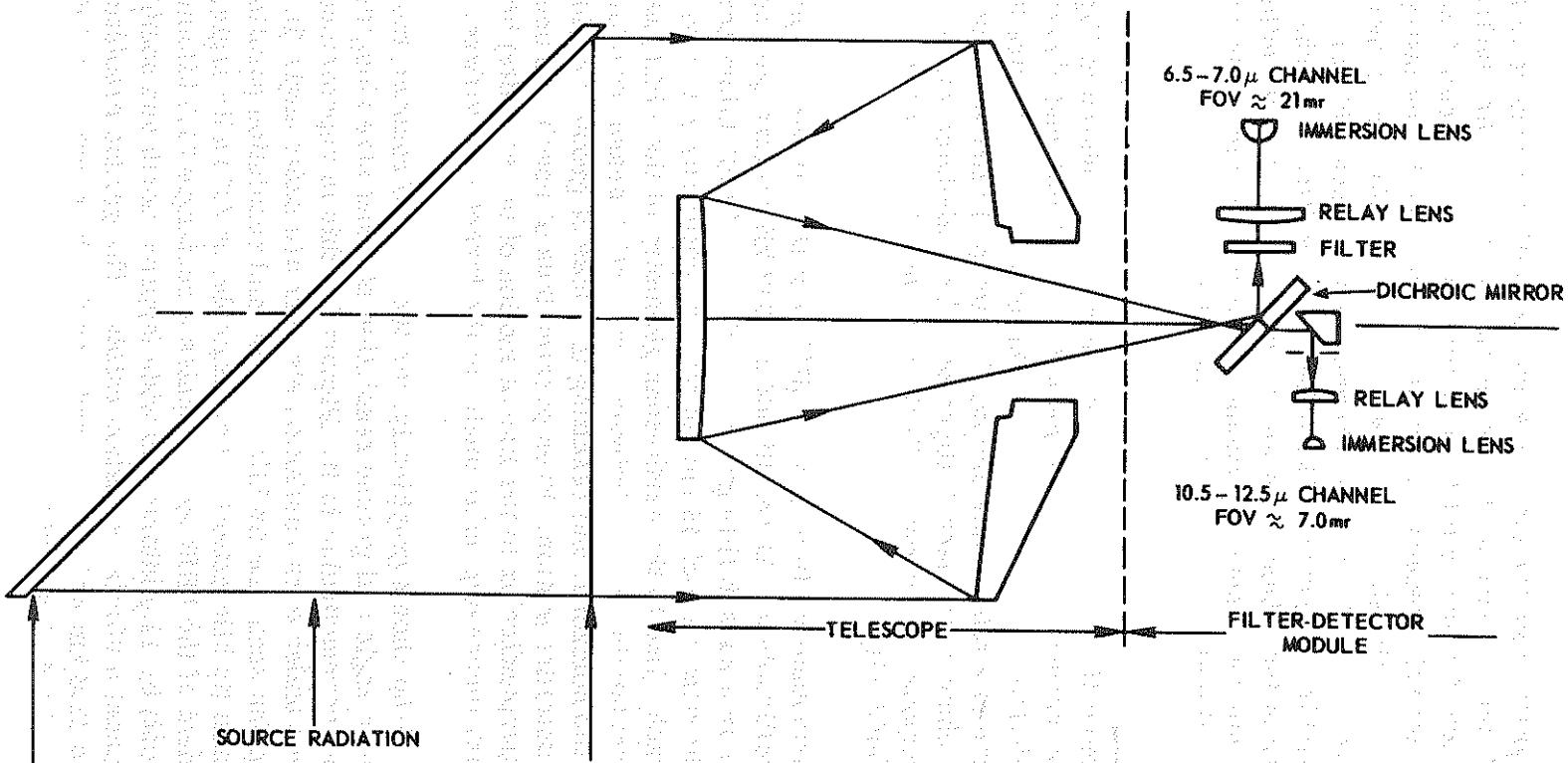

Figure 3-2. THIR Optical Schematic

The signals from the detectors are capacitively coupled to the preamplifiers, amplified and sent to the electronic module. In the electronic module, the signals are further amplified and corrected for detector time constant to provide the overall frequency response as required by the subsystem optical resolution. The signals are processed out of the electronic module through buffer amplifiers. The 6.7 micron channel output is available on a full time basis as the shifted level channel. The offset of the shifted level channel is provided in the buffer of that channel. A second video output selects either the 6.7 micron or the 11.5 micron channel by means of a command relay. In addition to the two video output signals, there are fourteen telemetry channels: ten analog and four digital.

The actual fields of view for both channels are shown in Figures 3-3 and 3-4. These measurements were made in the azimuth and elevation directions which are defined by the scanner orientations shown in Figure 3-5. Also shown in this figure is a table summarizing the fields of view sizes (half widths) as well as the channel to channel alignment. The tabulated values of the relative spectral response are shown in Table 3-1 while Figures 3-6 and 3-7 illustrate the data graphically.

The instantaneous field of view (IFOV) of the window channel is approximately 7 milliradians. At an altitude of 1112 kilometers (600 nautical miles) this results in a subsatellite ground resolution of 6.67 kilometers (4.1 nautical miles). The scan rate of 48 rpm produces contiguous coverage along the subsatellite track. Due to the earth-scan geometry of the THIR, as nadir angle increases, overlapping occurs between consecutive scans, reaching 350 percent overlap at the horizons, and resulting in a loss of ground resolution in the direction of the satellite motion. Even greater loss of resolution occurs along the scan line (perpendicular to the line of motion of the satellite) because of the expansion, with increasing nadir angle, of the target area viewed.

Figure 3-8b shows graphically, for the window channel, the relationship between nadir angle and ground resolution element size along the path of the satellite and perpendicular to it. Pictorially this is represented in Figure 3-8a. The numbers under each resolution element are nadir angle (in degrees), resolution along the scan line (in kilometers), and resolution parallel to the satellite line of motion (in kilometers). For example, at 50° nadir angle, the ground resolution element of the THIR approximates a rectangle 31.8 kilometers long (approx. east and west) by 14.0 kilometers wide (approx. north and south). For the 6.7 micron channel a similar situation exists. The ground resolution at the subsatellite point is 22.6 km while at 50° nadir angle, the ground resolution element is 93.5 km long by 41.1 km wide.

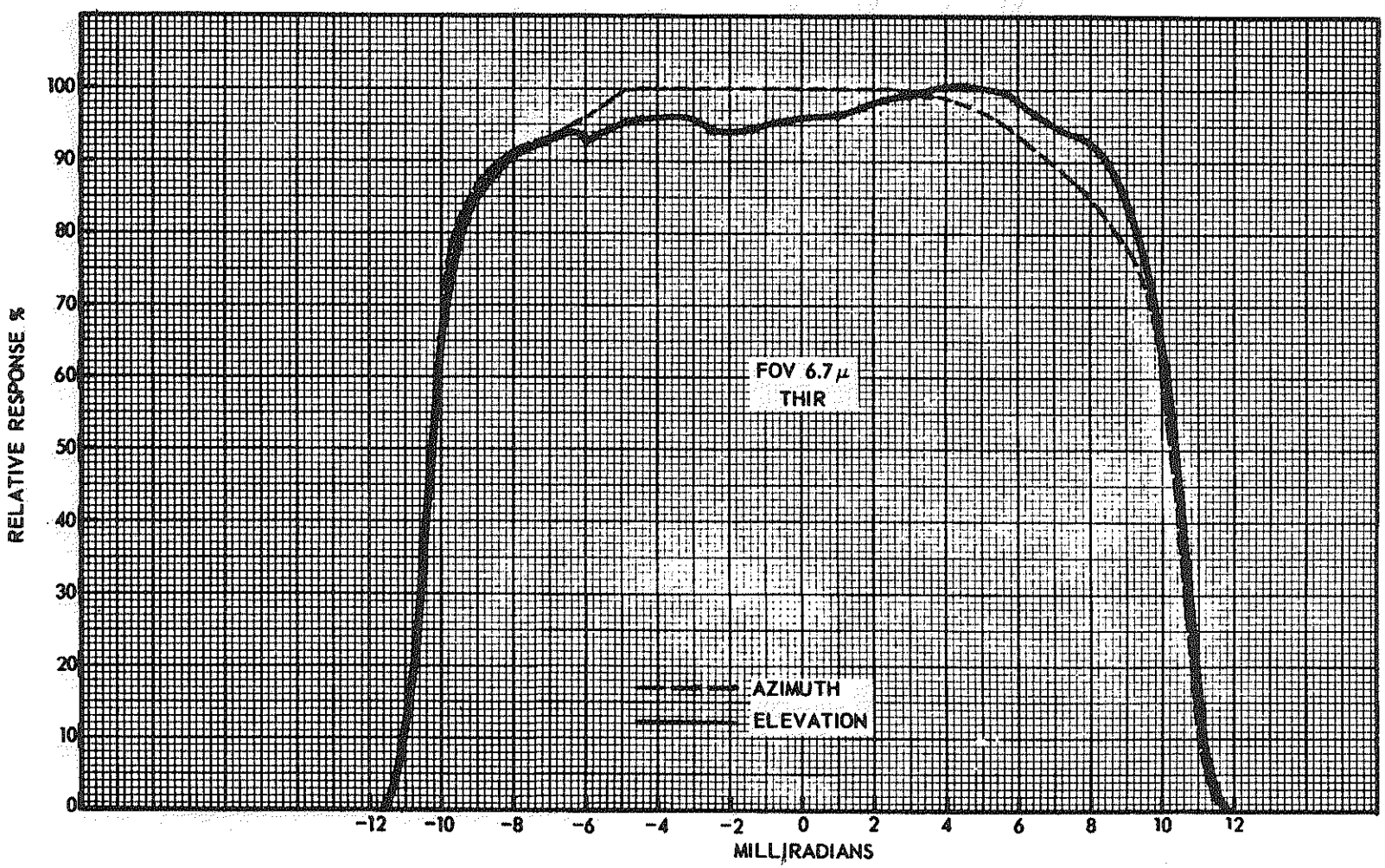

Figure 3-3. Field of View of the 6.7 Micron Channel

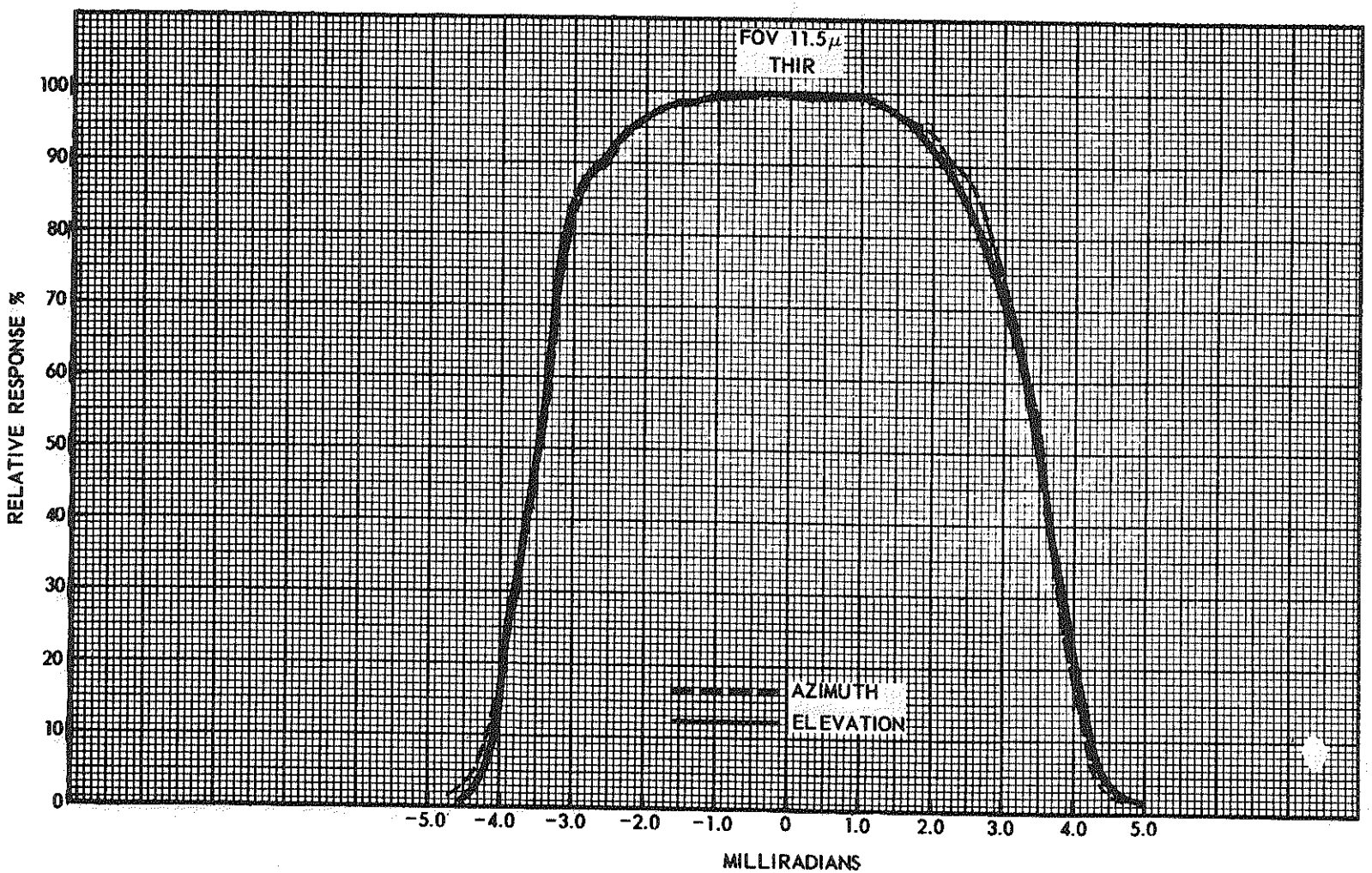

Figure 3-4. Field of View of the 11.5 Micron Channel

	FIELD OF VIEW		
	SIZE		ALIGNMENT
CHANNEL	AZ (mr)	EL (mr)	EL (mr)
6.7 μ	20.625	20.525	-2.940
11.5 μ	6.925	6.95	-3.025
CHANNEL TO CHANNEL ALIGNMENT	.10	.085	.085

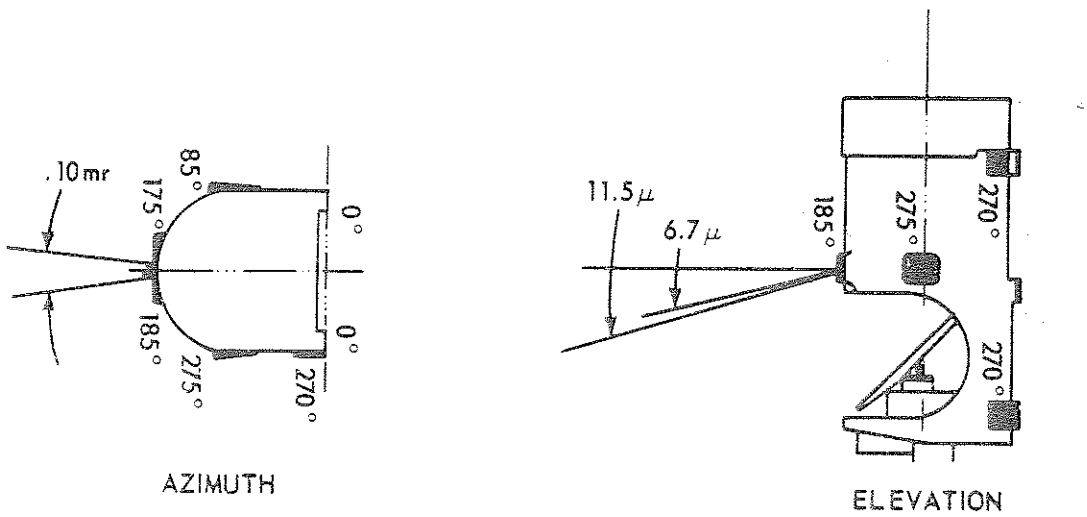

Figure 3-5. Scanner Orientations and Field of View Sizes

In contrast to television, no image is formed within the radiometer: the THIR sensor merely transforms the received radiation into an electrical (voltage) output with an information bandwidth of 0.5 to 360 Hz for the 10.5-12.5 micron channel and 0.5 to 120 Hz for the 6.7 micron channel. The radiometer scan mirror continuously rotates the field of view of the detector through 360 degrees in a plane normal to the spacecraft velocity vector. The detector views in sequence the in-flight black body calibration target (which is a part of the radiometer housing), outer space, Earth, outer space, and returns again to intercept the

Table 3-1
Relative Spectral Response, ϕ_λ

6.7μ Channel		11.5μ Channel			
λ Micron	Relative Response	λ Microns	Relative Response	λ Microns	Relative Response
6.20	0.00	9.90	0.00	12.7	0.4623
6.25	0.0061	10.0	0.0105	12.8	0.2513
6.30	0.0122	10.1	0.0282	12.9	0.1134
6.35	0.0761	10.2	.1306	13.0	0.0437
6.40	0.1399	10.3	.3019	13.1	0.0093
6.45	0.5088	10.4	.4327	13.2	0.00
6.50	0.8777	10.5	.4638		
6.55	0.9015	10.6	.6618		
6.60	0.9253	10.7	.8025		
6.65	0.8687	10.8	.8436		
6.70	0.8120	10.9	.8089		
6.75	0.8709	11.0	.8511		
6.80	0.9298	11.1	.9447		
6.85	0.9645	11.2	.9714		
6.90	0.9991	11.3	1.000		
6.95	0.9995	11.4	.9985		
7.00	1.0000	11.5	.9925		
7.05	.9471	11.6	.9923		
7.10	.8943	11.7	.9660		
7.15	.6972	11.8	.8761		
7.20	.5001	11.9	.9012		
7.25	.2859	12.0	.9662		
7.30	.0717	12.1	.9649		
7.35	.0422	12.2	.9682		
7.40	.0127	12.3	.9118		
7.45	.0097	12.4	.8148		
7.50	.0067	12.5	.8572		
7.55	.0033	12.6	.5987		
7.60	0.00				

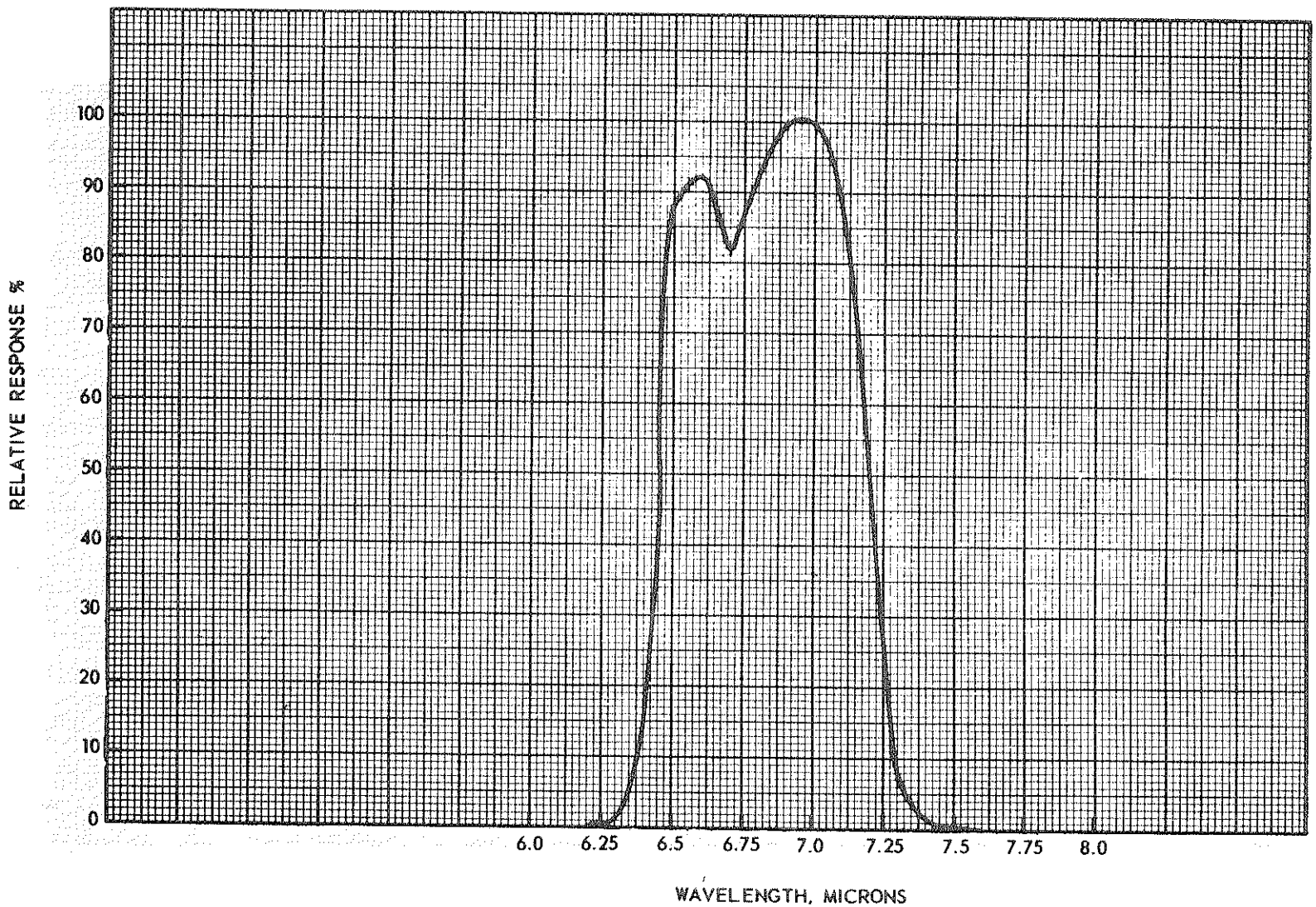

Figure 3-6. Relative Spectral Response of the 6.7 Micron Channel

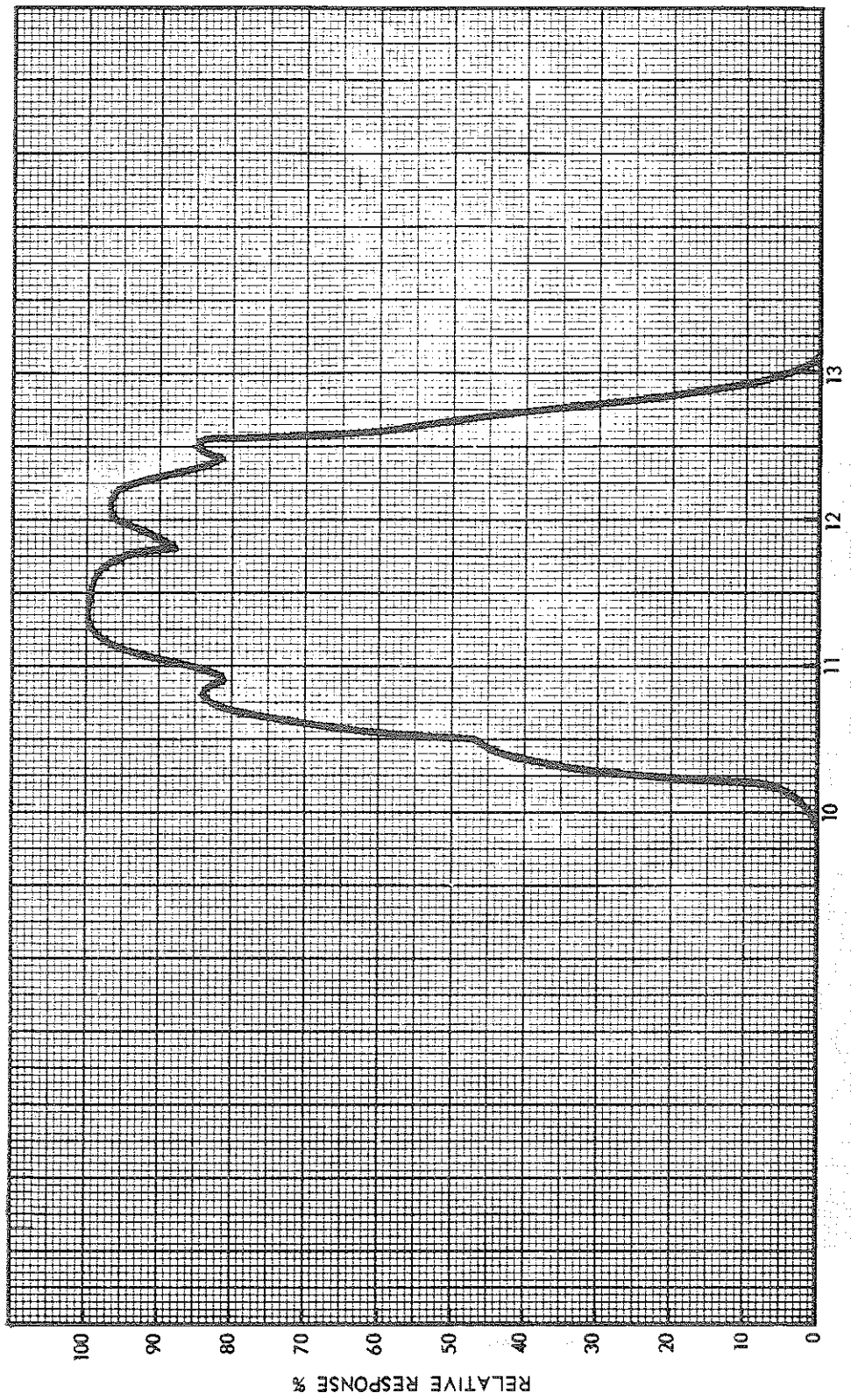

Figure 3-7. Relative Spectral Response of the 11.5 Micron Channel

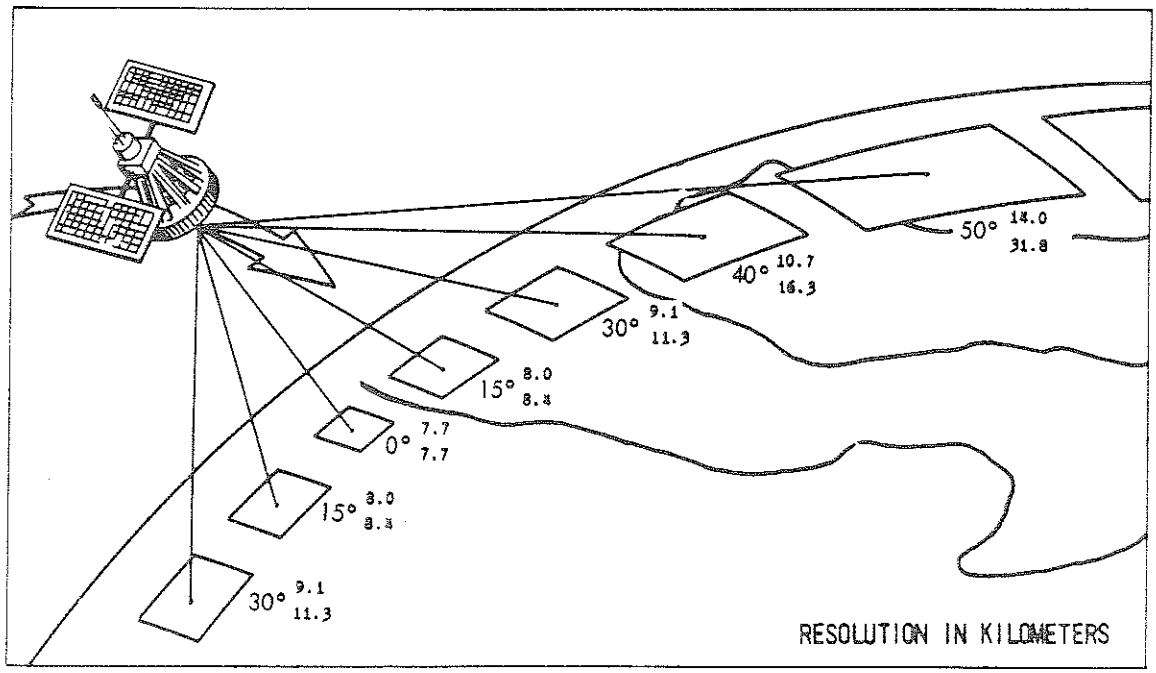

(a)

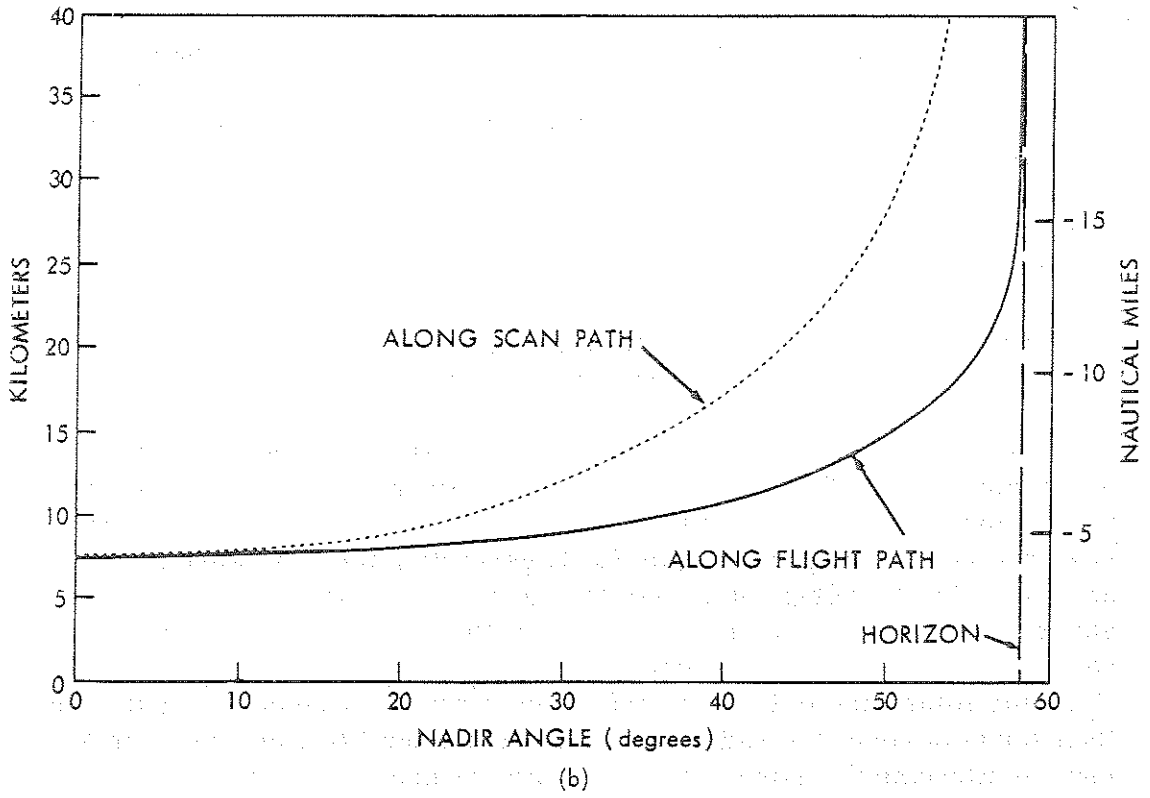

(b)

Figure 3-8. Relationship between Nadir Angle and Ground Resolution for the THIR 11.5 μ Channel at 600 N. Miles (a) Pictorial (b) Graphical

calibration target. The space and housing-viewed parts of the scan, which can be identified without difficulty, serve as part of the in-flight check of calibration. Information on housing temperature, which is monitored by thermistors, is telemetered to the ground stations and for calibration purposes is constantly compared with the temperature obtained from the radiometer housing scan. Even though the first stages of amplification are capacitor-coupled, the low frequency cutoff is so low that a dc restore circuit is necessary to provide a zero signal reference. This occurs during that portion of the scan when the optics are receiving zero radiation (space). The dc restore circuitry also provides additional gain to raise the signal to the desired output level and filtering to establish proper frequency characteristics.

An additional function of the dc restorer is to reduce the 6.7 micron channel gain to 1/3 of its former value when the bolometer views the housing. This is necessary to prevent saturation of the output signal when the housing temperature is beyond the dynamic range of the channel.

3.2.1.1 Scan Sequence

The scan mirror rotates at 48 rpm or 1.25 seconds per revolution. The scanner's total angular scan from the time the IFOV leaves the housing until it intercepts the housing again after scanning the earth is 150°. The earth subtends an arc of 128° at 400 nautical miles (nmi) and 117° at 600 nmi. This provides a minimum of 11° coverage above the horizon when scanning the earth. To assure an adequate scan period in space during dc restoration, the radiometer requires a mounting position rotated 5° about the spacecraft roll axis. This provides a minimum of 16° for operation of the dc restorer (for 400 nmi orbit).

Figures 3-9 and 3-10 illustrate the radiometer timing sequence relative to the angular position of the scan mirror for each scan cycle.

The sync word and calibration sequence is started by scan mirror position pulse (pip) No. 1. This pip is generated in the magnetic pick-off head when the magnet located on the scan mirror passes the pick-off. The logic circuit timing sequence is also triggered by pip No. 1, generating the sync word for 84 msec and the calibrate voltage staircase for 105 msec. At the end of the calibrate staircase, the radiometer IFOV is clear of the radiometer housing, and the restore period of 25 msec is started. After the restoration period, the radiometer IFOV for some time is in space before and after the scan of the earth. The IFOV then starts to cover the radiometer housing and pip No. 2 occurs. Pip No. 2 is used to attenuate the gain of the 6.7 micron channel by a factor of 3 to extend the dynamic range of that channel to include the housing radiation level. The gain is returned to normal by pip No. 1.

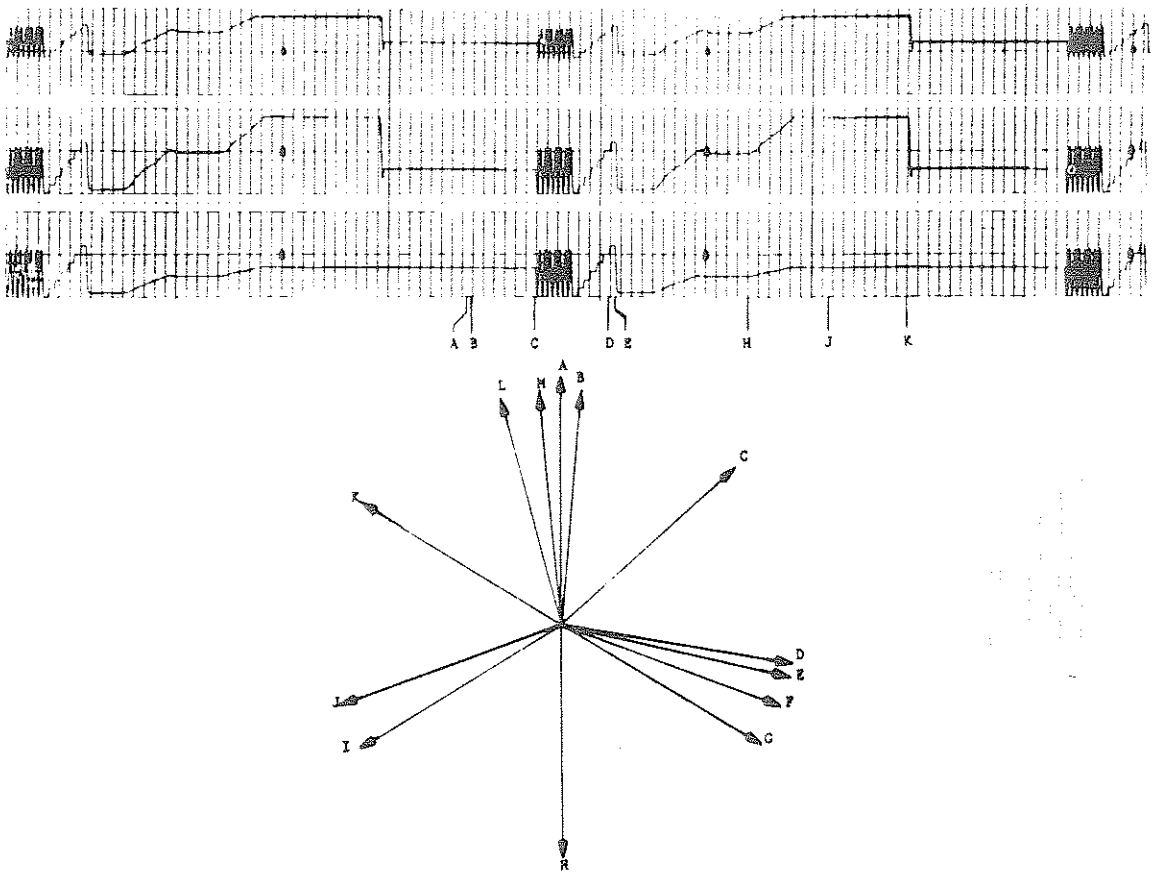

LEGEND

Reference Letter	Angle (degrees)	Time (msec)	Event
A:	0	0	Spacecraft zenith
B:	5	17.4	Radiometer IFOV just starting to leave housing.
C:	48	166.7	Scan mirror position pip No. 1 occurs and radiometer sync word and calibration signal sequence is started. 6.7 micron channel gain returned to normal.
D:	100	347.5	Radiometer IFOV just starting to see all of space.
E:	103.5	359.4	Calibrate signal sequence ends and restore period starts.
F:	110.7	384.4	Restore period ends
G:	121.5	422.2	Earth scan period begins (600-nmi orbit)
H:	180	625.0	Spacecraft nadir
I:	238.5	828.8	Earth scan period ends (600-nmi orbit)
J:	250	868.9	Radiometer IFOV just starting to see housing.
K:	302	1048.5	Scan mirror position pip No. 2 occurs and 6.7 micron channel gain is attenuated by a factor of 3.
L:	345	1197.9	Radiometer IFOV completely filled by housing.
M:	355	1232.6	Radiometer Z-axis

Figure 3-9. THIR Scan Angle Information

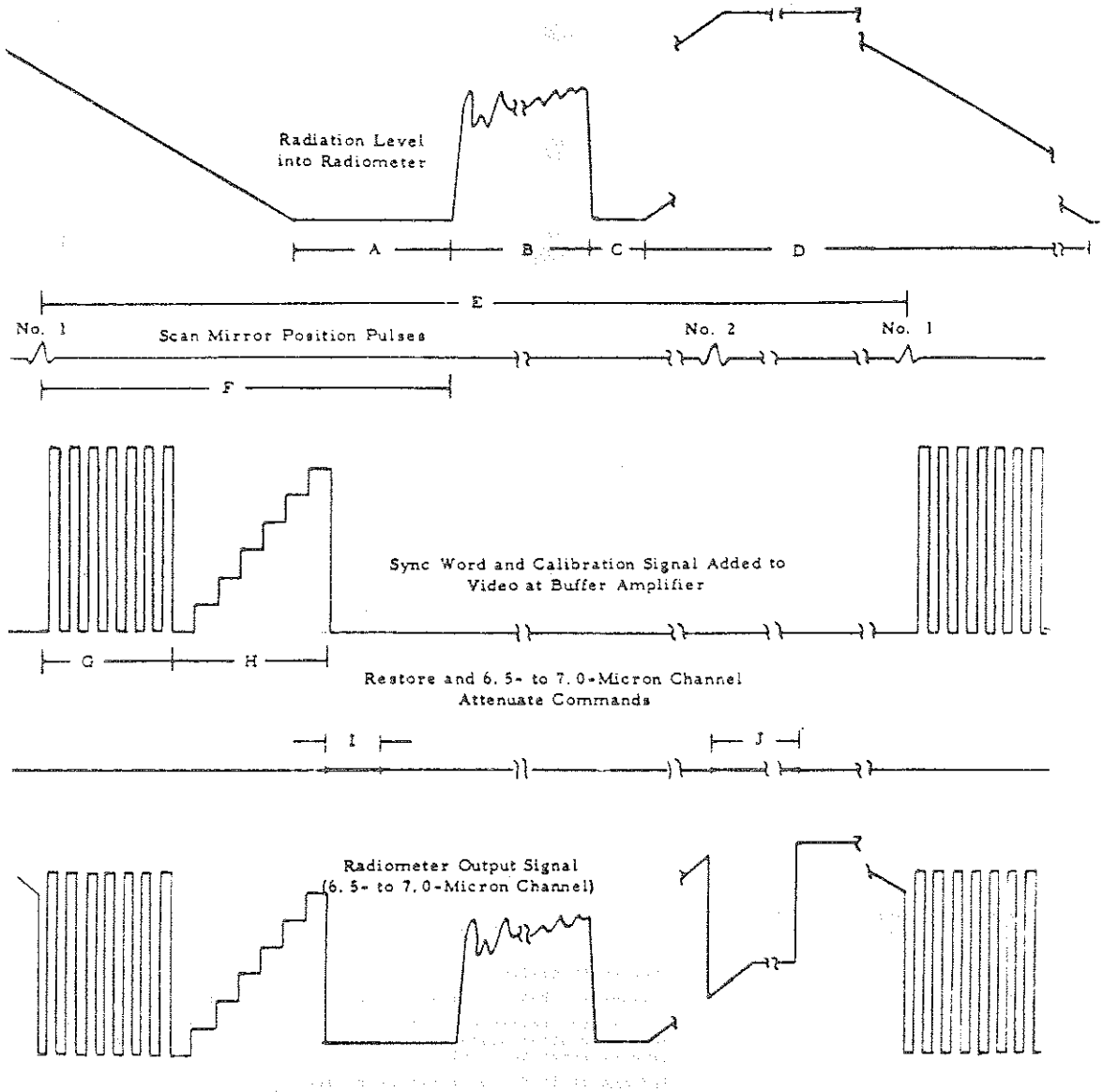

A - Space Scan (Prior to Earth Scan), 75 msec
B - Earth Scan, 407 msec
C - Space Scan (After Earth Scan), 40 msec
D - Housing Scan, 730 msec
E - Scan Period, 1250 msec
F - Sync Pulse to Earth Scan Period, 255.5 msec
G - Sync Word, 84 msec
H - Calibrate Signal, 105 msec
I - Restore Period, 25 msec
J - 6.5- to 7.0-Micron Channel Attenuate Period, 181 msec

Figure 3-10. THIR Voltage Waveforms During Scan Period

3.2.2 Subsystem

A simplified block diagram of the THIR subsystem is given in Figure 3-11. The radiometer produces three outputs. Two (2) of these have outputs of 0 to -6 volts dc while the third has a shifted level of -4.3 to -8.3 volts. The 11.5μ and 6.7μ channels time share one track of the tape recorder subsystems (High Data Rate Storage Subsystems HDRSS 'A' and 'B') while the shifted 6.7μ channel time shares with the IDCS another track of HDRSS. Information from the 11.5μ and 6.7μ channel is also available through the Nimbus D Versatile Information Processor (VIP) as well as alternating the IDCS on Real Time Transmission Subsystem (RTTS).

3.2.2.1 Stored Data

The THIR records on two tracks of the 5 track HDRSS tape recorder subsystem along with the other experiments and the time code. There are two (2) similar HDRSS's in the spacecraft for increased reliability and data coverage.

The varying dc voltage from the THIR modulates a VCO (voltage controlled oscillator) and is recorded on the HDRSS tape recorder. Upon command the recorder plays back (in reverse) 32 times faster than real time into two channels of the multiplexer (MUX). The signal is doubled and beat against an 805 kHz local oscillator, producing a 657.8 kHz to 602.8 kHz FM signal. This is directed into the S-band transmitter and broadcast to the Data Acquisition Facility (DAF) along with frequencies of the time code and other experiments.

3.2.2.2 Direct Readout Infrared Radiometer (DRIR)

The THIR Real-Time Transmission Subsystem (RTTS) is shared with IDCS. Generally Real Time IDCS (DRID) data will be broadcast in daytime and DRIR in nighttime. On a few selected occasions Real Time DRIR data will be transmitted in daytime to evaluate the daytime THIR (6.7 micron) experiment.

The THIR output is channeled into a mixer-modulator (HAX) where its amplitude modulates a 24 Hz signal from the spacecraft clock. This subcarrier in turn frequency modulates a 136.95 MHz transmitter which broadcasts continuously.

3.3 Calibration

3.3.1 Laboratory Calibration

The main parameters for calibration of all electromagnetic radiation detection devices are essentially the same. Three fundamental quantities must be defined: the effective spectral response, φ_λ; the effective radiance, $\bar{N}$; and the

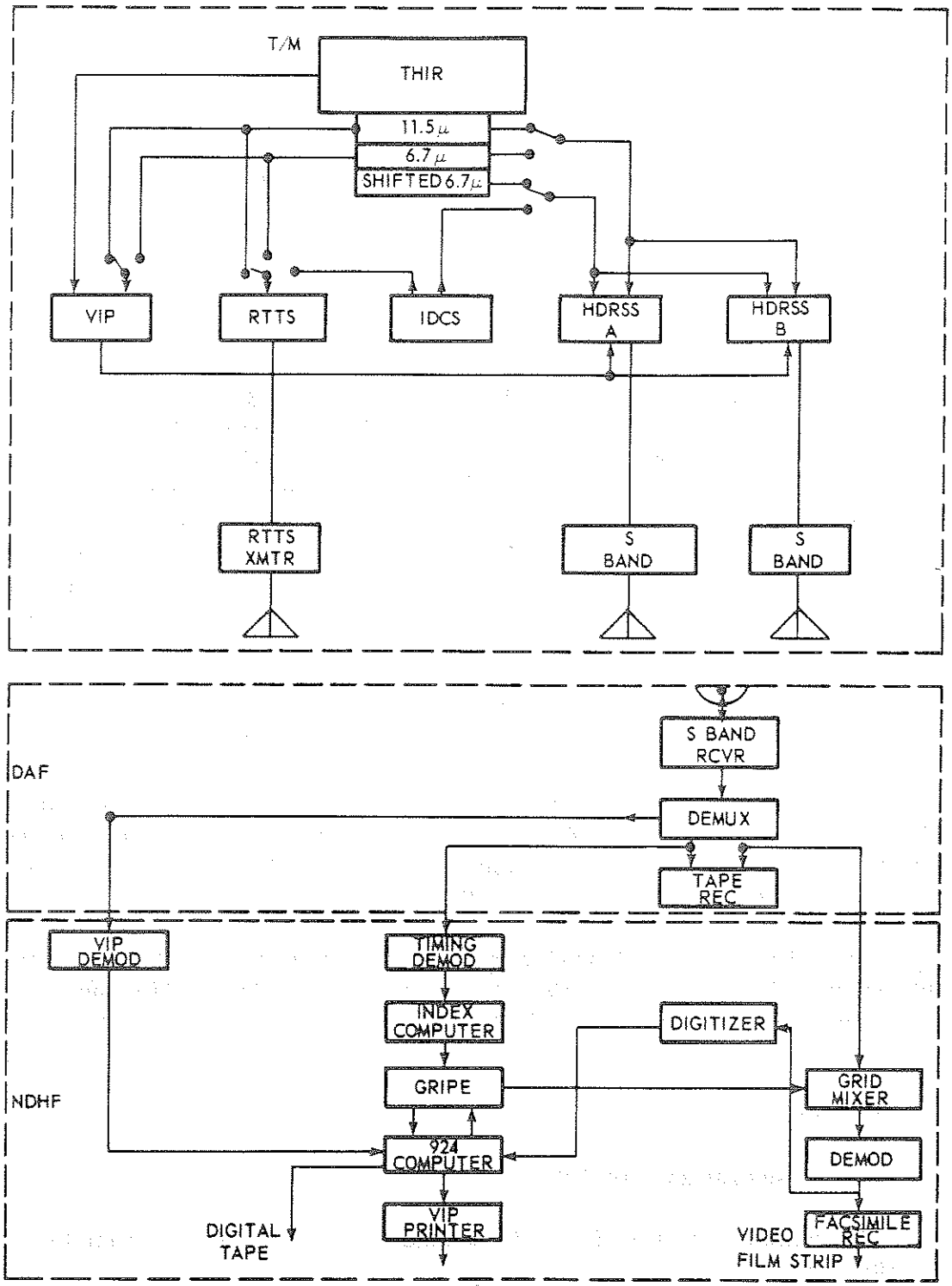

Figure 3-11. Simplified Block Diagram of the THIR Subsystem

equivalent blackbody temperature, T_{BB}. Here φ_λ is a composite function involving all of the factors which contribute to the spectral response of the instrument, such as filter transmission, mirror reflectances, and the spectral responsivity of the detector.

The effective radiance, $\bar{N}$, is defined as

$$\bar{N} = \int_0^\infty N_\lambda \, \varphi_\lambda \, d\lambda \tag{1}$$

where N_λ represents the generally non-Planckian radiation from the earth and its atmosphere.

Because of its narrow field of view, the THIR essentially measures beam radiation or radiance toward the satellite along the optical axis. In the preflight laboratory calibration, the field of view of the radiometer was filled by a blackbody target whose temperature could be varied and accurately measured over a range of 190 K to 340 K. From the temperature of the blackbody target, T_{BB}, the spectral radiance of the target is determined by the Planck function, B_λ. The integration of this function over the effective spectral response, φ_λ, yields that portion of the radiance of the target to which the radiometer responds, the "effective radiance", $\bar{N}$, given by

$$\bar{N} = \int_0^\infty B_\lambda \, (T_{BB}) \varphi_\lambda \, d\lambda \tag{2}$$

The preflight laboratory calibration set-up is shown in Figure 3-12.

3.3.2 Equivalent Blackbody Temperature

The effective radiance to which the orbiting radiometer responds may be expressed by

$$\bar{N} = \int_0^\infty N_\lambda \, \varphi_\lambda \, d\lambda \tag{3}$$

where N_λ is the spectral radiance in the direction of the satellite from the Earth and its atmosphere. It is convenient to express the measurement from orbit in terms of an equivalent temperature of a blackbody filling the field of view which would cause the same response from the radiometer. From Equations 2 and 3 it is seen that this "equivalent blackbody temperature" corresponds to the target

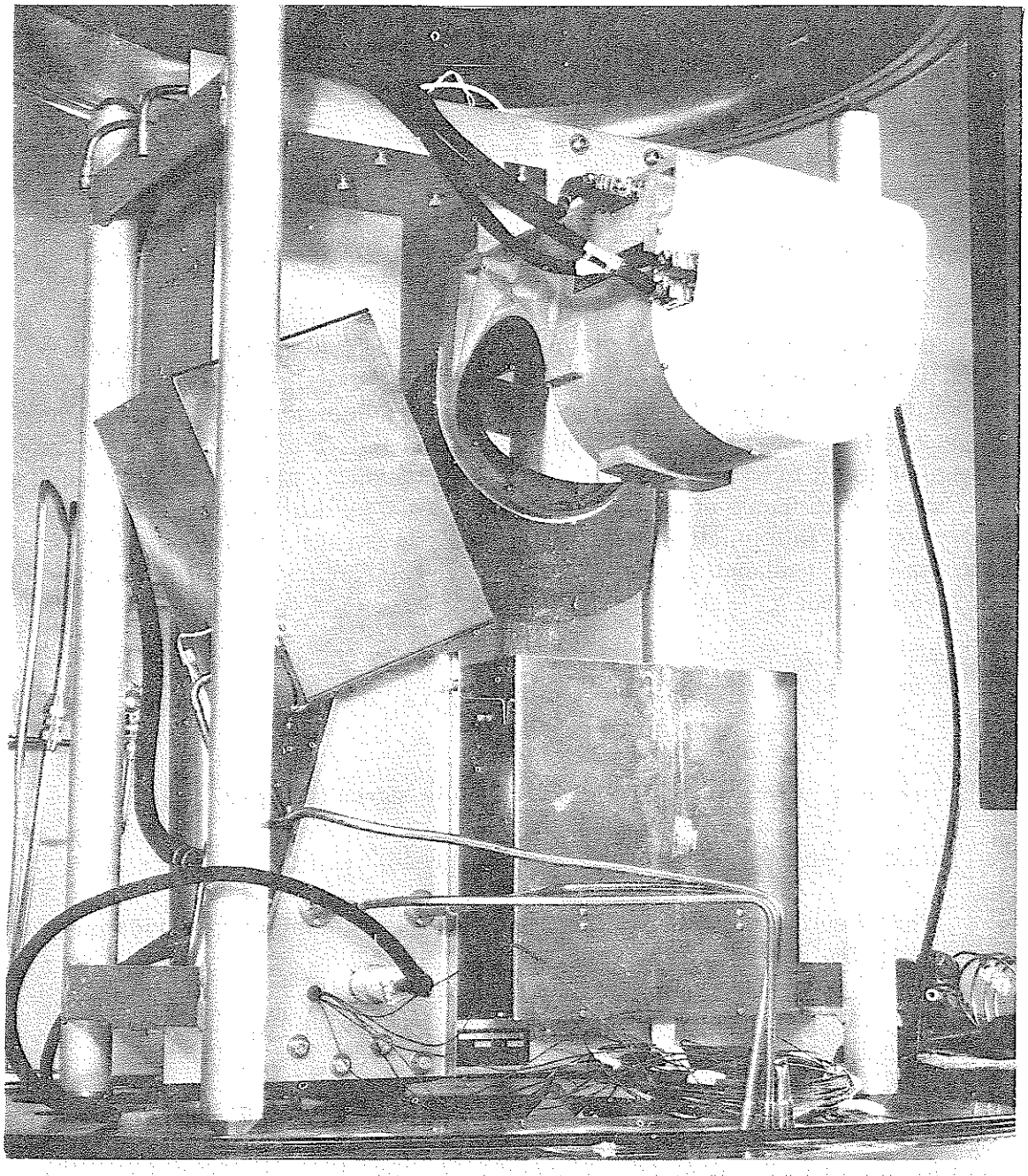

Figure 3-12. Preflight Laboratory Calibration Set-up for THIR

temperature, T_{BB}, of the blackbody used in the laboratory calibration, Therefore, the radiometer measurements can be expressed either as values of effective radiance, $\bar{N}$, or as equivalent black body temperatures, T_{BB}. The $\bar{N}$ versus T_{BB} function from Equation 2 is given in Figures 3-13, 3-14 and Table 3-2 for both channels.

THIR output voltages versus equivalent blackbody temperatures for both channels are given in Tables 3-3 and 3-4. The output voltages for the HDRSS are also valid for DRIR.

Table 3-2
Effective Radiance ($\bar{N}$) Versus Equivalent
Blackbody Temperatures(T_{BB}) — THIR SN 103

T_{BB} °K	6.7 Micron Channel $\bar{N}$ (W/M^2/Ster)	11.5 Micron Channel $\bar{N}$ (W/M^2/Ster)
150	.0047	.3019
160	.0113	.5050
170	.0244	.7960
180	.0484	1.193
190	.0892	1.716
200	.1548	2.380
210	.2550	3.202
220	.4016	4.195
230	.6079	5.371
240	.8891	6.738
250	1.262	8.306
260	1.743	10.08
270	2.352	12.06
280	3.106	14.25
290	4.025	16.66
300	5.126	19.27
310	6.429	22.10
320	7.951	25.13
330	9.708	28.37
340	11.72	31.80
350	13.99	35.44

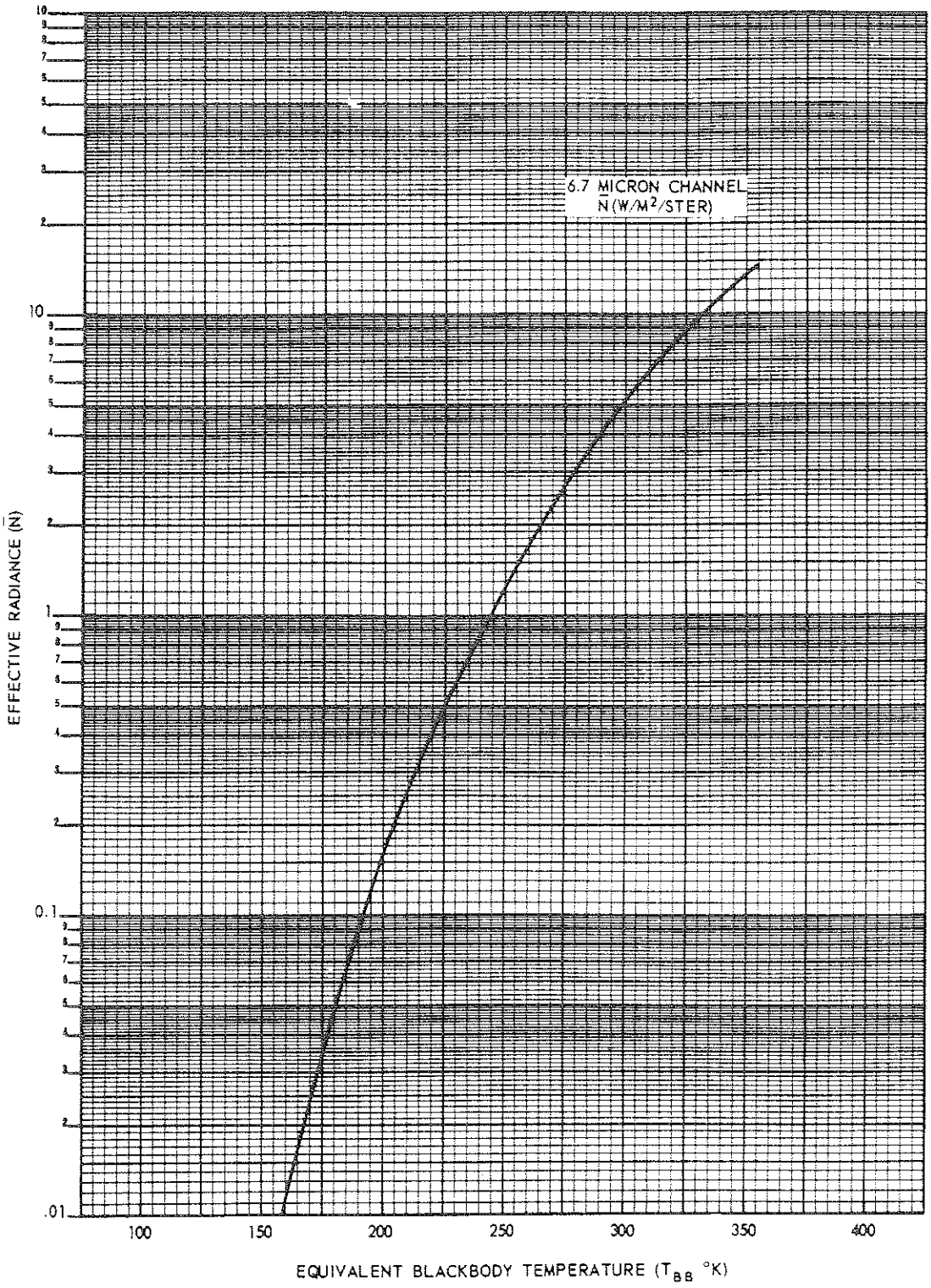

Figure 3-13. Effective Radiance versus Equivalent Blackbody Temperature for the 6.7 Micron Channel

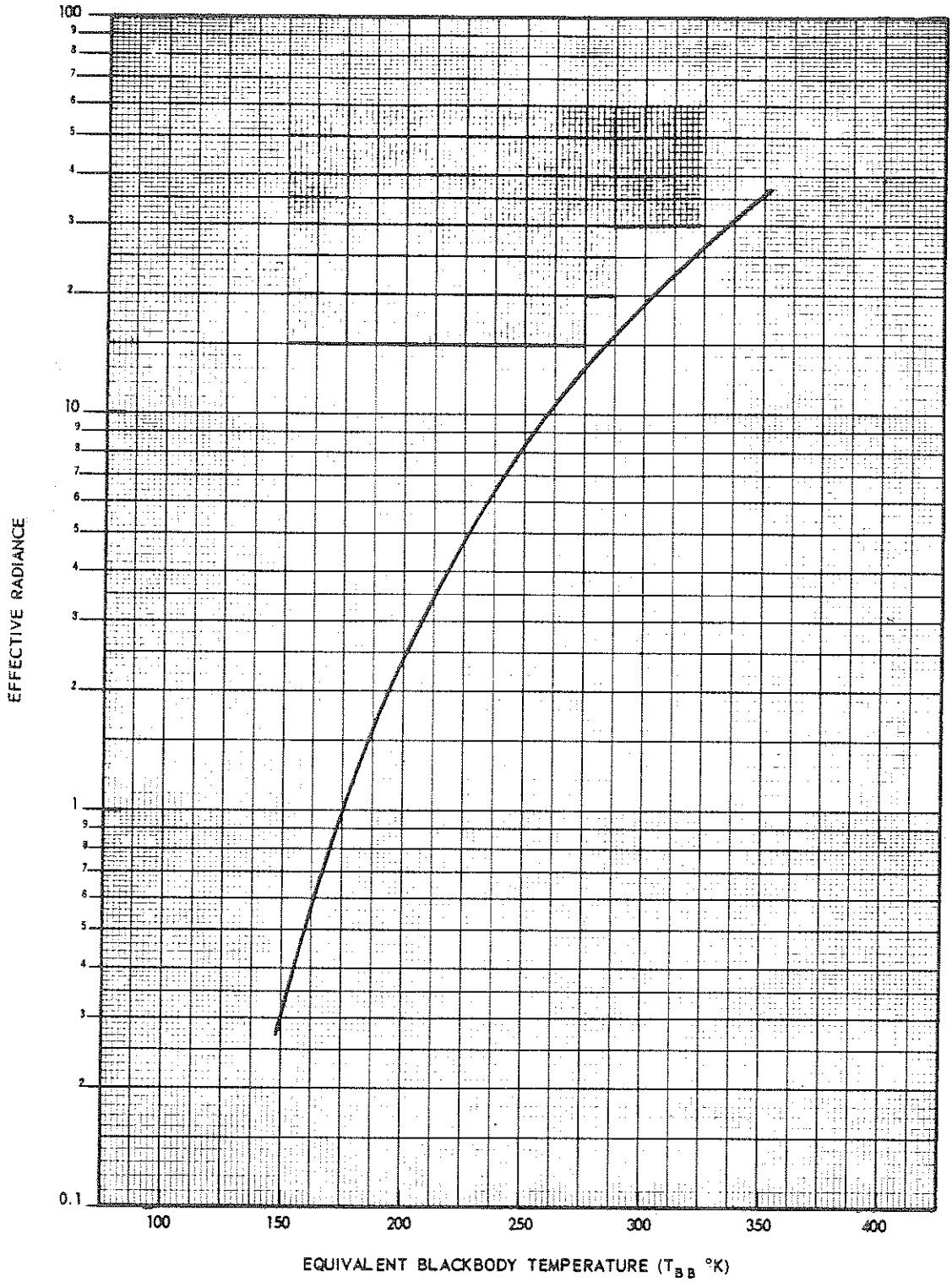

Figure 3-14. Effective Radiance versus Equivalent Blackbody Temperature for the 11.5 Micron Channel

Table 3-3
THIR Output Voltages versus Equivalent Blackbody Temperature at Different Bolometer Temperatures for the 11.5 Micron Channel (THIR SN-103)

	11.5 Micron Channel					
	HDRSS			VIP		
Bolometer Temperature	4°	17.5°	24°	4°	17.5°	24°
T_{BB} (°K) ↓						
< 190	-.52	-.52	-.52	-.52	-.52	-.52
190	-.857	-.848	-.843	-.808	-.820	-.809
200	-.952	-.975	-.940	-.904	-.946	-.909
210	-1.08	-1.10	-1.07	-1.04	-1.08	-1.04
220	-1.25	-1.24	-1.24	-1.20	-1.24	-1.21
230	-1.44	-1.43	-1.44	-1.40	-1.43	-1.42
240	-1.68	-1.66	-1.67	-1.64	-1.66	-1.65
250	-1.95	-1.94	-1.94	-1.91	-1.93	-1.92
260	-2.25	-2.25	-2.25	-2.22	-2.23	-2.23
270	-2.59	-2.59	-2.59	-2.56	-2.58	-2.57
280	-2.96	-2.95	-2.96	-2.94	-2.96	-2.95
290	-3.37	-3.36	-3.37	-3.36	-3.37	-3.36
300	-3.82	-3.81	-3.81	-3.81	-3.81	-3.80
310	-4.29	-4.29	-4.29	-4.29	-4.29	-4.28
320	-4.80	-4.78	-4.80	-4.81	-4.81	-4.79
330	-5.35	-5.33	-5.34	-5.37	-5.39	-5.34

3.4 Data Processing, Archiving and Availability

Nimbus IV THIR data are available from the NSSDC in three (3) general forms: Photofacsimile film strips (Figure 3-15); computer processed digital data shown in Figure 3-19, and raw analog records (not shown). The film strips are separated into day-night files and by channel. The user has the choice of ordering positive or negative transparencies or paper print.

The form of data most readily available to the user is the film strip.

Computer processing of the complex and voluminous data however, will be accomplished whenever requested by a user, as indicated in Section 3.4.2. The

Table 3-4
THIR Output Voltages versus Equivalent Blackbody Temperature at Different Bolometer Temperatures for the 6.7 Micron Channel (THIR SN-103)

	6.7 Micron Channel					
	HDRSS			VIP		
Bolometer Temperature	4°C	17.5°C	24°C	4°C	17.5°C	24°C
T_{BB} (°K) ↓						
< 190	-.54	-.54	-.54	-.54	-.54	-.54
190	-.788	-.765	-.801	-.685	-.70	-.748
200	-.916	-.828	-.944	-.821	-.84	-.886
210	-1.09	-1.02	-1.13	-1.03	-1.05	-1.08
220	-1.35	-1.35	-1.41	-1.33	-1.34	-1.37
230	-1.72	-1.79	-1.81	-1.76	-1.75	-1.79
240	-2.26	-2.35	-2.38	-2.34	-2.33	-2.37
250	-2.98	-3.08	-3.14	-3.12	-3.10	-3.14
260	-3.94	-4.07	-4.15	-4.11	-4.09	-4.13
270	-5.15	-5.36	-5.44	-5.38	-5.37	-5.39
280						
290						
300						
310						
320						
330						

analog data records require a comprehensive knowledge of the THIR subsystem for interpretation and reduction. The format of the analog data display makes it practical only for studies requiring extreme accuracy and detail over small areas.

Nimbus IV THIR recorded data are always received from the spacecraft in the reverse mode, i.e., the data are read out with the tape traveling in the opposite direction from that in which it was recorded.

3.4.1 Photofacsimile Film Strips

At the Data Acquisition Facility (DAF), the THIR information is demultiplexed and recorded on magnetic tape. It is then transmitted to the Goddard

Space Flight Center where the FM signal is demodulated, synchronized and displayed by a photofacsimile processor. The facsimile processor converts the radiometer output signals into a continuous strip picture, line by line, on 70 mm film. Blanking circuits in the recorder reject unwanted sections of each scan line. Only the Earth scan and, for calibration purposes, very small portions of the space scan are recorded on the film strip. 6.7 micron and 11.5 micron data will be split and separate files compiled for user convenience. All of the THIR data are available on photofacsimile film strips.

Figure 3-15 shows a typical example of a portion of a nighttime orbital film strip from the Nimbus III HRIR. It shows a tropical cyclone in the Central Indian Ocean about 600 miles east of Malagasy. The film strip from the window channel of the THIR is expected to be similar.

3.4.1.1 Photographic Processing of Film Strips

The original photofacsimile film strips are processed by the NDUC photographic laboratory and archived at the NSSDC for safe and permanent storage. A copy created from the original film with uniform density exposure is then used as a master for producing all film strips requested by the user. Uniform density exposure positive or negative film strips and paper prints are available to the THIR data user. In the positive copy, higher temperatures are indicated by darker areas, hence, the colder clouds appear white as in television pictures.

3.4.1.2 Grey Scale Calibration

The photofacsimile recorder is provided with the means for automatically producing on the film data a ten-step calibration grey scale wedge (Figure 3-16). A frequency generator provides ten (10) distinct frequencies to the demodulator just prior to the receipt of THIR data. These frequencies which cover the dynamic range of the radiometer cause the demodulator to produce ten (10) voltage levels which are recorded on the film. The ten levels correspond to ten equivalent blackbody temperatures on the film strips allowing a good estimate of the temperatures to be made.

Because film processing is such that variations in density can and do occur, these values are only approximate and accurate quantitative measurements cannot be obtained from the film.

3.4.1.3 Film Strip Identification

THIR data are archived in separate 6.7 micron and 11.5 micron daytime and nighttime swaths. A full swath therefore covers a distance approximately pole to pole and may include in rare cases more than one block of data. Each swath

NIMBUS III HRIR NIGHTTIME ORBIT 2406 10 OCTOBER 1969
TROPICAL CYCLONE IN THE CENTRAL INDIAN OCEAN
ABOUT 600 MILES EAST OF MALAGASY WITH WINDS IN EXCESS
OF 65 KNOTS.

Figure 3-15. Nimbus III HRIR Photofacsimile Film Strip. Nimbus IV THIR Photofacsimile Film Strips Would be of Same Format and Quality

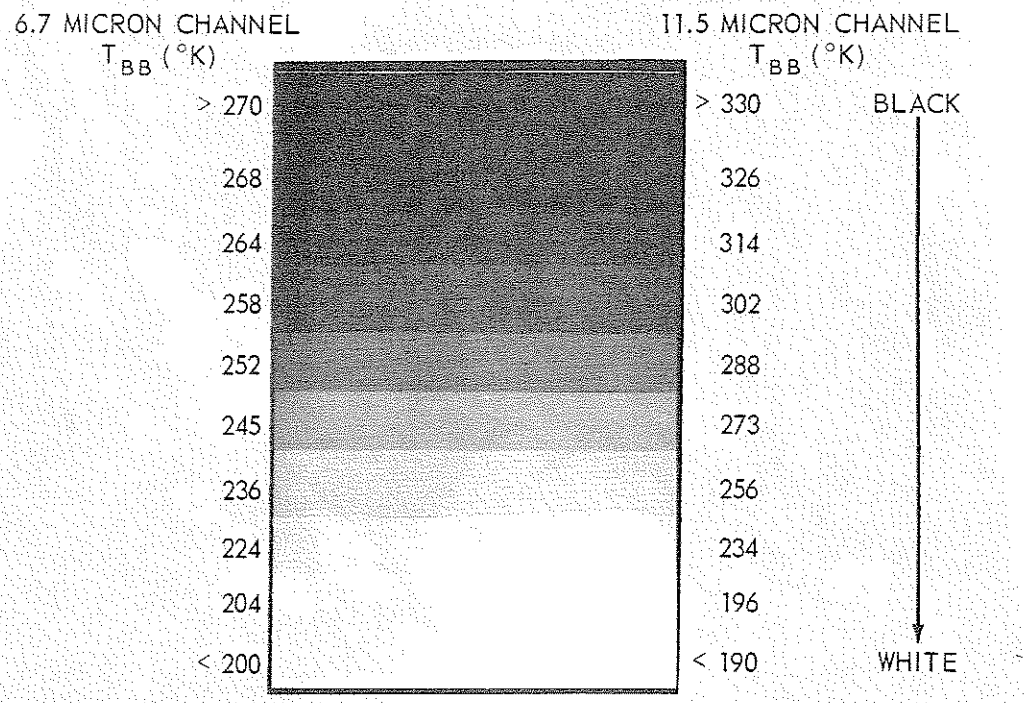

Figure 3-16. THIR Calibration Grey Scale Wedge for Positive Film. The Equivalent Blackbody Temperatures (T_{BB}) are for an Expected Bolometer Temperature of 17.5°C.

is identified by a label with the data orbit number, the channel (6.7 micron or 11.5 micron) and whether it is daytime or nighttime. The nighttime swath is labeled with the orbit number followed by N. The daytime swath crossing the ascending node is identified by the higher orbit number followed by D. Each block is also provided with a label showing the correct universal time of the first data scan nearest the label.

Figure 3-17 shows a film strip containing sample Nimbus III label formats, and computer produced grids with sensory data. The film strip has been gridded for nighttime data. The affixed label gives the data orbit number 2406. The end time is given in the affixed label and is 283: 19:30:30 UT. This time is given, in order, day: hour: minute: second.

A series of time marks in increments of two minutes are found on the left side of the film (Figure 3-17). The first time mark for nighttime data represents the first even minutes before the end time given in the affixed label (for daytime data it would represent the first even minute after the time given in the affixed label). In Figure 3-17 the first time mark is 19:30:00 UT, the second

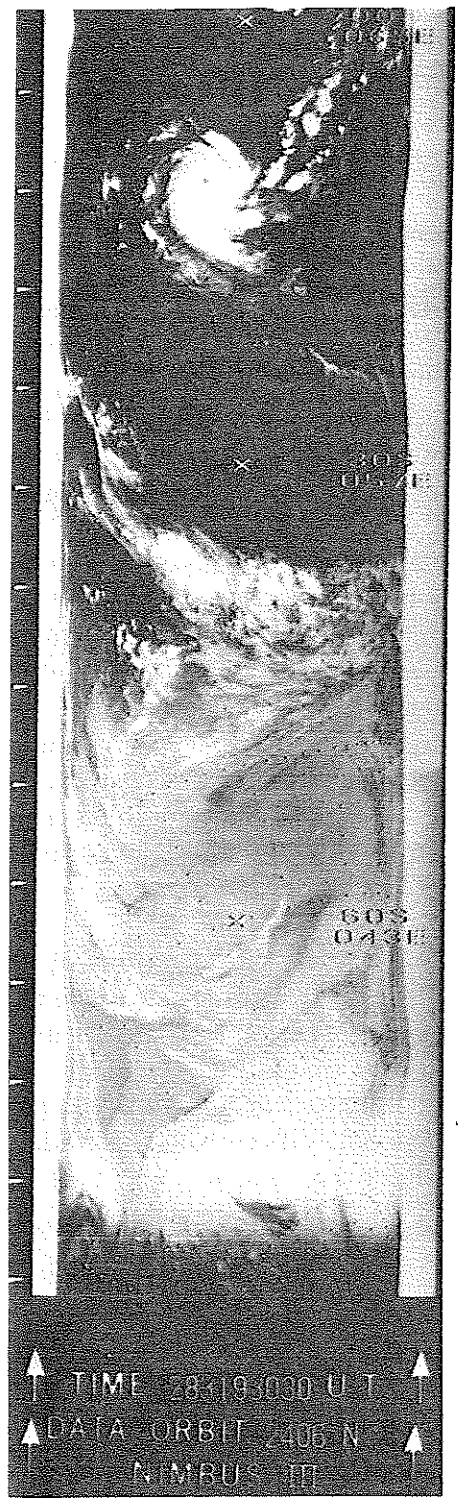

Figure 3-17. Nimbus III HRIR. Format of Computer Produced Grids

is 19:28:00 UT, etc. The time identifies the data to have been recorded during orbit 2406. The data are properly oriented when the film is held (shiny side toward the viewer) with the label at the bottom as shown in Figure 3-17.

3.4.1.4 Film Strip Gridding

The geographical location of each picture element scanned by the radiometer depends on the stability of the spacecraft. The Nimbus IV control system has a pointing accuracy of about ±1 degree in pitch, roll, and yaw. A pointing error of 1 degree corresponds to a subsatellite error of 20 km (11 nm) in the location of a picture element from an altitude of 1100 km (600 nm). On a global basis, this is an acceptable error for most meteorological analyses.

Automatic gridding of the data is accomplished by utilizing a CDC 924 computer to compute geographic coordinates, and a grid mixer which generates the grid points and adds them to the THIR data in analog form. These grid points are electronically superimposed on the film and manually checked to maintain an accuracy of better than ±1 degree of great circle arc at the subsatellite point. Referring to Figure 3-17 the grid point array makes up lines for every 10° of latitude and longitude, with points spaced at 2° intervals along each line between 60°N and 60°S latitude. Outside of 60°N and 60°S latitude, there are latitude lines each 10° and longitude lines each 20°, and latitude points each 2° and longitude points each 5°.

A small cross is placed at the intersections of the 60°N, 30°N, 0°, 30°S, and 60°S latitude lines with the subsatellite track. The first cross from the bottom of Figure 3-17 marks the intersection of the subsatellite track and 60°S at 43°E latitude. The full subsatellite track is not gridded. The longitude and latitude of each cross (rounded to the nearest degree) is displayed at the extreme right hand edge of the picture opposite that cross (latitude above longitude). The latitude format is XXY where $00 \leq XX \leq 90°$, and Y is N or S. The longitude format is XXXY where $000 \leq XXX \leq 180°$, and Y is E or W.

3.4.1.5 Ordering THIR Film Strips

When ordering THIR photographic data from NSSDC the following information should be given.

1. Satellite (e.g., Nimbus IV)
2. Date of data
3. Data orbit number, channel (11.5μ or 6.7μ) and whether day or night data
4. Data format, i.e., positive, negative, transparencies or prints

3.4.2 Digital Data

Quantitative data results when the original analog signals are digitized with full fidelity and the digital data are processed by an IBM 360 computer where calibration and geographic referencing is applied automatically.

A simplified block diagram of the A/D processing system is shown in Figure 3-18. The analog magnetic tape is fed to an A/D converter which utilizes a CDC 924 computer to prepare a digital tape. This tape is then operated upon by the IBM 360 which prepares a reduced radiation data tape called the Nimbus Meteorological Radiation Tape-THIR (NMRT-THIR). The NMRT can be used to generate grid print maps or to accomplish special scientific analyses. The format of this tape, nearly the same as for Nimbus III HRIR, is given in Section 3.5.

An example of a grid print map presentation is shown in Figure 3-19, where the central portion of Typhoon "Marie" is displayed. This map was made from Nimbus II HRIR data. The presentation from THIR is expected to be nearly identical. The advantages of this form of presentation are the display of absolute values of temperatures in their approximate location, geographical rectification

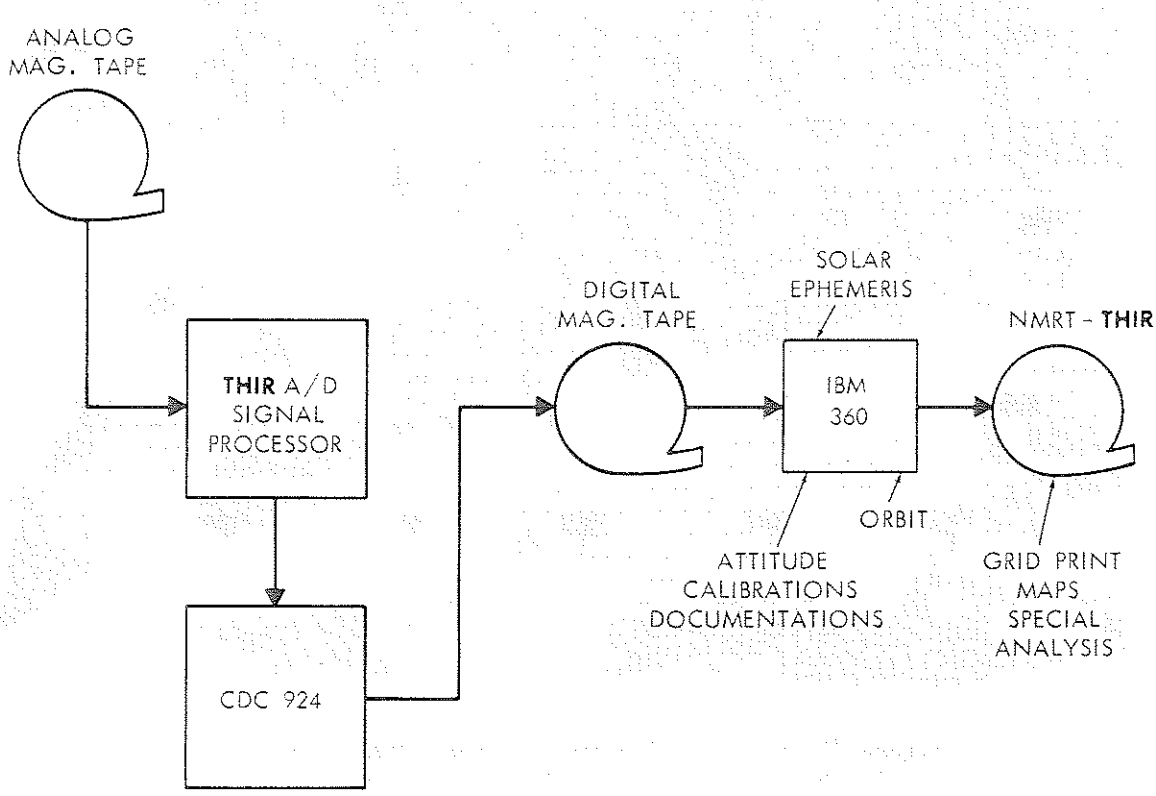

Figure 3-18. Simplified Block Diagram of the A/D Processing System

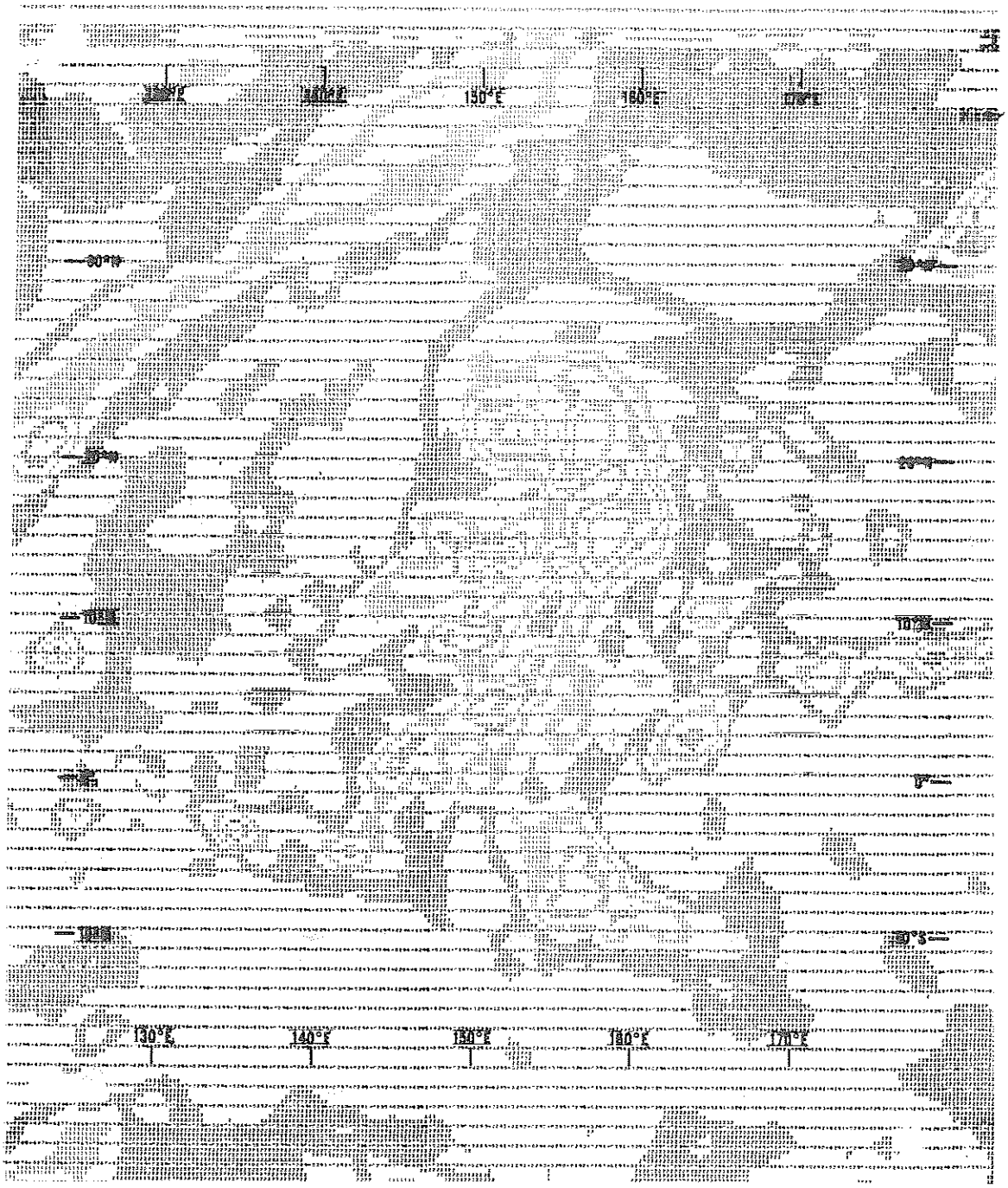

Figure 3-19. Computer Produced Grid Print Map of Typhoon "Marie" of 1966 Utilizing Nimbus II HRIR Data. Nimbus IV THIR Data will have the same Format

of the data, and the possibility of automatically composing measurements from consecutive orbits into quasi-synoptic aerial maps. However, due to the scanning geometry, either a loss of detail will result from smoothing in the center portions of each swath or data gaps (being larger than the grid interval) will occur at some distance from the subsatellite point. Figure 3-20 shows a portion of the rectified composite of three (3) consecutive orbits giving equivalent blackbody temperatures. The lowest temperatures shown over typhoon "Marie" in this map indicate cloud top heights above 11 kilometers. The printed values are averages of up to 200 data points within areas of up to 140 kilometers by 140 kilometers. Figure 3-20 shows an analysis of the typhoon developed using several forms of HRIR data.

3.4.2.1 Availability of Processed Digital THIR Data

Due to the large volume of data and the long computer running time required for processing it into NMRT's, Nimbus IV THIR digital data are not routinely reduced to final NMRT Format. Only those data which are specifically requested by the user will be processed. Requests should be made through NSSDC. It is anticipated that requested THIR-NMR tapes will begin to be available through NSSDC six months after launch. The user is urged to make full use of the film strips which are abundantly available in nearly real-time from the NSSDC.

A series of programs produce printed and contoured data referenced to a square mesh grid on polar stereographic or Mercator map bases. Grid print maps may be produced for either a single orbit or a composite of several orbits. The following standard options are available and should be specified when requesting grid print maps from NSSDC:

1. Map and Approximate Scale
   a. Polar Stereographic 1/30 million (approx.)
   b. Polar Stereographic 1/10 million (approx.)
   c. Multi-Resolution Mercator maps are available down to 1/1 million scale.

2. Maximum Sensor Nadir Angle (50° is practical limit)

3. Field Values and Contouring. Unless otherwise specified, all maps will include field values and contouring except Mercator maps of scales larger than 1/20 million. A data population map, indicating the number of individual measurements contained in each grid point average, as well as a latitude-longitude description for geographically locating the data, will be provided along with each grid print map.

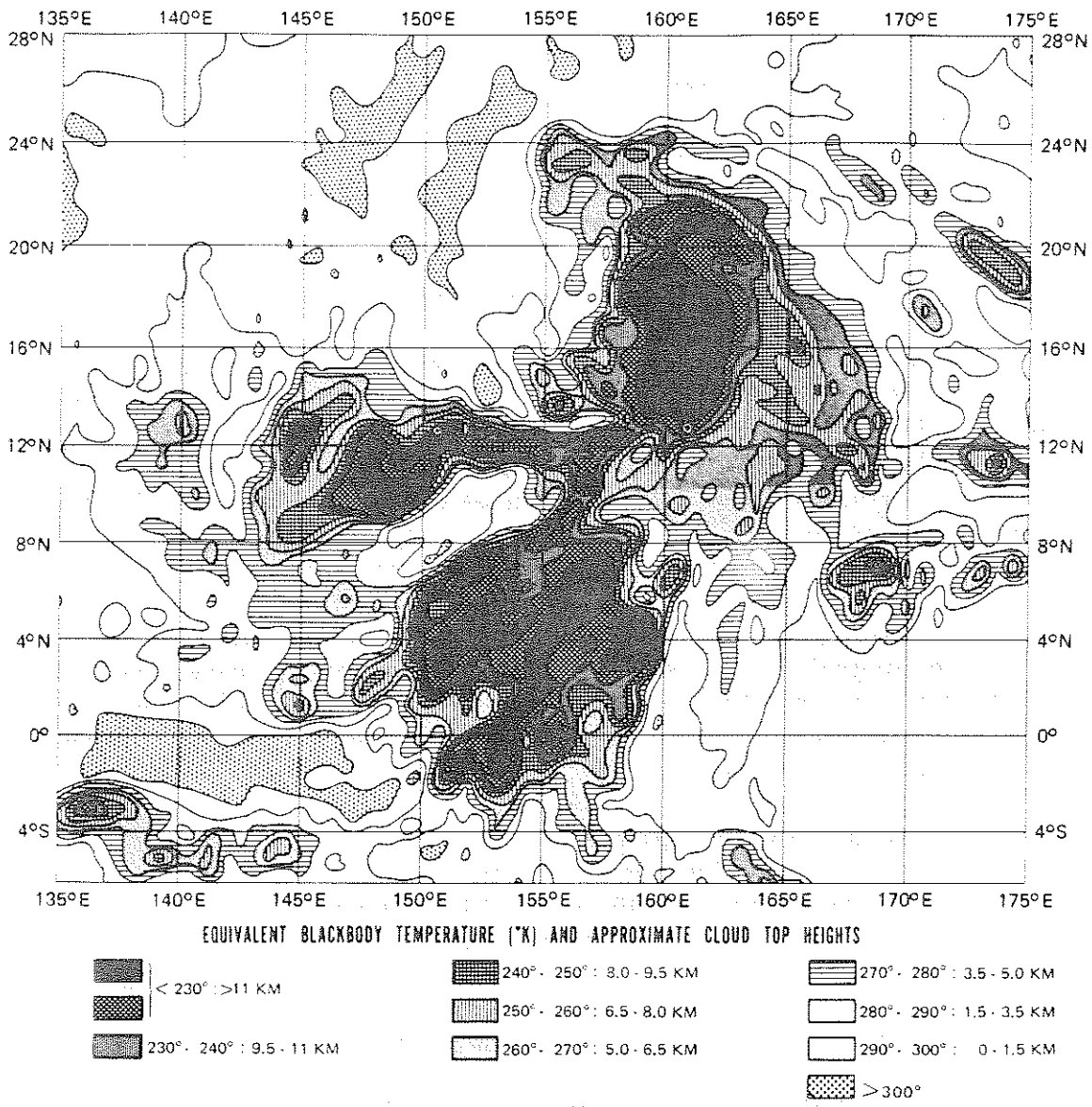

Figure 3-20. Analysis of Typhoon "Marie" Using Several Forms of HRIR Data

When ordering "hard copy" data, the following identifying information should also be given:

1. Satellite (e.g., Nimbus IV)
2. Sensor (THIR)
3. Channel (6.7μ or 11.5μ)
4. Data Orbit No.
5. Calendar Date of Equator Crossing
6. Beginning and Ending Times of Data in GMT
7. Format Desired (see 3.4.2.1, items 1; 2; 3)

When ordering NMR Tapes, only items 1, 2, 3, 4, and 6 above need to be given.

3.4.3 Analog Data

Analog records can be made from the original spacecraft interrogation records (not shown). These Visicorder oscillograph records permit accurate measurement of temperature as a function of time and sensor scan angle as long as the user has adequate knowledge of the workings of the instrument and all parameters involved.

However, the requirements for a comprehensive knowledge of the total THIR subsystem and the sheer volume of the data prohibits the use of this method except for extremely special case studies.

3.5 Format of the NMRT-THIR

The Nimbus Meteorological Radiation Tape-THIR will be a basic repository for requested radiation data from the Nimbus Temperature-Humidity Infrared Radiometer. This tape will contain data in binary mode at a density of 800 bits per inch.

The first file on this tape contains a BCD label. The label consists of fourteen words of BCD information followed by an end-of-file. The remaining files on this tape contain formatted THIR data in the format described on the following pages. The first record in this data file is a documentation record which describes the data to be found in the succeeding records. This first record contains seventeen words (see Table 3-5). The remaining records in the file will be of variable length, but this length will be consistent within the file (see Table 3-6). The length (L) of the data record can be computed as follows:

$$L = (\text{SWATHS PER RECORD}) \times (\text{WORDS PER SWATH}) + (\text{NUMBER OF NADIR ANGLES}) + 7$$

Table 3-5
NMRT-THIR Documentation Record Format

Word No.	Quantity	Units	Scaling	Remarks
1	Channel ID	Integer	B=35	Equals 115 for 11.5μ channel and 67 for 6.7μ channel
2	Date	MMDDYY	B=35	Date of interrogation for this orbit, i.e., 2/5/64 would be $(020504)_8$. Only the last digit of year is used.
3	Nimbus Day	–	B=35	Start time for this file of data
4	Hour	Z Hour	B=35	
5	Minute	Z minute	B=35	
6	Seconds	Z seconds	B=35	
7	Nimbus Day	–	B=35	End time for this file of data
8	Hour	Z hour	B=35	
9	Minute	Z minute	B=35	
10	Seconds	Z seconds	B=35	
11	Mirror Rotation Rate	Deg/Sec	B=26	Rotation rate of radiometer mirror
12	Sampling Frequency	Samples/Sec	B=35	Digital sampling of frequency per second of vehicle time
13	Orbit Number	–	B=35	Orbit Number
14	Station Code	–	B=35	DAF Station identification code
15	Swath Block Size (325)	–	B=35	Number of 35-bit words per swath
16	Swaths/Record	–	B=35	Number of swaths per record
17	Number of Locator Points	–	B=35	Number of anchor points per swath for which latitudes and longitudes are computed.

Table 3-6
NMRT-THIR Data Record Format

Word No.	Quantity	Units	Scaling	Remarks
1D	Nimbus Day	–	B=17	Start time for this record of data
1A	Hour	Z hour	B=35	
2D	Minutes	Z minute	B=17	
2A	Seconds	Z seconds	B=35	
3D	Roll Error	Degrees	B=14	Roll error at time specified in words one and two.
3A	Pitch Error	Degrees	B=32	Pitch error at time specified in words one and two.
4D	Yaw Error	Degrees	B=14	Yaw error at time specified in words one and two.
4A	Height	Kilometers	B=35	Height of spacecraft at time specified in words one and two.
5D	Detector Temperature	Degrees K	B=17	Measured temperature of detector cell at time specified in words one and two.
5A	Electronics Temperature	Degrees K	B=35	Measured temperature of electronics at time specified in words one and two.
6D	Reference Temperature A	Degrees K	B=17	Measured temperature of housing at time specified in words one and two.
6A	Reference Temperature B	Degrees K	B=35	
7D	Reference Temperature C	Degrees K	B=17	
7A	Reference Temperature D	Degrees K	B=35	

Table 3-6 (Continued)

Word No.	Quantity	Units	Scaling	Remarks
8 . . . N	Nadir Angle Nadir Angle	Degrees Degrees	B=29 B=29	Nadir angles corresponding to each locator point, and measured in the plane of the radiometer
(N+1)D	Seconds	Z Seconds	B=8	Seconds past time in words 1A & 2D for beginning of this swath.
(N+1)A	Data Population	–	B=35	Number of data points in this swath.
(N+2)D	Latitude	Degrees	B=11	Latitudes of subsatellite point for this swath
(N+2)A	Longitude	Degrees	B=29	Longitude of subsatellite point for this swath, positive westward 0 to 360°.
N+3	Flags	–	–	Reserved for flags describing this swath
(N+4)D	Latitude	Degrees	B=11	Latitude of viewed point for the first anchor spot
(N+4)A . . . MD MA	Longitude Latitude Longitude	Degrees Degrees Degrees	B=29 B=11 B=29	Longitude of viewed point for first anchor spot, positive westward 0 to 360°. Latitude and longitude for Mth anchor spot
(M+1)D (M+1)A . . . K(A or D)	THIR Data THIR Data THIR Data	– – –	B=14 B=32 B=32 B=14	THIR measurements. Tag and prefix reserved for flags. Last THIR data measurement

The above data constitute what is essentially the documentation portion of a data record. These data will be followed by several blocks of data with each block representing a swath. The number of these blocks in a record as well as the size of each block is specified in the documentation record represented on the previous page.

All remaining or unused portions of a swath data block are set to zero, giving a swath block size as specified in the documentation record. The above data on this page are repeated for the number of swaths in each record.

Ninety degrees are added to all latitudes and attitude data to eliminate negative signs.

Table 3-7 defines the flags which appear in the data records.

Table 3-7
Definition of Flags Describing Each THIR Swath

Flag	Bit	Definition	Yes	No
1	35	Summary flag. All checks defined by flags 2 thru 12 are satisfactory. (each flag is zero)	0	1
2	34	Consistency check between sampling rate and vehicle time is satisfactory	0	1
3	33	Vehicle time is satisfactory	0	1
4	32	Vehicle time has been inserted by flywheel	1	0
5	31	Vehicle time carrier is present	0	1
6	30	Vehicle time has skipped	1	0
7	29	Water vapor data	1	0
8	28	Sync pulse recognition was satisfactory	0	1
9	27	Dropout of data signal was detected	1	0
10	26	Window data	1	0
11	25	Unassigned		
12	24	Swath size is satisfactory when compared with the theoretical swath size	0	1
13	23	Unassigned		

Flags For Individual Measurements

Prefix	Tag	Definition	Yes	No
S	18	The particular measurement is below the earth-space threshold	1	0
1	19	Unassigned		
2	20	Unassigned		

REFERENCES AND BIBLIOGRAPHY

1. King, Jean I. F., "Meteorological Inferences from Satellite Radiometer." J. of Atmos. Sciences, 20, 245-250, July 1963.

2. Nordberg, W., McCulloch, A. W., Foshee, L. L., and Bandeen, W. R. "Preliminary Results from Nimbus II," Bulletin of the American Meteorological Society, Vol. 47, No. 11, Nov. 1966.

3. London, Julius, "Satellite Observations of Infrared Radiation." Scientific Report No. 1, Contract No. AF 19(604)-5955, College of Engineering, New York University, New York 53, N.Y., December 1959.

4. London, Julius, Katsuyuki Ooyama, and Herbert Viebrock. "Satellite Observations of Infrared Radiation." Report No. 2, Contract No. AF 19(604)-5955, College of Engineering, New York University, New York 53, N.Y., July 1960.

5. London, Julius, Katsuyuki Ooyama, and Herbert Viebrock. "Satellite Observations of Infrared Radiation." Final Report, Contract No. AF 19(604)-5955, College of Engineering, New York University, New York 53, N.Y., October 1961.

6. Pederson, Finn, and Tetsuya Fujita. "Synoptic Interpretation of TIROS III Measurements of Infrared Radiation." Research Paper No. 19, Mesometeorology Project, Department of Geophysical Sciences, The University of Chicago, October 1963.

7. Rasool, S. I., "Cloud Heights and Nighttime Cloud Cover from TIROS Radiation Data." J. of the Atmos. Sciences, 21, 152-156, March 1964.

8. Wark, D. Q., G. Yamamoto, and J. H. Lienesch. "Methods of Estimating Infrared Flux and Surface Temperatures from Meteorological Satellites." J. of the Atmos. Sciences, 19, 369-384, September 1962. (Also "Infrared Flux and Surface Temperature Determinations from TIROS Radiometer Measurements." Meteorological Satellite Laboratory Report No. 10 (1962) and Supplement thereto (1963), U.S. Weather Bureau, Washington, D.C.).

9. Wexler, R., "Satellite Observations of Infrared Radiation." First Semiannual Technical Summary Report, Contract No. AF 19(604)-5968, Allied Research Associates, Inc., Boston, Mass., December 24, 1959.

10. Wexler, R., "Satellite Observations of Infrared Radiation." Second Semi-annual Technical Summary Report, Contract No. AF 19(604)-5968, Allied Research Associates, Inc., Boston, Mass. June 30, 1960.

11. Wexler, R., "Interpretation of Satellite Observations of Infrared Radiation." Scientific Report No. 1, Contract No. AF 19(604)-5968, Allied Research Associates, Inc., Boston, Mass., April 20, 1961.

12. Aeronomy and Meteorology Division, 1965: Nimbus I High Resolution Radiation Data Catalog and User's Manual, NASA, Goddard Space Flight Center, Greenbelt, Maryland.

13. Nimbus Project, 1966: Nimbus II User's Guide, NASA, Goddard Space Flight Center, Greenbelt, Maryland.

14. Nimbus Project, 1966: Nimbus II HRIR Montage Catalog, NASA, Goddard Space Flight Center, Greenbelt, Maryland.

15. NASA Special Publication SP-89, Observations from the Nimbus I Meteorological Satellite, 1966.

16. Warnecke, G., Allison, L., Kreins, E., and McMillin, L., A Typical Cyclone Development as Revealed by Nimbus II High Resolution Infrared and ESSA-3 Television Data, NASA X-622-68-39, January 1968.

17. Nordberg, W., A. W. McCulloch, L. L. Foshee, W. R. Bandeen, Preliminary Results from Nimbus II, NASA X-620-66-349, August 1966.

18. Nimbus Project, 1969, The Nimbus III User's Guide, NASA, Goddard Space Flight Center, Greenbelt, Maryland.

19. Nimbus Project, 1969, The Nimbus III Data Catalog, Volumes 1, 2, 3, 4, 5, NASA, Goddard Space Flight Center, Greenbelt, Maryland.

SECTION 4

THE INFRARED INTERFEROMETER SPECTROMETER (IRIS) EXPERIMENT

By
R. Hanel, B. Conrath and B. Schlachman
National Aeronautics and Space Administration
Goddard Space Flight Center

The purpose of this section is to describe the nature and format of the IRIS "D" data so researchers in the field may be prepared to interpret and use the data as soon as they become available through the National Space Science Data Center.

The IRIS instrument is, in many respects, similar to the instrument which was flown on Nimbus III. The prime differences are in construction details of the instrument which permitted an increase in spectral resolution from 5 to 2.8 wave numbers, improvements in the signal to noise ratio, and an extension of the spectral range towards longer wave length. While the first two improvement factors have been implemented, the extension of the spectral range to 50 microns is, at the present time, questionable. The prime instrument presently on the spacecraft has a potassium bromide beamsplitter which restricts the long wave length response of the instrument to 25 microns as in the case of Nimbus III.

4.1 Scientific Objectives

The IRIS experiment is to provide information on the vertical structure of the atmosphere and the emissive properties of the surface. In the spectral region covered, water vapor, carbon dioxide, and ozone bands are available in addition to spectral features associated with minor constituents as methane and nitrous oxide. The specific intensity measured in the absorption bands and in the more transparent "windows" may be used to derive vertical profiles of temperature, water vapor and ozone, in addition to other parameters of meteorological interest.

The techniques used to recover the temperature, water vapor and ozone profiles are described, for example, by Wark and Fleming, 1966, and Conrath, 1969 (References 1, 2). Results from a similar instrument flown on Nimbus III

are discussed by Hanel and Conrath, Prabhakara et al, Conrath et al (References 3, 4, 5). The Nimbus III interferometer description can be found in a paper by Hanel et al (Reference 6). Typical results are shown in Figure 4-1.

For convenience, the objectives of IRIS may be divided into the following categories:

1. Derivation of atmospheric temperature and humidity structure on a global scale to be used in numerical studies of the general circulation

2. Observation of temperature, water vapor, and ozone fields for synoptic meteorological studies

3. Collection of spectra for research studies in meteorology, in radiative transfer, and for nonmeteorological purposes

4.2 The IRIS Instrument

The instrument is a Michelson interferometer constructed by Texas Instruments Inc. The optical module is shown in Figure 4-2. Table 4-1 summarizes the more important parameters and Figure 4-3 shows a simplified diagram of the instrument.

The essential part of the interferometer is the beam splitter which divides the incoming radiation into two approximately equal components. After reflection on the fixed and moving mirrors, respectively, the two beams interfere with each other with a phase difference proportional to the optical path difference between both beams. The recombined components are then focused onto the bolometer detector where the intensity is recorded as a function of path difference, δ. Since the mirror motion is phase locked to the spacecraft clock, the mirror path difference is also proportional to time. For quasi-monochromatic radiation, a circular fringe pattern appears at the focal plane of the condensing mirror. The detector size is chosen to cover just the smallest central fringe for the highest wave number of interest. The aperture at the detector and the interferometer mirrors constitute the limiting apertures and determine the 5° field of view of the instrument.

The central fringe may be light or dark depending on the path difference δ between the two beams. For polychromatic radiation and neglecting constant terms the signal at the detector, called the interferogram, is

$$i(\delta) = \int_0^\infty K_\nu (B_\nu - B_\nu(T_{instr})) \cos(2\pi\nu\delta - \phi_\nu)\, d\nu \qquad (1)$$

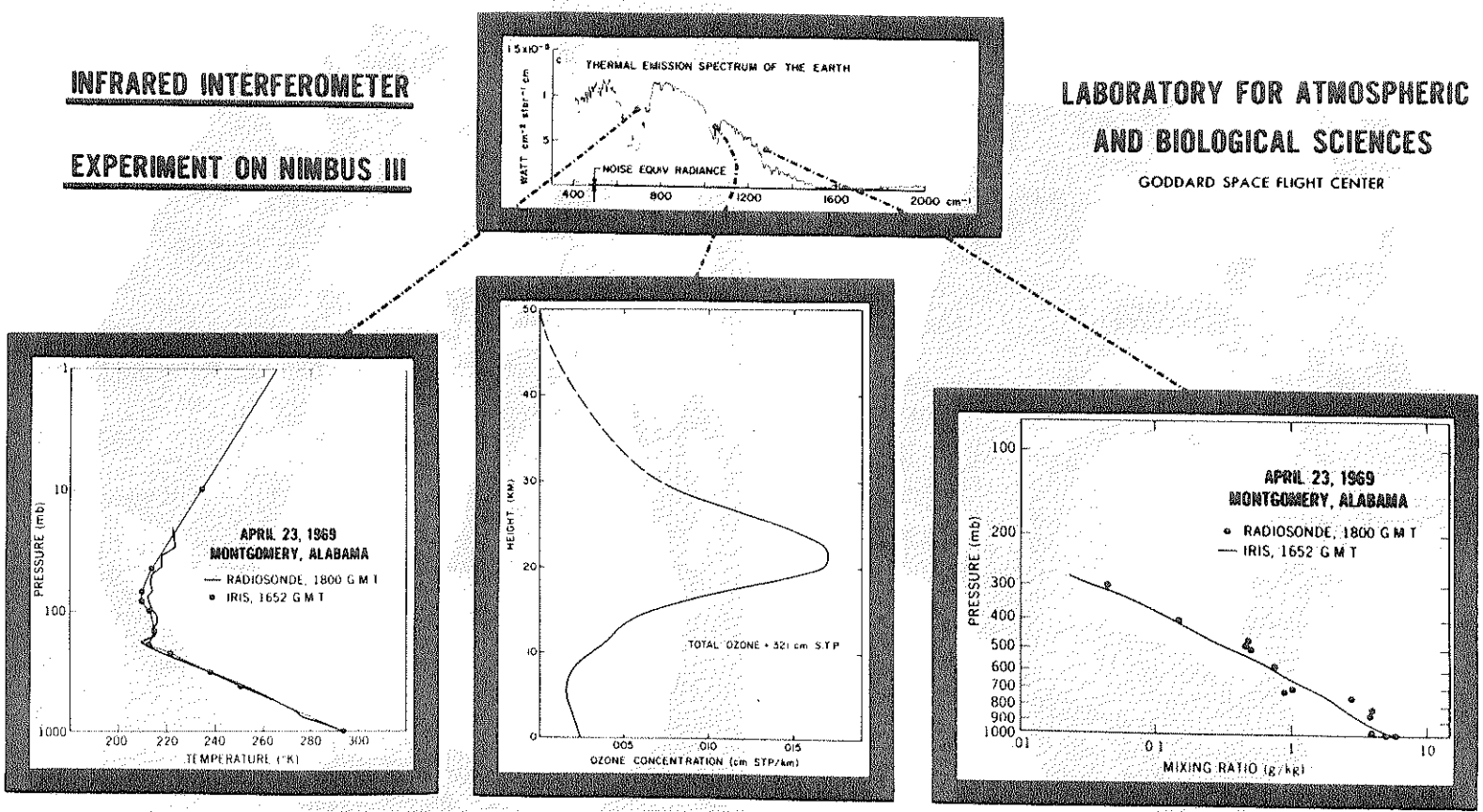

Figure 4-1. Typical Results of the Infrared Interferometer Experiment on Nimbus III

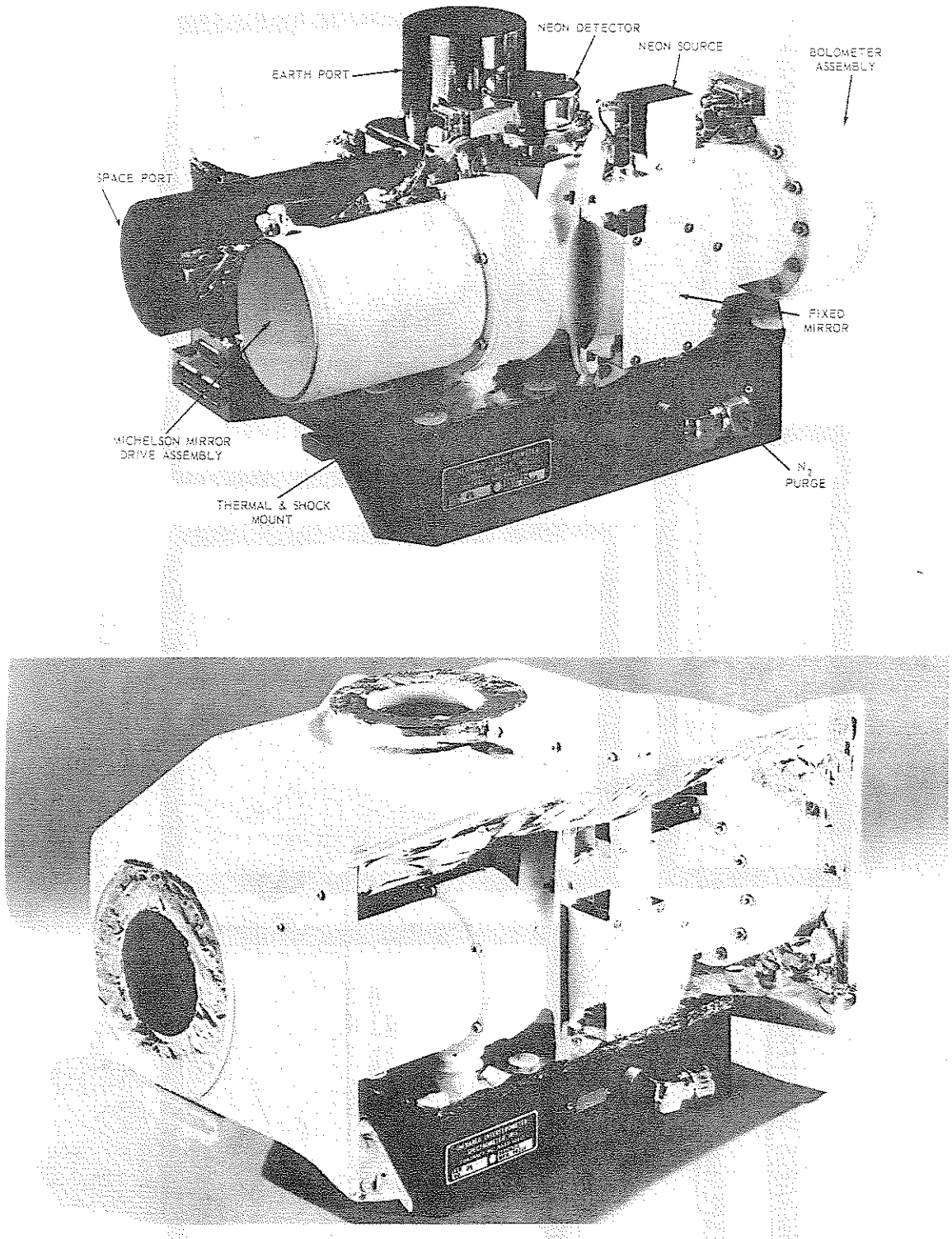

Figure 4-2. Optical Module of the IRIS Instrument with and without Thermal Shroud

Table 4-1
Summary of the More Important Parameters of the IRIS "D" KBr Version

Nominal Spectral Range	400 to 2000 cm^{-1} (5 - 25μ)
Spectral Resolution Element (apodized)	2.8 cm^{-1}
Spectral Resolution (unapodized)	1.4 cm^{-1}
Field of view	Circular, 2.5° half angle
Diameter of view area from 1100 km altitude	Approx. 94 km
Motion of moving mirror	0.36 cm
Velocity of moving mirror	0.0275 cm/sec
Duration of interferogram	13.107 sec
Wavelength of fringe control	0.5852μ
Data Words per interferogram	4096
Word Rate	312.5 Words/sec
Bits per Word	12 (2 Sync, 1 Gain, 9 Data)
Bit rate	3.75 k bits/sec
IMCC rotation rate	0.4 deg/sec
Operating temperature of	
Optical Module	250±2.5°K
Electronic Module	298±25°K
Weight	
Optical Module	32.1 lbs
Electronic Modules (2)	9.8 lbs. (4/0), 6.8 lbs (2/0)
Total	48.7 lbs
Dimensions	
Optical Module	11.0 × 17.3 × 15.3 inches
Electronic Modules (2)	8 × 6 × 6.5 and 4 × 6 × 6.5 inches
Power consumption	28 Watts average, 32 Watts peak

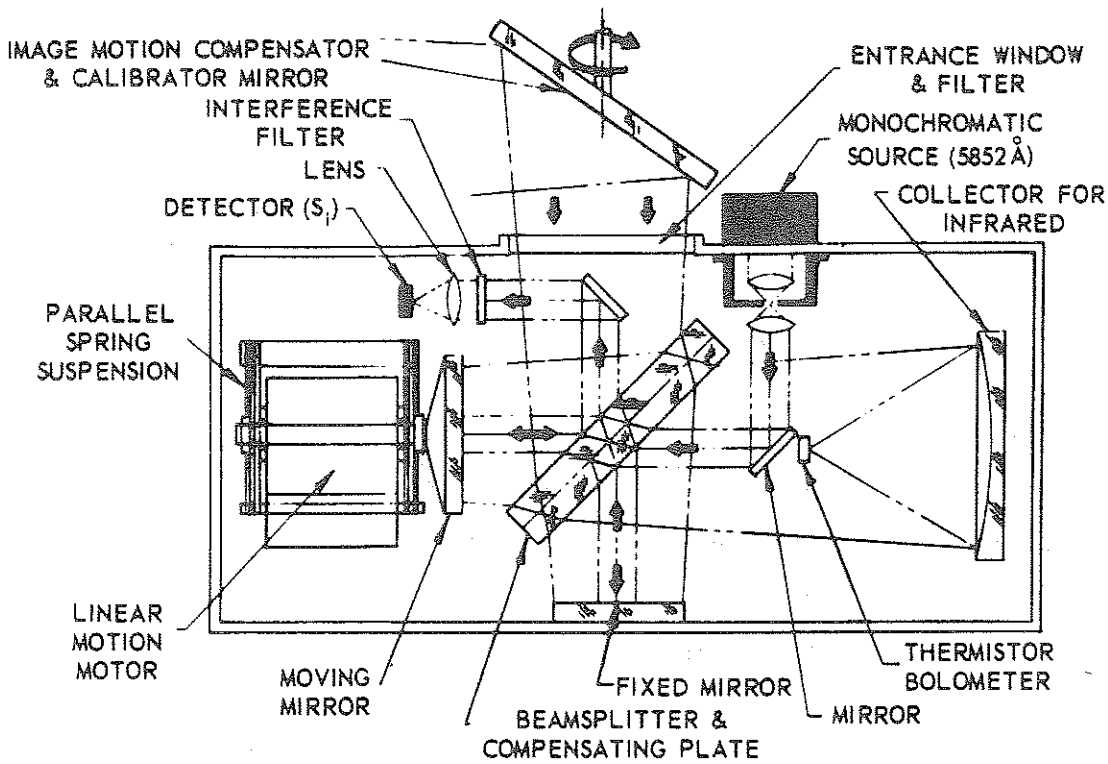

Figure 4-3. Schematic Diagram of Michelson Interferometer. The Monochromatic Source is a Neon Discharge Tube

The amplitude is proportional to a responsivity factor $K(\nu)$ and the difference in radiance between the scene within the field of view B_ν and the instrument $B_\nu(T_{instr})$. The phase is defined with respect to a point chosen as close as possible to, but not necessarily at, the zero path difference point. Imperfect optical compensation and residual phase shift in the analog part of the data channel cause the angle ϕ to depend on the wave number. Reconstruction of the spectrum by a ground based computer will be discussed later. A detailed block diagram of the instrument is shown in Figure 4-4.

The beamsplitter, made of potassium bromide (KBr) and supplied by Perkin-Elmer, is polished optically flat to a fraction of a visible fringe. It has a multi-layer dielectric coating which is optimized to the 5-25μ region except for a small area in the center where it is coated to perform well in the visible. In this center region the fringe control interferometer operates. It utilizes not only the same beam-splitter but also the prime infrared interferometer mirrors. The fringe control interferometer generates a sine wave of 937.5 Hz at the silicon diode detector from a nearly monochromatic spectral line (0.5852μ) of a

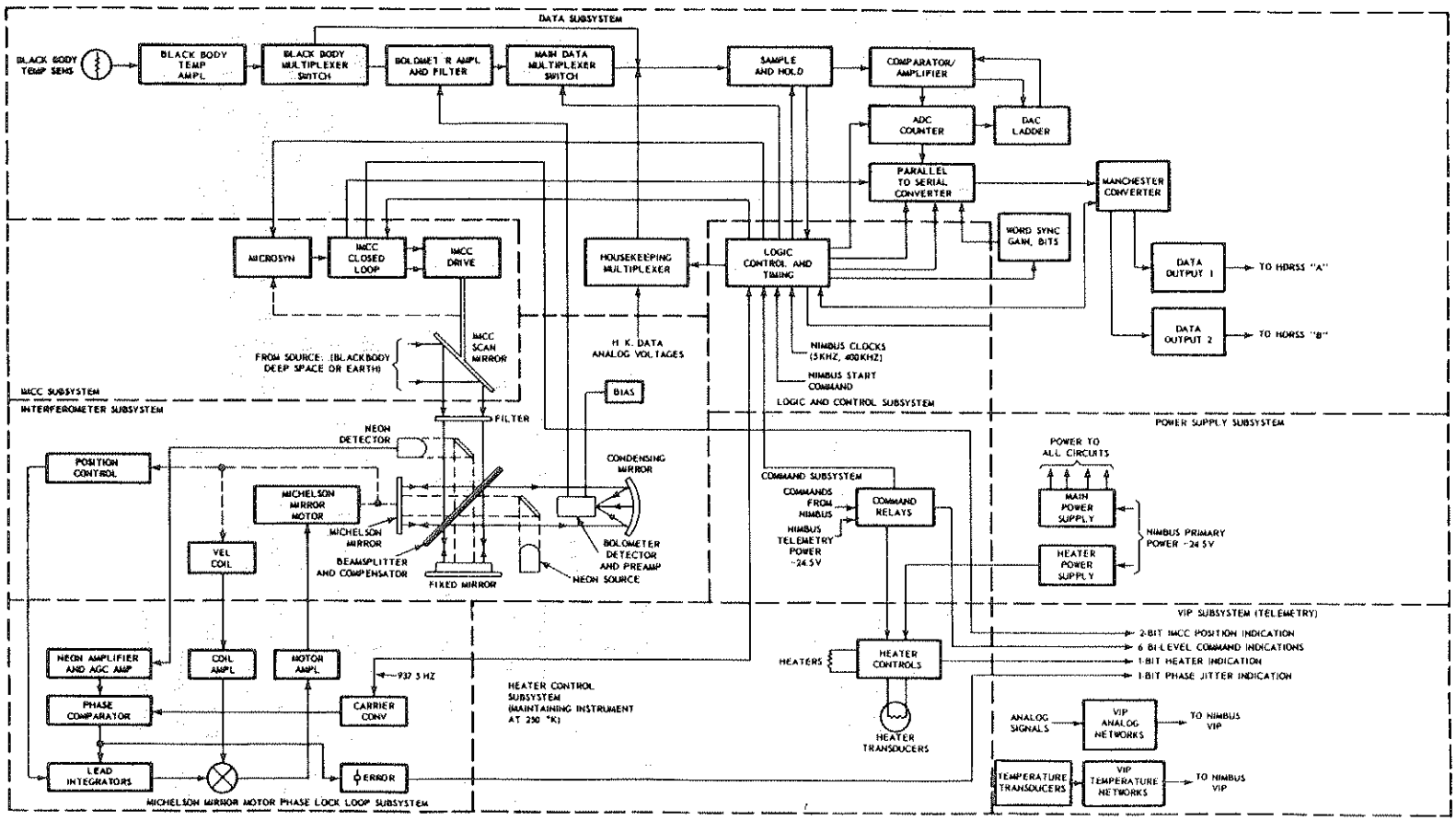

Figure 4-4. Simplified Block Diagram of the IRIS System

neon discharge lamp. The line is isolated by an interference filter. The 937.5 Hz signal serves two purposes. First, after being divided by three, it serves as a sample command and assures equal distance sampling. Secondly, it is compared in phase to a spacecraft clock derived frequency to provide the error signal for the phase locked loop.

The Michelson mirror assembly has an electromagnetic drive coil and also a pick-up coil to generate a voltage proportional to mirror velocity. The velocity signal is also used in a feedback arrangement to provide electrical damping and to make the system less sensitive to external vibration. The phase locked condition of the Michelson mirror provides a constant mirror velocity and permits a constant data rate; moreover the data stream is synchronized with the spacecraft clock.

The Image Motion Compensation and Calibration system channels radiation from several sources to the interferometer. After 14 interferograms are taken in the operating mode, one is taken from a built-in blackbody kept at spacecraft temperature followed by an interferogram from outer space which is considered a nearly zero degree sink. The interferograms from the hot blackbody and cold interstellar background serve calibration purposes. The inflight calibration will be discussed later. During the normal mode where the earth is in the field of view, the IMCC mirror rotates slowly at a rate of 0.4 degree/sec to assure image motion compensation. The calibration mode is prohibited near the north polar region where danger of viewing the sun exists.

Typical interferograms recorded by the Nimbus III IRIS are shown in Figure 4-5. The large central peak is reduced in a signal conditioner. The transfer function of the signal conditioner is shown in Figure 4-6. The inverse function must be applied in the computer. The purpose of the signal conditioner is to preserve dynamic range to 9 bits in the analog to digital converter without a great sacrifice in accuracy. A tenth bit, the gain bit, indicates that the signal exceeded ±1.25 volts input to the range standardization transfer curve.

The instrument generates main data and housekeeping data. Some of the housekeeping data are multiplexed with the main data and are then transmitted just before and just after an interferogram. This set of housekeeping data is required in the computer for the data reduction process. Another set of housekeeping data is transmitted via the Nimbus VIP subsystem. It is needed for engineering evaluation. Table 4-2 lists the housekeeping information recorded together with the interferogram and Table 4-3, the housekeeping channel available for performance evaluations.

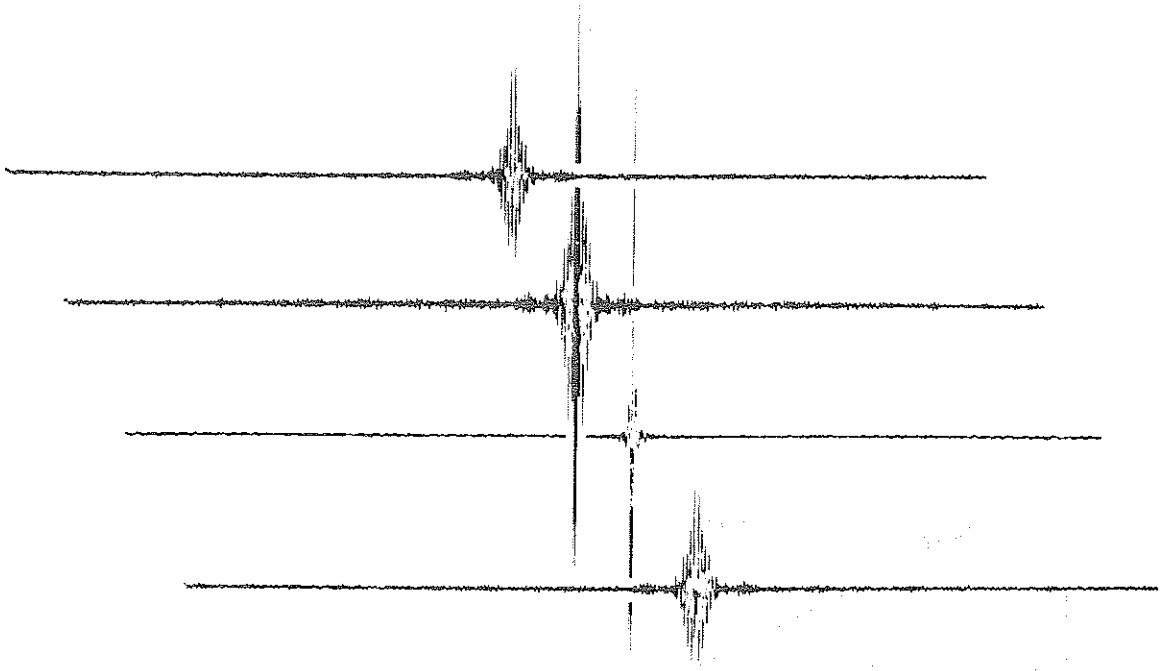

Figure 4-5. Typical Interferograms Recorded by the Nimbus III IRIS

4.3 Data Flow

The main bit stream of data is recorded at one of the HDRSS recorders in the spacecraft. Real time transmission capability exists also via the VIP subsystem and the beacon transmitter. Another channel of the HDRSS recorder carries a time code signal. The data format and timing is shown in Figure 4-7. The data flow in the spacecraft is shown in Figure 4-8 and on the ground in Figure 4-9.

At STADAN Data Acquisition Facility, the receiver output is demultiplexed and recorded on tape. The IRIS data are transmitted from ALASKA by a land-line data link to the Nimbus Data Handling System (NDHS) at GSFC. In some cases, a small fraction is transmitted from ROSMAN via the microwave links when transmission time is available. At the NDHS a Telemetric 670 computer formats the data, performs several checks, such as parity checks etc., and produces an IBM 360 compatible digital tape.

The NDHF also displays the housekeeping data for engineering purposes and provides weekly plots of the on-off time of the IRIS experiment and tables of height and position of the spacecraft as well as a table of the ascending and descending nodes. The IBM compatible digital tape is then carried to the LABS IBM-360 computer where the actual data reduction takes place.

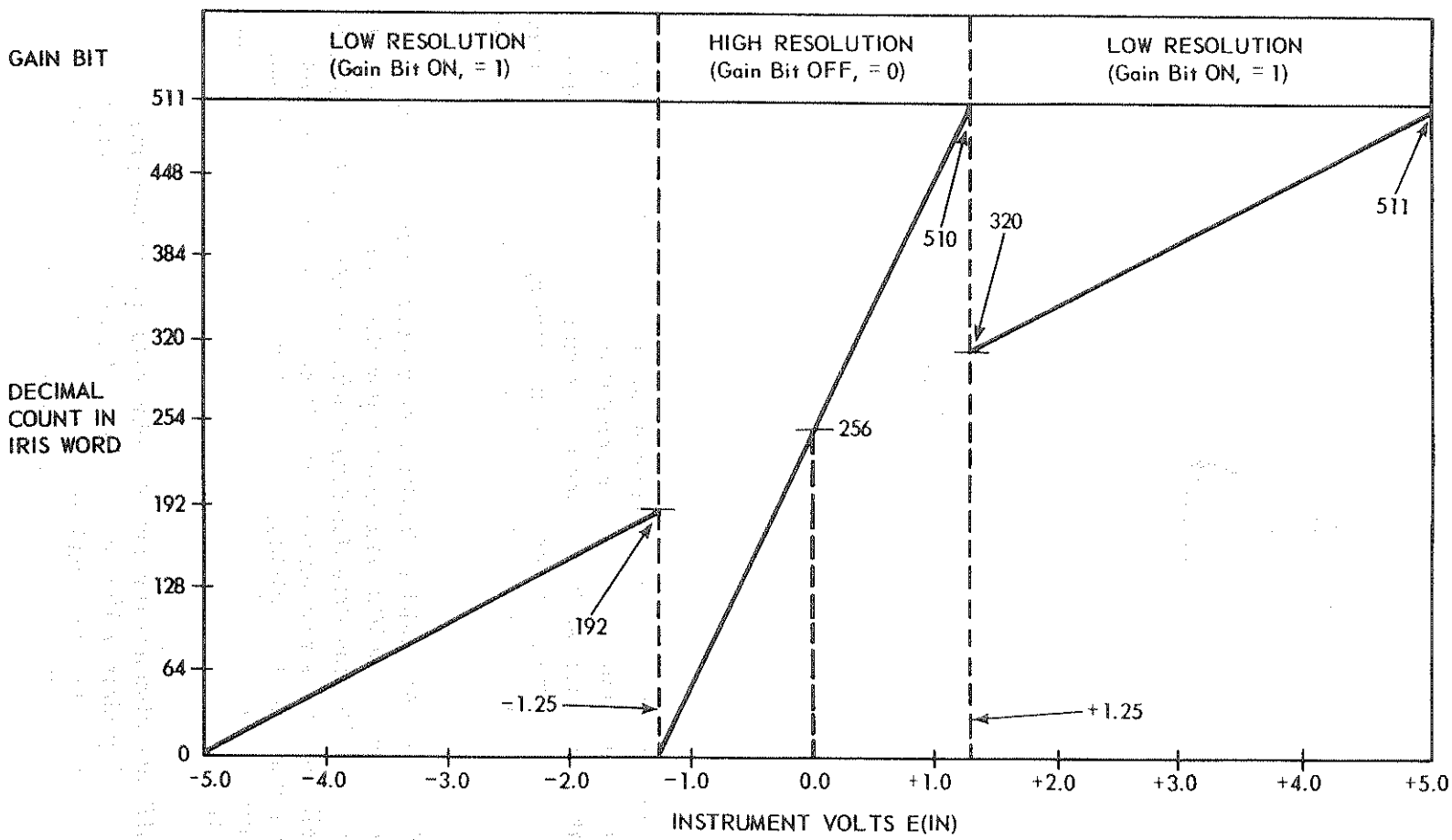

$$E(IN) = \frac{1}{4^A}\left[\frac{N}{512}(10.000) - 5.000\right]$$

where N = base 10 equivalent of 9 binary data bits
A = 0 for low resolution
A = 1 for high resolution

Figure 4-6. Range Standardization Transfer Curve and Conversion Equation

Table 4-2
IRIS Telemetry (HDRSS)

Channel No.	Channel No.
0. Sync Word	8. 0.0 Volt Calibration
1. Blackbody temp. (fine)	9. Transducer Calibration
2. Bolometer temp.	10. Blackbody temp. (coarse)
3. Beamsplitter temp.	11. -0.6 Volt Calibration
4. MMDA Housing temp.	12. Spare
5. +0.6 Volt Calibration	13. Spare
6. IMCC Drive temp.	14. IMCC Position & Phase Lock Condition
7. Radiating Surface temp.	15. Sync Word

Table 4-3
IRIS Telemetry (PCM Subsystem)

Analog	B1-Level
1. Reference Interferometer amplitude	1. IMCC Stowage (Blackbody Position Command Relay Monitor)
2. IMCC Earth Scan Indicator	2. Heater Power Command Relay Monitor (on or off)
3. Bolometer Temperature	3. IRIS Power Command Relay Monitor (on or off)
4. Blackbody Temperature	4. Calibration Mode Command Relay Monitor (Manual or Auto)
5. Radiating Surface Temperature	5. Calibration Command Relay Monitor (Inhibit or Enable)
6. Electronics Module Temperature (4/0)	6. Calibration Switch (Auto) Relay Monitor (Inhibit or Enable)
7. Electronics Module Temperature (2/0)	7. IMCC Mirror Position (2 Adjacent Channels coded for Position)
8. 0.6 Volt Zener Reference	8. Heater Output (on or off)
	9. Phase Lock Condition

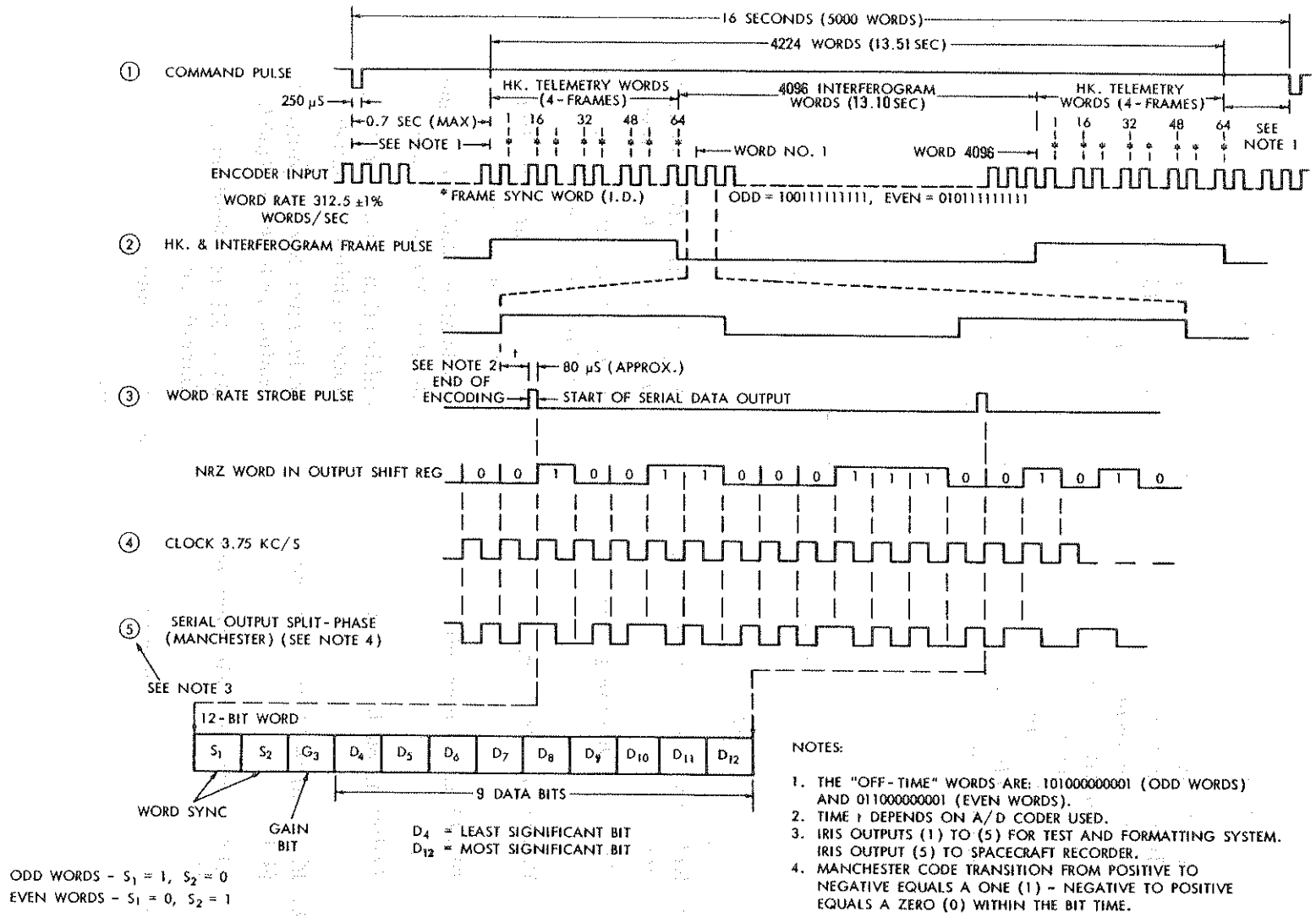

Figure 4-7. Timing Diagram of a Single Frame of Data

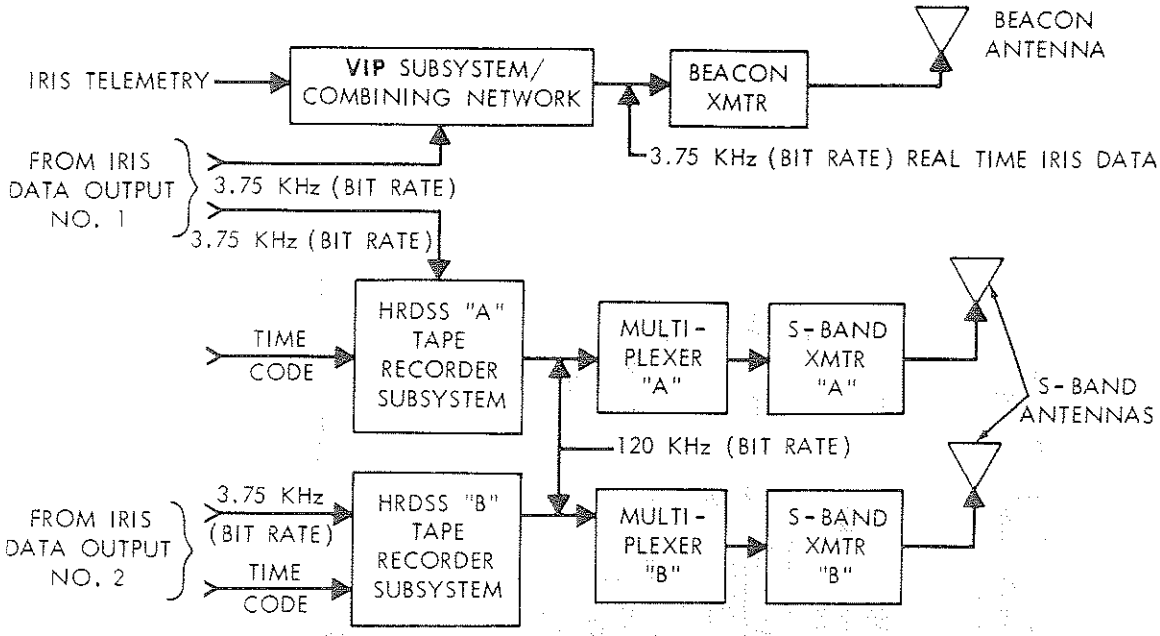

Figure 4-8. Flow Diagram of IRIS Data in the Nimbus Satellite

4.4 Data Reduction in the IBM-360 Computer

The data reduction process consists of four steps:

1. A check of consistency and completeness of input tape and processing of housekeeping information

2. Fourier transformation of each interferogram including consideration of phase

3. Application of calibration procedure

4. Production of IRIS archival tape containing the calibrated spectra, housekeeping information and orbital parameters

In the check of consistency and completeness, the total number of words per interferogram and the value, sign and position of the peak word in each interferogram are determined. Furthermore, a scan for gain switch pulses outside the central region of the interferogram and errors in the word sync bits are performed and the results printed out. Only interferograms which show a number of sync errors less than some upper limit will be processed further. This upper limit will be established in operation.

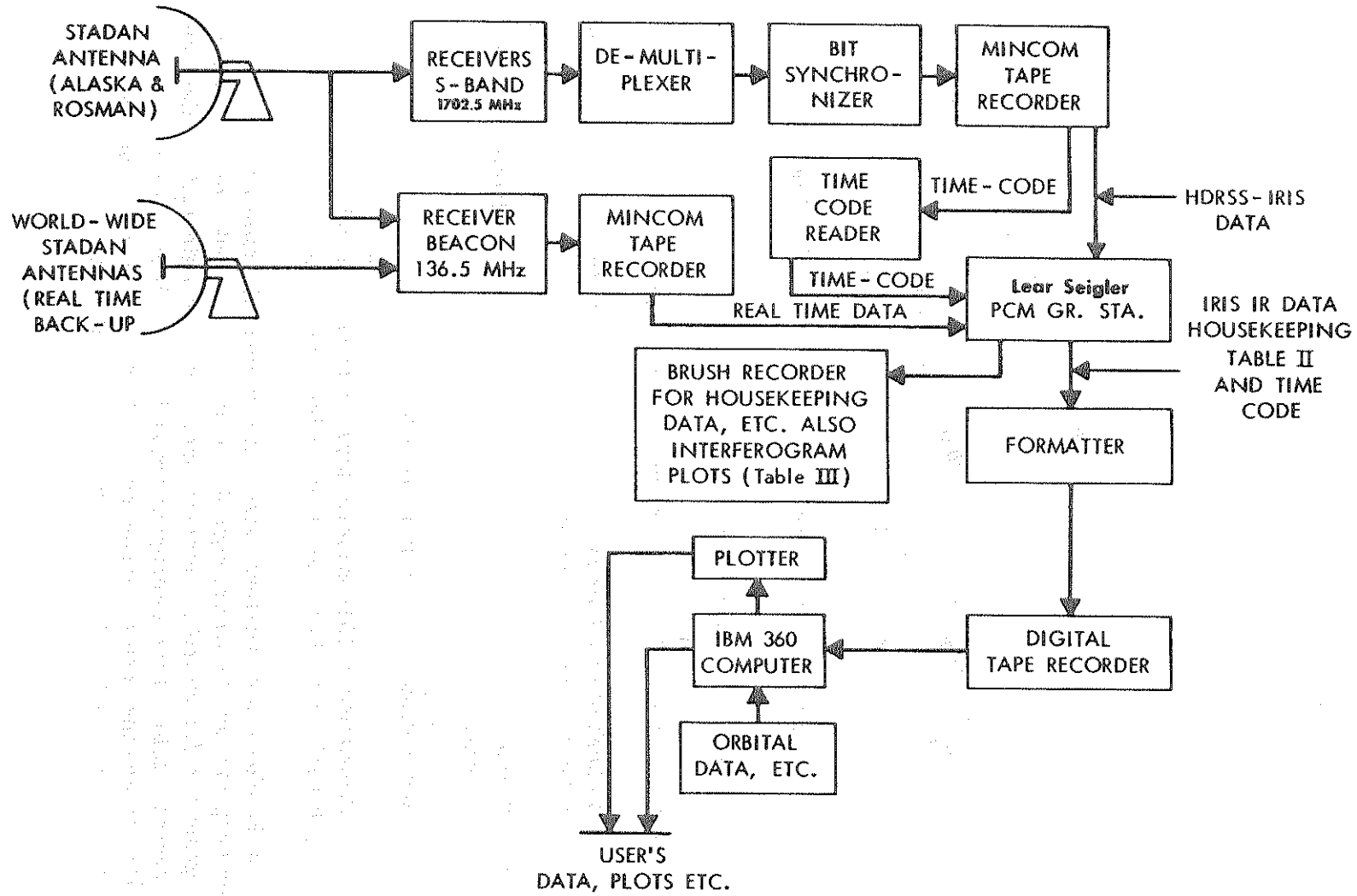

Figure 4-9. Flow Diagram of the Ground Station System and Computer Complex

Housekeeping data are converted into engineering units such as temperatures by application of conversion tables established during preflight calibrations.

Interferograms which passed the screening procedure mentioned above will be transformed by the means of the Cooley - Tukey method (References 7 and 8). A smoothing or apodization function is applied to each interferogram prior to transformation in order to reduce side lobes of the instrument function. The particular apodization function to be applied is the same one which was used on Nimbus III.

It is

$$0.54 + 0.46 \cos 2\pi \tau / T$$

where τ is the distance from the center and T is the total length of interferogram. This apodization function and its effects are discussed by Blackman and Tukey, 1958 (Reference 9). Should a researcher need unapodized spectra, they can be made available in limited numbers.

The Fourier transformation yields two amplitudes

$$a_\nu = \int_{-\infty}^{\infty} A(\delta)\, i(\delta) \cos 2\pi \nu \delta \, d\delta$$

and

$$b_\nu = \int_{-\infty}^{\infty} A(\delta)\, i(\delta) \sin 2\pi \nu \delta \, d\delta$$

where $A(\delta)$ is the apodisation function. From a_ν and b_ν a magnitude and phase is computed

$$c_\nu' = \sqrt{a_\nu^2 + b_\nu^2}$$

and $\phi_\nu = \arctan b_\nu / a_\nu$. The location of the pronounced central peak of the calibration interferograms is taken as the phase reference point. For atmospheric interferograms which may or may not have a strong central peak, the average phase reference point of several calibration interferograms is used.

The phase information is required to distinguish between a target radiance larger (warmer) or smaller (colder) than the radiance corresponding to the

instrument temperature. Wherever the brightness temperature of the target changes from colder to warmer than 250°K or vice versa, a 180° change in phase of the particular frequency component takes place.

Between 640 cm^{-1} and 690 cm^{-1}, the strongest portion of the CO_2 band, only brightness temperatures colder than 250°K are to be expected. In that spectral interval the phase is therefore taken equal to 180° and the magnitude c_ν is assigned a negative sign; wherever the phase changes by ±90°, the sign is alternated.

The slope of the phase curve versus wave number between 640 and 690 cm^{-1} is also used as a check on the selection of the proper phase reference point. In contrast to the interferometer on Nimbus III, this instrument has better control of the position of the central peak. Typical amplitude and phase spectra are shown in Figure 4-10.

After the proper sign of each amplitude is established, the calibration is performed. The instrument is exposed every 16th frame to a built-in calibration blackbody, and to the interstellar background, considered to be near zero, by rotation of the IMCC mirror. The calibration interferograms are processed in the same manner as the interferograms obtained while viewing the atmosphere. The amplitude c_ν in the spectrum is proportional to the difference in radiance between the instrument and the target.

$$c_\nu = r_\nu (B_{target} - B_{instrument}).$$

The factor of proportionality is the responsivity of the instrument. The dimensions of the responsivity are count per count maximum per radiance or just per radiance.

One obtains a set of three equations; one for the target (index 1), one for the cold blackbody (index 2), and one for the warm blackbody (index 3).

$$C_1(\nu) = r_\nu (B_1 - B_i)$$

$$C_2(\nu) = r_\nu (B_2 - B_i)$$

$$C_3(\nu) = r_\nu (B_3 - B_i).$$

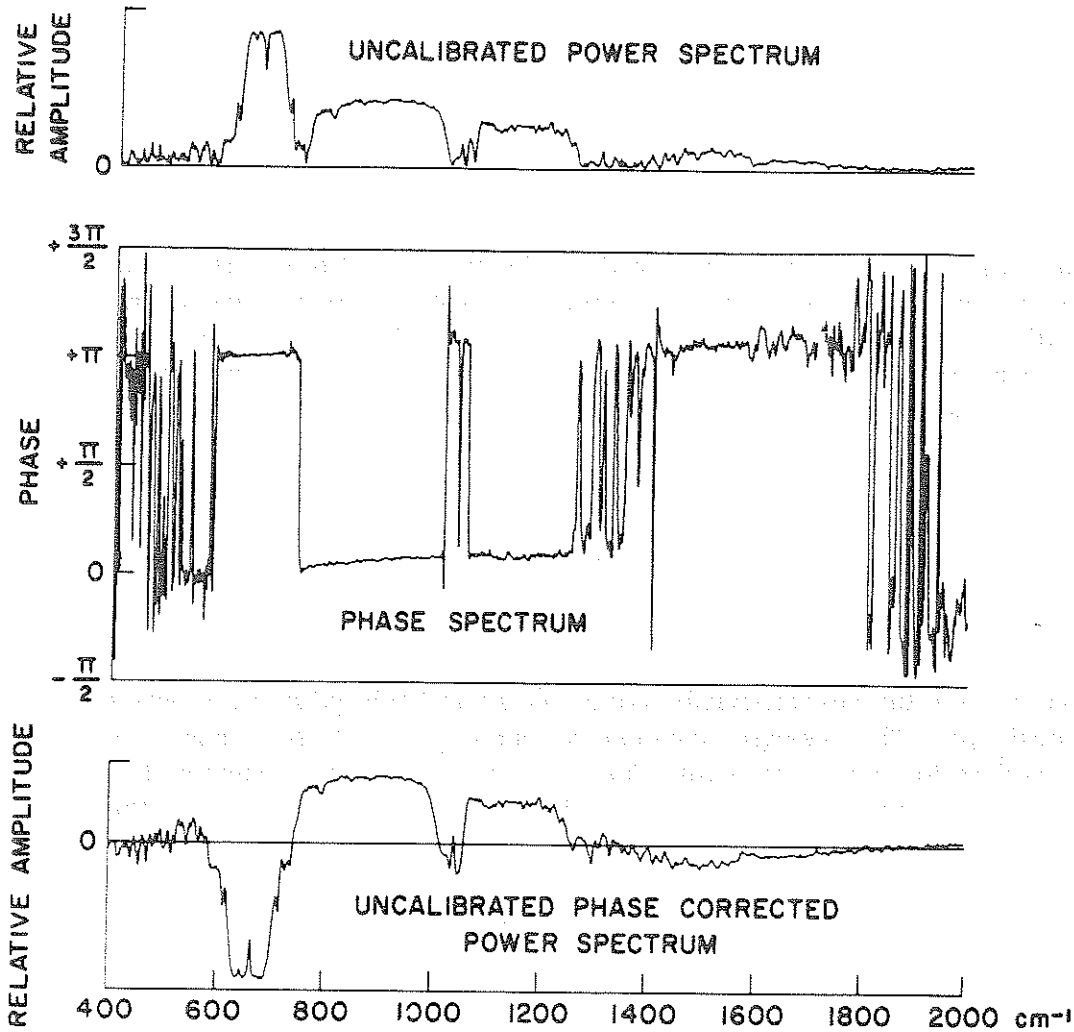

Figure 4-10. Power Spectra and Phase Plot Derived from Nimbus III Interferograms

Under the assumption that the responsivity, r_ν, is independent of the target brightness and that the detection and amplification is a linear process, the 3 equations may be solved to yield B_1 as well as r_ν and B_i. If one uses the interstellar background as the cold reference (~4°K), then B_2 is for all practical purposes zero and the equations simplify to

$$B_1 = B_3 \frac{C_2 - C_1}{C_2 - C_3},$$

$$r_\nu = \frac{C_2 - C_3}{-B_3},$$

$$B_i = B_3 \frac{C_2}{C_2 - C_3},$$

The equation for B_1 is used to reduce the spectra. Neither the responsivity nor the instrument temperature are contained explicitly in this equation. The calibration spectra C_2 and C_3 are the average of about 25 individual spectra so that the random effects in these spectra are greatly reduced. Then the sample standard deviation s of the responsivity is determined for each orbit.

$$s = \left(\frac{\sum_{i=1}^{k} (r_i - \bar{r})^2}{k - 1} \right)^{1/2}$$

The r_i are the responsivities computed from each calibration pair (hot and cold blackbody). The average responsivity per orbit is called $\bar{r}$ and k is the number of calibration pairs per orbit. Instead of tabulating the standard deviation of the responsivity the noise equivalent radiance (NER) calculated from the calibration spectra is employed. The NER is calculated from

$$NER = \frac{\sqrt{2}\, s\, B_3}{\bar{r}}$$

The same level of the NER may be expected to exist in the individual atmospheric spectra.

The NER gives the short time repeatability of the instrument and a comparison of the average orbital responsivity for each spectral interval from orbit to orbit, and from day to day yields the long term drift.

The instrument temperature, T_i, which is calculated from B_i and the instrument temperature measured by the thermistors imbedded in the housing should be in close agreement. A deviation from this agreement is used as a caution flag which calls for a special investigation if it should occur.

Figure 4-11 shows the average warm and cold calibration spectra, responsivity and Noise Equivalent Radiance, all from Nimbus III IRIS.

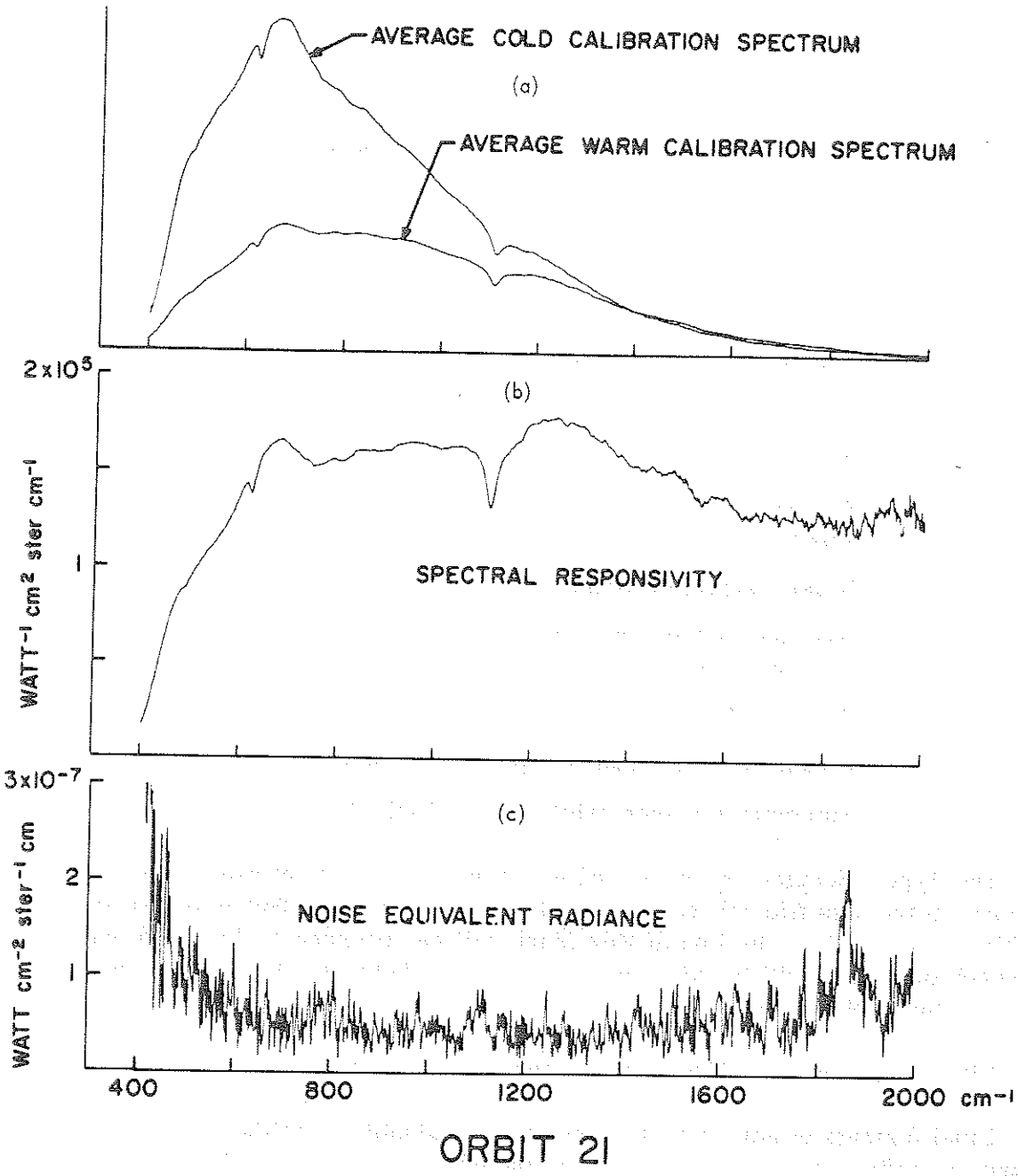

Figure 4-11. Average Cold and Warm Calibration Spectra (a), Spectral Responsivity (b) and Noise Equivalent Radiance (c) Derived from Nimbus III IRIS Data

4.5 Format of the IRIS Archival Tape

The IRIS Archival Tape will be the basic repository for radiation data from the Nimbus Infrared Interferometer Spectrometer (IRIS). This tape will be generated on the IBM 360 System with 9 track recording in binary mode at 1600 bits per inch, and will be available to the scientific community through the NSSDC several months after launch.

The IRIS Archival Tape contains one file for each readout orbit of data processed from the Nimbus spacecraft. Within each file there are several types of records. These are listed below and each type is described in detail in the following tables 4-4 through 4-12.

Record Type	Description
1	Documentation information for each file (Table 4-4)
2	Average cold reference calibration spectrum (Table 4-5)
3	Average warm reference calibration spectrum (Table 4-6)
4	Average Responsivity, R_ν, calculated from the calibration spectra (Table 4-7)
5	Noise Equivalent Radiance (Table 4-8)
6	Average instrument temperature, T_i, calculated from calibration spectra (Table 4-9)
7	Standard Deviation of T_i (Table 4-10)
8	Calibrated Atmospheric Spectrum (Table 4-11)
9	Summary for each orbital pass (Table 4-12)

The Type 1 documentation record will consist of 18 32 bit words. All other records in the data file will consist of 1080 32 bit words, or 960 36 bit words, or 576 60 bit words. The End of File Mark will be recorded at the end of each playback orbit, and will be repeated at least twice following the last readout orbit on any reel of tape.

Ninety degrees are added to all latitudes to eliminate negative signs.

Final formats of any computer printouts obtainable from the archival tapes cannot be defined at present, and will be included in a future Nimbus IV data catalog.

Table 4-4
Documentation Record

Word No.	Quantity	Units	Scaling	Remarks
1	Record Type	–	B31	Type = 1 indicates this record contains documentation data for this file.
2	Satellite I.D.	–	B31	Nimbus IV = 4
3	Orbit Number	–	B31	Readout Orbit No.
4	Day	Days	B31	Time for first calibrated spectrum in this orbit.
5	Hour	Z Hours	B31	
6	Minute	Z Minutes	B31	
7	Second	Z Seconds	B31	
8	Day	Days	B31	Time for last calibrated spectrum in this orbit.
9	Hour	Z Hours	B31	
10	Minute	Z Minutes	B31	
11	Second	Z Seconds	B31	
12	Initial Wave No.	cm^{-1}	Fl. Pt.	Initial wave number for each calibrated spectrum. Normally $\nu_1 \simeq 200$ cm^{-1}
13	Final Wave No.	cm^{-1}	Fl. Pt.	Final wave number for each calibrated spectrum. Normally $\nu_{1051} \simeq 1660$ cm^{-1}.
14	Wave No. Increment	cm^{-1}	Fl. Pt.	The wave number increment. Normally $\Delta\nu \simeq 1.39052333$ cm^{-1}.
15	Spare			
16	Spare			
17	Spare			
18	Spare			

Table 4-5
Cold Reference Calibration Spectra

Word No.	Quantity	Units	Scaling	Remarks
1	Record Type	–	B31	Type = 2 indicates this record contains the average cold reference calibration spectrum.
2	Orbit No.	–	B31	Readout orbit over which the average cold reference calibration spectrum was computed.
3	Number of Cold reference calibration spectra	–	B31	Number of cold reference calibration spectrum averaged.
4	Average peak value	–	Fl. Pt.	Average peak value of the cold reference calibration interferograms.
5	Standard Deviation of Peak Value	–	Fl. Pt.	Standard deviation of peak values from the cold reference calibration interferograms.
6	Average Position of Peak Value	–	Fl. Pt.	Average location of peak values in the cold reference calibration interferograms.
7	Standard Deviation of Position of Peak Value	–	Fl. Pt.	Standard deviation of the location of peak values in the cold reference calibration interferograms.
8 . . . 29	Spares			
30	Averaged Cold Reference Calibration Spectrum Intensity Count	–	Fl. Pt.	Spectral intensity for the averaged cold reference calibration spectrum at $\nu_1 \simeq 200\ cm^{-1}$.

Table 4-5
Cold Reference Calibration Spectra (Continued)

Word No.	Quantity	Units	Scaling	Remarks
31	Averaged Cold Reference Calibration Spectrum Intensity Count		Fl. Pt.	Spectral intensity for the Averaged cold reference calibration spectrum at $\nu_1 \simeq 200$ cm^{-1}. $\nu_2 = \nu_1 + \Delta\nu$.
.	"		"	"
.	"		"	"
.	"		"	"
.	"		"	"
1080	Averaged Cold Reference Calibration Spectrum Intensity Count	–	Fl. Pt.	Spectral intensity for the Averaged cold reference calibration spectrum at $\nu_{1051} \simeq 1660$ cm^{-1}.

Table 4-6
Warm Reference Calibration Spectra

Word No.	Quantity	Units	Scaling	Remarks
1	Record Type	–	B31	Type = 3 indicates this record contains the average warm reference calibration spectrum.
2	Orbit No.	–	B31	Readout orbit over which the average warm reference calibration spectrum was computed.
3	Number of warm reference calibration spectra	–	B31	Number of warm reference calibration spectrum averaged.
4	Averaged Peak Value	–	Fl. Pt.	Average Peak value of the warm reference calibration interferograms.
5	Standard Deviation of Peak Value	–	Fl. Pt.	Standard deviation of peak values from the warm reference calibration interferograms.
6	Average position of Peak Value	–	Fl. Pt.	Average location of peak values in warm reference calibration interferograms.
7	Standard deviation of the position of Peak Value	–	Fl. Pt.	Standard deviation of the location of peak values in the warm reference calibration interferograms.
8 . . . 29	Spares			
30	Average warm reference calibration spectrum intensity count	–	Fl. Pt.	Spectral Intensity for the Averaged warm reference calibration spectrum at $\nu_1 \simeq 200\ cm^{-1}$.
31	Average warm reference calibration spectrum intensity count			Spectral intensity for Averaged warm reference calibration spectrum $\nu_2 = \nu_1 + \Delta\nu$.

Table 4-6
Warm Reference Calibration Spectra (Continued)

Word No.	Quantity	Units	Scaling	Remarks
.	Average warm reference calibration spectrum intensity count		"	"
.	Average warm reference calibration spectrum intensity count		"	"
.	Average warm reference calibration spectrum intensity count		"	"
1080	Averaged warm reference calibration spectrum intensity count	–	Fl. Pt.	Spectral intensity for the averaged warm reference calibration spectrum at $\nu_{1051} \simeq 1660\ cm^{-1}$.

Table 4-7
Average Responsivity

Word No.	Quantity	Units	Scaling	Remarks
1	Record Type	–	B31	Type = 4 indicates this record contains the average responsivity for the orbit.
2	Orbit No.	–	B31	Readout orbit over which the average responsivity was calculated.
.	Spares			
.	Spares			
.	Spares			
.	Spares			
.	Spares			
.	Spares			
29				
30	Average responsivity for the orbit at a given ν.	(watts cm^{-1} $ster.^{-1})^{-1}$	Fl. Pt.	Average responsivity for the orbit at $\nu_1 \simeq 200$ cm^{-1}.
.	"	"	"	"
.	"	"	"	"
.	"	"	"	"
1080	Average responsivity for the orbit at a given ν.	(watts cm^{-1} $ster.^{-1})^{-1}$	Fl. Pt.	Average responsivity for the orbit at $\nu_{1051} \simeq$ 1660 cm^{-1}.

Table 4-8
Noise Equivalent Radiance

Word No.	Quantity	Units	Scaling	Remarks
1	Record Type	–	B31	Type = 5 indicates this record contains the standard deviation of the responsivity for the orbit.
2	Orbit No.	–	B31	Readout orbit over which the standard deviation of the responsivity was calculated.
3	Spare			
.	Spare			
.	Spare			
.	Spare			
.	Spare			
29	Spare			
30	Noise Equivalent Radiance at given ν.	–	Fl. Pt.	NER at $\nu_1 \simeq 200$ cm^{-1}.
.	"		"	"
.	"		"	"
.	"		"	"
.	"		"	"
.	"		"	"
1080	NER at given ν.	–	Fl. Pt.	NER at $\nu_{1051} \simeq 1660$ cm^{-1}.

Table 4-9
Average Instrument Temperature

Word No.	Quantity	Units	Scaling	Remarks
1	Record Type	–	B31	Type = 6 indicates this record contains the average instrument temperature.
2	Orbit No.	–	B31	Readout orbit over which the average instrument temperature was calculated.
3	Spare			
.	Spare			
.	Spare			
.	Spare			
.	Spare			
.	Spare			
29	Spare			
30	Average Instrument Temperature at a given ν.	Degrees Kelvin	Fl. Pt.	Average instrument temperature at $\nu_1 \simeq 200$ cm^{-1}.
.	"	"	"	"
.	"	"	"	"
.	"	"	"	"
1080	Average Instrument Temperature at a given ν.	Degrees Kelvin	Fl. Pt.	Average instrument temperature at $\nu_{1051} \simeq$ 1660 cm^{-1}.

Table 4-10
Standard Deviation of the Instrument Temperature

Word No.	Quantity	Units	Scaling	Remarks
1	Record Type	–	B31	Type = 7 indicates this record contains the standard deviation of the instrument temperature.
2	Orbit No.	–	B31	Readout orbit over which the standard deviation of the instrument temperature was computed.
3	Spare			
.	Spare			
.	Spare			
.	Spare			
.	Spare			
29	Spare			
30	Standard Deviation of the instrument temperature at given ν.	–	Fl. Pt.	Standard deviation of the instrument temperature at $\nu_1 \simeq 200$ cm^{-1}.
.	"	"	"	"
.	"	"	"	"
.	"	"	"	"
1080	Standard Deviation of the instrument temperature at given ν.	–	Fl. Pt.	Standard deviation of instrument temperature at $\nu_{1051} \simeq 1660$ cm^{-1}.

Table 4-11
Calibrated Atmospheric Spectrum

Word No.	Quantity	Units	Scaling	Remarks
1	Record Type	–	B31	Type = 8 indicates this record contains a calibrated atmospheric spectrum.
2	Orbit No.	–	B31	Readout orbit in which the calibrated spectrum was calculated.
3	Spectrum No.	–	B31	Sequential number assigned to a given spectrum in a given orbit.
4	Day	Days	B31	Time associated with this interferogram.
5	Hour	Z Hours	B31	
6	Minute	Z Minutes	B31	
7	Second	Z Seconds	B31	
8	Latitude	Degrees	Fl. Pt.	Latitude and Longitude of the center of the viewed area
9	Longitude	Degrees	Fl. Pt.	
10	Height of satellite	Kilometers	Fl. Pt.	Height of the satellite at the time stated in words 4-7.
11	Bolometer Temperature	Degrees K	Fl. Pt.	Bolometer temperature (average of two readings before and after interferograms).
12	Bolometer temperature redundant sensor	Degrees K	Fl. Pt.	Bolometer temperature from redundant sensor (average before and after interferogram).
13	Blackbody Temperature	Degrees K	Fl. Pt.	Blackbody temperature (average before and after interferogram).
14	Blackbody temperature from redundant sensor	Degrees K	Fl. Pt.	Blackbody temperature from redundant sensor (average before and after interferogram).
15	Beamsplitter Temperature	Degrees K	Fl. Pt.	Temperature of IRIS instrument beamsplitter.
16	Temperature of Michelson mirror drive motor	Degrees K	Fl. Pt.	IRIS Michelson mirror drive motor temperature.

Table 4-11
Calibrated Atmospheric Spectrum (Continued)

Word No.	Quantity	Units	Scaling	Remarks
17	IMCC Temperature	Degrees K	Fl. Pt.	IMCC Temperature
18	Temperature of cooling surface	Degrees K	Fl. Pt.	Cooling surface temperature
19	IMCC Position	–	B31	IMCC Position (2 bits digital) 0 = Warm Ref. 2 = Earth 3 = Cold Ref.
20	+0.6 Volt Calibration	–	Fl. Pt.	+0.6 Volt Calibration
21	0 Volt Calibration	–	Fl. Pt.	0 Volt Calibration
22	-0.6 Volt Calibration	–	Fl. Pt.	-0.6 Volt Calibration
23	Calibration Transducer	–	–	Calibration Transducer
24	Solar Elevation Angle	Degrees	Fl. Pt.	Solar deviation angle at the viewed point.
25	Number of sync bits errors	–	Fl. Pt.	Number of interferogram sync pulse errors.
26	Spare	–		
27	Number of Gain Pulses Outside Center	–	Fl. Pt.	Number of gain pulses outside center region of the interferogram.
28	Time Indicator	–	–	= 0, time code from raw data tape
29	Spare Position	–	–	= 1, time computed
30	Specific Intensity	watts cm^{-1} $ster^{-1}$	Fl. Pt.	Specific intensity at $\nu_1 \simeq 200$.
31	"	"	"	"
.	"	"	"	"
.	"	"	"	"
1080	Specific Intensity	watts cm^{-1} $ster^{-1}$	Fl. Pt.	Specific intensity at $\nu_{1051} \simeq 1660$.

Table 4-12
Summary Record For the Orbit
(Last Record in File)

Word No.	Quantity	Units	Scaling	Remarks
1	Record Type	–	B31	Type = 9 indicates this record is a summary for the orbit.
2	Orbit Number	–	B31	Readout Orbit No.
3	Number of Spectra per orbit	–	Fl. Pt.	Number of calibrated spectra computed for the orbit.
4	Day	Day	B31	Time of the first calibrated spectrum computed for the orbit
5	Hour	Z Hour	B31	
6	Minute	Z Minute	B31	
7	Second	Z Second	B31	
8	Day	Day	B31	Time of the last calibrated spectrum computed for the orbit
9	Hour	Z Hour	B31	
10	Minute	Z Minute	B31	
11	Second	Z Second	B31	
12	Orbital Mean of Bolometer Temperature	Degrees K	Fl. Pt.	Mean bolometer temperature for the orbit
13	Sample Standard Deviation of Bolometer Temperature	–	Fl. Pt.	–
14	Orbital Mean of Blackbody Temperature	Degrees K	Fl. Pt.	–
15	Sample Standard Deviation of Blackbody Temperature	–	Fl. Pt.	–
16	Orbital Mean Beamsplitter Temperature	Degrees K	Fl. Pt.	–
17	Sample Standard Deviation of Beamsplitter Temperature	–	Fl. Pt.	–

Table 4-12
Summary Record For the Orbit
(Last Record in File) (Continued)

Word No.	Quantity	Units	Scaling	Remarks
18	Orbital Mean Temperature of Michelson mirror drive motor	Degrees K	Fl. Pt.	–
19	Sample Standard Deviation of Michelson mirror motor temperature	–	Fl. Pt.	–
20	Orbital Mean IMCC Temperature	Degrees K	Fl. Pt.	–
21	Sample Standard Deviation of IMCC Temperature	–	Fl. Pt.	–
22	Orbital Mean Temperature of Cooling Surface	Degrees K	Fl. Pt.	–
23	Sample Standard Deviation of Temperature of Cooling Surface	–	Fl. Pt.	–
24	Number of Interferograms containing sync pulse errors	–	Fl. Pt.	Number of interferograms in the orbit containing sync pulse errors.
25	Number of Interferograms containing bits parity errors	–	Fl. Pt.	Number of interferograms in the orbit containing word parity errors.
26	Number of Interferograms containing gain switch pulses outside central region	–	Fl. Pt.	Number of interferograms in orbit containing gain pulses outside central region.

Table 4-12
Summary Record For the Orbit
(Last Record in File) (Continued)

Word No.	Quantity	Units	Scaling	Remarks
27	Number of warm calibration spectra used	—	Fl. Pt.	Number of warm calibration spectra used in the average to compute calibrated spectra.
28	Number of cold calibration used	—	Fl. Pt.	Number of cold calibration spectra used in the average to compute.
29	Spare	—	—	—
1080	Spare	—	—	—

REFERENCES

1. Wark, D. Q., and Fleming, H. E., Indirect Measurements of Atmospheric Temperature Profiles from Satellites: I, Introduction, Monthly Weather Review, 94, 35-362 (1966).

2. Conrath, B., 1969, On the Estimation of Relative Humidity Profiles from Medium-Resolution Infrared Spectra Obtained from a Satellite, J. Geophys. Res., Vol. 74, pp. 3347-3361.

3. Hanel, R. A., and B. J. Conrath, 1969, The IRIS Experiment on Nimbus III; Preliminary Results, Science, Vol. 165, pp 1258-1260 Sept. 19.

4. Prabhakara, C., B. J. Conrath, R. A. Hanel and E. J. Williamson, 1970, Remote Sensing of Ozone Using the 9.6μ Band, submitted to Journal of Atmospheric Sciences.

5. Conrath, B. J., R. A. Hanel, C. Prabhakara, 1970, Results of the IRIS Experiment on the Nimbus III Satellite, in preparation.

6. Hanel, R. A., B. Schlachman, F. D. Clark, C. H. Prokesh, J. B. Taylor, W. M. Wilson and L. Chaney, 1970, The Nimbus III Michelson Interferometer, submitted to Applied Optics.

7. Cooley & Tukey, Math. of Computation 19, 296 (1965).

8. Forman, 1966, J. Opt. Soc. of Amer., Vol. 56, No. 7, July pp. 978-979.

9. Blackman, R. B., and J. W. Tukey, The Measurement of Power Spectra, Dover Publications, New York (1958).

SECTION 5

THE SATELLITE INFRARED SPECTROMETER (SIRS) EXPERIMENT

By
D. Wark, D. Hilleary, S. Anderson, J. Lienesch
National Environmental Satellite Center
Environmental Science Services Administration

5.1 Introduction

The Satellite Infrared Spectrometer (SIRS) on the Nimbus IV satellite is a second step in a process of developing a means of determining the three-dimensional state of the atmosphere by indirect means. Similar to the instrument on Nimbus III, identified as SIRS-A, the new instrument, known as SIRS-B, has the added capabilities of spatial scan for greater area coverage, and of the determination of the tropospheric water vapor content.

The outputs of the Satellite Infrared Spectrometer are transformed to spectral radiances by the calibration procedure discussed in Section 5.3. The spectral radiances are then used ensemble to deduce the temperature and humidity profiles of the atmosphere within the field-of-view.

5.2 Description of the Experiment

Fourteen spectral intervals are examined simultaneously. One of these is located in the spectral window at 899 cm^{-1}; seven are located within the carbon dioxide band centered at 667 cm^{-1}; and the remaining six are located in the water vapor rotation band. Table 5-1 lists the 14 spectral intervals in terms of the center of each interval and of the spectral response within the interval. It may be noted that the nominal spectral response is trapezoidal, modified slightly by optical blur.

The measured radiances are related to the temperatures of the atmosphere, the surface, and clouds which may be within the field-of-view through the equation of radiative transfer. If one assumes that a single cloud layer exists, one can construct the set of integral equations

Table 5-1
SIRS-B Slit-Function Parameters.
The first column is the channel identification number, and the second column is the spectral location of the center of each channel. The next two columns give the slit-functions' widths at the maxima and the minima, defining the trapezoidal shape of these functions. The last column lists the radii of the optical blur circles.

Channel	ν_0 (cm^{-1})	$(\Delta\nu)_1$ (cm^{-1})	$(\Delta\nu)_0$ (cm^{-1})	Blur Radius (cm^{-1})
1	899.0	2.36	12.36	0.8
2	750.0	1.83	11.83	0.6
3	734.0	1.70	11.70	0.5
4	709.0	1.13	11.13	0.5
5	701.0	0.96	10.96	0.6
6	692.0	0.81	10.81	0.7
7	679.8	0.61	10.61	0.8
8	668.7	0.42	10.42	0.9
9	531.5	0.14	10.14	0.8
10	436.5	1.53	8.47	0.5
11	425.5	1.70	8.30	0.8
12	291.5	1.90	8.10	0.8
13	302.0	1.68	8.32	1.0
14	280.0	2.14	7.86	0.7

$$I(\nu_i) = N\left\{B\left[\nu_i, T(p_c)\right]\ \tau(\nu_i, p_c) - \int_1^{\tau_c} B\left[\nu_i, T(p)\right]\ d\tau(\nu_i, p)\right\}$$

$$+ (1 - N)\left\{B\left[\nu_i, T(p_s)\right]\ \tau(\nu_i, p_s) - \int_1^{\tau_s} B\left[\nu_i, T(p)\right]\ d\tau(\nu_i, p)\right\}$$

$$i = 1, \cdots, M$$

$I(\nu_i)$ = spectral radiance at wavenumber ν_i

$B\left[\nu_i, T(p)\right]$ = Planck radiance at wavenumber ν_i and temperature T; in the atmosphere temperature is a function of the pressure level, p.

$\tau(\nu_i, p)$ = fractional transmittance of the atmosphere in the spectral interval centered at wavenumber ν_i and from pressure level p to the satellite.

Subscripts c and s refer to cloud-top and surface.

N = the product of the fraction of cloud cover within the field-of-view and the cloud emissivity; if the cloud is thick the emissivity is unity, whereas if the cloud is not opaque it is assumed to be geometrically thin.

The solution of this equation has been discussed in the references given in the bibliography and in the more extensive bibliography of Chapter 6 in the Nimbus III User's Guide.

Experience from the SIRS A Data shows that satellite measurements can be used as a viable adjunct to other meteorological data, particularly over oceans and other data-sparse regions. The SIRS B experiment has been designed to extend the scope of this observational technique in two ways:

1. By the scan to each side of the sub-satellite track, described in Section 5.3, a mosaic of observations can be built. Figure 5-1 shows a 12-hour pattern of viewed areas over the northern hemisphere which could be obtained from seven consecutive full orbits of data. In the sub-arctic portions of this figure the average separation of the viewed areas is about 500 n.m.

2. Channels 9-14 will provide a means of estimating the vertical distribution of water vapor in the troposphere. Because of the dependence of the transmittances in channels 2-6 upon both carbon dioxide and water vapor, the determination of the water vapor distribution will improve the determination of temperature distribution as a by-product.

The SIRS B experiment is seen to be a reasonable extension of the SIRS A experiment. The extraction of the physical parameters of the atmosphere from the measurements will be somewhat more complicated with the new experiment, but the results should be more useful for most meteorological applications.

5.3 Description of the Instrument

The Sirs B instrument consists of the following two components:

a. Optical Unit

This component measures the difference in IR radiation between earth and space in fourteen narrow spectral intervals. AC output voltages produced from the detectors are proportional to the energy in each spectral

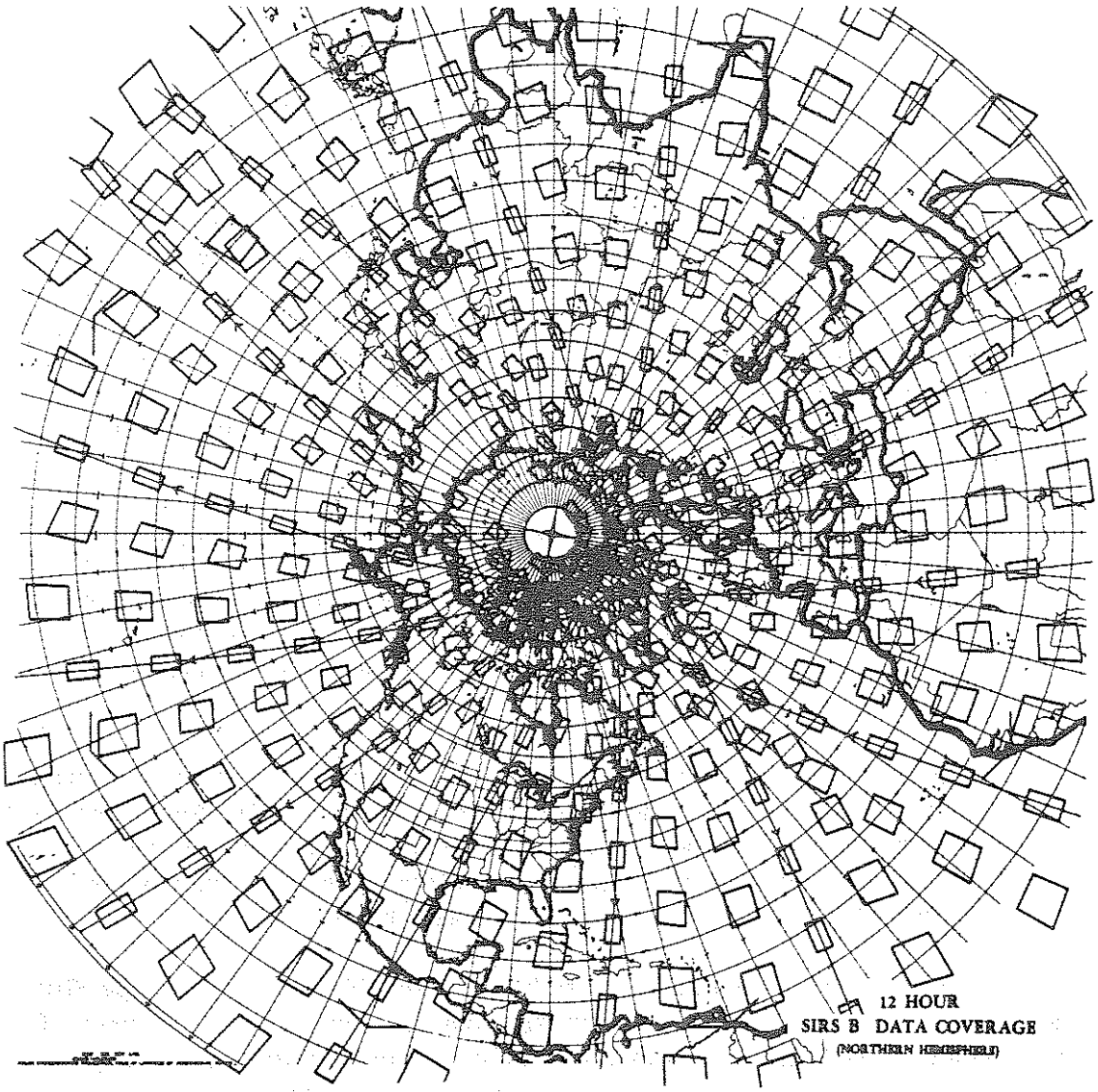

Figure 5-1. A Northern Hemisphere Pattern of Viewed Areas which could be Obtained from 12 Hours of Complete Data

interval. Each of these signals is amplified before leaving the optical unit. In addition to housing the monochrometer and detectors, the optical unit houses a chopper motor, a scan motor, and an in-flight wavenumber calibration system. This large cylindrical container, the optical unit, is suspended vertically in the central crossbeam area of the sensory ring. Table 5-2 summarizes the design of the optical unit.

Table 5-2
Optical Unit Design Summary

Type Instrument	f/5 Ebert-Fastie grating spectrometer, 12.5-inch focal length.
Field-of-View	Square 0.04-steradian FOV scanned up to 37.8° each side of orbital track.
Wavenumber Region	One detection channel in the atmospheric window (899 cm^{-1}), seven channels in the CO_2 band (668.7 to 750 cm^{-1}), and six channels in the H_2O band (280 to 531.5 cm^{-1}).
Spectral Bandpass	5 cm^{-1} equivalent energy bandpass.
Spectral Accuracy	Stability and accuracy, ±0.3 cm^{-1} at 669 cm^{-1}.
Spectral Calibration	Internal calibrator check to ±0.5 cm^{-1}.
Sensitivity	0.25 erg (sec cm^2 ster $cm^{-1})^{-1}$.
Dynamic Range	800 maximum of 200 ergs (sec cm^2 ster $cm^{-1})^{-1}$.
Accuracy	0.5 erg (sec cm^2 ster $cm^{-1})^{-1}$.
Calibration	Internal ambient blackbody reference cone and space.
Optical Design Summary	Programmed object-space scan mirror. 15-Hz earth-space reflective chopper. Grating ruled with 26.93 lines/mm operating in orders of 1 through 4. Immersed thermistor bolometer detectors. Approximately 21.5 inches long and 12 inches in diameter. Weight of 50 lbs.

b. Sensory Ring Module

This component accepts the output voltages from the optical unit, synchronously demodulates them, and converts these output voltages into ten-bit decimal words for output into VIP. In addition to housing the synchronous demodulators and A/D circuitry, the sensory ring module also houses the system power supply, command sequencer, stepping motor logic, and temperature monitoring circuitry. The sensory ring module

is housed in a 3 over 3 module ($6 \times 6 \times 13$ inches) mounted in the sensory ring. Table 5-3 summarizes the design of the electronics unit.

The SIRS B sensor is an f/5 Fastie-Ebert grating spectrometer having a 12.5-inch focal length. The mechanical-optical arrangement is shown in the artist's conceptual drawing, Figure 5-2. The spectrometer's 0.04-steradian field-of-view is positioned by the object-space scan mirror (nadir plane). Exact scan mirror positioning is accomplished with a stepper motor-encoder arrangement together with associated electronic logic. This method permits

Table 5-3
Electronics Design Summary

Analog Channel	Gain:	Variable, 1×10^5 to 5×10^6.
	Stability:	0.1%, 5°C to 55°C.
	Noise:	1.05 times the Johnson noise of a 300-Kohm wire-wound resistor (referred to input).
	Cross-talk:	-70 db.
	Time Constant:	6 ± 0.3 second.
	Output Ripple:	1 mv rms or less.
	Output:	10 volts with impedance of 1 ohm or less.
Detector Bias	Voltages:	±24 and ±37 volts.
	Regulation:	±0.1%
	Track:	Plus and minus equal to within 50 mv and track with each other within 0.1μv (peak-to-peak).
	Output Impedance:	0.1 ohm or less.
A/D System	Convert 36 analog channels to 10-bit digital word and store in a storage register. Sample 15 channels every 2 seconds and remaining every 16 seconds. Provide 30 go/no-go bits.	
Scan Control	Sequence stepper scan motor to 54 discrete positions at 59.6-second intervals. Operational programs include a calibration sequence mode in addition to the normal earth scan mode.	
Commands	Eleven command relays are provided.	

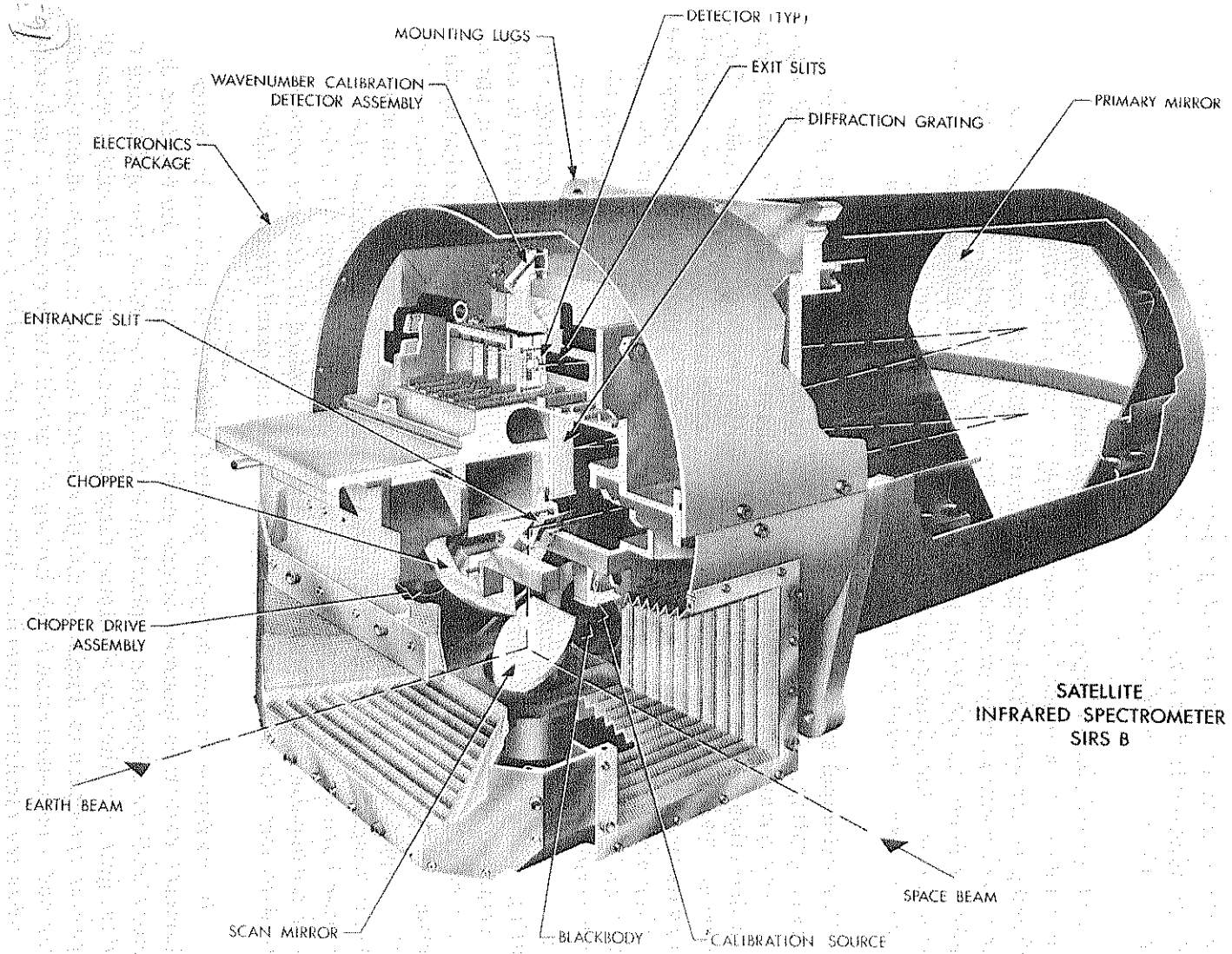

Figure 5-2. The Nimbus IV Satellite Infrared Spectrometer

pointing the field-of-view directly below the instrument and at nadir angles of 23.4°, 28.8°, 32.4°, 34.2°, 36.0°, and 37.8° each side of the orbital track. In addition, the scan mirror can be programmed to view space or a self-contained ambient blackbody reference cone. The latter two positions are used for in-flight confirmation of the instrument's radiometric calibration.

The spectrometer input is alternately switched from the unknown scene input radiance to a space reference having a minimum radiance. The optical switching is accomplished using a reflective chopper, the number of chopper blades and rotation rate producing a 15 Hz chop frequency. The chopper assembly includes an electrical pickoff arrangement for phasing the data processor demodulator. An optimum packaging arrangement is achieved by using a folding mirror mounted directly in front of the spectrometer entrance slit.

The principal spectrometer components are the entrance slit, primary mirror, grating, and the exit slits with the associated order filters and detectors. The parameters of these components have been optimized to obtain maximum detection sensitivity while maintaining the required spectrometer characteristics. The principal spectral characteristics are: The selected wavenumber intervals must be accurate and stable to ± 0.2 cm^{-1}; the equivalent energy bandpass for all channels must be 5 cm^{-1}; and the width of the exit slit for channel 8 (668.7 cm^{-1}) must be equal to the entrance slit width which guarantees that the slit function will be nearly triangular in shape. Energy from the entrance slit is collimated by the primary mirror which in turn illuminates the grating. The grating, ruled with 26.93 lines/mm, operates in the first four orders to cover the required spectral range. The entrance slit is imaged into the exit slit plane by a second reflection from the primary mirror following diffraction by the grating. A series of slits at the exit slit plane sample the dispersed spectrum in the required spectral intervals. Channel 1 is selected to be in an atmospheric window (899.0 cm^{-1}); Channels 2 through 8 in the carbon dioxide absorption band (668.7 to 750.0 cm^{-1}); and Channels 9 through 14 in the water vapor absorption band (280.0 to 531.5 cm^{-1}). Optical filters are associated with each exit slit to eliminate radiation from unwanted grating orders.

The radiation in each selected spectral interval is detected by thermistor bolometer detectors mounted behind each exit slit. Each of the fourteen detectors utilizes a hyperhemispherical immersion technique for optimizing the optical gain, and thereby obtaining maximum sensitivity. The output from the separate detectors is amplified and processed through a synchronous demodulator and a post-detection filter having a 6 second time constant. Each amplifier provides the electrical interface between the associated detector and the demodulator. The amplifier is composed of a preamplifier and two ac-coupled gain states. The preamplifier consists of a matched pair of low-noise field effect

transistors (FET) connected in a Middlebrook configuration which in turn drive an integrated circuit amplifier. The preamplifier is followed by two additional integrated circuit amplifiers. The gain control feedback loop of the first of these amplifiers is associated with a temperature compensating thermistor located in the detector housing. This temperature compensating circuit stabilizes the gains as a function of ambient equipment temperature. Figure 5-3 shows the signal flow in schematic form.

The optical unit also includes the detector bias supply regulators. One assembly supplies ±24 volts to the smaller bolometer detectors (Channels 1 through 9); the second assembly supplies ±37 volts to the larger detectors (Channels 10 through 14). The regulators are designed to provide minimum noise with low output resistance and good regulation.

The fourteen voltages are each sampled, encoded to ten binary bits, and stored in a register, all within 0.1 second. The fourteen binary numbers are read out in turn to the VIP Telemetry. During one 16-second major frame, the 14 IR data channels are each sampled eight times.

The electronics in the sensory ring module provide the interface between the optical unit and the spacecraft NIMBUS Versatile Information Processor (VIP). It contains 14 synchronous demodulators for the signal channels, A/D system, scan motor control and drive circuitry, temperature and voltage monitor circuits, control circuitry, and the SIRS B system power supply.

The circuits of the sensory ring buffer demodulate the outputs of the 14 signal channels from the optical unit. This information is multiplexed with 22 channels of other analog information (temperature and circuit monitors), and converted into 10-bit digital words. This digital information is sampled by external command. In addition to the analog data, three 10-bit digital words provide 30 go/no-go bits for added information monitoring. The data from the 14 signal channels and a reference channel are sampled each minor frame (2 seconds). The remaining data channels are sub-multiplexed and sampled each major frame (16 seconds).

The assembly contains a sequencer which provides drive pulses to the scan motor located in the optical unit. The logic drives the scan mirror to the various scan positions in the required sequence. Operation is determined from external commands which are received and stored by locking relays or momentary relays and flip-flops. Additional command relays receive and store commands necessary for other SIRS B functions.

All SIRS B power is provided from preregulators and dc-dc converters located in the sensory ring module.

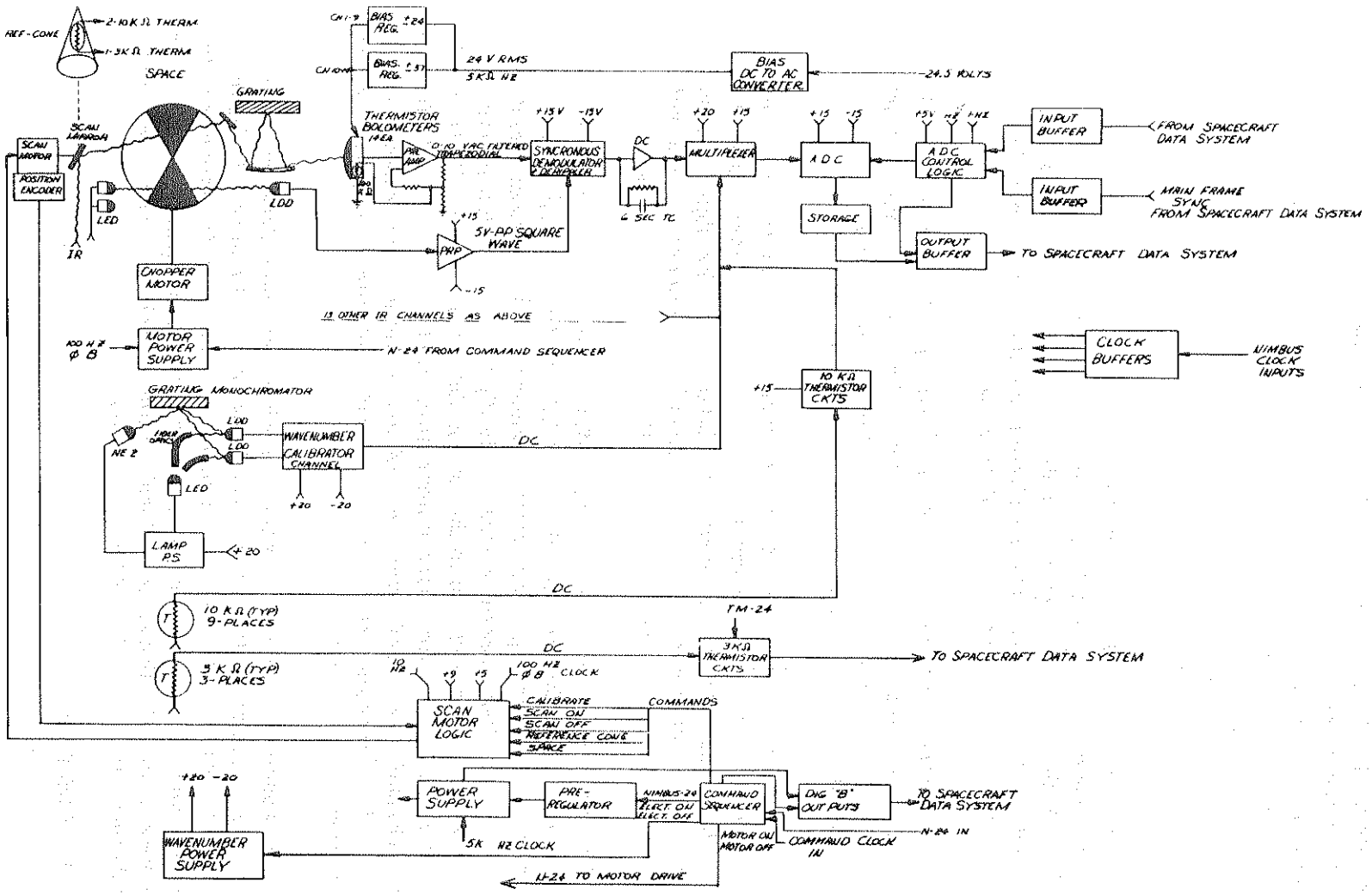

Figure 5-3. SIRS Signal Flow Diagram

There are two basic types of in-flight calibration: Radiance Calibration, and Wavenumber Calibration. Each of these calibration modes can only be actuated by ground command. To initiate the Radiance Calibration Mode the radiance calibration command is transmitted, actuating the calibration program at the end of the next 59.6-second step in the calibration mode sequencer. Once this step has been reached, the scan mirror will step to the reference cone position and remain there for 89.4 seconds, after which the mirror will be stepped to the space position. The mirror will remain in the space position for 89.4 seconds and then return to the appropriate step in the scan sequence.

Initiation of the calibration sequence will not advance or delay the scan mirror sequence and it will return to its correct position at the end of a calibration sequence.

The instrument includes an in-flight wavenumber calibration check. The calibrator essentially confirms that no physical displacement of the spectrometer components has affected the selected wavenumber calibration. It consists of a second entrance slit illuminated by a neon lamp and located near the primary entrance slit. An optical bandpass filter placed at the entrance slit is used to isolate the strong neon line at 14,216 cm^{-1}. This radiation then traverses the spectrometer in the usual manner. Two exit apertures are positioned adjacent to the normal spectrometer exit slits in a manner so that each intercepts a single order of this line. The apertures are shaped so that a change of the spectrometer parameters will cause a relative change in the detected energy from the two slits. Inaccuracies which may arise from lamp and detector decay and amplifier gain change as a function of temperature are eliminated by having a gallium arsenide emitter on during one-half of the wavenumber calibrator period. The pulsed radiation from this emitter is transmitted via light pipes to the same silicon detectors which view the neon line during the other half of the wavenumber calibrator period. The transfer function is calculated as a double ratio of each channel's output for the neon and gallium arsenide lamps. This transfer function is shown in Figure 5-4. The wavenumber calibrator operates only on command, and it is anticipated that it will be used primarily to confirm wavenumber calibration during the initial phase of the mission. Table 5-4 shows the variation of the transfer function with instrument temperature.

Ground calibration of the SIRS B is achieved by utilization of blackbody radiation sources in front of each beam. The thermocouple or thermistor sensor voltage in each radiation source is translated to temperature using a calibration curve. These temperatures define the component energies at each of the fourteen spectral intervals measured by the detectors. In flight the space beam energy is negligible, but during ground calibration the space source energy may be substantial and must be subtracted to give the correct AC differ-

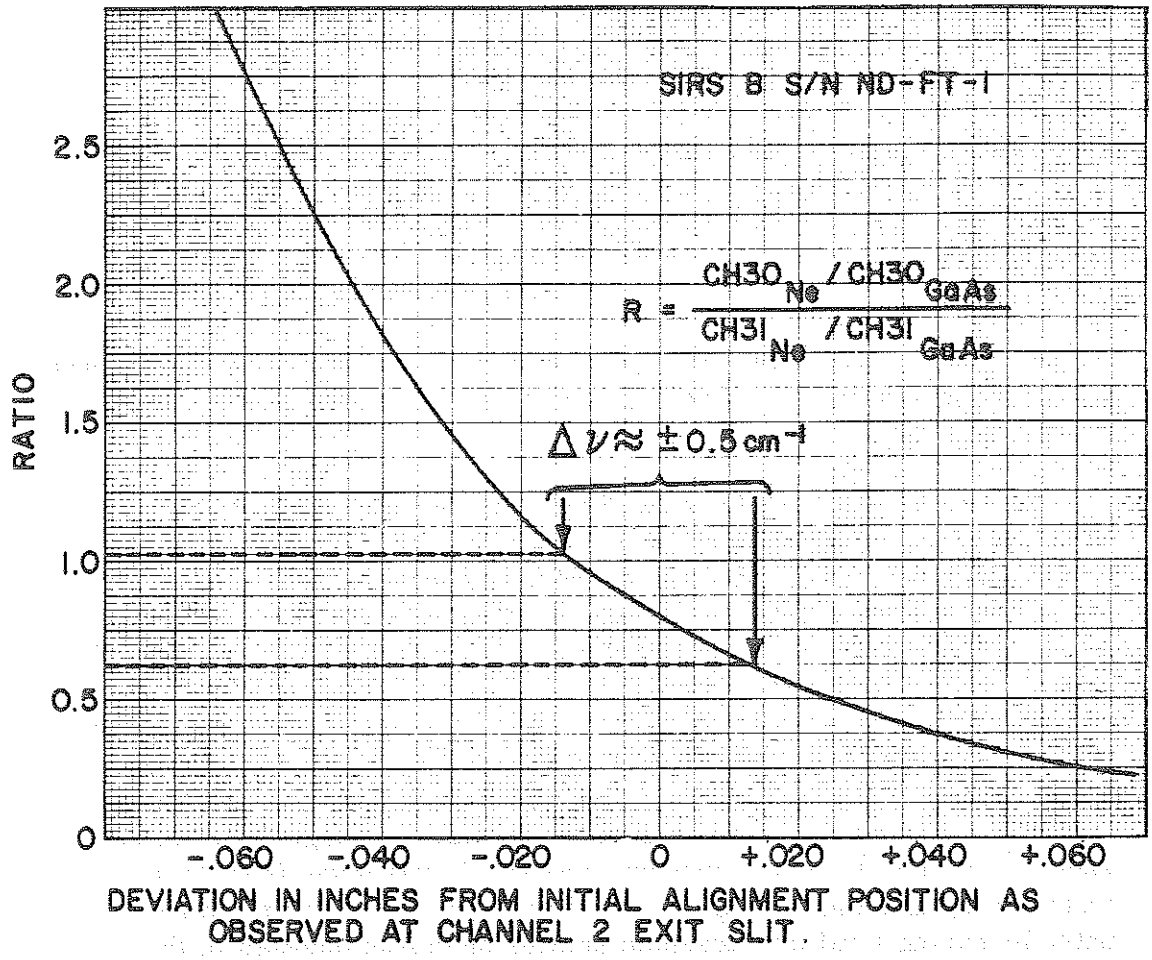

Figure 5-4. Wavenumber Calibration Transfer Function

ential seen by the bolometers. The net energies are converted to voltages by the fourteen bolometers. These voltages and the net radiance from the two radiation sources determine the calibration of the instrument. The calibration of the 14 channels at 25°C detector temperature is shown in Figures 5-5 to 5-18. Variations in sensitivity with detector temperature are given for all channels in Figures 5-19 and 5-20.

Fifteen temperature and three voltage monitors are sampled once every sixteen seconds and sub-commutated in the SIRS digital data. The identification of these monitors is given in Table 5-5 and the calibration curves are shown in Figures 5-21 and 5-22. Four analog temperatures are also monitored and identified in Table 5-5. Figure 5-23 shows the calibration applicable to these monitors.

Table 5-4
Flight Model Wavenumber Calibrator Operation as a Function of Instrument Temperature

Ambient Temp.	$CH30_{Ne}$	$CH30_{GaAs}$	$CH31_{Ne}$	$CH31_{GaAs}$	Ratio
0°	378	341	439	440	1.1
5°	370	328	466	420	1.0
15°	355	312	501	385	0.88
25°	337	283	547	357	0.78
31°	324	275	576	348	0.71
37°	307	260	615	334	0.63

Table 5-5
SIRS B Temperature and Voltage Monitors

Channel No.	Description	Channel No.	Description
15	Reference Cone Temp.	26	Primary Mirror Temp.
16	Detector #1 Temp.	28	Chopper Mirror Temp.
17	Detector #2 Temp.	32	+15 Volt Monitor
18	Detector #3 Temp.	33	A/D Conv. Ref. Voltage
19	Detector #4 Temp.	34	DC-DC Converter Temp.
20	Amplifier Package Temp.	35	A/D Converter Temp.
21	Bias Regulator Temp.	36	Sync. Demod. Temp.
22	Chopper Motor Temp.		Reference Cone Temp. (Analog)
23	Stepper Motor Temp.		Power Supply Temp. (Analog)
24	+5 Volt Monitor		Upper Dome Temp. (Analog)
25	Reference Cone Temp.		-15 Volt Monitor (Analog)

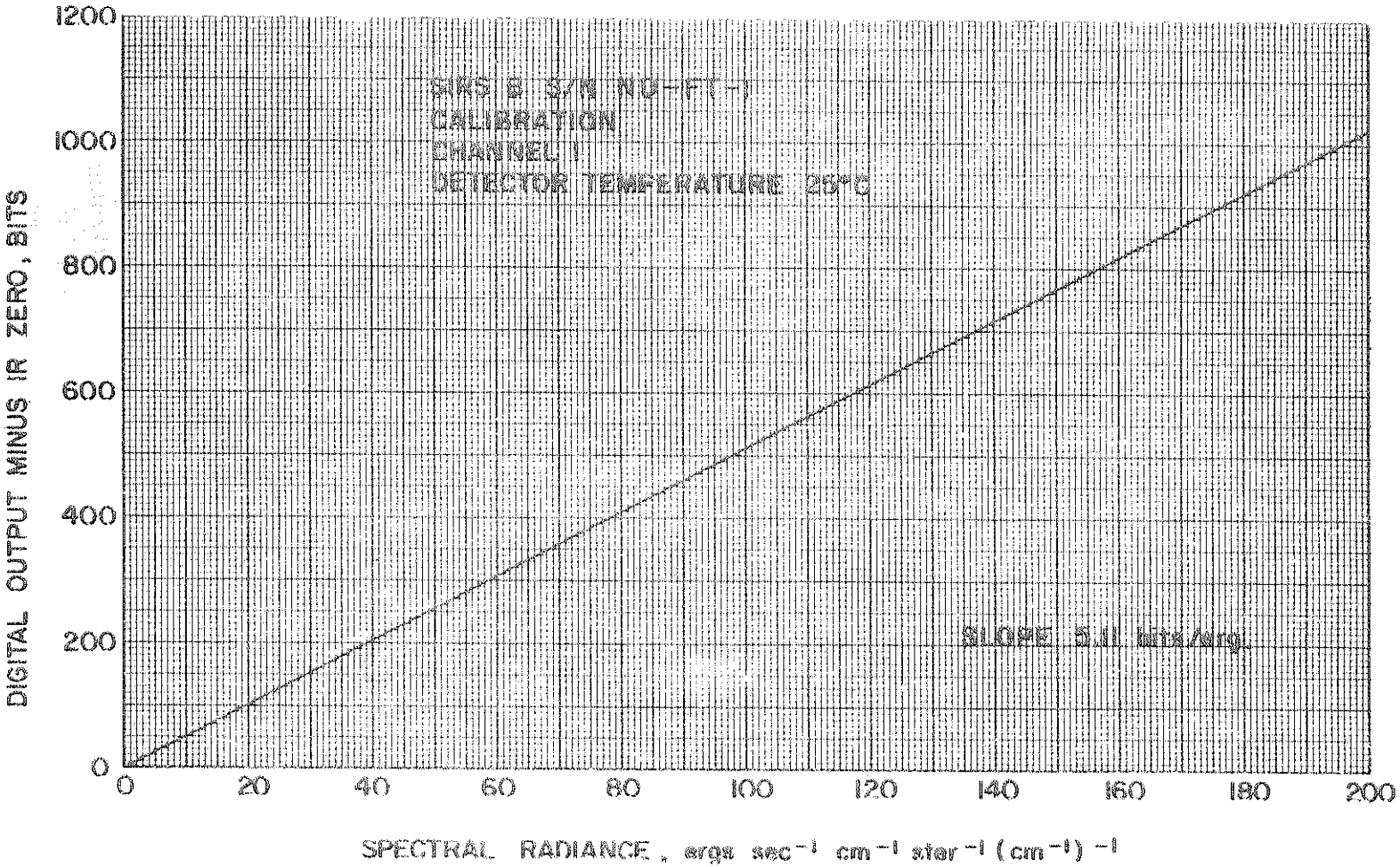

Figure 5-5. Channel 1 (899.0 cm^{-1}) Calibration Curve

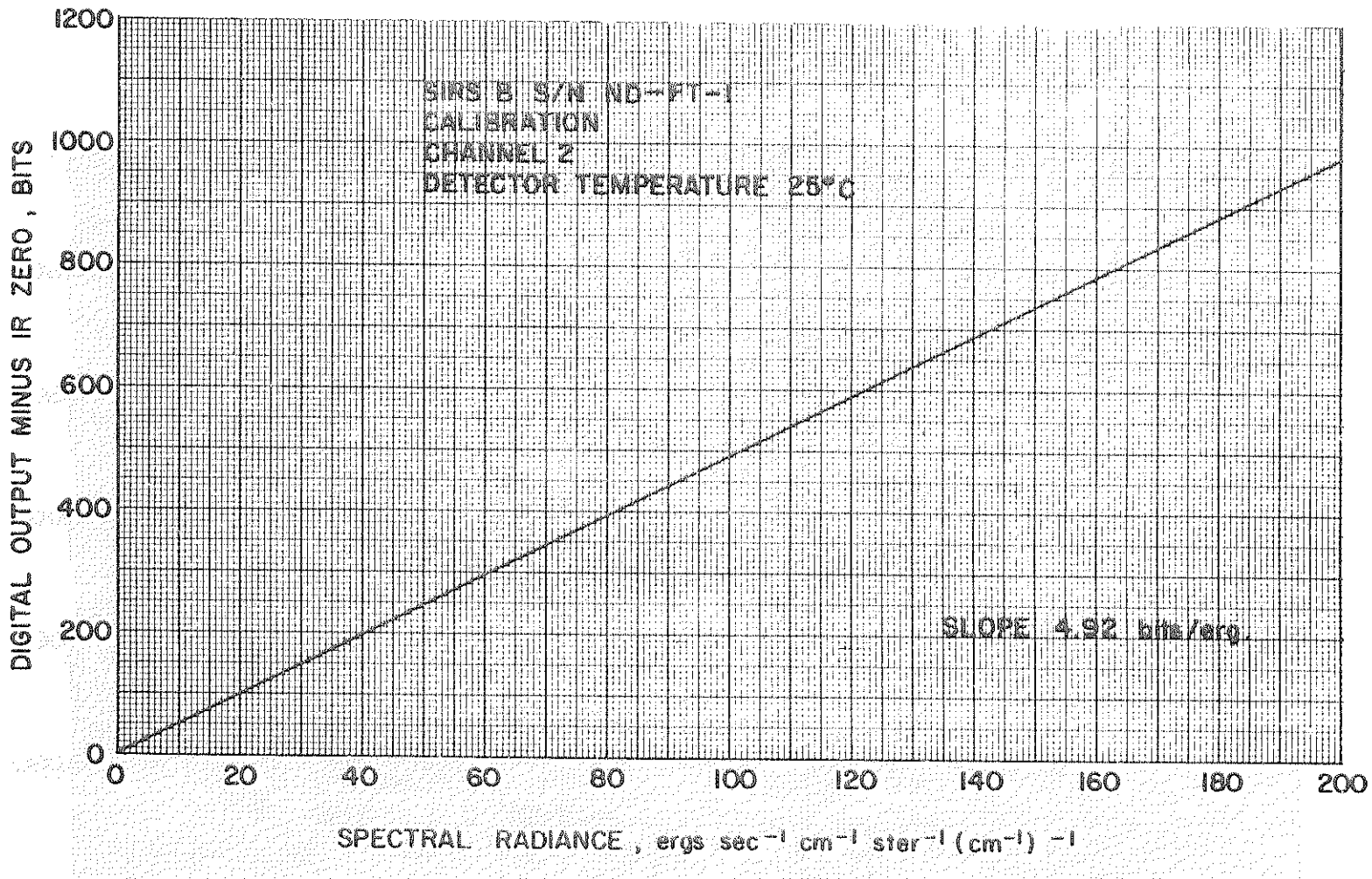

Figure 5-6. Channel 2 (750.0 cm^{-1}) Calibration Curve

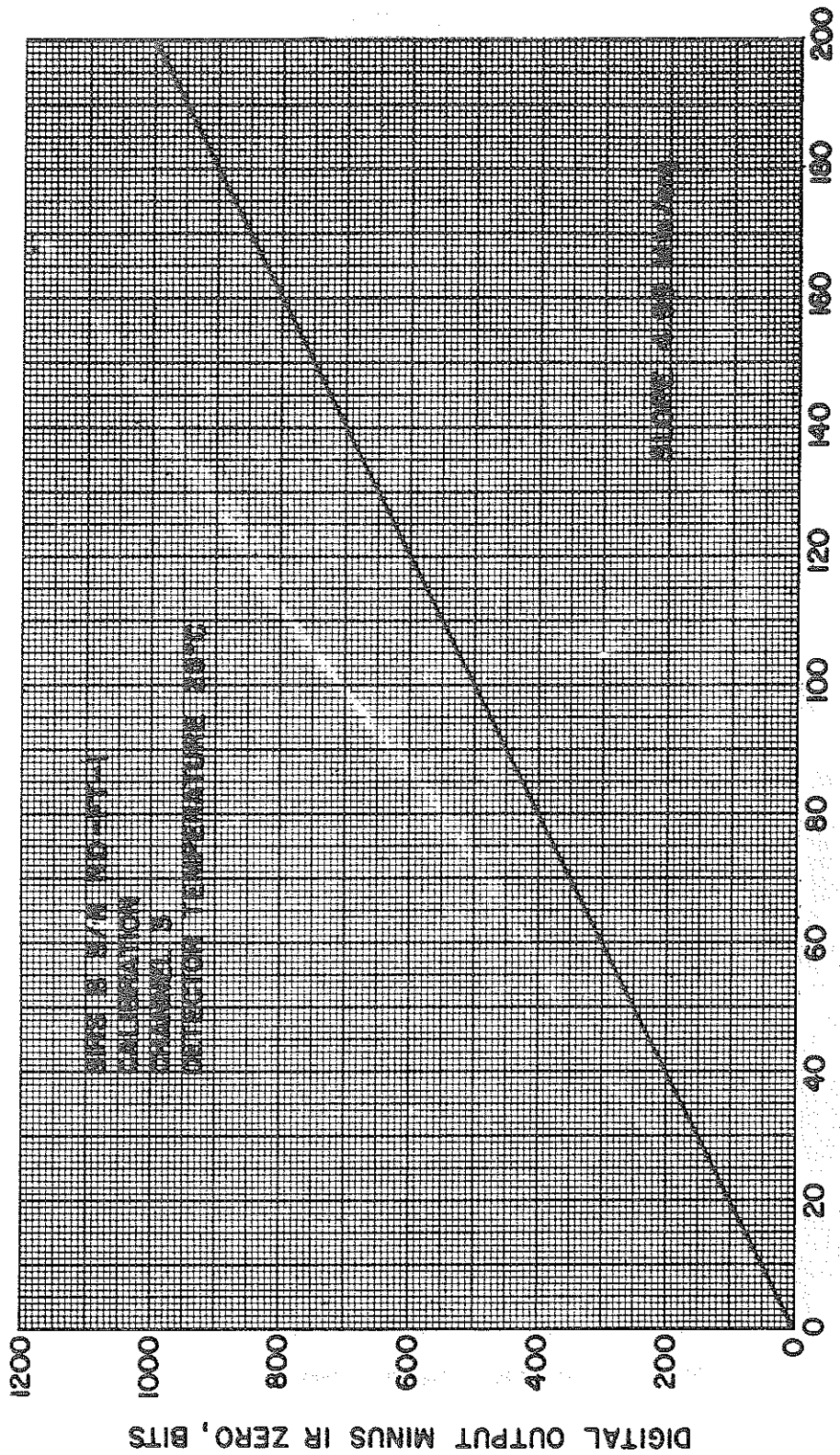

Figure 5-7. Channel 3 (734.0 cm^{-1}) Calibration Curve

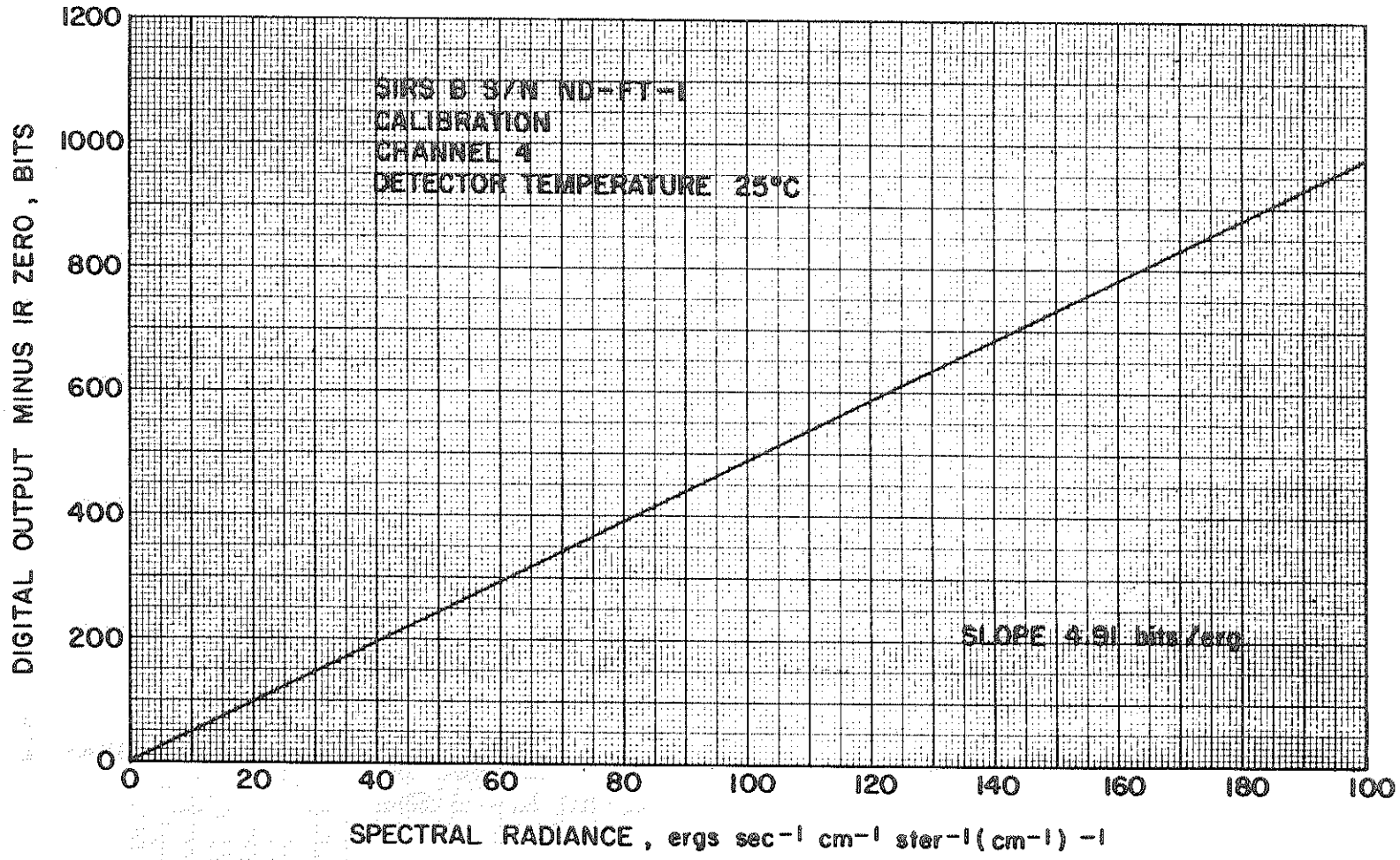

Figure 5-8. Channel 4 (709.0 cm^{-1}) Calibration Curve

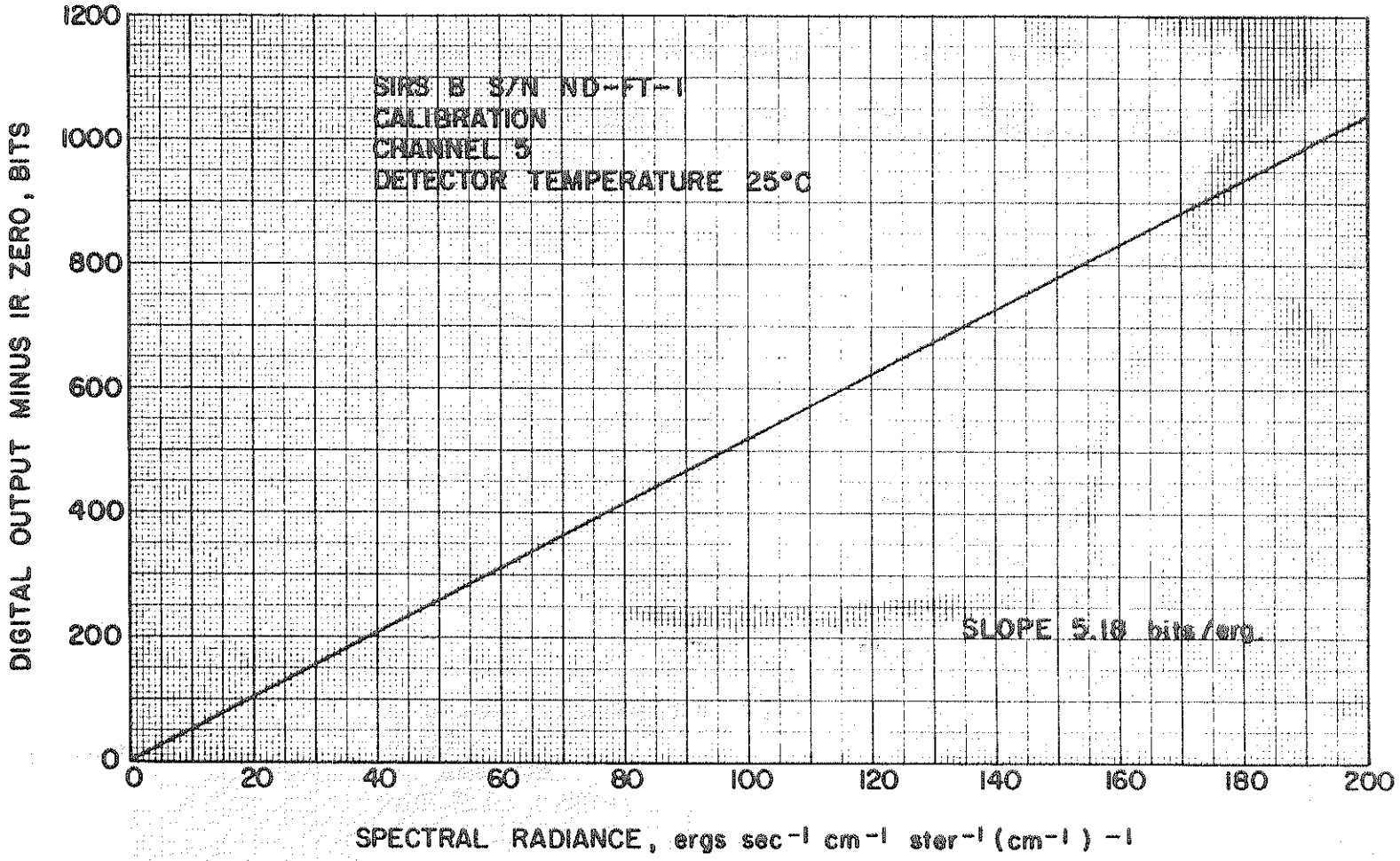

Figure 5-9. Channel 5 (701.0 cm^{-1}) Calibration Curve

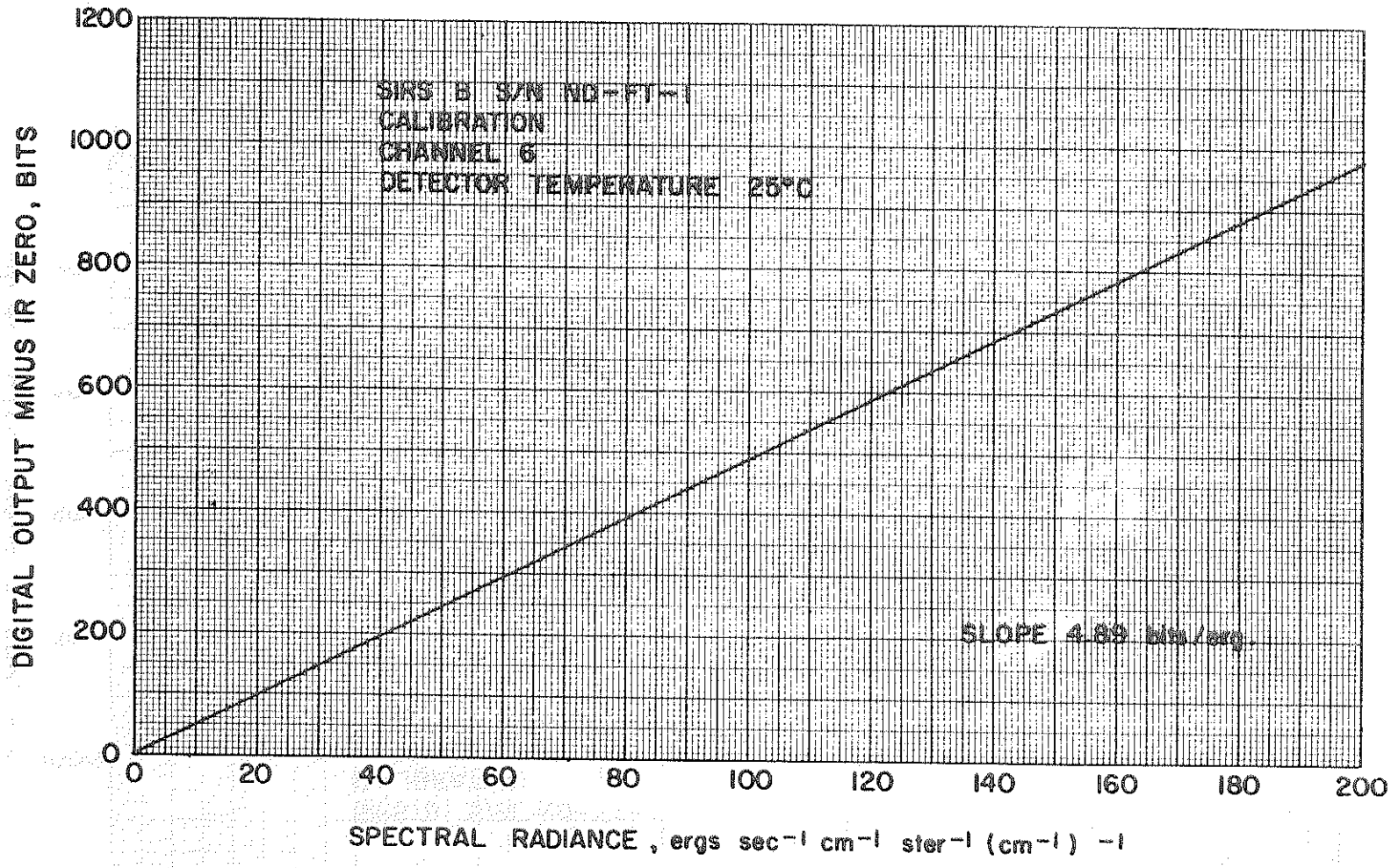

Figure 5-10. Channel 6 (692.0 cm^{-1}) Calibration Curve

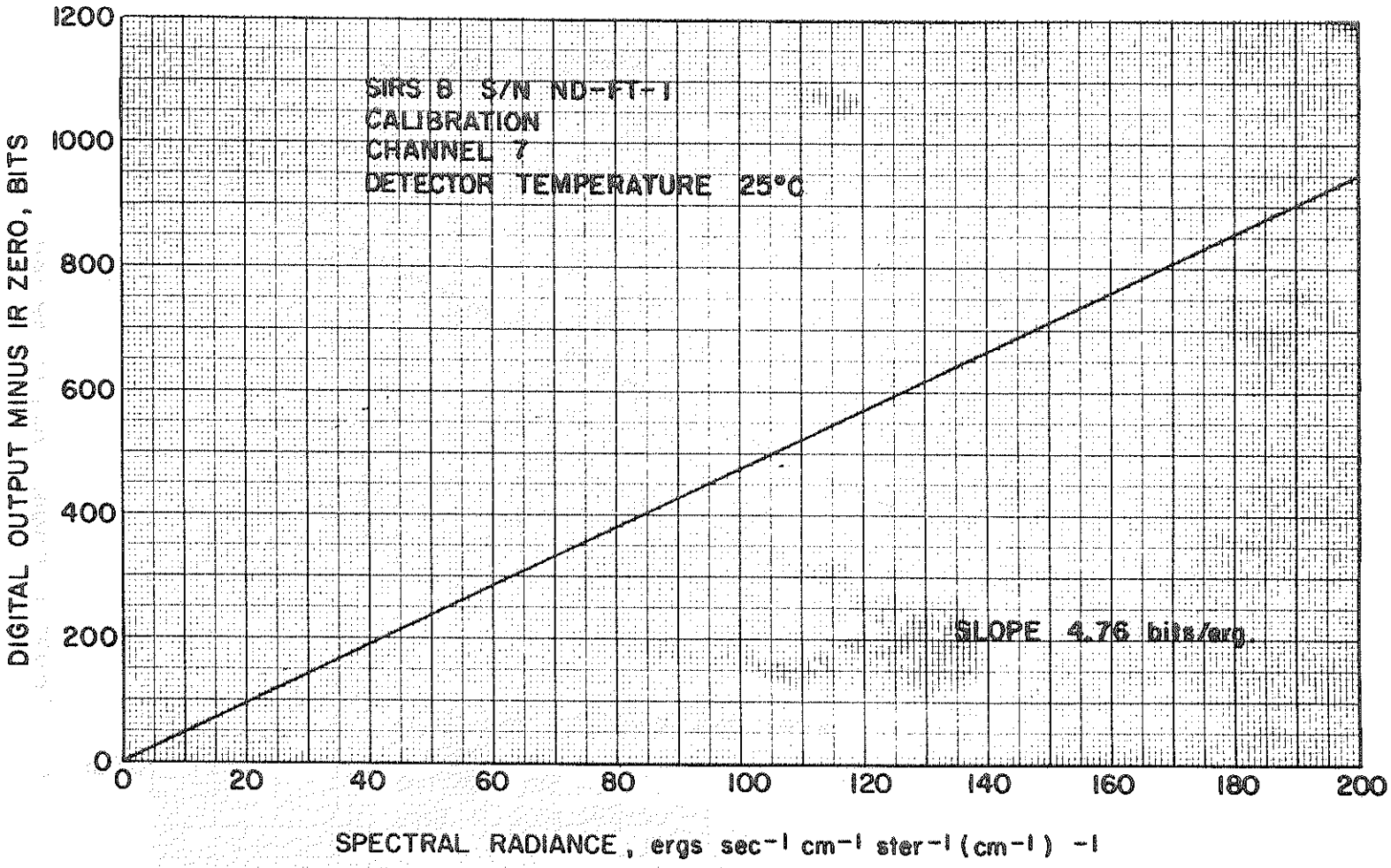

Figure 5-11. Channel 7 (679.8 cm^{-1}) Calibration Curve

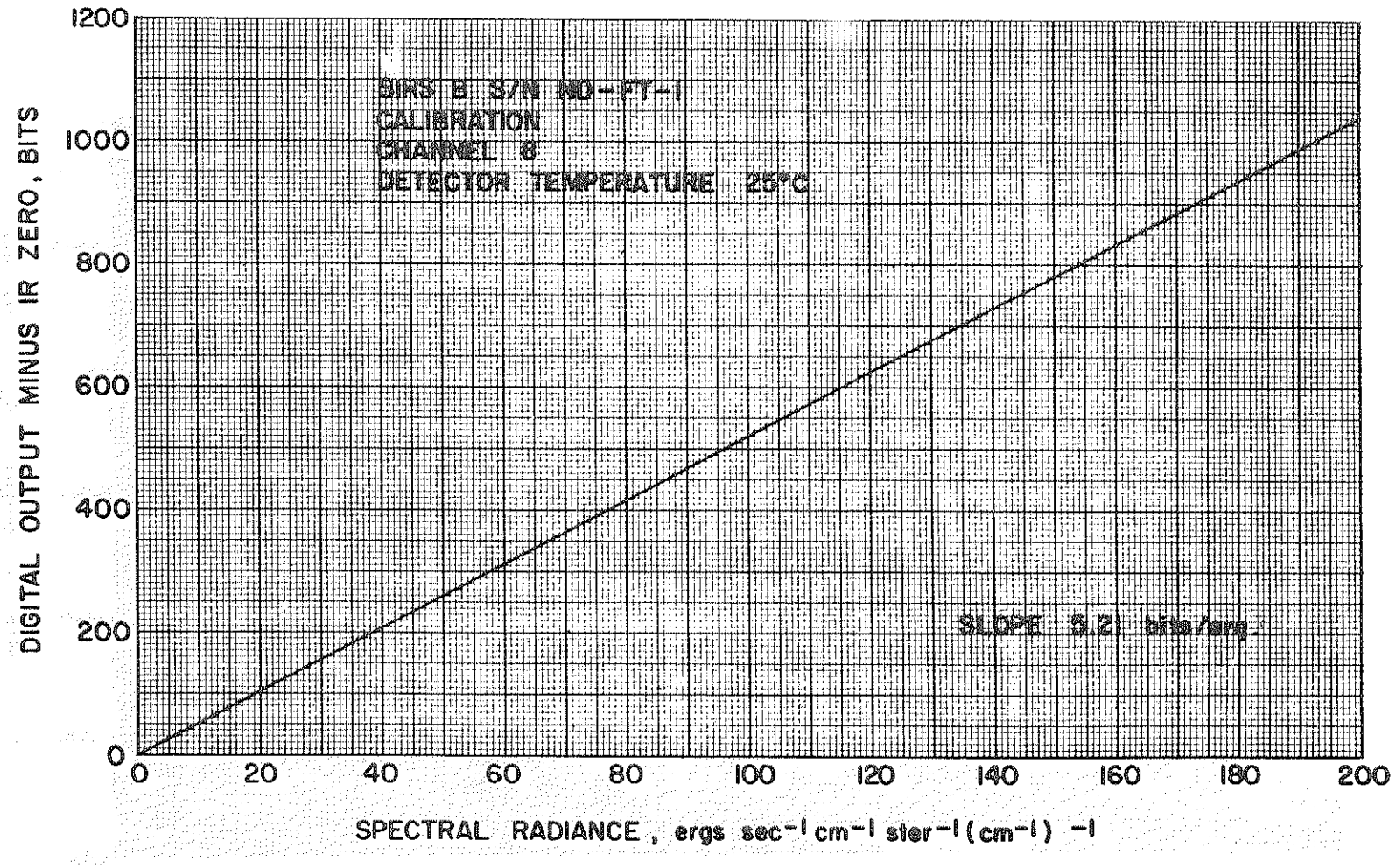

Figure 5-12. Channel 8 (668.7 cm^{-1}) Calibration Curve

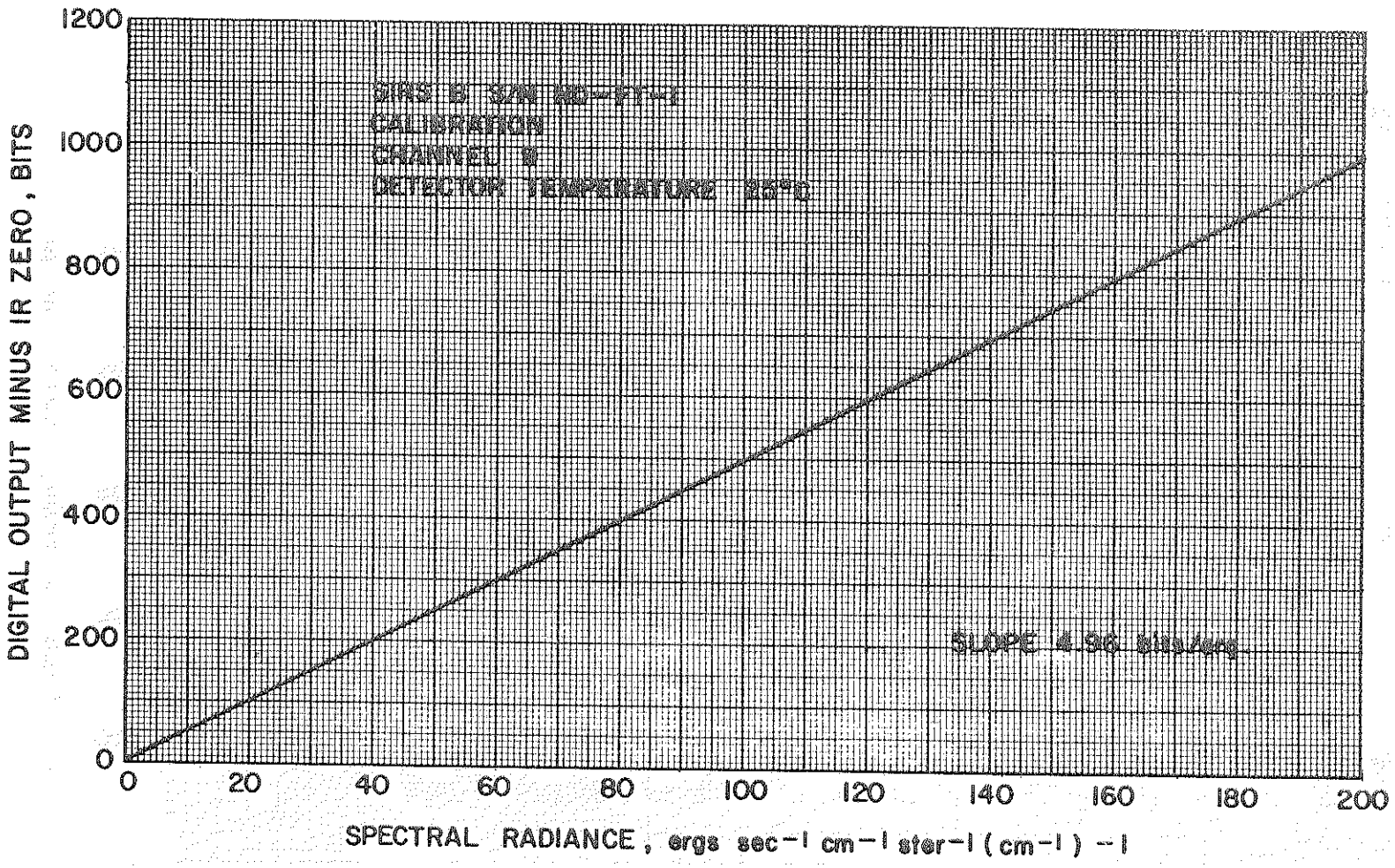

Figure 5-13. Channel 9 (531.5 cm^{-1}) Calibration Curve

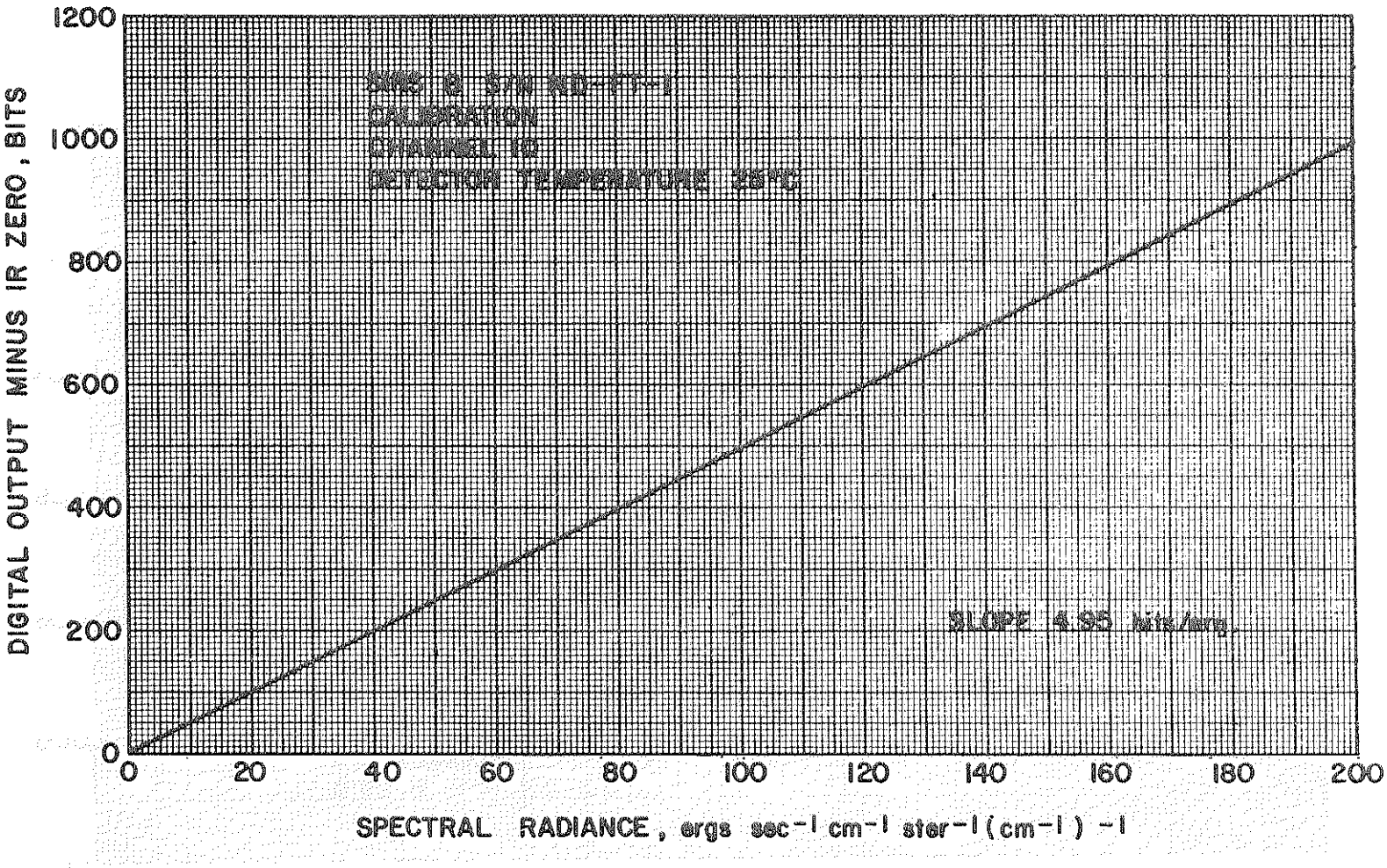

Figure 5-14. Channel 10 (436.5 cm^{-1}) Calibration Curve

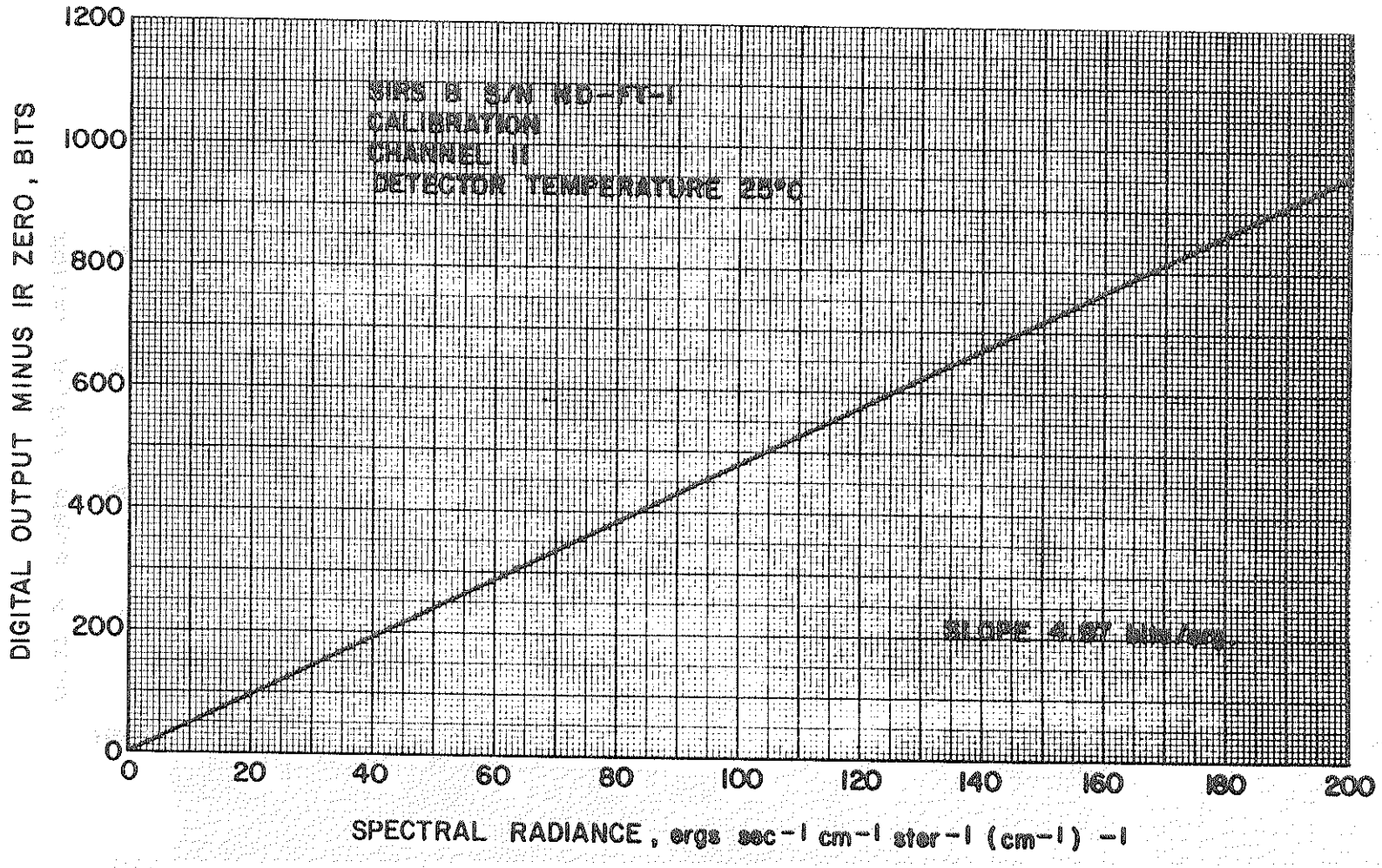

Figure 5-15. Channel 11 (425.5 cm^{-1}) Calibration Curve

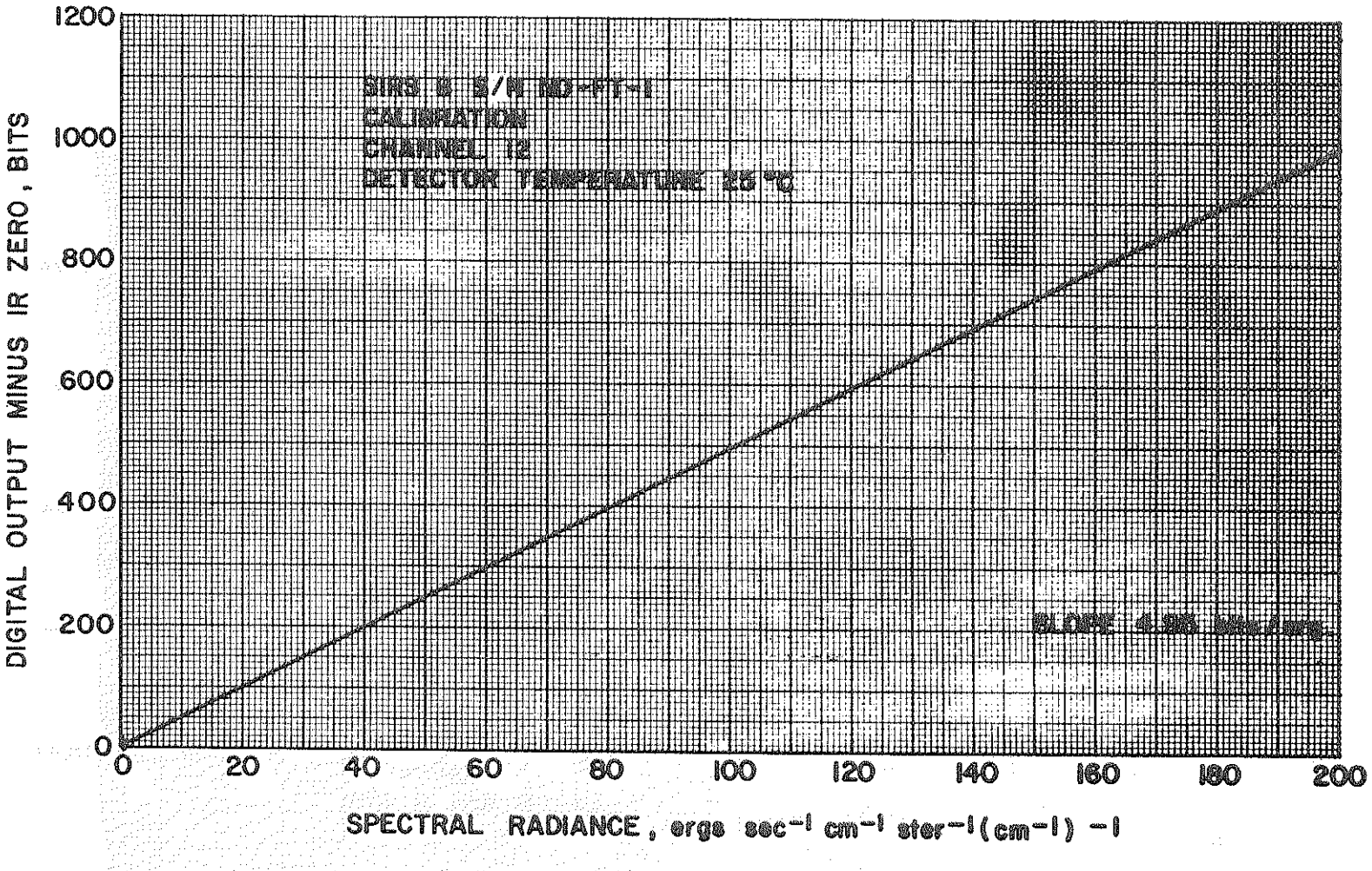

Figure 5-16. Channel 12 (291.5 cm^{-1}) Calibration Curve

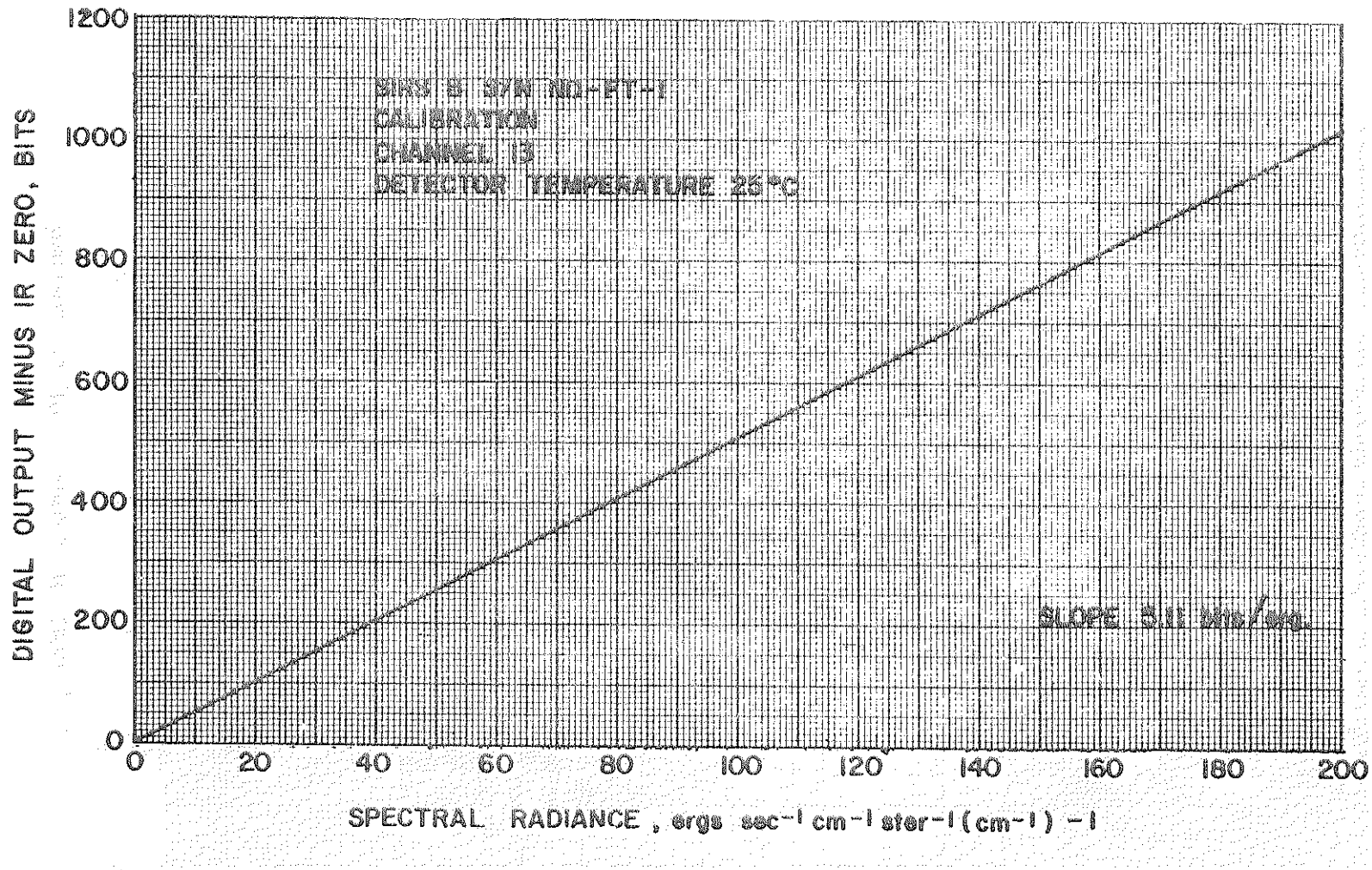

Figure 5-17. Channel 13 (302.0 cm^{-1}) Calibration Curve

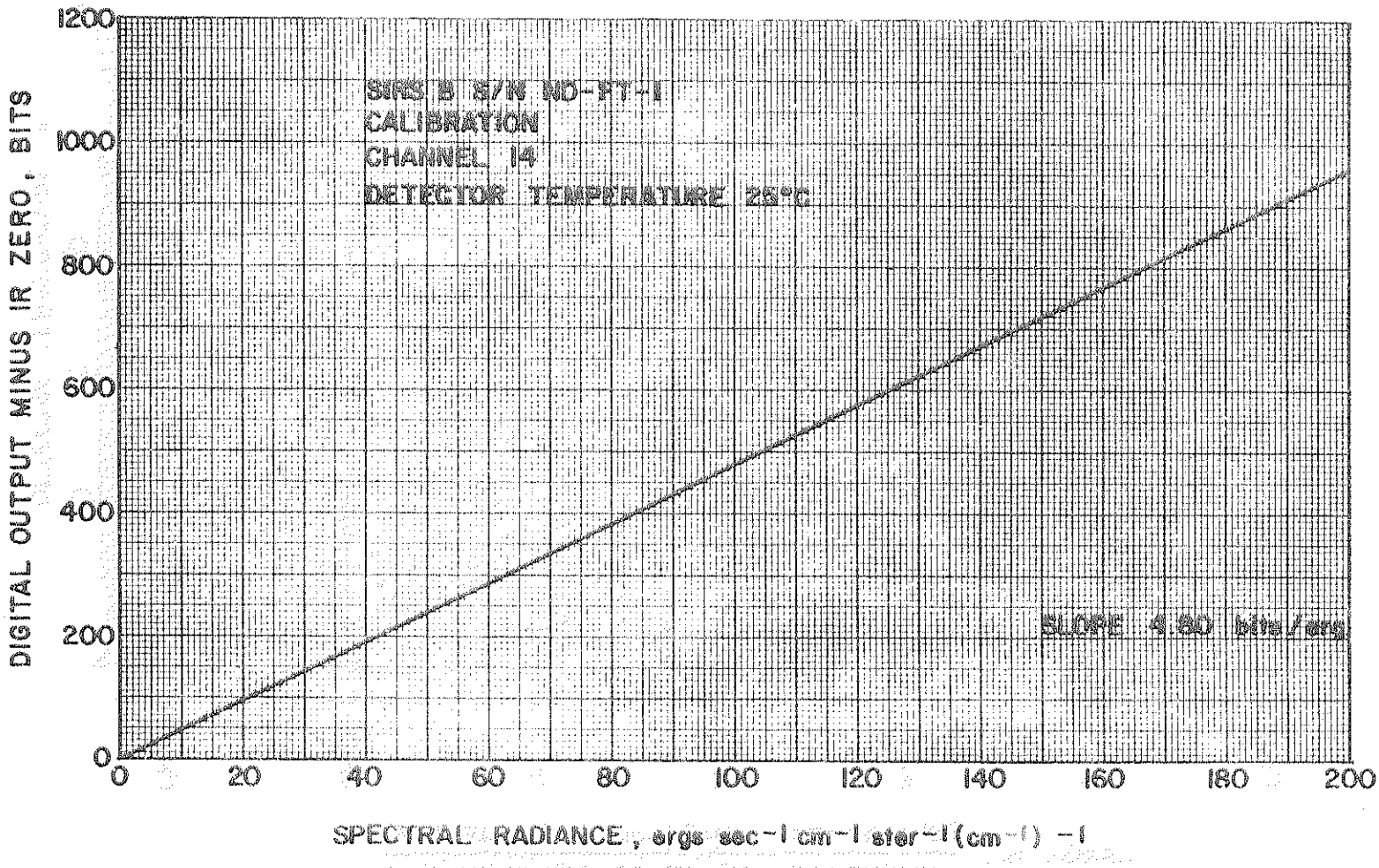

Figure 5-18. Channel 14 (280.0 cm^{-1}) Calibration Curve

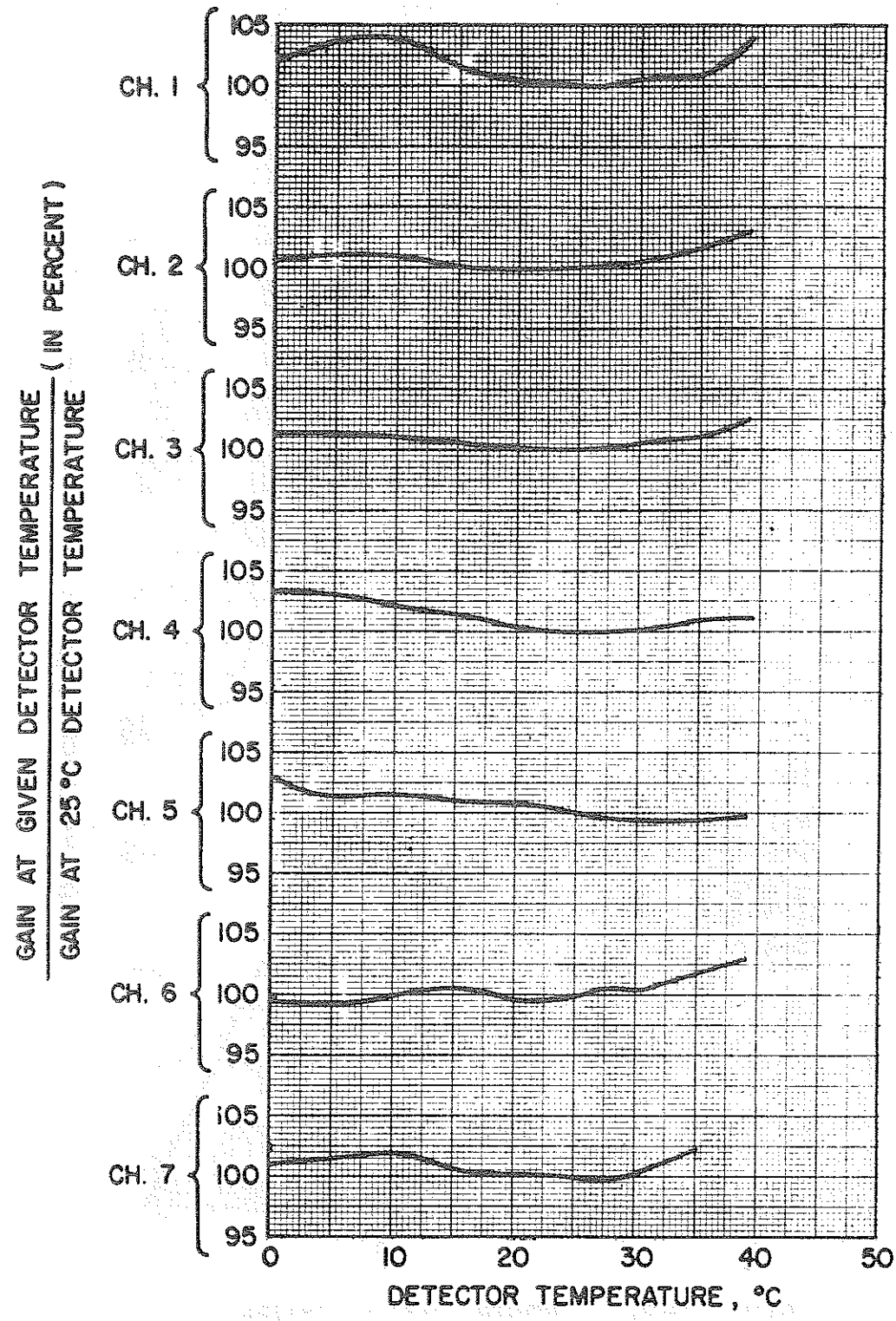

Figure 5-19. Flight Model Gain Compensation vs Detector Temperature (Channels 1 to 7)

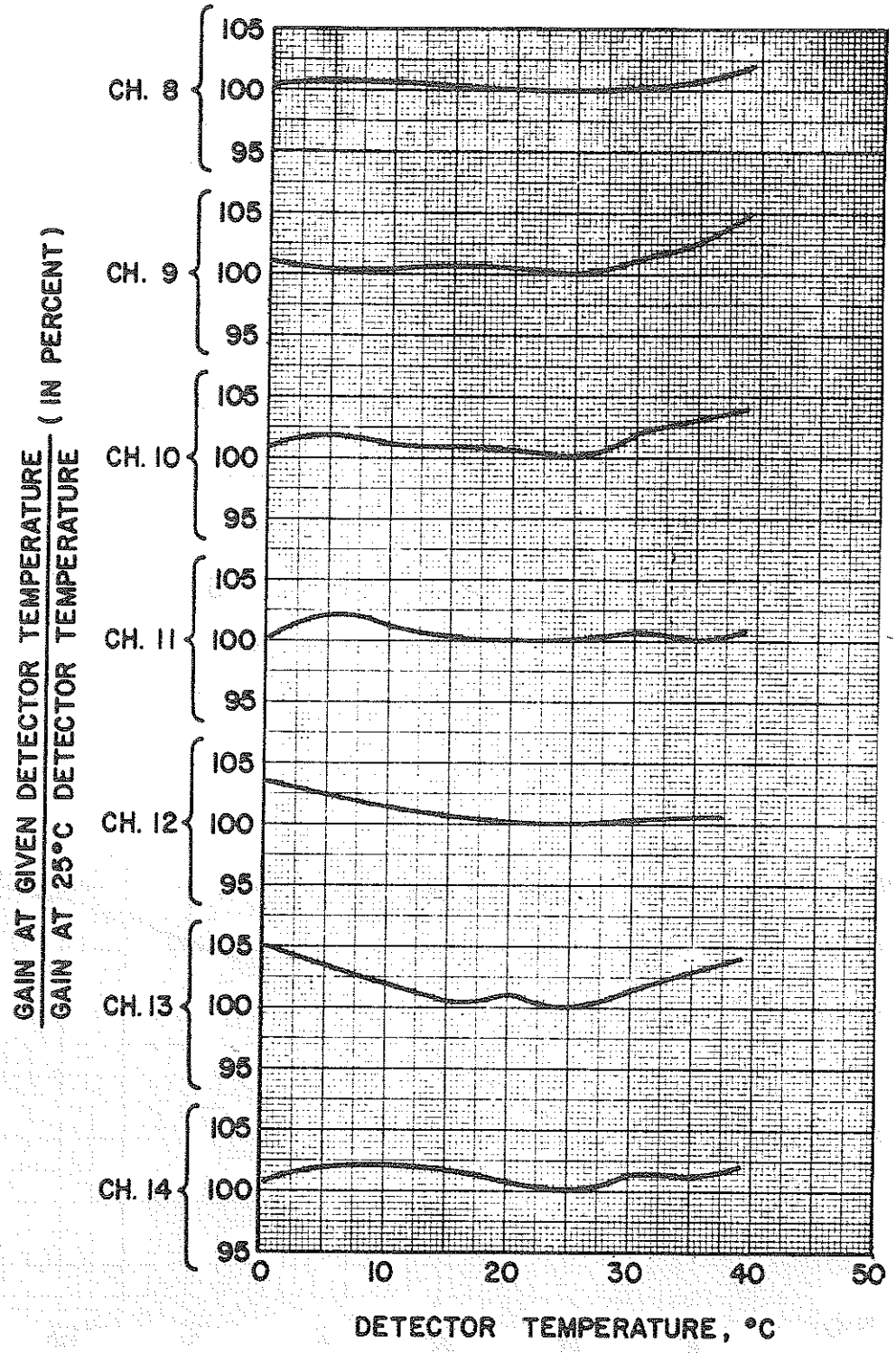

Figure 5-20. Flight Model Gain Compensation vs Detector Temperature (Channels 8 to 14)

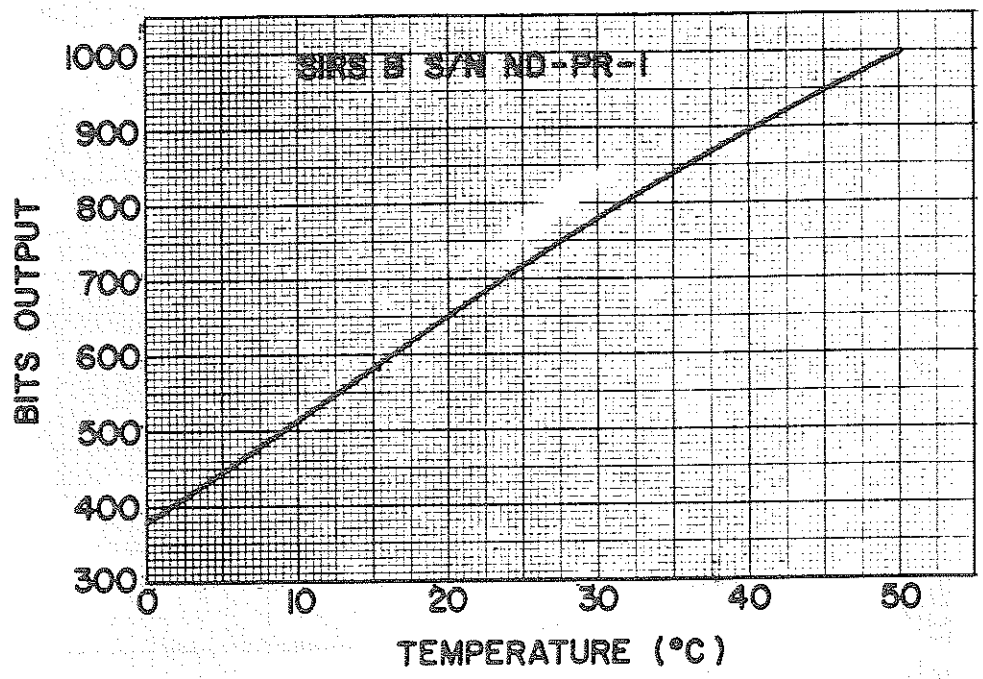

Figure 5-21. Temperature Monitor Thermistor Calibration, Channels 15-23, 25, 26, 28

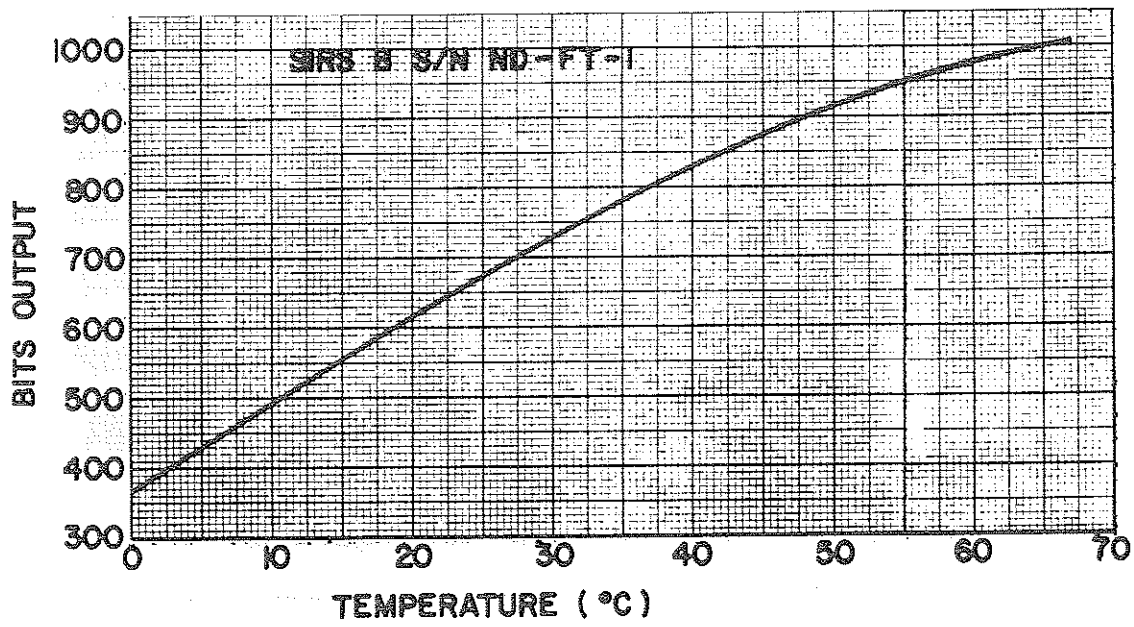

Figure 5-22. Temperature Monitor Thermistor Calibration, Channels 34, 35, 36

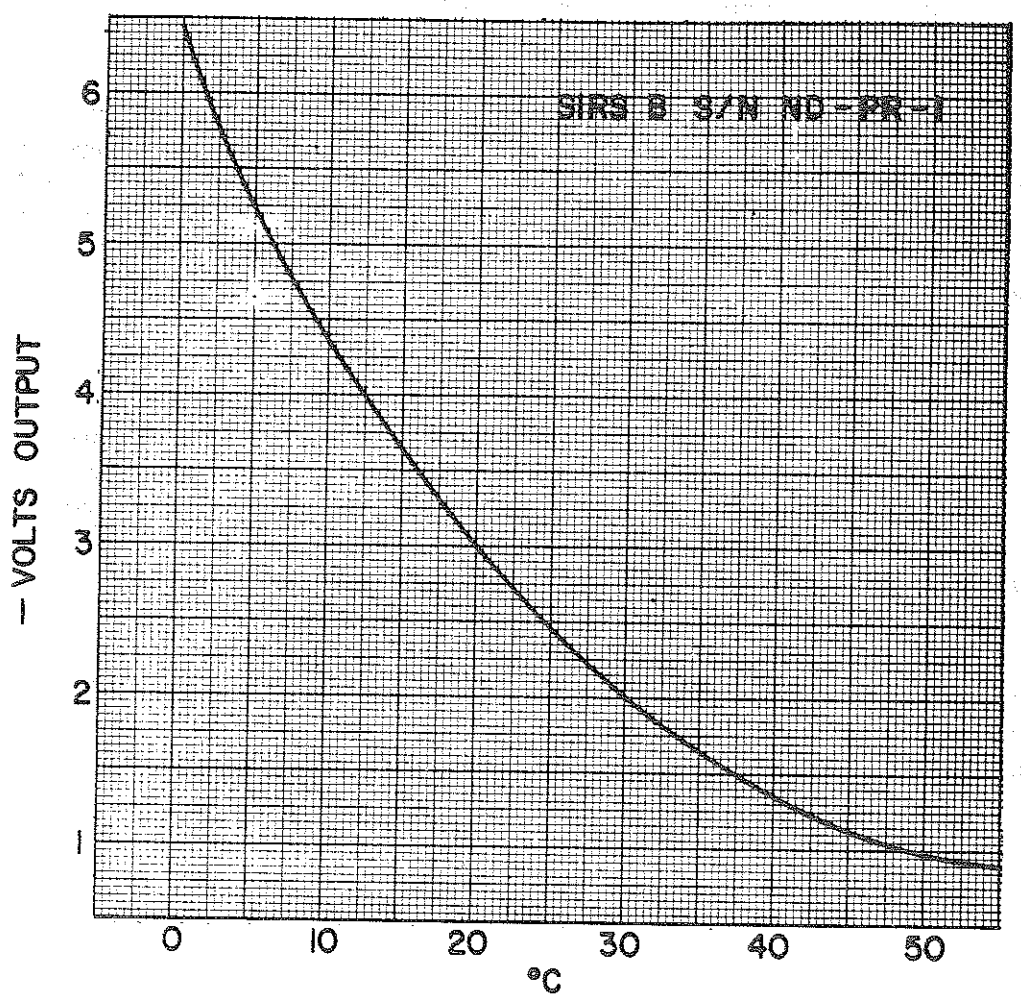

Figure 5-23. Analog Temperature Calibration Curve

5.4 SIRS Data Processing, Archiving and Access

The SIRS data will be transmitted from the Nimbus Data Handling Facility at the Goddard Space Flight Center to the National Environmental Satellite Center on an hourly basis. Digital data stripped from the Sensory Data Tapes will be processed by the CDC 6600 computer at NESC. At that time calibration information will be applied to the data, quality and location of the data will be determined and instrument evaluations and tests will be performed.

Data which pass the screening procedures will be used by a series of programs which compute the vertical temperature profiles for operational use. These profiles will become a part of the meteorological observations analyzed operationally by the National Meteorological Center of the U.S. Weather Bureau. The profiles accepted by the analysis programs become a part of the daily weather data included in the NMC-B3 tape and archived at the National Weather Records Center.

Archival tapes containing radiance values, associated space and time coordinates, and instrument parameters will be furnished to the National Space Science Data Center at Goddard Space Flight Center. These tapes will be produced by the CDC 6600 computer. The data will be furnished to the NSSDC after evaluation of the instrument and data quality. A period of 3 to 6 months will probably elapse after launch before the data tapes will be available.

The detailed format of the SIRS B archival tapes will be presented in Volume 1 of the Nimbus Data Catalog. These tapes will contain the acceptable radiance values from each viewed area, the corresponding space and time coordinates, housekeeping telemetry and other supporting information.

REFERENCES

1. D. Q. Wark and D. T. Hilleary, "Atmospheric Temperature: Successful Test of Remote Probing", Science, Vol. 165, 19 Sept., 1969, pp. 1256-1258.

2. R. Hanel and B. Conrath, "Interferometer Experiment on Nimbus 3: Preliminary Results", Science, Vol. 165, 19 Sept. 1969, pp. 1258-1260.

3. D. Q. Wark, "SIRS, An Experiment to Measure the Free Air Temperature from a Satellite", submitted to Applied Optics, 1970.

4. W. L. Smith and H. M. Woolf, "A Regression Method for Obtaining Real Time Temperature and Geopotential Height Profiles from Satellite Spectrometer Measurements and its Application to Nimbus III 'SIRS' Observations", submitted to Journal of Applied Meteorology, 1970.

5. D. Q. Wark, D. T. Hilleary, H. E. Fleming, W. L. Smith, and J. H. Lienesch, "Atmospheric Temperature Determinations from the SIRS-A on Nimbus III", Proceedings of the Sixth International Symposium on Remote Sensing of Environment, Infrared and Optics Laboratory, Willow Run Laboratories, Institute of Science and Technology, University of Michigan, Ann Arbor, Oct. 1969.

6. Staff, National Environmental Satellite Center, "SIRS: A Major Breakthrough in Meteorological Observation", WMO Bulletin, Vol. XIX, No. 1, January 1970, pp. 2-10.

7. W. L. Smith, H. M. Woolf, and D. Q. Wark, World Weather Watch Planning Report No. 30, Appendix H, World Meteorological Organization, Geneva, 1969.

SECTION 6

THE MONITOR OF ULTRAVIOLET SOLAR ENERGY (MUSE) EXPERIMENT

By
Donald Heath and Raymond D. Westcott
National Aeronautics and Space Administration
Goddard Space Flight Center

6.1 Description of the Experiment

The purpose of the MUSE experiment is to look for changes with time in the ultraviolet solar flux in five bands from 1150 to 3000Å, to measure the solar flux in these regions, and to measure the atmospheric attenuation at these wavelengths as the sensors on board view the setting sun after the spacecraft has crossed the terminator in the northern hemisphere.

The sensors have their maximum response to solar radiation at Lyman α (1216Å) and the solar continuum 1350-1600Å, 1800Å, 2100Å, 2800Å, and 2600-3300Å. The solar flux from 1150 to 3000Å provides the major source of energy input into the upper atmosphere.

An important part of this experiment is the monitoring of solar radiation which produces the photochemical equilibrium that governs the amount and distribution of ozone in the upper stratosphere. S. I. Rasool (Reference 1) has analyzed the effect on the ozone content, and the heating of the upper stratosphere which could result by changes in the solar flux at 2000Å and 2600Å.

The wavelength regions, each with a brief description of its purpose are as follows:

1216Å, (1350-1600Å) — This channel monitors the solar radiation which originates in the chromosphere, and plays a major role in the production of the D-region of the ionosphere and atomic oxygen in the lower thermosphere.

1800Å — Solar radiation at this wavelength comes from the top of the photosphere, and produces the flourescence of O_2 and the production of atomic oxygen through a predissociation effect at the 90 Km level in the atmosphere.

2100Å — Photospheric radiance of this wavelength produces the photodissociation of O_2 at the level of the ozone layer via the Herzberg continuum.

2800Å — This channel encompasses the MgII lines at 2795 and 2802Å whose emission cores could account for changes in solar radiation producing the photo-destruction of ozone.

2600Å (2600-3300Å) — Photospheric radiation over a broad wavelength interval encompassing radiation which is responsible for the photodissociation of ozone. Radiation in this wavelength region in conjunction with that seen by the 2100Å sensor determines the photochemical equilibrium of ozone.

The MUSE instrument is shown in Figure 6-1. The appropriate bands of ultraviolet flux enter the photodiodes, producing a current which is measured by an electrometer and digitized by the Nimbus VIP system. Simultaneously an Adcole solar aspect system measures the angle of incidence of the solar rays and transmits its digital information to the VIP system. The VIP data are stored on magnetic tape and transmitted on playback to the Data Acquisition Facility (DAF) and retransmitted to the Nimbus Data Handling Facility at GSFC. At the NDHF the VIP data are decommutated and selected housekeeping and MUSE sensory data are processed by a CDC 924 computer to create an IBM-360 compatible Sensory Data Tape (SDT) for final data processing. The MUSE instrument has only an in-flight electrical calibration sequence, as there are no known suitable ultraviolet sources capable of providing an in-flight optical calibration.

6.2 Sensors

The sensors are vacuum photodiodes which were fabricated by EMR Photoelectric, Division of Weston Instruments, Inc. All except the shortest wavelength sensor have semi-transparent photocathodes which are deposited on an Al_2O_3 window. The 1216Å sensor utilizes a solid tungsten cathode.

The spectral regions of the sun to which three of the sensors respond (1216Å, 1800Å, and 2600Å) are determined by filter transmittance on the short wavelength side, while the long wavelength cut-off is produced by varying degrees of "solar blindness" of the photocathode materials. Two of the sensors (2100Å and 2800Å) use interference filters fabricated by Baird Atomic for the spectral isolation while the "solar blindness" of CsTe is used to suppress the longer wavelength radiation which is passed by the filter.

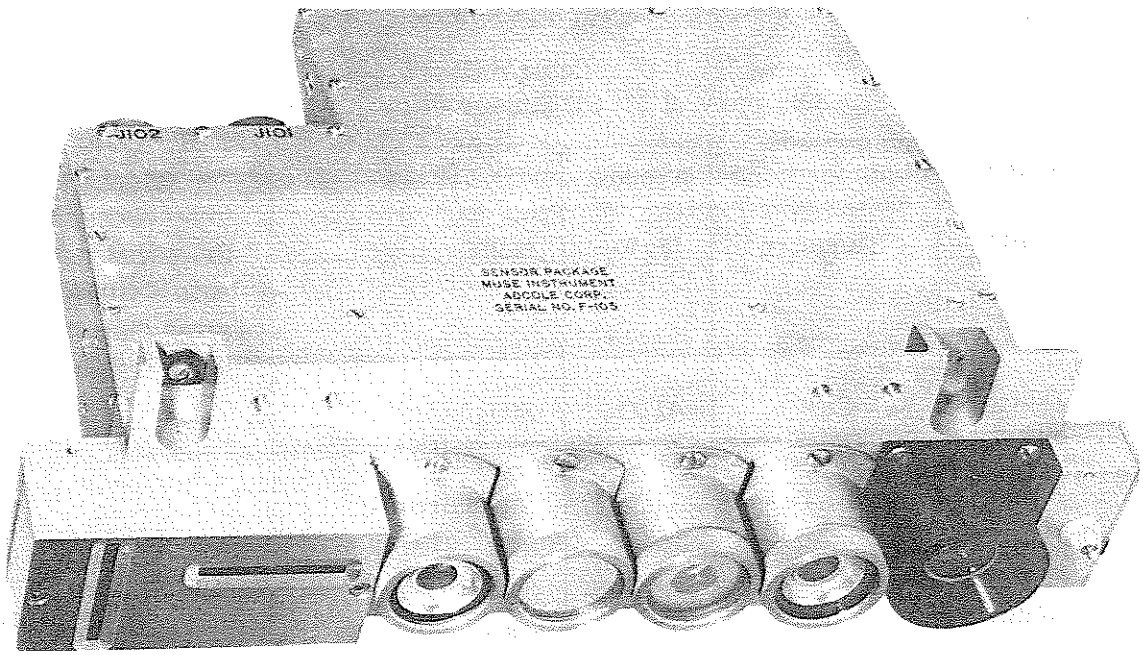

Figure 6-1. MUSE Sensor Package

A summary of the characteristics of the five channels is given in Table 6-1. The final sensor calibration curves and characteristics will be included in the first Nimbus IV monthly Catalog.

The sensors nominally called 1216Å, 1800Å, and 2600Å are identical to those currently operating on Nimbus III, while the sensors 2100Å and 2800Å, utilizing interference filters, are new and replace the two which malfunctioned on Nimbus III.

The character of the interference filters centered at 2100Å and 2800Å change with the angle of incidence of solar radiation. The parameters which change are the transmittance, wavelength of peak transmittance, and the equivalent width or the full width at 1/2 maximum transmittance (FWHM). A summary of these characteristics is contained in Figures 6-2 and 6-3. The change of transmittance and equivalent width with angle of solar illumination are shown in Figure 6-2 and the corresponding shift in wavelength of maximum transmittance are given in Figure 6-3.

Table 6-1
Summary of MUSE Sensor Characteristics

Sensor	Photocathode	Window	Filters	Remarks
1216Å	Tungsten	MgF_2	None	Principal response is to Lyman-α and solar continuum 1350-1600Å
1800Å	CuI	Al_2O_3	SiO_2 Al_2O_3(G)*	
2100Å	CsTe	Al_2O_3	Interference Neutral Density Al_2O_3(G)*	
2600Å	CsTe	Al_2O_3	Calcite (C_aCO_3) Neutral Density Al_2O_3(G)*	Principal Response (2600-3300Å)
2800Å	CsTe	Al_2O_3	Interference Neutral Density Al_2O_3 (G)*	

* G refers to a vacuum-deposited metal grid on the outer element.

The current output of a sensor is related to the solar flux incident normal to the photocathode by the formula:

$$I_{(amps)} = \sum_i f_0(\lambda_i)\, \Delta\lambda_i\, AS(\lambda_i)\, 1.6 \times 10^{-19} \qquad (1)$$

Where $f_0(\lambda_i)$ is the solar flux at the top of the atmosphere in quanta/cm^2-sec-Å at λ_i

$\Delta\lambda_i$ is the wavelength interval centered at λ_i

A is the area of the photocathode which is illuminated

$S(\lambda_i)$ is filter transmittance × quantum efficiency at λ_i

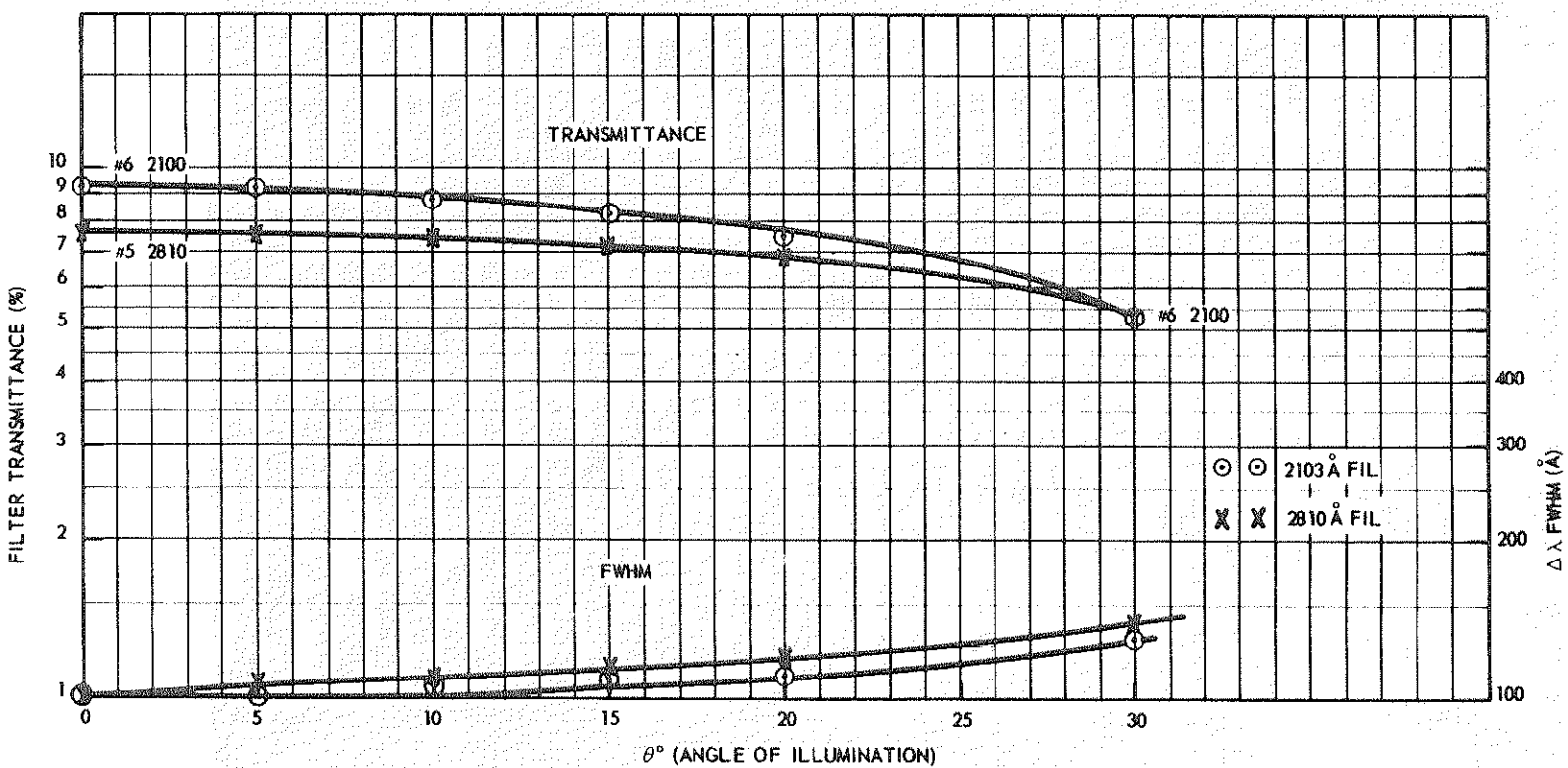

Figure 6-2. Change of Transmittance and Equivalent Width with Angle of Solar Illumination

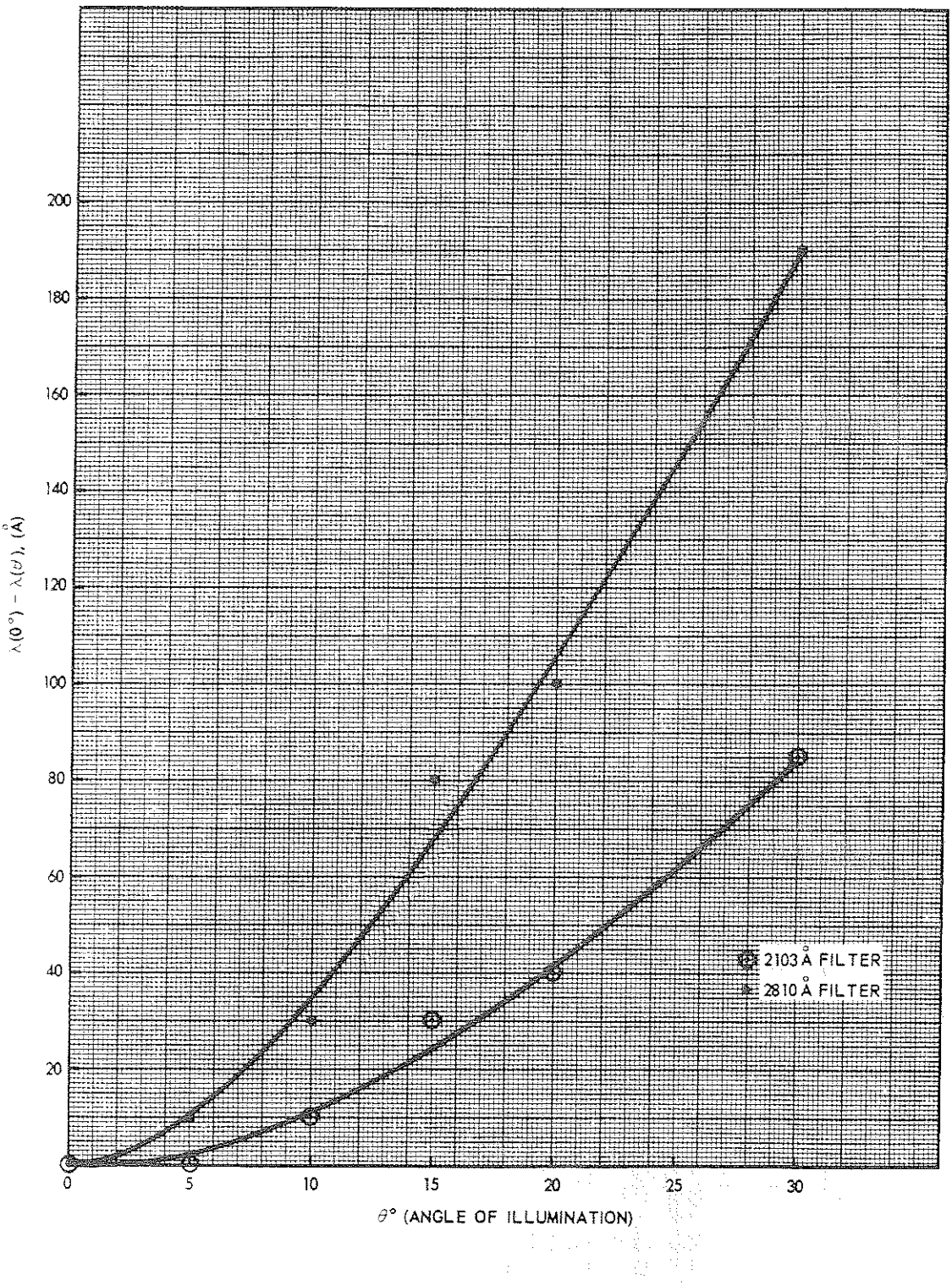

Figure 6-3. Shift in Wavelength of Maximum Transmittance

One must assume a distribution of solar flux with wavelength. If the measured sensor current is different from that calculated with Equation 1, one can determine the solar flux at the effective wavelength of the sensor by the relationships:

$$f_0(\bar{\lambda}) = f(\bar{\lambda})_{assumed} \frac{I_{meas}}{I_{calc}} (\text{quanta/cm}^2\text{-sec-Å}) \quad (2)$$

$$\bar{\lambda} = \sum_i R(\lambda_i)\,\lambda_i \Big/ \sum_i R(\lambda_i) \quad (3)$$

Where $R(\lambda_i)$ = (Filter transmittance at λ_i) × (Quantum efficiency of photocathode at λ_i) × (Solar flux in specified interval centered at λ_i in quanta/cm^2-sec.)

To convert Equation 2 to ergs/cm^2-sec-Å multiply by the energy/quanta $\left(E = \frac{hc}{\lambda}\right)$

The instrument is housed in an electronics package and a sensor package, located in the rear of the Nimbus spacecraft. The field of view of the sensors is about 90° with the center of the field of view parallel to the spacecraft velocity vector. Solar acquisition will, therefore, begin at 45° prior to the earth day/night terminator and completely cease at the satellite day/night transition. Just prior to the day/night transition, the solar flux will be partially occulted by the earth's atmosphere.

The instrument can operate in either the automatic or manual mode. In the automatic mode, the instrument has a basic 48 second cycle and a D/A conversion rate of 2 samples per second. In the manual mode, the instrument will lock on a selected sensor and will remain there (with 2 samples per second) until the instrument is commanded back into the automatic mode.

The following description of the instrument assumes automatic mode operation. Figure 6-4 shows the MUSE analog data output resulting from the internal commutation of the sync pattern, electrometer calibration, and sensor outputs.

A block diagram of the instrument is shown in Figure 6-5. The five radioactive current sources and the five ultraviolet sensors are sequentially switched into a four decade automatic range switching electrometer. The analog output, along with 3 bits of range information, is sampled twice per second by the PCM system.

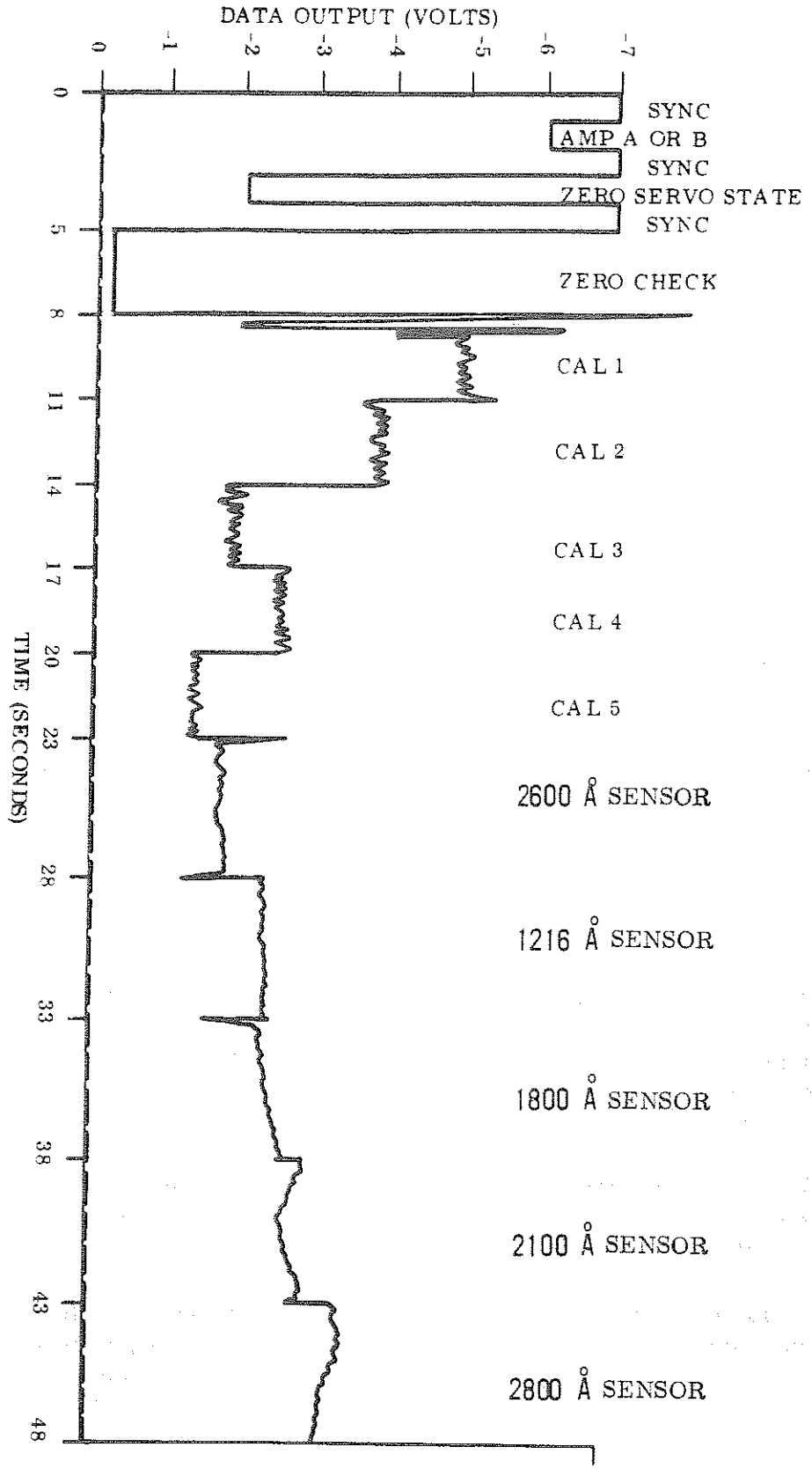

Figure 6-4. Typical MUSE Experiment Cycle in the Automatic Mode

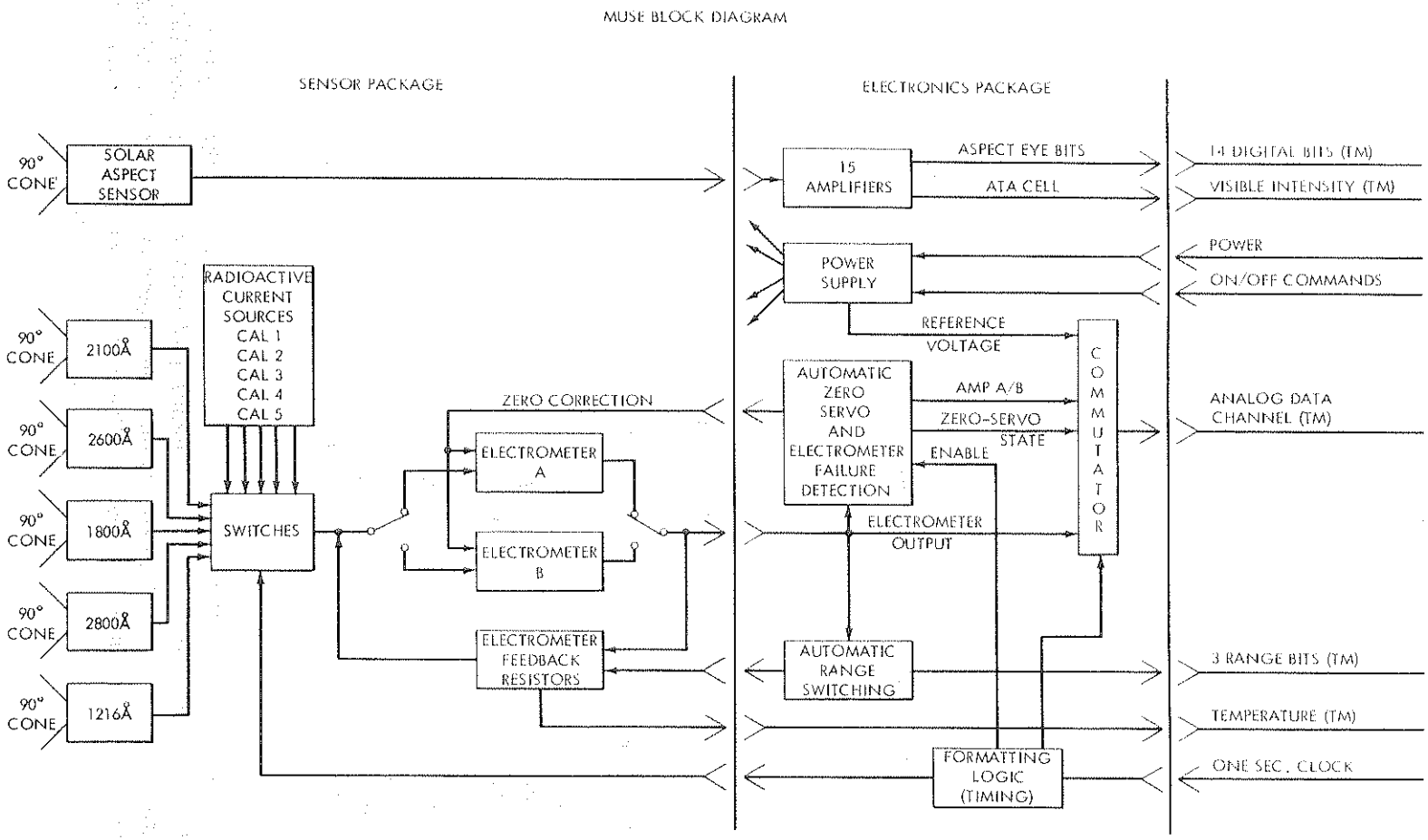

Figure 6-5. MUSE Block Diagram

The input current to the electrometer may be calculated using the following equation and Table 6-2:

$$I = M(V_{tm} - V_0 + V_b) - I_0 \quad (4)$$

Where I = electrometer input current

M = slope of calibration curve for a particular decade

V_{tm} = electrometer output voltage

V_0 = 0.20 volts = electrometer output voltage with no input current (zero check)

V_b = 5.40 volts, which is a level removed from the analog output when the range falls in the upper half of a decade

I_0 = offset current due to ionizing radiation (assumed to be negligible)

Table 6-2
Conversion of Telemetry Voltage to Sensor Current

Range Bits	Vb (volts)	M (amps/volt)
000	0.00	0.836×10^{-11}
100	5.458	0.836×10^{-11}
010	0.00	0.828×10^{-10}
110	5.458	0.828×10^{-10}
001	0.00	0.750×10^{-9}
101	5.458	0.750×10^{-9}
011	0.00	0.881×10^{-8}
111	5.458	0.881×10^{-8}

During the first 8 seconds of the MUSE 48 second cycle, the electrometer is preprogrammed to the least sensitive decade (not indicated with range bits) and an automatic zero servo is enabled. Should the electrometer output voltage (zero check) exceed 0.250 volts or fall below 0.150 volts the zero will be digitally adjusted in 0.050 volt increments to bring the zero within these limits. If the range

of adjustment is no longer sufficient for zero correction, a redundant electrometer will be automatically switched into the circuit and automatically rezeroed. The redundant electrometer may also be switched by an external command.

Due to the high orbital altitude of the Nimbus spacecraft, considerable work was done to determine what effects the high energy particles in the Van Allen belts would have on the transmittance of the optical filters and the quantum efficiencies of the photocathodes. These results are contained in the papers of Heath and Sacher, Sacher, and Heath and McElaney (References 2, 3, 4).

A brief summary of the MUSE/NIMBUS III performance can be found in the paper by Heath (Reference 5).

6.3 Optical Calibration

The measurement of the quantum efficiencies of the photocathodes was made using the standard technique of calibrating a freshly deposited film of sodium salicylate in front of a photomultiplier against a calibrated nitric oxide ionization cell at H-Lyman alpha. The calibration was checked in the long wavelength region by calibrating the sodium salicylate — photomultiplier against a thermopile. It was assumed that the response of the sodium salicylate was uniform between 1216Å and 2537Å. This in turn was used to calibrate two standard diodes, tungsten and CsTe which are used as standard detectors for the calibration of the flight sensors.

The filters were calibrated by measuring their transmittances as a function of wavelength under vacuum.

The 3rd and 4th samples of the 48 second cycle indicate which electrometer is in use. Electrometer A is represented by 5.90 ± 0.20 volts and electrometer B by 2.80 ± 0.15 volts.

The 7th and 8th samples of the 48 second cycle indicate the state of the zero servo. The zero servo corrects amplifier drift of the input MOS-FET's (Metal Oxide Field Effect Transistor) in 64 steps of 0.025 volts referred to the electrometer input. A step of 0.025 volts on the electrometer input will cause a 0.050 volt change in the electrometer output (verified by zero check). The zero servo state is indicated by a voltage of 0.10 to 6.3 volts in 64 levels corresponding to the 64 input levels available for adjustment. Initially, the zero servo is set at mid-range for launch (2.9 volts).

Samples 11 through 16 of the cycle indicate the zero check. This value should be between 0.150 and 0.250 volts at all times.

Samples 17 through 46 contain calibration data for the gain settings of each decade of the electrometer. Because of the electrometer and current-source time constants, the first 4 samples of Cal. 1 do not indicate the final correct value and should not be used in gain corrections. The first two samples of Cal. 2 through Cal. 5 should likewise be rejected. The statistically random variations in the calibration current are due to the low rate of alpha particle production within the Americium 241 constant current sources. It is, therefore, mandatory that one obtain a large number of samples and average them before attempting to correct the values of "M" found in Table 6-2.

The certified currents for these sources are contained in Table 6-3.

Table 6-3
Calibration Current Sources

Cal. 1	CK 1914-5 #2	6.85×10^{-11}	7/30/68
Cal. 2	NN 1-4	2.98×10^{-10}	6/28/67
Cal. 3	NM 9-11	5.95×10^{-10}	6/28/67
Cal. 4	CK 1913-3 #4	6.46×10^{-9}	7/30/68
Cal. 5	NM 4-14	1.04×10^{-8}	6/28/67

The electrometer decade resistors have a non-linear temperature coefficient. Since the temperature of the internal resistive element cannot be measured, no attempt will be made, at this time, to provide a temperature-dependent gain correction factor.

The 48th through 96th samples indicate the sensor current outputs. Each sensor is switched into the electrometer for five seconds. The first and second samples of each sensor may be higher than the last three samples because of the electronics and sensory time constants. This will have to be determined by data inspection after launch. The sensors are commutated in the following order given in Table 6-4.

The MUSE instrument provides supporting measurements of the solar aspect angle, photodiode temperature and feedback resistor case temperature.

The solar aspect angle is measured using an Adcole Corporation solar aspect sensor. Essentially the aspect sensor measures two orthogonal angles between

Table 6-4
Sensor Commutation

Samples 47 through 56	2600 Å Band
Samples 57 through 66	1216 Å Band
Samples 67 through 76	1800 Å Band
Samples 77 through 86	2100 Å Band
Samples 87 through 96	2800 Å Band

the sun and the normal vector of the MUSE optical axis. Assuming no spacecraft roll or pitch errors and assuming the MUSE optical axis coincides with the spacecraft velocity vector, the solar aspect pitch angle will indicate zero degrees at the day/night terminator. The solar aspect yaw angle measured at the terminator will indicate the angle between the orbital plane and the high noon meridian. The quantization of these angles is 90/128 of a degree with an absolute accuracy of 50/128 of a degree. The aspect angle will be measured correctly only when the "ATA" voltage is below 6.35 volts. When this is the case, the data tapes will indicate "ATA" on.

The photodiode temperature (cathode temperature) is measured by a thermistor located in the 1800Å sensor (middle sensor in Figure 6-1). The thermistor is fastened to the metal housing in the proximity of the photocathode surface of the photodiode.

The feedback resistor case temperature is measured by a thermistor embedded in the teflon block supporting the feedback resistors.

There are three anticipated sources of erroneous signal levels. These are:

1. Ultraviolet flux from the earth's albedo entering the field of view of the sensors.

2. Contamination of sensor surfaces during the launch process.

3. Degradation of optical transmission due to ionizing radiation.

The contribution of the earth's albedo to the total ultraviolet flux is expected to be quite low. The extent of the albedo, if any, may be extrapolated by inspection of the curves of sensor outputs as a function of solar angle of incidence.

6.4 The NMRT-MUSE Archival Tape

The NMRT-MUSE archival tape will be the basic repository for radiation data from the Nimbus Monitor of Ultraviolet Solar Energy (MUSE) experiment. This tape will be available to the scientific community through the National Space Science Data Center within one year after launch of Nimbus IV. The format of the NMRT-MUSE archival tape will be given in the Nimbus IV Catalog.

REFERENCES

1. S. I. Rasool, "Effects of Assumed Changes in the Near Ultraviolet Radiation on the Photochemical Distribution of Atmospheric Ozone and on Heating Rates in the Stratosphere", XII General Assembly of IUGG, August 19-31, 1963.

2. D. F. Heath and P. A. Sacher, "Effects of a Simulated High Energy Electron Space Environment on the Ultraviolet Transmittance of Optical Materials Between 1050 and 3000Å", Applied Optics, 5, 937 (1966).

3. P. A. Sacher, "The Effects of a Simulated Proton Space Environment on the Ultraviolet Transmittance of Optical Materials Between 3000Å and 1050Å", NASA, X-622-G7-416, August 1967.

4. D. F. Heath and J. H. McElaney, "Effects of a High Energy Particle Environment on the Quantum Efficiency of Spectrally Selective Photocathodes for the Middle and Vacuum Ultraviolet", Applied Optics, 7, 2049 (1968).

5. D. F. Heath, "Observations of the Intensity and Variability of the Near Ultraviolet Solar Flux from the Nimbus III Satellite", J. Atmos. Sci., 26, 1157 (1969).

B07747

SECTION 7

THE BACKSCATTER ULTRAVIOLET SPECTROMETER (BUV) EXPERIMENT

By
Donald Heath and Arlin J. Krueger
National Aeronautics and Space Administration
Goddard Space Flight Center
and
C. L. Mateer*
National Center for Atmospheric Research
Boulder, Colorado

7.1 Introduction

The Backscatter Ultraviolet (BUV) System consists of a double Ebert-Fastie monochromator and a parallel filter radiometer. Both channels simultaneously view identical fields in the nadir or, on command, the sun reflected from Lambertian diffuser plates. The monochromator serially monitors 12 selected narrow wavelength bands in the spectral region 2500 to 3400 Å while the radiometer monitors the light in a fixed band centered at 3800 Å. The system is intended for use in measuring atmospheric ozone when the atmosphere is illuminated by the sun, and with restricted capability, with light from the moon. To achieve both objectives the electronic system can operate over a dynamic range approaching 10^9 in input light level.

7.2 Scientific Objectives

The BUV experiment is designed to measure the vertical distribution and total amount of ozone on a global scale. The technique depends on the combined effects of Rayleigh scattering and ozone absorption on ultraviolet light incident on the atmosphere from the sun or moon. The light emerging from the atmosphere, sampled by the BUV, originates in a relatively thin layer at a wavelength-dependent height and is modified by the ozone in and above the layer. Methods used to recover the ozone information from backscattered ultraviolet measurements have been described in the literature (Ref. 1, 2, 3, 4). From the nature of the scattering layers, three distinct types of evaluations are possible:

---

*Present Affiliation, Canadian Meteorological Service, Toronto, Canada

1. The ozone distribution above 30 km can be derived from monochromator measurements at wavelengths less than 3000 Å. The inversion problem is most straightforward at these wavelengths in that primarily single scattering occurs.

2. The total ozone amount can be determined from monochromator measurements at wavelengths longer than 3000 Å (Ref. 5). These wavelengths penetrate deeply in the atmosphere and are subject to multiple scattering.

3. At heights below 30 km the general character of the ozone distribution can be derived from the longer wavelengths (Ref. 6).

In the latter two cases, the light can penetrate to the lower troposphere and the surface where it is scattered or reflected. To compensate for the effects on the ozone calculations (Ref. 7) measurements are made with the photometer at 3800 Å which is outside the ozone absorption band.

7.3 Physical Description

The BUV Subsystem includes two units: a sensor or optical module and an electronics module. The sensor module houses the optical components of the subsystem, the high voltage power supplies, and the first stages of the signal processing electronics. The electronics module houses the bulk of the signal processing electronics plus the circuitry required to support the subsystem. The physical characteristics of each module are summarized in the following list:

Characteristic	Sensor Module	Electronics Module
Location	Bay 9	Bay 8
Component Module	4/4 ABCD (extended)	3/0 ABC
Envelope Dimensions	6 × 8 × 22 in.	6 × 6 × 6.5 in.
Weight	27.6 lb	7.5 lb
Power	3.9 watts	8.1 watts

7.4 Optical Design

The Backscatter Ultraviolet (BUV) Instrument is a satellite-borne scientific instrument designed to measure ozone concentrations in the earth's atmosphere. The experiment is designed to optically measure the backscattered radiation from ozone in a selected wavelength range.

The BUV Instrument, as shown in Figure 7-1, is basically a precision monochromator and a precision photometer with supplementary optical, mechanical, and electronic equipment.

The monochromator has a wavelength range from 2500 Å to 3400 Å. Twelve steps in this range are selected for sample wavelengths. The instrument continuously scans the wavelength range and remains on the selected wavelength steps a certain time interval to take readings.

The BUV Instrument is designed for maximum flux transfer for this wavelength range with the total unwanted radiant flux output (stray light) less than one percent of the wanted spectral radiant flux output; a double monochromator is employed to obtain the desired stray light level.

The wavelength resolution of the monochromator is 10 Å at all wavelengths, using gratings as the dispersive element.

The optical elements in the monochromator render the BUV Instrument selectively sensitive to polarized radiation. A depolarizer is installed in-front of the entrance slit to minimize the polarization effect.

Wavelength calibration is provided by an internal mercury-argon lamp. The 2537 Å mercury line is scanned by the wavelength cam in seven discrete steps. The location of the line with respect to the steps indicates the wavelength accuracy.

Photometric calibration is provided by an internal radioactive phosphor source. The broad emission band of the source covers almost the entire wavelength range of the Instrument. The response of the photomultiplier to the photometric source flux is used to monitor the optical transmission efficiency of the Instrument.

A photometric calibration of the photometer is provided which is identical to the system employed in the monochromator, except for the different wavelength response of the phosphor.

A different means of calibration is provided which uses the sun's radiation. Upon command, diffuser plates for photometer and monochromator are deployed which direct the sun's direct radiation into the Instrument, instead of the backscattered ozone radiation from the earth's atmosphere.

The Instrument is designed to perform trouble-free for a minimum of one year in orbit. Figure 7-2 is a schematic representation of the satellite viewing attitude at various orbital positions.

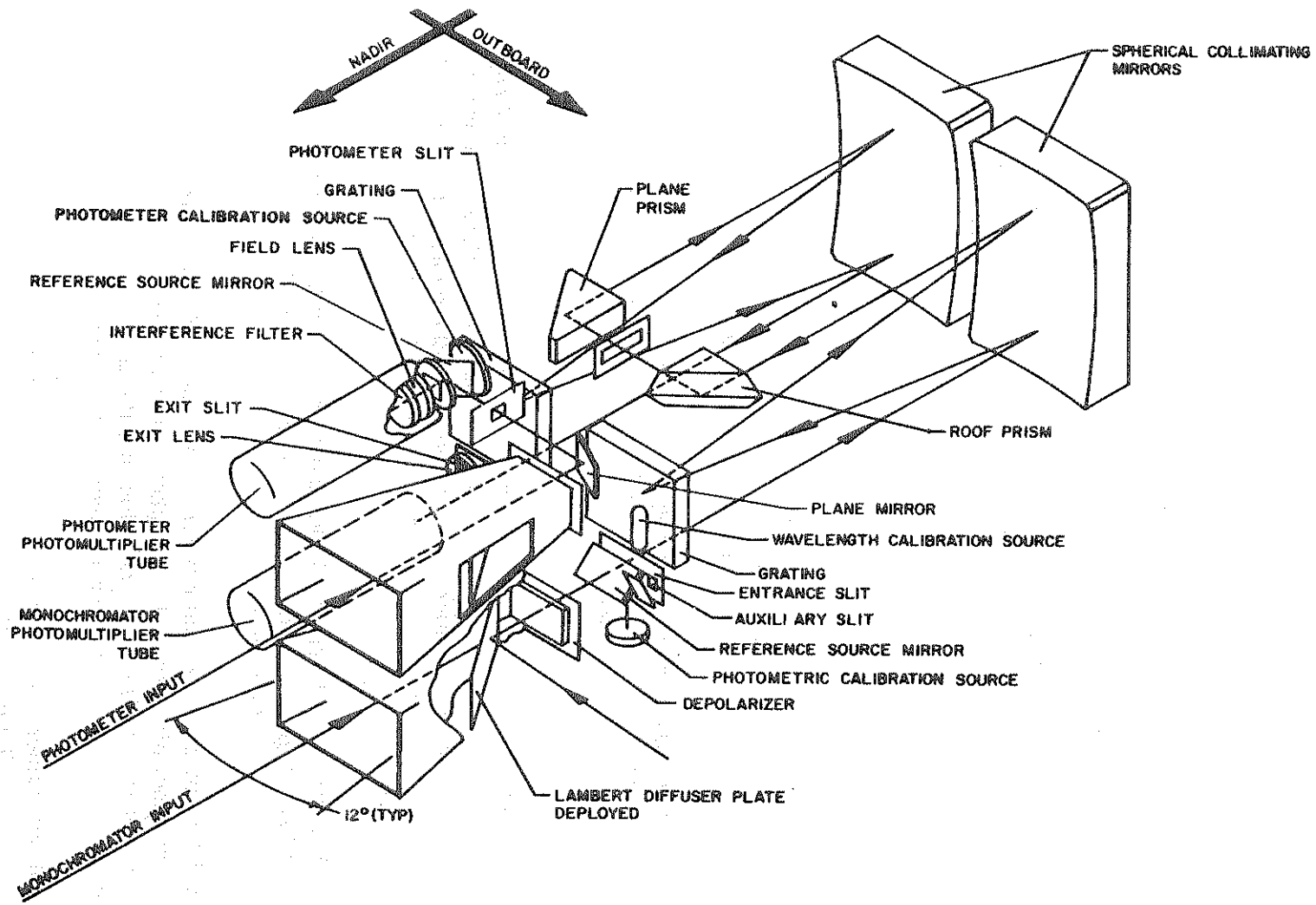

Figure 7-1. Optical Diagram of the BUV Photometer and Monochromator

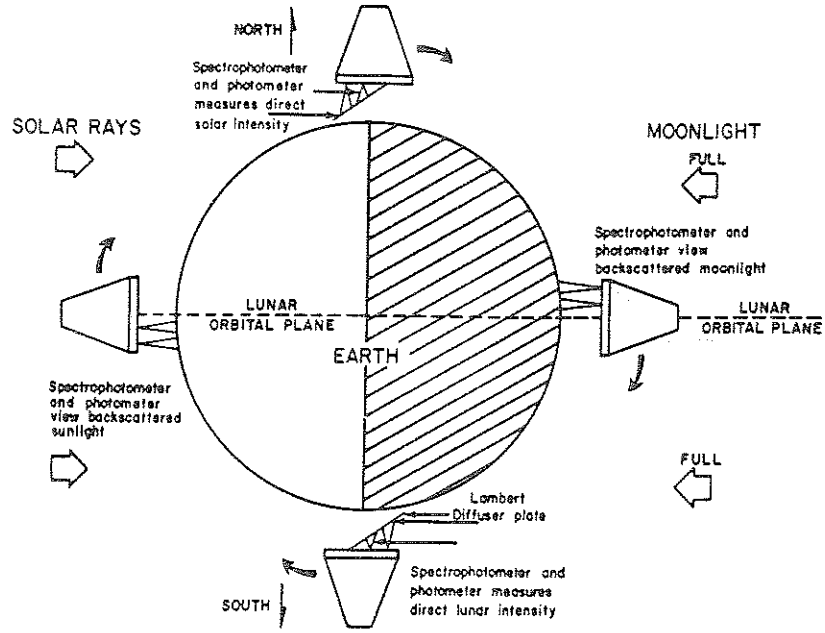

Figure 7-2. Schematic Representation of the Satellite Viewing Attitude at Various Orbital Positions

7.4.1 Spectrometer

The spectrophotometer is a Fastie-Ebert design which employs two monochromators. Each monochromator uses a single spherical collimating mirror. The entrance and exit slits are on a common circle which encircles the grating (Figure 7-3). Each point on this circle is imaged by the monochromator on the opposite side of the same circle (180° away) for all wavelengths. The entrance slit is imaged on the exit slit with unit magnification. The focal length of the monochromator is 250 mm. The height of both the entrance and exit slits is 25 mm.

Single-grating monochromators have high stray-light levels. Stray light is the generally accepted term to describe the total radiant flux of all unwanted wavelengths which pass through the exit slit of a monochromator.

The stray light arises primarily from two different optical mechanisms; (1) the direct "white light" scattered from the dispersive element, and (2) the indirect "white light" and spectral scattering from the dispersive element and from other mirrors in the monochromator.

(1) In reference to direct scattering, the surface texture of the prisms and grating, internal imperfections in prisms, and dust and foreign matter on the

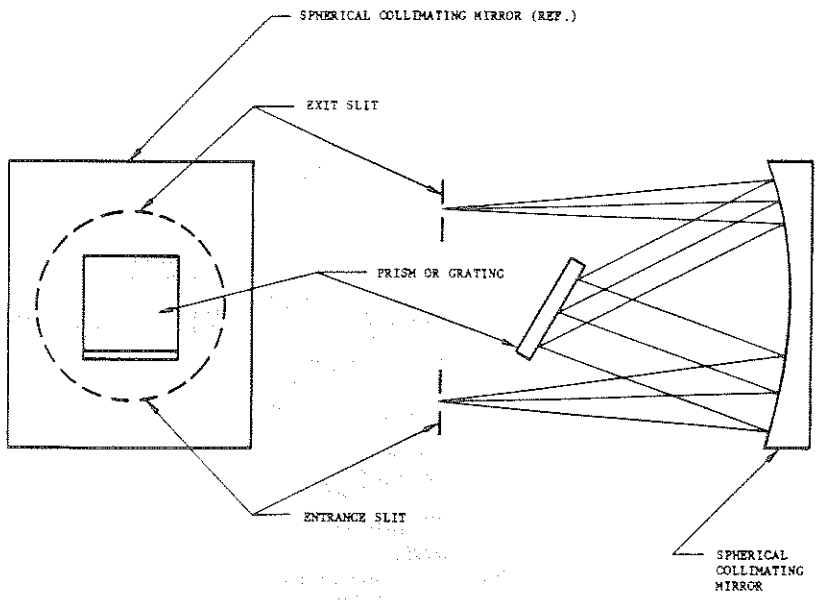

Figure 7-3. Fastie-Ebert Monochromator

dispersive surface, scatter a certain percentage of the incident radiant flux directly through the exit slit without the process of dispersion.

(2) In reference to the indirect "white light", the monochromator volume can be thought of as comparable to a black integrating sphere. The walls of the monochromator are generally illuminated by many decades more radiant flux than that which passes through the exit slit. This includes the direct scattering of the input radiant flux from imperfect mirror surfaces and Fresnel reflection from the prism face or the zero order reflection of the grating. Usually the major source of radiant flux in the monochromator is the spectral radiant flux in the portion of the spectral image which does not pass through the exit slit.

Another source of stray light may be secondary dispersion which occurs when the primary spectral image is not only spread across the exit slit, but also across the dispersing element. Those wavelengths which fall on the dispersive element are redispersed and a certain bandwidth of these unwanted wavelenghts passes through the exit.

Several means to reduce the stray light in the Instrument have been employed. One is the double monochromator design used in the BUV Instrument. The dispersed radiant flux passes from the first into the second monochromator through the intermediate slit. This slit is only slightly larger than the image of the entrance slit formed at the intermediate slit. The second monochromator

and intermediate slit effectively reduce the indirect "white light" scattering in the second monochromator.

Another means of reducing stray light is the field lens located at the exit slit of the second monochromator which images the dispersive area of the grating in the second monochromator onto an optical stop in front of the photo detector. This stop matches the size of the image of the dispersive area. Therefore, rays arising from outside the dispersive area cannot directly reach the photodetector.

All optical elements slits, gratings, collimating mirrors, and transfer prisms are supported by a single compact casting giving maximum rigidity, heat transfer, efficiency, and minimum weight.

The double monochromator of Figure 7-4 places the first monochromator on top of the second in such a way that the two identical gratings are fixed to a common bearing axis with identical angular orientation.

The entrance slit is mounted immediately above the exit slit in the same plane, both slits are mounted on a common slit plate. Two transfer prisms are used to divert the optical path through the intermediate slit. The volume required by this double monochromator structure is $11 \times 6 \times 7$ inches.

The imaging characteristics of the spectrometer are shown in Figure 7-5. An image of the earth and the photomultiplier aperture are traced through the optical system. As discussed in the stray light paragraph, the aperture opening falls well within the dispersing surface of the second grating, with the aperture (grating) defining the f-5 field-of-view.

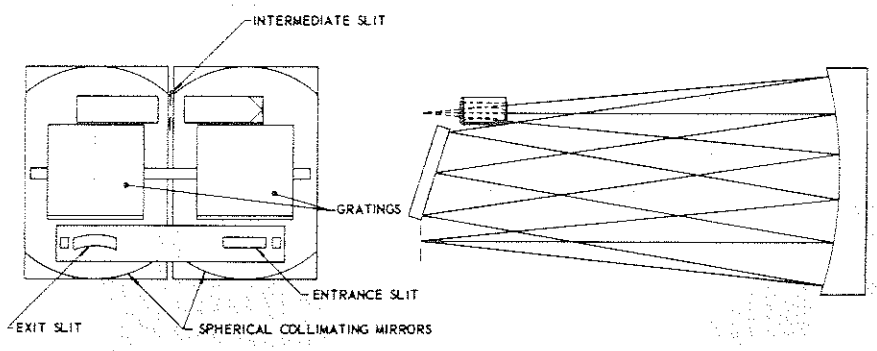

Figure 7-4. Common Bearing Axes with Identical Angular Orientation

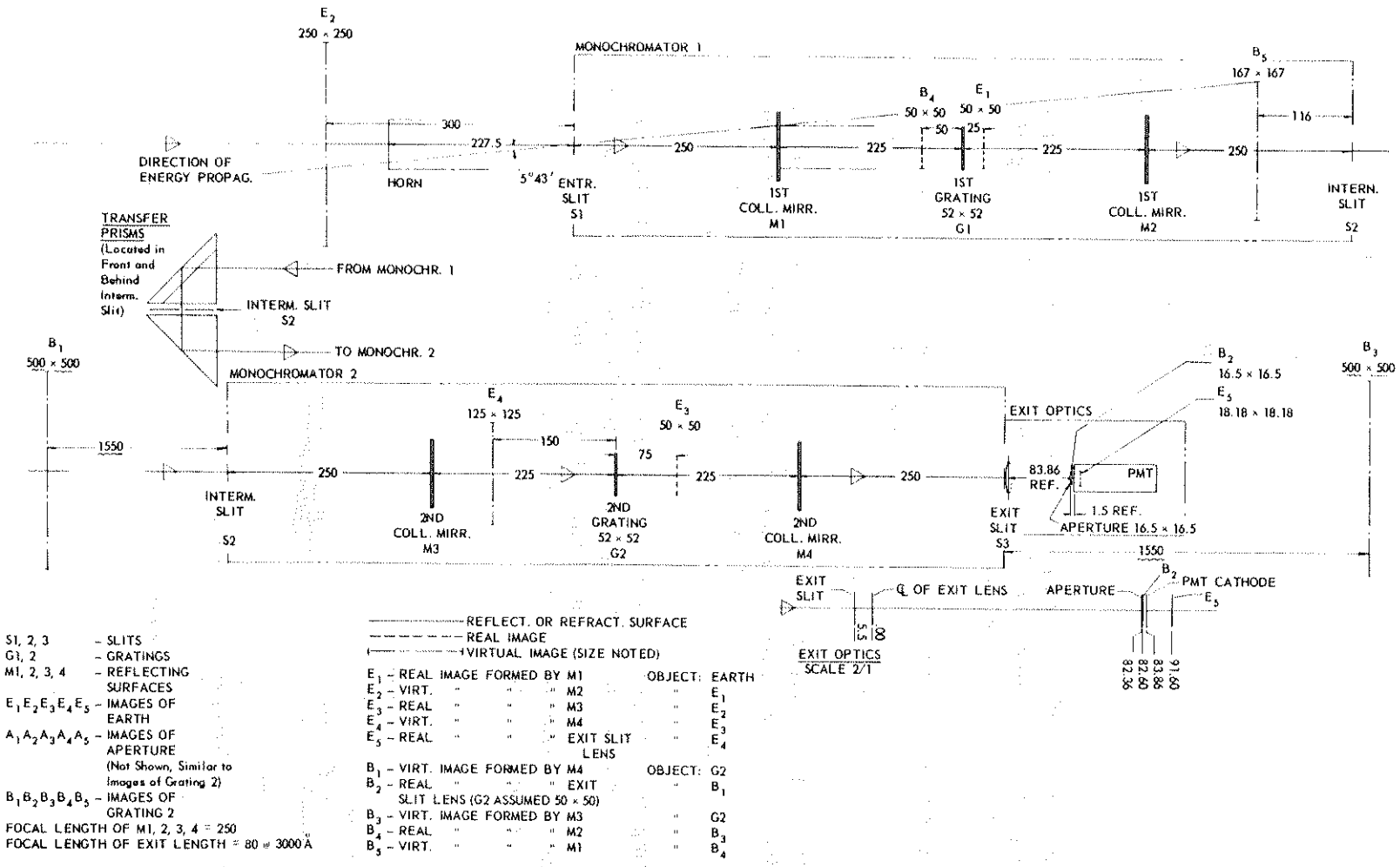

Figure 7-5. BUV Monochromator Imaging Characteristics (Horizontal Beam)

7.4.2 Photometer

The photometer is designed to optically parallel the monochromator. The same type of photomultiplier is used for the two detectors. The entrance horns and diffuser plates are the same for both systems.

The fields-of-view have been matched to ±3 percent. A lens focuses the incident radiant flux in such a way that the illuminated area of the photomultiplier matches that of the monochromator. The photometer system is depicted in Figure 7-6.

The respective field of views of the flight and back-up models are shown in Figures 7-7 and 7-8.

The BUV Instrument, without the depolarizer, exhibits selective sensitivity to polarized light, called in this abstract "Residual Polarization Sensitivity". The use of a depolarizer reduces this sensitivity to an acceptable level.

The depolarizer consists of three parts: a 5-mm-thick sapphire shield and two calcite plates 6 and 3-mm thick. Orientation of the optical axis is very important in all three items. In the sapphire shield, the optical axis is oriented along the direction of propagation of the incoming beam into the BUV. The optical axes of the calcite are perpendicular to the incoming beam; Figure 7-9 shows the critical angular relationship between the two calcite plates as well as the critical orientation of the optical axes. The thickness ratio between the 6 and the 3-mm calcite plates is held to 2.000 ±.003.

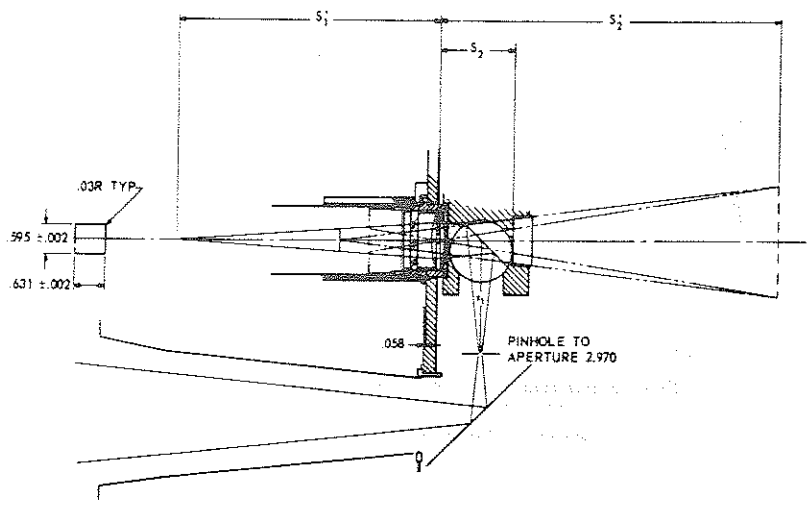

Figure 7-6. Photometer Optical Layout

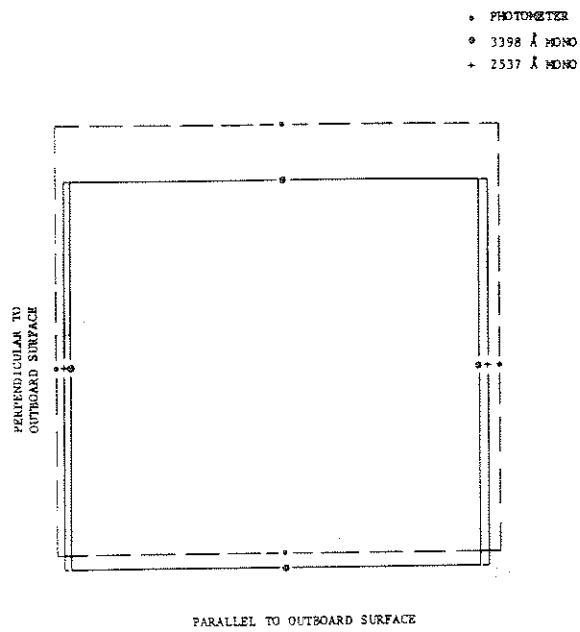

Figure 7-7. BUV–Field-of-View of the P-103 Model (Scheduled to be Flown)

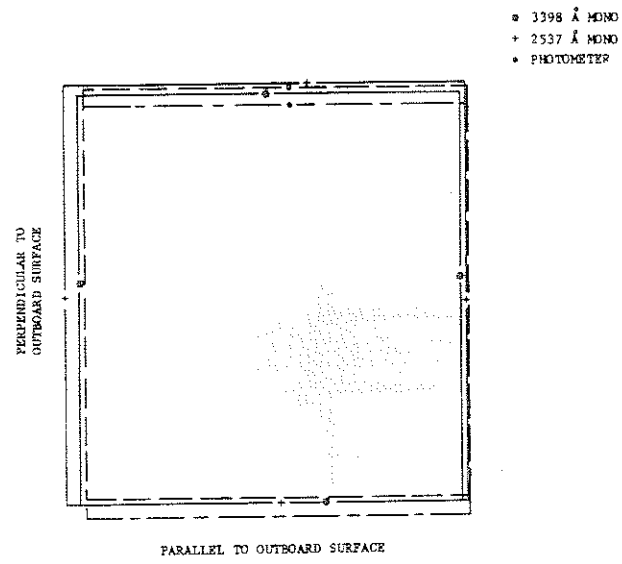

Figure 7-8. BUV–Field-of-View of the F-104 Model (Back-up Unit)

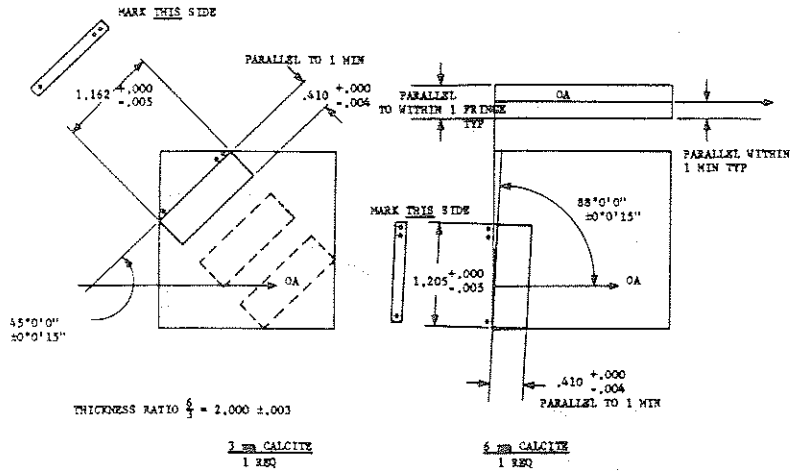

Figure 7-9. Calcite Depolarizer

The residual polarization of the prototype (Model P-103 scheduled to be flown) with and without the depolarizer are shown in Figures 7-10 and 7-11.

After installation of the depolarizer, the residual polarization of the backup unit (Model F-104) is shown in Figure 7-12.

7.4.3 Wavelength Scan and Accuracy

The wavelength scan of the Instrument contains twelve sampling steps in the wavelength range 2500 to 3400 Å and seven wavelength calibration steps grouped around the 2537 Å mercury line. The half-bandwidths of all steps are nominally 10 Å wide.

A wavelength scan starts at 3400 Å and continues sequentially through the sampling steps, the seven calibration steps, and returns to the 3400 Å starting point.

The scan dwells for two seconds at each sampling step and moves to the next step in 0.5 seconds. During the 2-second measuring interval, any given wavelength is displayed at the exit slit to an accuracy of ±0.2 Å. A complete scan is accomplished in 32 seconds with 2 seconds for each sampling step, and 0.5-second movement to the next step.

The sequence of the wavelength scan is cut into a continuous cam. One cam revolution contains all sampling and calibration steps. The sampling steps are 10° wide, the calibration steps 8° wide. Table 7-1 shows sampling and calibration wavelengths, and separation between steps:

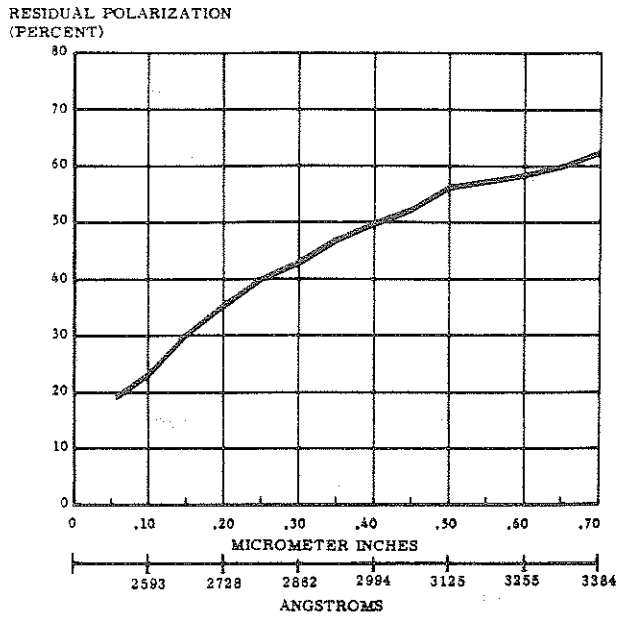

Figure 7-10. P-103 Model Residual Polarization Sensitivity Without Depolarizer

To Be Included

In First Data

Catalog

Figure 7-11. P-103 Model Residual Polarization Sensitivity With Depolarizer

To Be Included

In First Data

Catalog

Figure 7-12. F-104 Model Residual Polarization Sensitivity With Depolarizer

Table 7-1
Sampling, Calibration Wavelengths, and Separation between Steps

Step Number	Wavelength Å	Separation Å	Step Number	Wavelength Å	Separation Å
00	3398	86	10	2735	180
01	3312	137	11	2555	
02	3175	50	19	2522	5
03	3125	67	20	2527	5
04	3058	39	21	2532	5
05	3019	44	22	2537	5
06	2975	53	23	2542	5
07	2922	46	24	2547	5
08	2876	46	25	2552	5
09	2830	95			

Calibration Steps

Table 7-2 lists the final values for the cam steps of the BUV Prototype and Flight Models:

Table 7-2
Cam Steps of the BUV Prototype and Flight Models

		Actual Wavelength Step (Å)	
Step Number	Wavelength Step Desired (Å)	BUV Prototype	BUV Flight
00	3398	3400.26	3401.27
01	3312	3313.85	3315.07
02	3175	3177.23	3178.05
03	3125	3126.90	3127.94
04	3058	3060.03	3061.35
05	3019	3021.34	3022.20
06	2975	2977.27	2978.56
07	2922	2923.69	2925.49
08	2876	2877.85	2879.78
09	2830	2831.85	2833.90
10	2735	2737.93	2739.32
11	2555	2558.24	2559.01
12	2537	2539.21	2540.94

The wavelength accuracy of the Prototype and Flight Models were monitored through all environmental tests. The manual PEN RAY external and the mercury lamp internal calibration methods were used employing the micrometer screw after the vibration, acceleration, and thermal vacuum tests. The internal mercury lamp method was employed during all environmental tests with the resultant data recorded on printed tape.

The absolute photometric calibration of the BUV system will be given in the first edition of the Nimbus IV Data Catalog. This includes the angular response of the diffuser plates and their absolute reflectance as a function of wavelength.

7.5 Electronic Design

A block diagram of the BUV subsystem appears in Figure 7-13.

The signal processing electronics of the monochromator and photometer channels are virtually identical and only one channel will be described. The dynamic range of optical signal levels expected, approximately nine decades, is provided by a programmable high voltage power supply, a three-range electrometer, and a two-mode digital ratemeter. The photomultiplier is operated at two discrete gain states by automatically adjusting the high voltage power supply. In the low gain state only analog current signals are obtained while in the high gain state pulse count data are available in addition to the analog signals.

In the analog mode the signal processing channel consists of an electrometer, an automatic range sequencer, and a logarithmic analog to digital converter. The electrometer produces an output voltage which is proportional to the average input current.

The output voltage is sensed by an automatic range sequencer and is utilized to select any of the three feedback resistors and the two high voltage levels, hence controlling the system gain. Gain changes can occur every 200 milliseconds except during the automatic reference adjustment period. Gain changes are permissible in single steps (i.e. from 10^7 to 2×10^9 to 3×10^{10} and the reverse in the low voltage and from 3×10^{10} and low voltage to 1×10^7 and high voltage).

The buffered output of the electrometer is compared to an exponential voltage ramp. The comparator gates a 1 MHz clock signal to a counter for the interval during which the exponential ramp voltage exceeds 100 millivolts and is less than or equal to the electrometer output voltage. The analog to digital conversion is performed every 400 milliseconds. The eight most significant bits of the counter and two range bits denoting the electrometer gain are commutated as a single word into the digital "A" bit stream.

The signal processing channel in the pulse counting mode consists of an electrometer (common to both analog and pulse counting modes), a pulse amplifier — shaper, a single channel pulse height selector, and a digital ratemeter. In the pulse counting mode the electrometer serves as a wide-band pulse amplifier. The pulses from the electrometer are further amplified and appropriately shaped for input to the discriminators. The high and low level discriminators and the anti-coincidence circuit form a single channel analyzer. The low level discriminator removes noise while the upper discriminator is

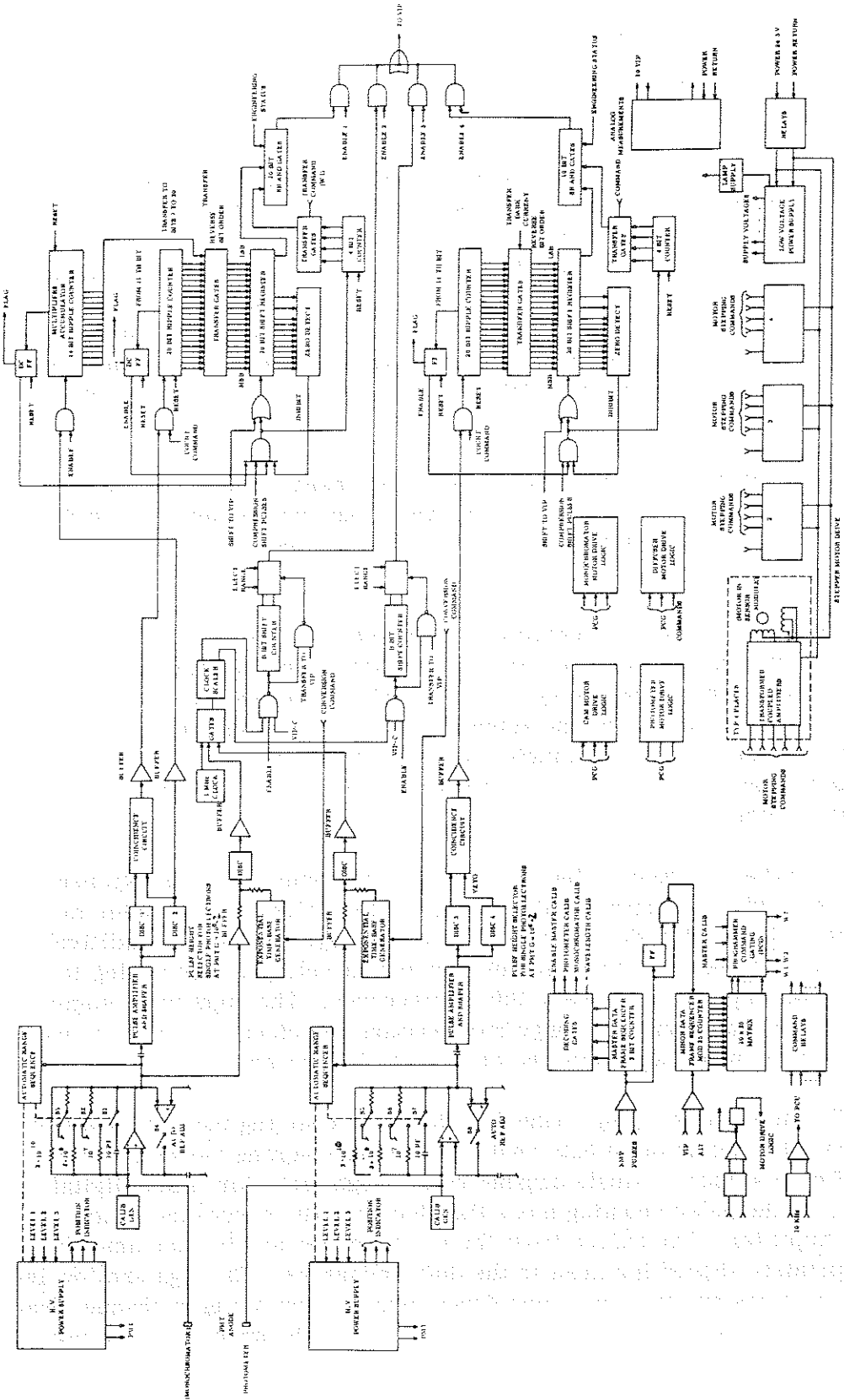

Figure 7-13. Backscatter Ultraviolet Spectrometer Subsystem Block Diagram

utilized to compensate for radiation induced pulses. The output pulses from the anticoincidence circuit are counted for 1.8 seconds. At low counting rates the contents of the counter are commutated directly into the digital "A" data stream while at high count rates ($>10^5$/sec) the counter contents are logarithmically compressed prior to commutation into the data stream.

In addition to the signal channels the major electronic circuitry is comprised of the following:

calibration generator
automatic reference adjust
low voltage power supply
calibration sequencer
cam sequencer
motor drivers
housekeeping telemetry
command and timing circuitry
output logic elements.

The calibration generator provides reference current levels and pulse trains which are utilized for in-flight calibration of the signal processing channels. The automatic reference adjust circuitry re-zeros the electrometers subsequent to each wavelength scan. The power supplies provide appropriate voltages for the photomultipliers and the mercury calibrations lamp in addition to those voltage levels required by the circuitry. The calibration and cam sequencer circuitry provide the logic required for wavelength scanning in the monochromator and inserts the calibrations at the appropriate times in the instrument sequence.

7.6 Experiment Sequence

The BUV subsystem experiment cycle requires 6144 seconds. Each cycle is partitioned into 192 BUV frames of 32 second duration. Calibrations are performed in 26 of the 192 frames, the others being utilized for experimental measurements. Four types of calibration (described in the following paragraphs) are performed during each experiment cycle. The experiment sequence is described in Table 7-3. The diffusers may be deployed twice during each orbit and remain deployed for two BUV frames (64 seconds). Time of deployment is a function of orbital position, not experiment sequence, and hence, during diffuser deployment, calibration is inhibited. Since the BUV Power ON command does not reset the sequencer, the position in the experiment cycle cannot be predicted prior to power on and, in fact, can only be determined by observing operation for a maximum of 104 BUV frames.

Table 7-3
BUV Experiment Sequence

BUV Frame No.	Sequence (Normal Mode Diffuser Retracted)	BUV Frame No.	Sequence (Normal Mode Diffuser Retracted)
1	MCS-D	96	MCS-A
2	MCS-E	97-103	DATA
3-7	DATA	104	MCS-A
8	MCS-A	105-111	DATA
9-15	DATA	112	MCS-A
16	MCS-A	113-119	DATA
17-23	DATA	120	MCS-A
24	MCS-A	121-127	DATA
25-31	DATA	128	MCS-A
32	MCS-A	129-135	DATA
33-39	DATA	136	MCS-A
40	MCS-A	137-143	DATA
41-47	DATA	144	MCS-A
48	MCS-A	145-151	DATA
49-55	DATA	152	MCS-A
56	MCS-A	153-159	DATA
57-63	DATA	160	MCS-A
64	MCS-A	161-167	DATA
65-71	DATA	168	MCS-B,C
72	MCS-A	169-175	DATA
73-79	DATA	176	MCS-A
80	MCS-A	177-183	DATA
81-87	DATA	184	MCS-A
88	MCS-B,C	185-191	DATA
89-95	DATA	192	MCS-A

The wavelength transition time is alternately 0.8 and 0.6 second. During the last 2.76 seconds of each frame, the diffraction grating is returned to its initial position.

7.6.1 Data Frames

During each data frame the monochromator measures the intensity of ultraviolet radiation in each of 12 wavelength bands, while the photometer measures the ultraviolet intensity in a single wavelength band. Monochromator wavelength scans are accomplished by changing the position of the diffraction

grating in discrete steps. The dwell time at each wavelength is 1.8 seconds, and during this interval four analog ultraviolet intensity measurements are taken at 400 msec intervals in addition to an integrated pulse count measurement of the ultraviolet intensity and energetic particles.

7.7 Optical Calibration and Instrument Parameters

The principal method of radiometric calibration in flight is the direct observation of sunlight by means of the diffuser plates. Since the ozone measurement requires only the backscattered radiance relative to the incident irradiance, this technique minimizes the effects of any instrument changes.

The four types of internal calibration performed during a BUV experiment cycle are:

a. MCS-A: Dark current and Electronics Calibration
b. MCS-B,C: Photometric Calibration
c. MCS-D: Primary Wavelength Calibration
d. MCS-E: Secondary Wavelength Calibration

Master Calibration Sequence A (MCS-A) — MCS-A is performed on the monochromator and photometer channels simultaneously. During this calibration sequence, the monochromator entrance shutter is placed in the photometric calibrate position, the exit shutter is closed, the photometer shutter is closed and the High Voltage Power Supplies are fixed in the precalibration modes. The following calibrations are taken:

a. Photomultiplier Dark Currents.
   Sixteen analog and four pulse count measurements of the pmt dark current of each channel are performed. The pulse counters are enabled over 9.2 seconds. The fourth measurement (i.e., the fourth W5 and W6) represents the count rate integrated over 9.2 seconds and the first three W5 and W6's represent intermediate count totals.

b. Energetic Particle Counter Check.
   The calibrator circuits provide pulse inputs to both electrometers for 1.8 seconds. The pulse train is comprised of 8-volt (amplitude) pulses at a 100 Hz rate. The 8 volt amplitude is twice the high level discriminator threshold.

c. High Level Pulse Height Discriminator Check.
   The calibrator circuits provide pulse inputs to both electrometers for 1.8 seconds. The pulse trains are comprised of 2-volt (amplitude)

pulses at a 125 kHz rate. The 2 volt amplitude is one-half the high level discriminator threshold.

d. Low Level Pulse Height Discriminator Check.
The calibrator circuits provide pulse inputs to both electrometers for 1.8 seconds. The pulse trains are comprised of 0.3-volt (amplitude) pulses at a 125 kHz rate. The 0.3 volt amplitude is twice the low level discriminator threshold.

e. Electrometer Gain, Low Range.
The calibrator circuits provide a constant current to both electrometers. The constant current source is a 9 volt/second voltage ramp across the capacitor resulting in a current of approximately 9×10^{-11} amperes.

f. Electrometer Gain, High Range.
The calibrator circuits provide a constant current to both electrometers. The constant current source is a voltage ramp of 50 volts/second across a capacitor, resulting in a current of approximately 5×10^{-10} amperes.

Master Calibration Sequence B, C (MCS-B, C) — Photometric calibration is performed on both channels simultaneously; monochromator photometric calibration referred to as MCS-B, photometer photometric calibration referred to as MCS-C, and the combination referred to as MCS-B, C. In this calibration, the entrance shutters in both channels are turned so that tritium-activated phosphor sources are viewed. Because the signals in the monochromator are very low, the electrometer is allowed to free range with the photomultiplier in the high gain state.

Note that B calibration data are meaningless for 3398, 2735 and 2555 Å because of moving shutters.

Master Calibration Sequence D (MCS-D) — Primary wavelength calibration (MCS-D) is performed on the monochromator only, and is accomplished by viewing a mercury lamp at seven discrete wavelengths near the 2537 Å line. Measurements are taken at the following nominal wavelength positions:

2522 Å, 2527 Å, 2532 Å, 2537 Å, 2542 Å, 2547 Å, and 2552 Å.

From these measurements the cam position for maximum response to the Hg line can be calculated. The calibration lamp is offset from the instance slit requiring a correction of +3Å to the observed wavelength. This calibration in conjunction with MCS-E checks the monochrometer for wavelength drift.

Master Calibration Sequence-E(MCS-E) — Secondary wavelength calibration (MCS-E) is performed once per experiment cycle. Since this calibration is performed immediately following MCS-D, the shutters are correctly positioned and the wavelength calibration lamp is on. In the MCS-E calibration cycle, the signals from the mercury lamp are monitored at each normal wavelength step from 3398 Å to 2735 Å. This calibration is used only in the event of major shifts in instrument wavelength positions.

7.8 Housekeeping and Status Functions

In addition to the sensory data as described above, certain other instrument functions are telemetered through the VIP system. The following Digital B signals are sampled 3 times per 16 seconds:

a) Power On/Off
b) 10 kHz clock received Yes/No
c) Mode Launch/Normal
d) Data Cycle 2nd/1st
e) Calibrations Inhibited/Enable
f) Command Verify Deploy Diffuser
g) Command Verify Store Diffuser
h) Diffuser Deployed No/Yes
i) Diffuser Stored No/Yes
j) Pre-wavelength calibrate
k) Electronics calibrate On/Off
l) Photometric Calibrate On/Off
m) Wavelength Calibration Lamp On/Off
n) Monochromator Shutters in Data Position
o) Monochromator Shutters in Photometric Calibration Position
p) Monochromator Shutters in Dark Current Position
q) Photometer Shutters in Data Position
r) Photometer Shutters in Photometric Calibration Position
s) Photometer Shutters in Dark Current Position

The following housekeeping functions are furnished to the VIP system as analog signals:

a) Logic Supply (+4 VDC)
b) Thermistor Bias Supply (-6.375 V)
c) Photometer High Voltage Monitor
d) Monochromator High Voltage Monitor
e) Housing Absolute Temperature

f) Photomultiplier Absolute Temperature
g) Sensor Module Electronics Temperature
h) Motor Current Limiter Temperature
i) Static Inverter #1 Temperature
j) Static Inverter #2 Temperature
k) Wavelength Arm Temperature Gradient
l) Housing Temperature Gradient

All of the housekeeping channels are monitored once every sixteen seconds.

7.9 Data Processing and Archiving

All BUV signals are sent to the VIP System and recorded on a HDRSS tape recorder for playback at a data acquisition station or, alternatively, transmitted real-time with the spacecraft beacon transmitter. At GSFC a Sensory Data Tape (SDT) is generated containing the data from all experiments. For BUV data processing an intermediate tape containing only BUV and related data is produced. This tape is then merged with the Minute-Vector Tape to produce the BUV Archival Tape. In this tape the monochromator and photometer signals are converted to photocathode currents and the calibrations housekeeping data are summarized. The format for the Archival Tape will be published in the Nimbus IV Data Catalog.

REFERENCES

1. Singer, S. F., and R. C. Wentworth. "A Method for the Determination of the Vertical Ozone Distribution From a Satellite", J. Geophys. Res., Vol. 62, No. 2 (June 1957), pp. 299-308.

2. Twomey, Sean. "On the Deduction of the Vertical Distribution of Ozone by Ultraviolet Spectra Measurements From a Satellite", J. Geophys. Res., Vol. 66, No. 7 (July 1961), pp. 2153-62.

3. Twomey, S., and H. B. Howell. "A Discussion of Indirect Sounding Methods With Special Reference to the Deduction of Vertical Ozone Distribution From Light Scattering Measurements", Mon. Weather Rev., Vol. 91, No. 10-12 (October-December 1963), pp. 659-64.

4. Kaplan, Lewis D. "On the Determination of Upper-Atmosphere Composition From Satellite Measurements", in Chemical Reactions in the Lower and Upper Atmosphere. New York, Interscience, 1961. pp. 269-74.

5. Dave, J. V. and C. L. Mateer, 1967b: "A preliminary study on the possibility of estimating total atmospheric ozone from satellite measurements". J. Atmos. Sci., 24, 414-427.

6. Herman, Benjamin M. and Douglas N. Yarger. "Estimating the Vertical Atmospheric Ozone Distribution by Inverting the Radiative Transfer Equation for Pure Molecular Scattering." J. Atmos. Sci., 26, 153-162 (1969).

7. Dave, J. V. and P. M. Furukawa. "The Effects of Scattering and Ground Reflection on the Solar Energy Absorbed by Ozone in a Rayleigh Atmosphere", J. Atmos. Sci., 24, 175-181 (1967).

SECTION 8

THE FILTER WEDGE SPECTROMETER (FWS) EXPERIMENT

By
W. A. Hovis, Jr., M. L. Forman and L. R. Blaine
National Aeronautics and Space Administration
Goddard Space Flight Center

8.1 Introduction

The Filter Wedge Spectrometer on Nimbus IV spectrally scans the 1.2 to 2.4 and 3.2 to 6.4 micron intervals of the infrared spectrum. The 1.2 to 2.4 micron interval observes reflected solar energy during daylight passes and will see virtually no energy during nighttime passes. The 3.2 to 6.4 micron channel simultaneously detects both reflected energy of solar origin and emitted energy of terrestrial origin between 3.2 and 4.2 microns during daylight hours. The strong absorption band of CO_2, centered at 4.3 microns, will absorb virtually all incident solar energy from 4.2 to 4.5 microns. Beyond 4.5 microns reflected solar energy will be inconsequential and only emitted radiation originating in either the atmosphere or surface of the earth will be observed. During nighttime observations only energy of terrestrial origin will be observed by the 3.2 to 6.4 micron channel.

The instrument utilizes a circular variable filter to scan the spectral intervals. The filter consists of two 180° segments, one covering the 1.2 to 2.4 micron interval, the other 3.2 to 6.4 microns. The performance of the instrument will be described in the sections dealing with calibration. Incident energy is reflected off a first surface mirror and collected by a telescope lens as shown in Figure 8-1a, a side view of the instrument. The telescope focuses the collected energy onto the edge of the multi-toothed chopper wheel that chops the energy at a rate of 333 cps.

After passing through the chopper the energy is refocused onto the edge of the circular variable filter at an aperture that acts both as the slit of the spectrometer and as the field stop of the system. After passing through the filter the energy is reimaged on a lead selenide detector mounted on the edge of a cold patch inside the radiative cooler. This cooler is designed to cool the detector to approximately 175°K in flight.

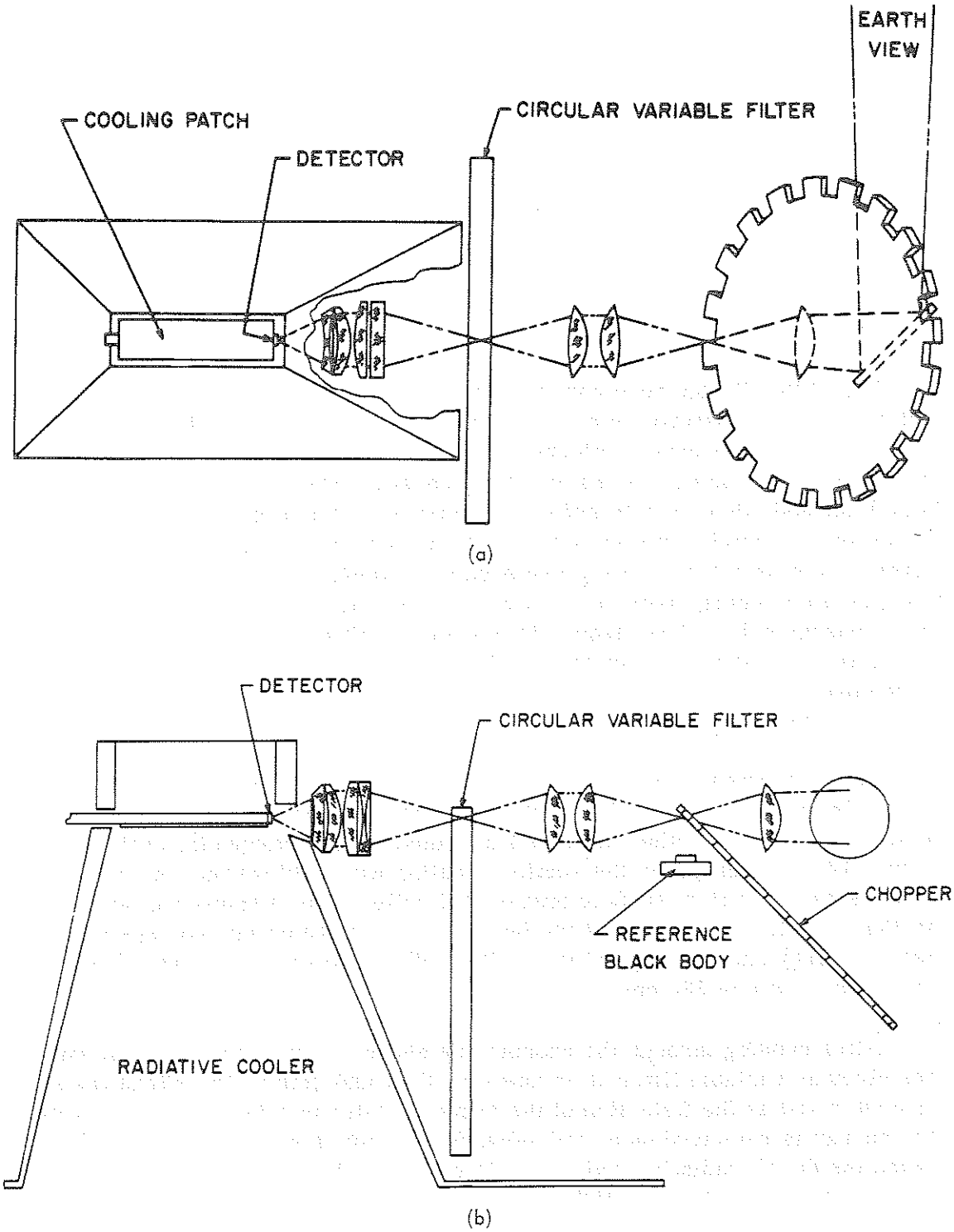

Figure 8-1. Nimbus IV Filter Wedge Spectrometer (a) Side View (b) Bottom View

Figure 8-1b shows another view of the instrument that more clearly illustrates the use of the chopper. The side of the chopper toward the circular variable filter is highly reflecting so that the detector alternately sees energy from the target and energy from a reference blackbody within the instrument. A calibration blackbody, not shown, can be inserted to cover the entrance port. Its function will be discussed under calibration.

8.2 Objectives

8.2.1 General

The purpose of this experiment is to accurately measure radiance from the earth, as a function of wavelength, in the 1.2 to 2.4 and 3.2 to 6.4 micron region for meteorological purposes.

The principal objective is in the area of atmospheric measurements. However, some data of use to the earth resources effort will also be obtained. It has become evident in recent years that the goals of operational meteorological satellites will be largely met by high spatial resolution, multi-channel scanning radiometry. The selection of wavelength intervals for these radiometers requires a detailed knowledge of the radiance spectrum in the wavelength intervals that show promise for remote sensing. This experiment should acquire that knowledge in the intervals covered.

8.2.2 1.2 to 2.4 Micron Interval

The interval, as previously mentioned, will observe only energy of solar origin reflected from earth or clouds. Within this interval there are several atmospheric "windows" as well as several strong atmospheric absorption bands. Included in this interval are the (1, 0, 1), (0, 2, 1) and (0, 1, 1) bands of H_2O and the (2, 0, 1) and (1, 1, 1) bands of CO_2. The 1.6 to 2.2 micron interval shows great promise for remote detection of cloud type and particle size. Aircraft measurements indicate that a multi-channel radiometer with channels in the 1.6 to 2.2 micron interval would accomplish this goal. The data from the Nimbus IV FWS will allow precise selection of the proper channels for the radiometer.

8.2.3 3.2 to 6.4 Micron Interval

The 3.2-4.2 micron interval will be of little use during daylight hours because this region is a mixture of reflected solar energy and emitted energy from the earth and there is no way of distinguishing between energy from two sources. The 4.3 micron band of CO_2 will absorb virtually all incident solar radiation so

only radiation of terrestrial origin will be observed in this region. Beyond the 4.3 micron band solar reflectance is inconsequential so only radiation of terrestrial origin will be observed, day or night.

The principal purpose of scanning the 3.2 to 6.4 micron region is to cover the emission spectrum due to the water vapor band centered at 6.3 microns. Emission from this band will be inverted to infer vertical water vapor profile in much the same manner that temperature profiles have been derived from emission from the 15 micron CO_2 band. Selection of optimum intervals for multi-channel radiometry will be accomplished utilizing the data obtained with these measurements.

8.3 Instrument Calibration

8.3.1 Wavelength

The wavelength as a function of filter position or time is obtained by utilizing a calibrated half meter Fastie Ebert spectrometer. The slit setting is such that the line width corresponds to about one half that of which the FWS is capable of resolving. Readings are taken every tenth of a micron across each of the two scanned intervals of the FWS.

Time is referenced to zero at the leading edge of the marker pulse for each side. Since the main data are sampled every .05 seconds without regard to filter position, the maximum error in wavelength determination is of the order of one half of a resolution element. Figure 8-2 shows the wavelength as a function of time.

8.3.2 Radiometric

The technique for radiometric calibration for the FWS depends on which wavelength interval is under consideration.

8.3.2.1 1.2-2.4 Micron Scan

This portion of the scan is calibrated by observing the output of a NBS standard quartz Iodide lamp which is reflected off of a 45° gold plated diffuser. The output is varied either by inserting neutral density filters at constant current to the lamp, or varying the current to the lamp. This calibrator, has in turn been calibrated by comparing its output with that of the six foot integrating sphere at GSFC. The observation instrument was an existing aircraft Filter Wedge Spectrometer which scanned the wavelength interval in question.

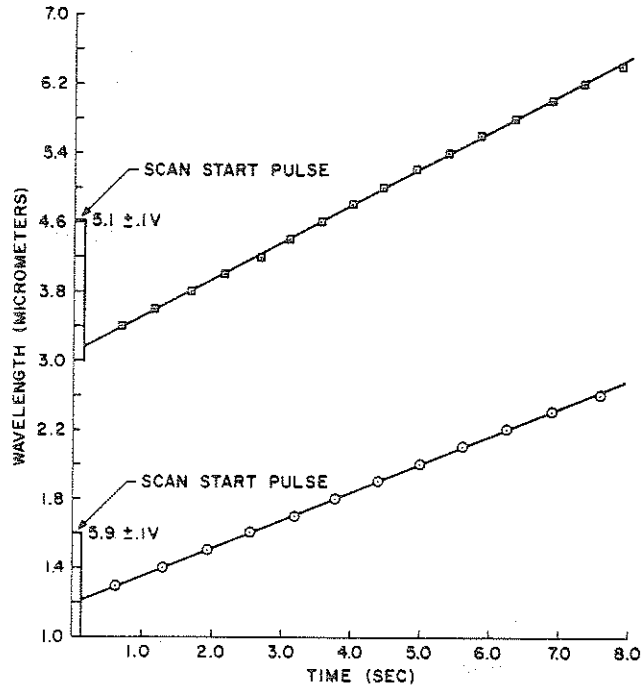

Figure 8-2. Wavelength as a Function of Time

Since the spectral response is a function of wavelength and source intensity (possibly baseplate and detector temperature also), a family of calibration curves, voltage vs milliwatts, is generated at predetermined wavelengths, and the appropriate curve is applied to the output of the FWS. The wavelengths involved will be discussed under data reduction.

As there is no inflight calibration for this portion of the scan, one assumes the FWS is stationary and that for varying conditions its behavior can be predicted on the basis of laboratory measurements. It is possible, however, to cross check the output with other Nimbus experiments such as THIR, or with concurrent aircraft observations using existing instruments. Of course, this must be done after launch.

8.3.2.2 3.2-6.4 Micron Scan

This portion of the scan is calibrated by utilizing the output of blackbody targets (emissivity > .98) at different temperatures. These targets are optically chopped against a built-in reference blackbody, hence the output of the FWS for this portion of the scan is a measure of energy difference.

The instrument electronics are set so that when observing a target colder than the reference blackbody, a negative voltage is generated. Conversely, observation of a target warmer than the reference blackbody yields a positive voltage.

A family of curves, voltage versus differential energy, is obtained at each predetermined wavelength for various detector and baseplate temperatures. For observed voltage at a particular wavelength, the differential energy is found and substituted into the following equation

$$\Delta E(\lambda, V) = E_T(\lambda, T) - E_R(\lambda, T) \quad (1)$$

where $\Delta E(\lambda, V)$ = differential energy at λ corresponding to voltage V (watts/cm^2-μ)

and $E_T(\lambda, T)$, $E_R(\lambda, T)$ = watts/cm^2-μ for the target and reference blackbody respectively

Since $E_R(\lambda, T)$ is known to follow the Planck Radiation Law, one can calculate the thermal emission of the target.

It appears that in the wavelength region beyond 5 microns, the response of the FWS is quite sensitive to both detector and baseplate temperature (Figure 8-3). This may be due to the fact that the detectivity of the detector is changing very rapidly in this region. However, preliminary calculations indicate that these variations can be handled by interpolation techniques with an error of less than 1°C for a 275°K target. It will be necessary to do this if the instrument stabilizes at a different temperature than those of the calibration runs.

A calibration cycle for this wavelength region occurs every 64th scan by inserting a blackbody of known temperature in front of the optical port. Thus a one point check at all wavelengths can be obtained for any stabilized condition and compared with the ground calibration. A posteriori checks can also be made. During this scan, telemetry is also checked during the 1.2-2.4 micron portion.

8.4 FWS Instrument Parameters

8.4.1 FWS Instrument Function

Two of the most significant characteristics of any spectrometer is its ability to resolve closely spaced spectral features and that its instrument (or slit) function be essentially triangular.

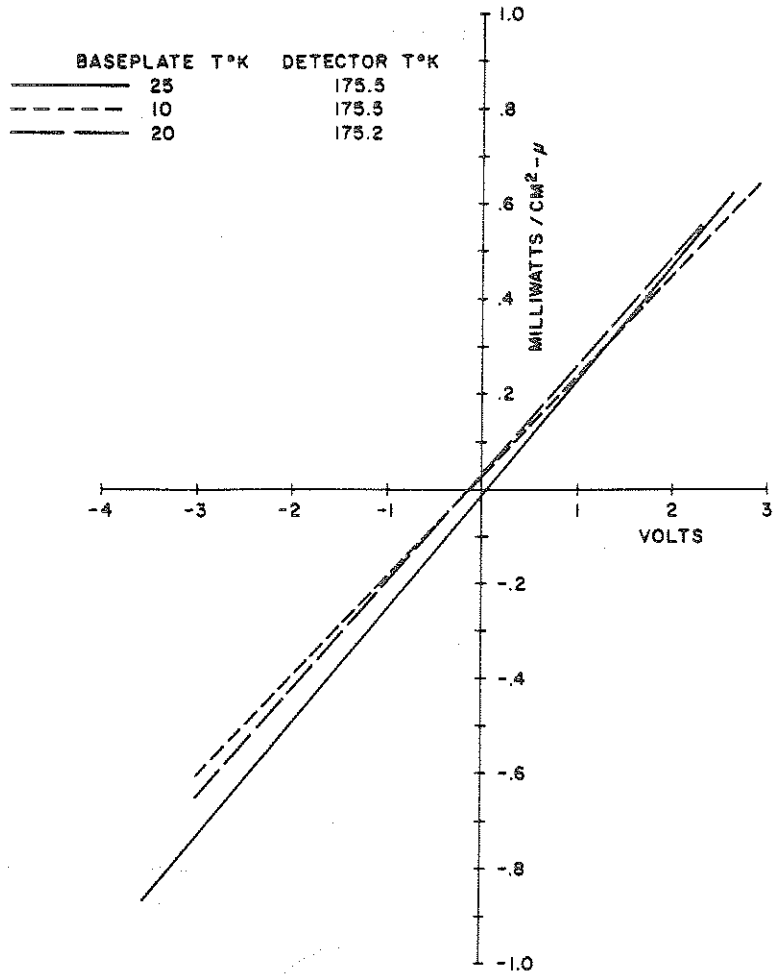

Figure 8-3. Response of the FWS at 5.45 Micrometers at Various Baseplate and Detector Temperatures

To demonstrate these features of the FWS, the following experiment was performed: A Nernst-Glower was placed at the entrance slit of a calibrated grating spectrometer and the energy leaving the exit slit was collimated, directed into the FWS entrance aperture and a scan was recorded. The slit of the grating spectrometer was then reduced to a spectral width well below the effective slit width of the FWS. At this point, the FWS demonstrated its minimum effective slit width and its true instrument function. Figure 8-4 shows a record of these results.

8.4.2 Field of View

The "Instantaneous Field of View" of the FWS is illustrated graphically by Figure 8-5. This parameter was obtained by directing collimated 3.8 micron

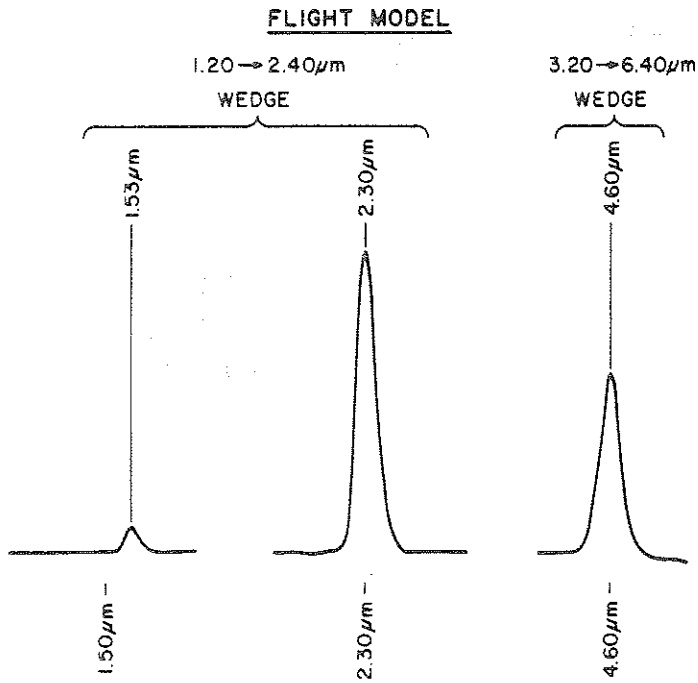

Figure 8-4. Filter Wedge Instrument Function

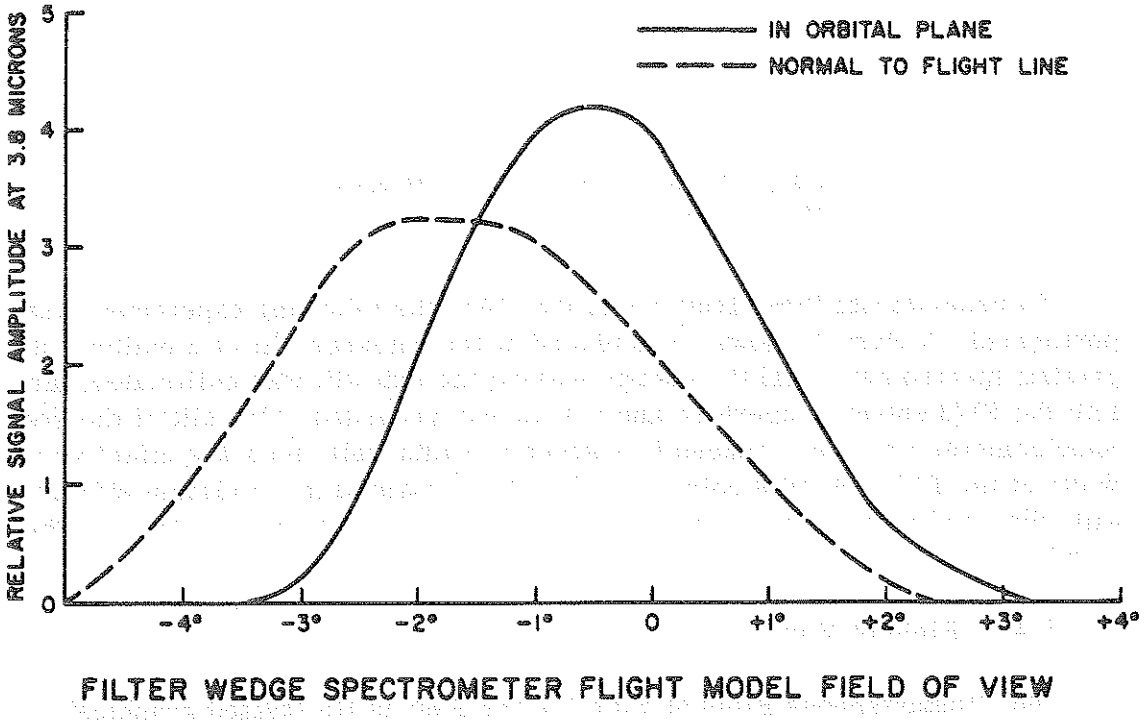

Figure 8-5. Instantaneous Field of View of the FWS

radiation into the center of the instrument's entrance aperture and rotating the instrument about a specific point in 0.5 degree increments. The fulcrum of rotation is a point in the plane of the entrance aperture and at its physical center. The analog signal generated was then plotted as a function of angular displacement from this apparent optic axis, yielding a sensitivity relation between the apparent and true optic axis of the instrument. The curve labeled "Horizontal" is in the satellite's orbital plane while the curve labeled "Vertical" is in the plane perpendicular to the velocity vector.

It is seen that the two axes are not perfectly aligned. This is in part due to the accumulated aberrations of the 5 optical components and in part due to the difficulty of lining up the collimator. The instrument's Field of View is defined as the half-width of these sensitivity curves, which is approximately 3.6°.

8.5 Data Reduction

Data from the FWS is returned to GSFC on the Sensory Data Tape (SDT) which also contains data from other experiments (MUSE, BUV, THIR). Pertinent data for each experiment will be stripped from the SDT, examined for fidelity and written out on separate tapes. It is probable that more than one orbit's data will be stacked on a given output tape. This output tape will be designated as the Filter Wedge Data Tape (FWDT) and includes all housekeeping as well as IR data. The FWDT will then be processed in a manner described in the next few paragraphs.

Initially a search of the IR data will be made for the beginning of a wedge position pulse. A pulse of magnitude 5.1 ± .2 volts means that data from the 3.2-6.4 micron scan follows; a pulse of night 5.9 ± .2 volts means data from the 1.2-2.4 micron scan follows. Referencing the first pulse point as t = 0, a wavelength is assigned to each data point by an interpolation process rather than according to the curves of Figure 8-3 since those curves are really not exactly linear. For ease of presentation new data values are calculated at intervals of .004 micron in the 1.2-2.4 micron region, and at intervals of .01 micron in the 3.2-6.4 micron region. This corresponds to a density of about four points per resolution element in each case.

The appropriate calibration is applied to this data, and the results will be stored and archived along with appropriate housekeeping information.

The output tape will consist of one file for each date readout orbit. Within each file records of the following type will exist:

Record Type	Description	
1	Documentation for each file	(Table 8-1)
2	Detector temp at 16 sec intervals	(Table 8-2)
3	Baseplate temp at 16 sec intervals	(Table 8-2)
4	Reference blackbody at 16 sec intervals	(Table 8-2)
5	Calibrated spectra 1.2-2.4 micron	(Table 8-3)
6	Calibrated spectra 3.2-6.4 micron	(Table 8-3)

It should be noted that all record types are read with the same format. Also orbits will be stacked on a daily basis.

Table 8-1
The Filter Wedge Data Tape Format
(Preliminary)

Word	Quantity	Units	Format	Remarks
1	Record Type	—	B31	Type = 1 indicates this record contains documentation data for this file
2	Satellite ID	—	B31	Nimbus IV = 4
3	Orbit No.	—	B31	Data Readout Orbit No.
4	Day	Days	B31)	
5	Hour	Z Hours	B31)	Time of first calibrated
6	Minute	Z Minutes	B31)	spectrum for this orbit
7	Second	Z Seconds	B31)	
8	Day	Days	B31)	
9	Hour	Z Hours	B31)	Time of last calibrated
10	Minute	Z Minutes	B31)	spectrum for this orbit
11	Second	Z Seconds	B31)	
12	Spare		B31	
13	Spare		B31	
14	Spare		B31	
15	Spare		B31	
16	Initial Wavelength	Microns	F.P.	1.260)
17	Final Wavelength	Microns	F.P.	2.440) 1.2-2.4 Micron Scan
18	Increment	Microns	F.P.	.004)
19	Initial Wavelength	Microns	F.P.	3.200) 3.2-6.4 Micron Scan
20	Final Wavelength	Microns	F.P.	6.400)
21	Increment	Microns	F.P.	.010)
22	)		F.P.	
.	)		.	
.	) Spare		.	
500	)		F.P.	

Table 8-2
The Filter Wedge Data Tape Format
(Preliminary)

Word	Quantity	Units	Format	Remarks
1	Record Type	—	B31	Type = 2, detector temp. Type = 3, baseplate temp. Type = 4, Reference temp.
2	Satellite ID	—	B31	Nimbus IV = 4
3	Orbit No.	—	B31	Data Readout Orbit No.
4	Day	Days	B31)	
5	Hour	Z Hours	B31)	Time of 1st temperature
6	Minute	Z Minutes	B31)	reading
7	Second	Z Seconds	B31)	
8	Increment	Seconds	B31	Normally 16
9	Spare		B31	
.	.		.	
.	.		.	
.	.		.	
15	Spare		B31	
16				0.0 means no reading available
.)	Temperature	Degrees	F.P.	999.9 means end of data
.)		Kelvin		
500)				Number of readings based on 108 minute orbit

Table 8-3
The Filter Wedge Data Tape Format
(Preliminary)

Word	Quantity	Units	Format	Remarks
1	Record Type	—	B31	Type 5 = 1.2-2.4 micron side Type 6 = 3.2-6.4 micron side
2	Satellite ID	—	B31	Nimbus IV = 4
3	Orbit No.	—	B31	Data Readout Orbit No.
4	Day	Days	B31)	
5	Hour	Z Hours	B31)	Time at wavelength
6	Minute	Z Minutes	B31)	marker pulse
7	Second	Z Seconds	B31)	
8			B31	
.				
.	SPARE			
.				
15			B31	
16	Latitude	Degrees	F.P.	Latitude and longitude of sub-
17	Longitude	Degrees	F.P.	satellite point at wavelength marker pulse
18	Height	Kilometers	F.P.	Height of satellite at wave-length marker pulse
19	Detector Temp.	°K	F.P.	
20	Ref BB Temp.	°K	F.P.	
21	Base Plate Temp.	°K	F.P.	
22	Optical Port Temp.	°K	F.P.	
23)				Words 23-317 if Type = 5
.)	Radiance	watts/cm^2-micron	F.P.	Words 23-342 if Type = 6
.)				9999.9 will indicate scan end
500)				

It is anticipated that FWD Tapes will be available through NSSDC approximately one year after launch.

SECTION 9

THE SELECTIVE CHOPPER RADIOMETER (SCR) EXPERIMENT

By
E. J. Williamson
Department of Atmospheric Physics, Clarendon Laboratories
Oxford University, England

9.1 General Description

The object of the Selective Chopper Radiometer (SCR) is to determine the temperature of six successive layers in the atmosphere, from earth or cloud top level to 60 km height, each layer being 10 km deep. The upper two channels have a circular field-of-view 100 miles in diameter, and the lower four have a rectangular field-of-view 70 miles square. A refinement of the system enables high spatial resolution measurements of earth or cloud top temperatures to be taken, the field-of-view in this case being a strip 7 miles long (in the direction of flight) by 70 miles wide. This channel may be selected by ground command as an option to the normal Channel 3 (40 km height) and makes SCR less dependent upon data received by other experiments.

9.2 Principles of Operation

The SCR temperature sounding is achieved by observing the emitted infrared radiation in the 15 micron band from atmospheric carbon dioxide. Height resolution is obtained by a combination of optical multi-layer filters, and selective absorption of radiation using carbon dioxide-filled cells within the experiment.

The four lower channels (3 through 6) are known as single cell channels. The optics of each channel consists of a cantilever-mounted blade shutter which oscillates at 10 Hz and successively chops the field-of-view between earth and a cold reference source (space). The chopped radiation is then passed through a 10 cm path length of carbon dioxide, the pressure being set for each channel to define the viewing depth in the atmosphere. Behind the CO_2 path is the narrow band filter, the centers of which are also different for each channel, and a light pipe which converges the radiation on a thermistor bolometer detector. In order to obtain adequate height resolution in the upper layers of the atmosphere, the upper two channels (1 and 2) operate on a slightly different principle

and are known as double cell channels. The technique consists of switching the radiation between two half-cells, semicircular in shape and of 1 cm path length, containing different pressures of carbon dioxide. The oscillating shutter used in the four lower channels is replaced by a vibrating 45 degree mirror. During one half-period earth radiation passes through one half-cell and space radiation through the other; the situation is reversed during the other half-period. This system assumes that, apart from the CO_2 pressures, both halves of a cell have equal optical transmissions. A special in-flight calibration procedure, known as "imbalance calibration" is required to verify this assumption.

9.3 Physical Description

The SCR consists of four units including three sensor housings (numbers 1, 2,3 containing the optics of channels 1 and 2, 3 and 4, 5 and 6, respectively), and an electronics module. In addition to the optics, choppers, and detectors, each sensor housing contains the following electronics for the two appropriate channels:

a. Signal head amplifiers (gain = 40,000).
b. Chopper drive and reference circuits.
c. Bolometer bias DC-DC converter (±120 volts).
d. Filtering and stabilizers for head amplifier supplies.
e. Some housekeeping telemetry circuits.
f. Stepper motors for rotating calibration mirrors and filter wheels.

The electronics module contains the following:

a. Further signal amplifiers and synchronous detectors.
b. Command and calibration logic system.
c. DC-DC power converter unit (low voltage supplies).
d. Remainder of housekeeping telemetry circuits.

Figure 9-1 is a drawing of one of the (single cell) sensor housings.

9.4 Functional Description

9.4.1 Optical System

The optical arrangement is similar for all six channels, with the exception of the chopping principle described in 9.2. Infrared radiation from earth enters the sensor and is reflected through 90 degrees by the calibration mirror. It is then chopped and passes through the lens/CO_2 cell system within the radiometer

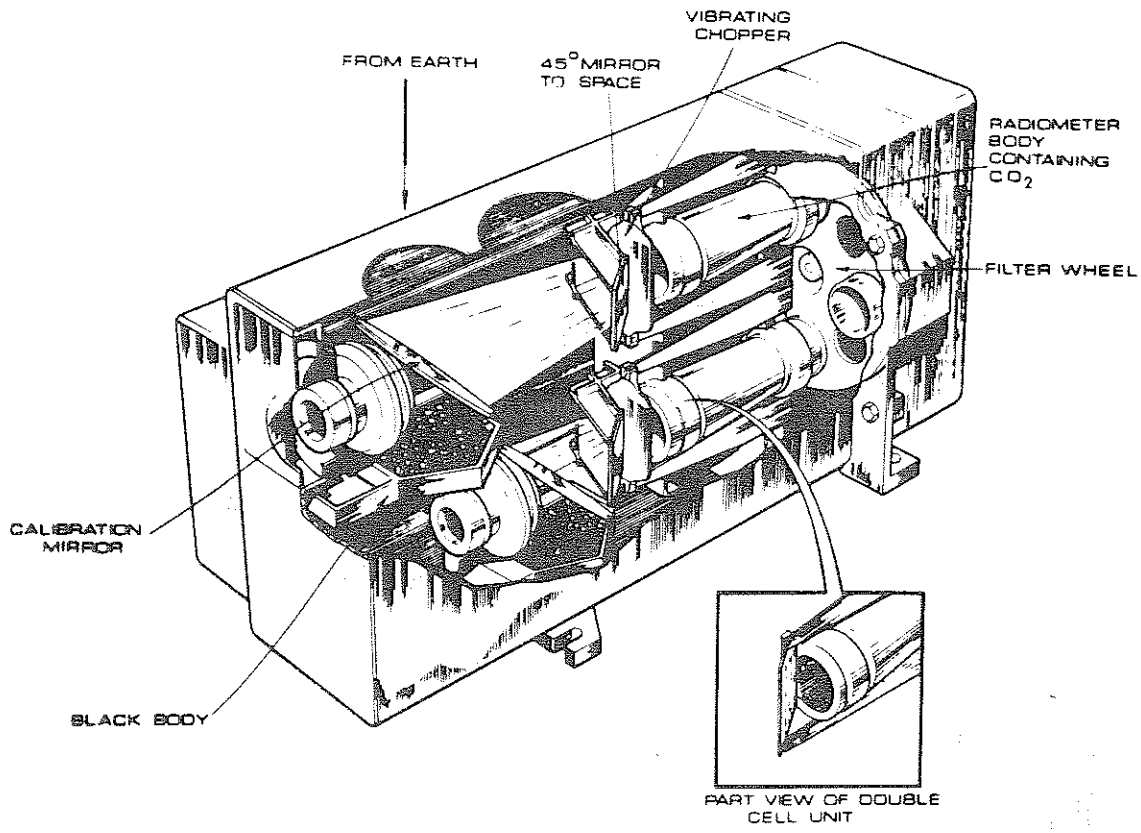

Figure 9-1. SCR Single Cell Housing (2 Channels)

body. The narrow band filter is located behind the radiometer body, and for the double cell channels is mounted on a wheel which may be rotated through 90 degrees, thus replacing the normal filter with one tuned to a CO_2 window to enable "imbalance calibration measurements" to be performed. A similar arrangement is used in Channel 3 to replace the normal filter with one that enables the channel to see ground or cloud top, and simultaneously switches in a strip shaped field stop to give the narrow field-of-view. The filters in Channels 4, 5 and 6 are fixed. Behind the narrow band filter is another lens and low pass filter. Final condensing of the radiation is achieved by a gold-plated conical light pipe. The radiation then falls on to the flake of the bolometer detector. All lenses and filter substrates are manufactured of germanium and are anti-reflection coated.

9.4.2 Electronic System

Located immediately behind the bolometer is a head amplifier with low noise input stage, and total gain of 40,000. The output signal (noise and 10 Hz signal) feeds via the interconnection harness to the signal channel located within

Table 9-1
Optical Characteristics of SCR Channels

Channel No.	SC or DC	Path Length of CO_2 (cm)	Pressure of CO_2 (atm)	Pass Band Center (cm^{-1})	Filter Bandwidth (cm^{-1})	Equivalent Bandwidth after CO_2, Chopping Absorption	Type of Filter
1a	DC	1	0.01/0.05	668	3	1.3	FP
1b		1	0.01/0.05	775	12	N/A	DHW
2a	DC	1	0.05/0.02	668	3	1.6	FP
2b		1	0.05/0.02	775	12	N/A	DHW
3a	DC	10	0.03	668	3	2.5	FP
3b		10	0.03	935	—	N/A	FP
4	SC	10	0.2	675	10	6.3	DHW
5	SC	10	0.6	697	10	3.5	DHW
6	SC	10	0.3	712	10	10.3	DHW

SC = Single Cell
DC = Double Cell
FP = Fabry Perot
DHW = Double Half Wave

the electronics module. It is synchronously filtered, amplified, and synchronously detected. The design of the circuit is such that the signal is integrated for approximately one second to give a true average for the integrating period. The integrator is reset immediately after being sampled by the VIP (1/second).

The command and calibration logic circuits are located within the electronics module and have three main purposes:

a. Switch on and off individual parts of the experiment
b. Generate the calibration cycle waveforms to operate the calibration mirrors and filter wheels
c. Operate the gain change and zero shift facilities in each signal channel (by ground command)

The SCR is provided with a considerable number of housekeeping sensors to:

a. Check voltage power supplies
b. Monitor the temperature of the sensors housing and electronics module
c. Monitor the amplitude of oscillation of each chopper
d. Monitor the gain and zero settings of each channel
e. Monitor the settings of the relays
f. Monitor the position of the calibration mirrors and filter wheels
g. Check for the presense of 1 Hz and 10 KHz signals

9.4.3 Operational Modes

9.4.3.1 Normal Mode

The SCR subsystem will normally be operated under the following conditions:

a. All power supplies ON
b. Calibration mirrors viewing EARTH
c. Double cell imbalance calibration filter wheel in NORMAL position
d. Channel 3 filter wheel in either NORMAL or GROUND FILTER position as required
e. All gain and zero shifts PRESET. In this setting the gain is set to the 4th of the eight positions, and zero shift to a 10 percent telemetry zero offset. The settings will be changed from PRESET if it is required to compensate for optical degradation or drift

9.4.3.2 Calibration Cycle

The in-flight calibration sequence consists of rotating the calibration mirrors by means of stepper motors so that they view in turn:

a. An internal reference black body target, whose temperature is accurately monitored and will be at the ambient temperature of the sensor housing. This provides a high level signal, approximately full scale on the telemetry.
b. Space, under which condition both half cycles of the chopped radiation are derived from the cold space reference and zero signal output should be obtained.

Turning the mirrors from the normal "earth view" to the "black body" positions involves a 180 degree rotation; this must be accomplished in two 90 degree steps, with the intermediate "space" position regarded as spurious. The calibration sequence is as follows:

a. Spurious space position = 16 seconds
b. Black body position = 32 seconds
c. Space position = 32 seconds

The mirrors then return to the normal (earth view) position for 32 minutes, 48 seconds. This cycle is continuously repeated.

A further calibration involves measurement of the "imbalance" of the double-cell channels (1 and 2) in the No. 1 Sensor Housing. This is achieved by changing optical filters in both channels by means of a 90 degree rotation of a filter wheel. This calibration is performed upon receipt of a ground command which "enables" the double-cell filter wheel to move into the "IMBAL CAL" position whenever the mirrors are viewing "space" or "black body". It should be necessary to perform this calibration only at infrequent intervals. In this manner any signal components other than those due to the pressure difference in the two halves of the double-cell may be determined and allowed for.

Calibration tables and/or graphs for the six SCR channels will be presented in the Nimbus IV Catalog.

9.5 SCR Data Flow

Housekeeping and sensory data from the SCR (and other experiments) are sampled by the VIP and transmitted to the Data Acquisition Facilities (DAF) via the PCM 136.5 MHz beacon, and/or the HDRSS S-band transmitter.

At the DAF the housekeeping and sensory data (including SCR) are formatted into the Sensory Data Tape (SDT) which in turn is operated upon by the CDC 924 computer to prepare the STS (SCR/THIR/SIRS) Tape. From the STS tape a CDC 160 computer extracts and formats the data which are sent via cableline to the SCR Experimenter at the Clarendon Laboratories, Oxford, England. The data sent to England include: SCR experimental and housekeeping data, THIR data corresponding to the field of view of the SCR, time and attitude information.

The SCR Experimenter will provide NSSDC with final SCR data tapes for archiving purposes. The format and anticipated availability of the SCR tape sent to NSSDC will be published in the Nimbus IV Catalog.

B-7750

SECTION 10

THE INTERROGATION, RECORDING AND LOCATION SYSTEM (IRLS) EXPERIMENT

by
Charles E. Cote
National Aeronautics and Space Administration
Goddard Space Flight Center

10.1 IRLS General Description

10.1.1 IRLS System Objectives

The IRLS is designed to collect meteorological, geophysical and other experimental data from remote, unmanned data collection stations (platforms) deployed on a global scale. The IRLS system will also determine the location of the platforms and track the movement of such platforms as balloons, buoys and ships. Figure 10.1 illustrates the IRLS concept.

The Nimbus IV/IRLS Experiment contains two meteorologically significant features: (1) The ability to make 370 platform interrogations per orbit and to store up to 100 kilobits of meteorological and range data, and (2) The flight demonstration of a number of constant altitude meteorological balloons carrying lightweight, low power packages.

The objectives of the IRLS are:

1. To provide a world wide remote platform location and data collection system.

2. To prove feasibility of selective interrogations of remote platforms from an orbiting satellite and acknowledge receipt of an automatic response.

3. To determine system performance in resolving location of both fixed and moving platforms.

4. To demonstrate the dissemination of the data collected and the locations determined within an orbital period.

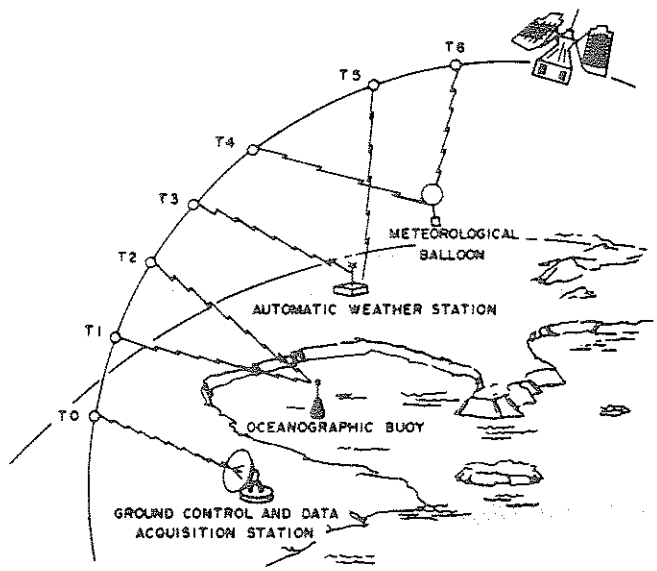

Figure 10-1. Interrogation, Recording and Location System

10.1.2 System Description

The elements making up the IRLS system are a set of remote platforms, a satellite, and a ground station. The platforms accept analog data from various sensors, convert the measurements to digital form, and transmit these data to the satellite via a PCM communication link. On each orbital pass, when in the vicinity of an IRLS ground station (located at ALASKA and GSFC), the satellite command memory is programmed by the IRLS Ground Acquisition and Command Station (GACS) to communicate with selected platforms during the coming orbit. The satellite stores both the address (number) of each platform and the desired time each should be contacted. At the designated times in orbit, the satellite interrogates each platform, measures the satellite-to-platform distance by determining the propagation time of the RF signal, and receives and stores the platform data. Upon return to the locale of the ground stations, the station commands the satellite to transmit all stored data and to accept new commands for use during the next orbit.

The system uses a coded digital message for transmission of all data, for timing synchronization between satellite and platforms or ground station, and for measurement of satellite-to-platform range.

The system employs a 100,000 bit satellite data memory capable of storing data measurements during each orbit for up to 370 different interrogations stored in the command memory. Two interrogations are required per platform

if a location computation is to be made. The range measurements between satellite and platform are made to an accuracy of ±500 meters.

With a knowledge of satellite orbit parameters and past platform locations, two such range measurements are sufficient to establish the position of a moving platform, such as a buoy or balloon.

The analog sensor data are converted by the platform electronics into a digital format. In transmitting data to and from the IRLS subsystem via the IRLS RF link, all bits of data are treated as twelve minor bits in a manner that provides noise protection in communication and the sensitivity to perform an accurate range determination.

Major characteristics of the IRLS system are tabulated below:

Satellite Data Capacity:	100,640 bits per orbit
Range Measurement Accuracy:	±500 meters (±0.27 nautical miles)
Accuracy of Data:	1% maximum error, 0.2% linearity and repeatability, 0.8% resolution
Number of Interrogations:	370 Maximum/orbit
Data Measurements per Platform:	630 Maximum (21 per frame, 1 to 30 frames per platform)/interrogation
Available Orbit Time for Data Collection:	3.64 hours maximum (can be extended for blind orbits)
Data Transfer Time:	Platform to Satellite - 4 frames per second Satellite to Ground - 30 second maximum for completed data dump and new command entry (1.041 Kilobits/second major bit rate) (12.5 Kilobits/second minor bit rate)

10.2 Platform Elements

The remote data stations from which the IRLS spacecraft equipment collects its data consist of three main elements: the sensor, the platform electronics, and the antenna.

10.2.1 Sensor

The source of the data collected from the individual platform is a sensor provided by the individual platform experimenter. The output of the sensor is generally an analog voltage although the platforms are also equipped to handle digital inputs.

10.2.2 Platform Electronics

The platform consists of the data conditioning equipment, the synchronizing equipment and the communication equipment including the transmitter and receiver. A standard "all weather" platform has been designed as part of the IRLS program.

The data inputs are quantized into 7 bit digital words. On the technological evaluation platforms, 6 out of the 21 data words placed into each frame are reserved for platform housekeeping telemetry utilized in the technical evaluation of the platform performance under extreme environmental conditions.

They are:

data word
1. transmitter power amplifier temperature
2. transmitter plate current
3. receiver module temperature
4. data and range module temperature
5. data and range module 3.4v logic level
6. power control and dist. module 24v input level

The platform transmitter operates at 466.0 MHz and the receiver at 401.5 MHz. The RF output of the Balloon Interrogation Packages is 6 watts and the output of the Technical Evaluation Platforms is 25 watts.

10.2.3 Antennas

There are several types of antennas developed for the IRLS application, each having about 6db peak gain. The general purpose antenna is a loop vee type having a bifolium pattern. This, overhead, has reduced gain for arc pass but has improved performance at lower elevation angles at which interrogations are generally contemplated. Another antenna is a cavity-backed spiral with a cardioid pattern. It has higher gain overhead than at the lower angles but has the advantage of not having its pattern affected by the bobbing action of ocean activity and therefore is more suitable for buoy applications than the loop vee. The balloon antenna is a crossed dipole, specially designed to have a bifolium pattern.

10.3 Interrogation of Nimbus from IRLS Ground Acquisition and Command Stations and Unloading Data

The Nimbus satellite is interrogated each orbital pass over the Alaska and Rosman Data Acquisition Facility (DAF) stations. The DAF stations transmit a command through the normal spacecraft command system to place the IRLS system on the satellite in a readout mode allowing data readout to be initiated. The data output from the satellite is shown in Figure 10-2 for one frame of platform data when the IRLS to GACS RF communication line is established. This is composed of a barker code for synchronization, the address complement of the platform, 21 data words of seven major bits each, three words containing ranging vernier time, plus parity and range data information. Data transfer is accomplished at 1041 bits per second until the entire contents of the 100,000 bit data memory have been transmitted. The memory content is destroyed after each data readout cycle.

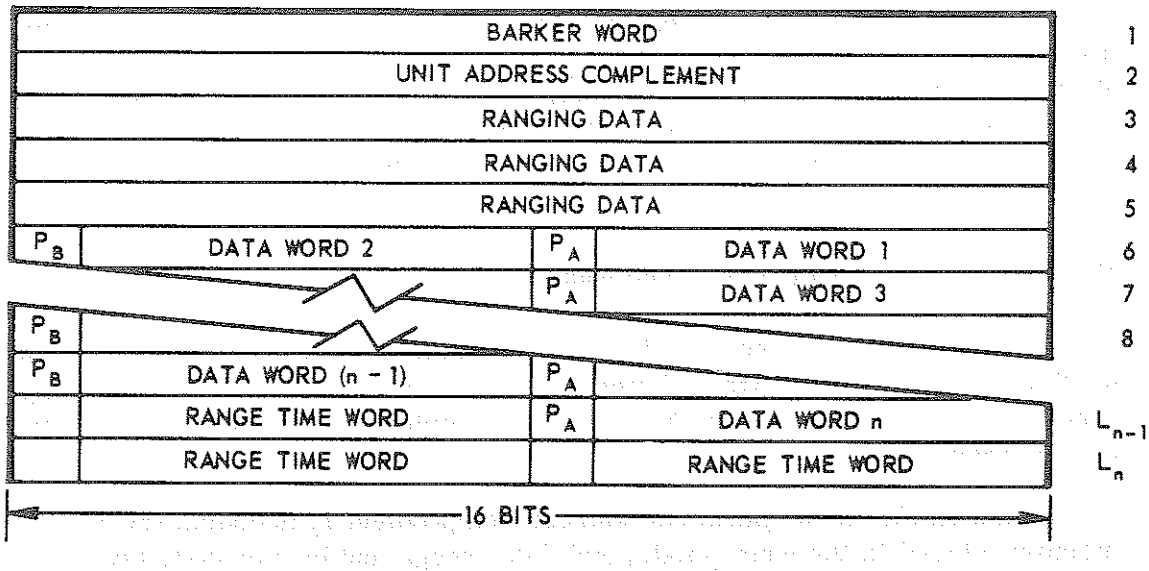

NOTES: P_A IS ODD PARITY FOR BITS 2^0 THROUGH 2^6

P_B IS ODD PARITY FOR BITS 2^0 THROUGH 2^{14}, EXCLUDING BIT 2^7

L_n = LINE 17 (PLATFORM), OR LINE 10 (BIP)

DATA WORD (n) = DATA WORD 21 (PLATFORM), OR DATA WORD 7 (BIP)

Figure 10-2. Data Output from the Satellite to DAF for One Frame of Platform Data

Following the receipt of the spacecraft data, the IRLS GACS Station transmits twenty 31 bit command words which the satellite loads into the IRLS command memory. Each command word contains a platform address and a time of interrogation. This entire cycle of data dump and command load takes less than 35 seconds.

10.4 Interrogation of Platform

The 31 bit command word is composed of a 16 bit platform address and a 15 bit time code. The time code is a count of .4 second units that establishes when the platform is to be interrogated. The time code count is continuously being compared to a counter driven by the Nimbus spacecraft clock 10 cps reference frequency. The counter is reset to zero at the beginning of the command load cycle. When count coincidence occurs, the interrogation cycle is initiated by continuously transmitting the platform address portion of the command word and placing the data memory into the write mode. Receipt of this address by the platform causes it to continuously transmit its own address to the satellite. After the address is received by the spacecraft, the complement of the address is transmitted by the spacecraft for the duration of the interrogation. A timer in the IRLS spacecraft equipment limits each platform interrogation to 3 seconds. At the end of the 3 second interval, the transmitter is turned off, the data memory is placed in a static mode and if the command was not the last, the next command is placed in the command register. After the last programmed command, the command memory is empty and goes into a static mode.

10.5 Receipt of Platform Data and Ranging

When the platform receives its address complement, it retransmits it immediately and follows it with ranging data and 21 word data frame and a range time word and closes with another address complement. Up to 30 data frames may be transmitted.

At the satellite, the platform address complement is decoded, the data memory placed in the write mode, and data, range and barker code (synchronization) are written into the data memory. At completion of transmission, the data memory is returned to static condition.

The ranging vernier times are the units of time used to accurately establish the time when ranging function was actually performed. Ranging is accomplished by measuring time between transmission and reception of the signal.

Geometry of the ranging measurement is shown in Figure 10-3. If a measurement is made from the satellite at time T_1, the propagation time may

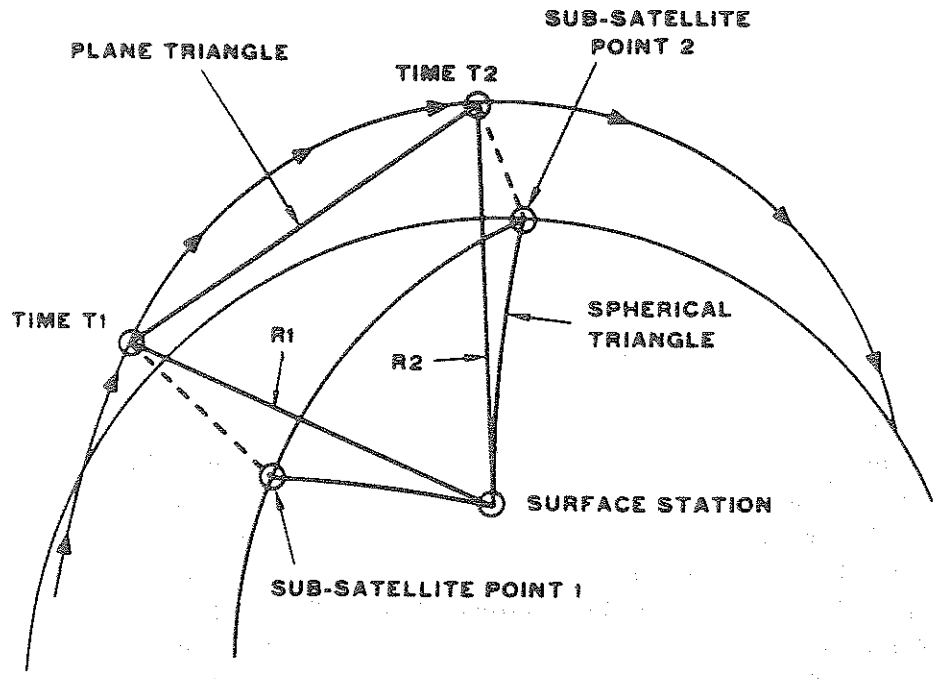

Figure 10-3. Platform Positioning Geometry

be converted to a radial distance R_1. As the height of the satellite is known above point 1 on the earth's surface (dashed line), this signal measurement would essentially indicate that the platform is somewhere on the circumference of a circle of radius r_1. A similar measurement at time T_2 would indicate location on the circumference of a circle of radius r_2. Knowing the locations of the two subsatellite points from the spacecraft Ephemeris and the time of interrogation, the location of the platform is found by determining the intersection of the two circumferences. Two solutions are obtained by this procedure: a correct one and a mirror image on the opposite side of the subsatellite track. Utilizing either the knowledge of the previous general location or when data are available from two successive satellite passes, the unique location can be determined. To optimize the calculations, the interrogations are scheduled for the included angle between R_1 and R_2 to be approximately 90°. For nominal spacecraft orbit, this varies from 2 to 4 minutes, depending on the platform offset from the satellite subpoint track.

10.6 IRLS Platforms

The platforms of the IRLS experiment are classified into three groups: (1) Balloon Interrogations Packages (BIP), (2) Technological evaluation platforms

and (3) other platforms utilized by cooperating government agencies and non-profit organizations to evaluate the usefulness of IRLS in their scientific programs. The technological evaluation group is further subdivided into the Integration Support Equipment (ISE) platforms which are under direct NASA Goddard supervision and the Field Test platforms which are installed and maintained by supporting organizations at a variety of global locations. All IRLS participants provide their own sensors for obtaining data to be collected. The platform addresses are assigned by the National Aeronautics and Space Administration.

10.6.1 Balloon Interrogation Packages

The major experiment will consist of the tracking of a number of constant altitude meteorological data collection balloons, each carrying a Balloon Interrogation Package (BIP). These balloons will be released in groups of three at periodic intervals from Ascension Island in the Atlantic between Africa and South America. The balloons will ascend to an altitude of between 10 and 20 kilometers and will stabilize to within 300 meters. Each BIP will have a unique address and will be interrogated by the Nimbus IV satellite on every orbit in which it is within the range of the satellite transmitter. A minimum of two range measurements per orbit will be made on each balloon within communication view of the satellite. The data for all balloons taken during an orbit will be telemetered to the ground when the satellite passes over the ground station at either Alaska or Rosman, N.C., and a new set of interrogation sequences will be relayed to the satellite. The new interrogation sequences will be based on a ground solution of balloon position, calculation of average wind, and a prediction of balloon position at the next interrogation time.

10.6.2 Technological Evaluation Platforms

These platforms are supplied to the installing organizations by the IRLS project office at GSFC.

10.6.2.1 Integration Support Equipment Platforms

Two of these platforms will be located at the Goddard Space Flight Center and their positions will be known. Data transmitted to the satellite will consist of calibrated reference voltages and typical sensor measurements such as temperature and/or pressure.

These platforms are used to evaluate system parameters over the expected lifetime of the satellite and to determine the accuracy of the platform location technique and the data coding and transmission system.

10.6.2.2. Field Test Platforms

10.6.2.2.1 National Science Foundation

This platform will be located aboard the Antarctic Research Ship HERO operating in the waters off the coast of Antarctica, near Palmer Station. Data to be transmitted during each interrogation will consist of weather conditions at reporting time, including cloud condition, wind speed and direction, barometric pressure, air and sea temperatures, sea state, and ice floe status. The position of the ship at the time of interrogation and the expected position 24 hours later will also be transmitted.

10.6.2.2.2 U.S. Naval Oceanographic Office

This platform will be deployed on a Monster Buoy located in the Pacific Ocean, north of Hawaii. The purpose of this platform is to compare the relative performances of a satellite relay data acquisition system (IRLS) and a direct high frequency platform-to-shore data communication link. Since the location of the platform is essentially fixed, the positioning feature of IRLS is of secondary importance.

10.6.2.2.3 Environmental Science Services Administration

This platform will be deployed at several locations. Two possible locations are at Tungsten, Canada, and in the Antarctic area. The purpose of this platform is to enable ESSA to make geophysical (magnetic) measurements near the polar regions of the earth. This experiment is being conducted with the cooperation of the University of California.

10.6.2.2.4 University of California, San Diego

This platform will interface with a deep ocean (3000 fathoms) instrument capsule to relay temperature, pressure and current data daily via the IRLS system to the shore station. Sensor data in the capsule will be recorded at intervals of two to fifteen minutes on a digital magnetic tape. The taped information will be relayed to a surface buoy twice a day, corresponding to the satellite overpass time. The interface between the capsule and the surface buoy is an acoustic link. The IRLS package will be installed in the surface buoy.

This experiment will be performed by the La Jolla Laboratories of the U. of C. Institute of Geophysics and Planetary Physics and is expected to be conducted over a period of one year.

10.6.2.2.5 Smithsonian Institution

This is a special platform package designed for use in animal migration studies. The package is shaped in the form of a collar to be fitted on an elk's neck. Besides tracking the whereabouts (location and altitude) of the elk, its skin temperature and the local solar light intensity will be recorded. This experiment will be conducted at the National Elk Refuge near Jackson, Wyoming.

10.6.3 Co-operative Scientific Experimenter Platforms

These platforms are supplied by the participating scientific experimenters.

10.6.3.1 U.S. Naval Oceanographic Office

The U.S. Naval Oceanographic Office will have several platforms deployed at various locations. Among them will be (a) the Bermuda reference station, (b) the PLOT experiment, (c) the Acoustic Reverberation Buoy, and (d) free floating buoys.

Bermuda Reference Platform: This platform will be located at the Tudor Hill U.S. Navy Facility on Bermuda and will serve as a reference and calibration station. Its position will be accurately known.

PLOT Experiment Platform: The Position Location through Orbital Tracking (PLOT) experiment involves the services of the Applications Technology Satellite (ATS-3) to relay the IRLS ranging information to and from the central computing center to provide near real time position determination for the platform user. The objectives are: (1) to prove the feasibility of real time position location determination from low orbiting satellites via synchronous satellite data relay; (2) to provide a reliable, accurate and portable positioning aid for ships of opportunity; and (3) to ascertain the real time position location capability of the IRLS.

A hybrid IRLS/ATS-OPLE platform will be deployed aboard an ocean vessel crossing the Atlantic. During each Nimbus orbit in which the satellite is in communication range with the ship, the hybrid platform will be interrogated, ranged and given the ranging data immediately by the Nimbus satellite. The ranging data will then be transmitted via the ATS-OPLE relay to the IRLS computing center. The computed position information will then be relayed back via the ATS satellite to the hybrid OPLE/IRLS platform where the position will be displayed on a readout device.

Acoustic Reverberation Study Buoy: This buoy will be moored off the coast of Puerto Rico. The objective of this platform is to study the scattering of acoustic energy by marine organisms, which imposes operational limits on sonar systems.

Free Drifting Buoy Platforms: Two buoys will be deployed in the Atlantic Ocean off Bermuda. These buoys will be allowed to drift freely in the Gulf Stream, and their passage tracked as a part of the study of ocean currents and their effect on oceanographic and meteorological forecasting. Data acquisition will include wave heights, wind speed and direction, sea surface and air temperatures.

10.6.3.2 Woods Hole Oceanographic Institution Platforms

One or two platforms are located in the Gulf Stream off Cape Hatteras and one on Georges Bank (off Cape Cod).

Data Content on all platforms:

1. temperature at 300 meters
2. temperature at 150 meters
3. temperature at surface
4. temperature of air above the surface

The purpose of the platforms in the Gulf Stream is to determine the location and characteristics of eddies. The purpose of the platform on Georges Bank is to determine the characteristics of current flow. The use of the positioning feature of IRLS is of primary importance to the Woods Hole Oceanographic Institute.

10.6.3.3. Bureau of Commercial Fisheries Platform

Platform is on a drifting buoy in the North Pacific south of Alaska.

Data Contents:

1. temperature of the water at the surface
2. temperature of the water at a depth of 50 meters
3. pressure at a depth of 50 meters
4. Salinity of sea water at a depth of 2 meters

The primary purpose of the Bureau of Commercial Fisheries' participation in the IRLS program is in the utilization of the positioning feature of IRLS in order to determine current flow (rate and direction) in the North Pacific. The secondary purpose of this experiment will be to utilize the data received from the platform in a scientific program.

10.6.3.4 Naval Air Systems Command Platforms

Two platforms are used in conjunction with Air-Sea Rescue beacons.

Only one channel is used to indicate the presence or absence of signal on an Air-Sea Rescue receiver from an Air-Sea Rescue beacon.

The purpose of the Naval Air System Command's participation is to demonstrate the use of a satellite system (IRLS) in the Air-Sea Rescue Program.

10.7 Data Dissemination, Archiving and Access

The IRLS Ground Acquisition and Command Station transmits the IRLS data collected from the spacecraft to a CDC 924 computer in the Nimbus Data Handling Facility at GSFC. The CDC 924 computer performs the location calculations for the various platforms, and separates the data for the individual platform experimenters on printed computer outputs. The computer outputs will be mailed to the IRLS platform experimenters, and copies will be retained in the Nimbus/ATS Data Utilization Center, NASA, Goddard. During special test periods the output data may also be punched on paper tape in teletype format for dissemination to the experimenters within the orbital time period.

The computer printouts will show platform location at given times. Any geophysical data collected will be expressed in voltages. Calibration charts and tables necessary to translate these voltages measurements into corresponding measurements of temperature, wind velocity, etc., are available through the individual platform experimenters listed in 10.6.2, and 10.6.3.

BIBLIOGRAPHY

1. Hogan, G. and Cressey, I., The Interrogation Recording and Location System, National Telemetry Conference, November 1965.

2. Survey of Requirements for a Geophysical Data Collection Satellite System, Contract No. NAS r 49612. Stanford Research Institute, August 1963.

3. The Feasibility of a Global Observation and Analysis Experiment, National Academy of Sciences, National Research Council, Publication 1290, March 1966.

4. Operations Analysis of the IRLS Experiment, Contract No. NAS 5 3747, Operations Research Inc., Phase I - Simulation Modes and Error Analysis, March 1966, Phase II - Composite Error Analysis, August 1966.

5. Final Engineering Report for IRLS, Contract No. NAS 5 9559, Radiation Inc., June 1967.

SECTION 11

THE REAL TIME TRANSMISSION SYSTEMS (RTTS) EXPERIMENT

11.1 General

A detailed discussion of the Real Time Transmission System will not be presented here. The reader interested in detailed information for APT station operational usage, including gridding techniques is referred to the "Nimbus IV Real Time Transmission System (DRID and DRIR)" (Reference 9).

The THIR or IDCS data can be instantaneously transmitted by the spacecraft to APT stations within satellite acquisition range while being simultaneously stored on tape for subsequent transmission to a central Data Acquisition Facility. The instantaneous transmission modes of the IDCS and the THIR are referred to, respectively, as the DRID and the DRIR system. The DRID system is the same IDCS camera experiment flown on Nimbus III providing daytime meteorological data. The DRIR system is also similar to the DRIR experiments tested on Nimbus II and III which provided nighttime meteorological data. Both DRID and DRIR systems produce data in pictorial format.

DRID and DRIR data are transmitted from the satellite at a frequency of 136.95 MHz. Automatic Picture Transmission (APT) ground stations (References 1, 2 and 8) throughout the world can acquire the direct readout data when the satellite is within line of sight of the local antenna. Nimbus IV DRID picture reception requires no modification of facsimile equipment presently set up to receive Nimbus III APT pictures. Some modifications to the APT ground equipment are necessary to properly acquire the DRIR data (References 3, 4, 5 and 8). However, stations set up to acquire Nimbus III DRIR need no modification for Nimbus IV DRIR.

Participating APT stations not routinely receiving the transmitted daily APT Predict messages will if requested receive Nimbus APT Ephemeris messages twice each month to aid them in tracking the Nimbus Satellite. Daily APT Predict messages (TBUS-2) giving both day and night Nimbus ephemeris information will be furnished over the National and International Radio teletypewriter weather circuits.

DRID and DRIR grids which have been provided in the Nimbus III Real Time Transmission Systems (DRID and DRIR) document (Reference 7) can be used for

Nimbus IV with the new enlargement factors given in the Nimbus IV Real Time Transmission Systems (DRID and DRIR) document (Reference 9).

Request for information and grids relating to the Nimbus IV Real Time Transmission Systems (both DRID and DRIR) should be directed to:

Nimbus Project, Code 450
National Aeronautics and Space Administration
Goddard Space Flight Center
Greenbelt, Maryland 20771 U.S.A.
Attn: NADUC Manager.

DRID and DRIR data are only available from the local acquisition facilities. Potential users desiring information concerning these data for specific applications, should contact the agencies responsible for the various APT receiving stations. However, the same DRID and DRIR data as recorded on board the spacecraft, can be obtained in the higher quality IDCS and THIR film formats from the appropriate archival source.

11.2 Direct Readout Image Dissector Camera System (DRID)

Although the Image Dissector Camera flown on Nimbus IV (and Nimbus III) differs from the APT cameras flown on previous TIROS, TOS, ESSA and Nimbus I and II satellites, the real time operation of the system is almost identical to the Nimbus I, II and III APT. Previous APT cameras consisted of a wide angle lens, a mechanical shutter, and a storage vidicon on which the complete scene was exposed, slowly scanned, and then erased. Thus, all the pictorial information contained in a single frame was exposed instantaneously from a fixed position in space. The image dissector is a shutterless electronic scan and step tube mounted behind a wide angle lens. Scanning and stepping functions occur continuously while the satellite is progressing along its orbital path, i.e., the earth scene is not exposed instantaneously from a fixed location in space. The 108° lens used on the camera is identical to the lenses used on previous Nimbus APT systems. The side to side camera field of view is 98.2° (nominal) providing a ground coverage of about 1600 x 1600 nautical miles from a 600 nautical mile altitude.

The video presentation contains no fiducial marks and the line sync pulse consists of seven black to white pulses instead of the conventional APT type of black sync pulses. The 3 second start time, 5 second phasing period, and 5 per cent line blanking are identical to those of previous Nimbus APT, as are the 4 hz line rate and 200 second active picture period.

A more detailed description of the IDCS may be found in Section 2 of this Guide.

11.3 Direct Readout Temperature Humidity Infrared Radiometer (DRIR)

Transmission of Nimbus IV Temperature Humidity Infrared Radiometer (THIR) data in real time to APT stations is known as Direct Readout Temperature Humidity Infrared Radiometer system referenced by the acronym DRIR.

The Nimbus IV THIR is a scanning (48 rpm) radiometer with a window channel at 11.5 microns and a water vapor channel at 6.7 microns, with resolutions of about 4 and 12 n. miles respectively at the subpoint. The window channel provides cloud top or surface temperature. The water vapor channel will permit estimates of the water vapor in the upper troposphere.

Although either channel can be transmitted to APT ground stations during both the daytime and nighttime, the normal operational mode will be nighttime transmission of the window (11.5μ) channel. Daytime DRIR data can be transmitted only if the DRID system is not activated. Daytime DRIR transmission, if and when it occurs, will be announced in advance in the TBUS-2 message.

Nimbus IV DRIR video display for the window channel (11.5μ) is similar to the Nimbus III DRIR with shades of gray related to the temperature of the scene. Cold clouds, snow and ice show up white, while the warmer land and waters show up gray to black. A detailed meteorological interpretation of infrared pictorial data is contained in Reference 6. The DRIR display for the water vapor channel if transmitted would not be as sharp as the window channel because of its lesser resolution and the effect of the water vapor. Shades of gray in the display represent the intensity of radiant energy: the darker the picture, the greater the radiation and the lesser the atmospheric moisture content.

The typical APT facsimile recorder used to display the DRIR shows the total 360° scan of the radiometer including the earth, space and the interior of the radiometer. The data from earth and atmosphere (from horizon to horizon) occupies about 1/3 of the total horizontal display of the facsimile.

A more detailed description of the THIR may be found in Section 3 of this Guide.

REFERENCES

1. Goldshlak, L., 1963: APT Users' Guide, Scientific Report No. 1, Contract No. AF 19(628)-2471, Allied Research Associates, Inc. (Out of print. May be available through the Defense Document Center or Federal Clearing House for Scientific and Technical Information).

2. National Weather Satellite Center, ESSA, 1969. Direct Transmission System Users Guide, Environmental Science Services Administration; for sale by the Superintendent of Documents, Government Printing Office, Washington, D.C. 20402. Price $2.25.

3. Radio Corporation of America, 1965: User Guide for HRIR Modifications to the APT Ground Stations, Contract No. NAS 5-667, Astro-Electronics Division, Defense Electronic Products, Issued 23 November 1965, changed 4 November 1966, changed 31 March 1967.

4. Radio Corporation of America, 1966: Instruction Manual for HRIR Modifications to the APT Ground Stations Using Fairchild Facsimile Recorders, Contract No. NAS 5-667, Astro-Electronics Division, Defense Electronic Products, Issued 10 January 1966, Revision 1 issued 18 November 1966, Change 1 issued 6 January 1967.

5. Radio Corporation of America, 1962: Instruction Manual for HRIR Modification to the APT Ground Stations Using Muirhead Facsimile Recorders, Contract No. NAS 5-667, Astro Electronics Division, Defense Electronic Products, Issued 22 February 1962, Change 1 issued 22 November 1966.

6. Widger, W. K., Jr., J. C. Barnes, E. S. Merritt and R. B. Smith, 1965: Meteorological Interpretation of Nimbus High Resolution Infrared (HRIR) Data, Final Report, Contract No. NAS 5-9554, ARACON Geophysics, A Division of Allied Research Associates, Inc. (Republished as NASA Contractor Report-352, January 1966).

7. Goldshlak, L., 1968: Nimbus III Real-Time Transmission Systems (DRID and DRIR), Technical Report No. 5, Contract No. NAS 5-10343, Allied Research Associates, Inc., Concord, Massachusetts.

8. Vermillion, C. H., 1969: Weather Satellite Picture Receiving Station - Inexpensive Construction of APT Ground Equipment, Report NASA SP-5080. For sale by the Clearinghouse for Federal and Scientific and Technical Information, Springfield, Virginia 22151. Price $3.00

9. Allied Research Associates, 1970: Nimbus IV Real Time Transmission Systems (DRID and DRIR), Technical Report No. 12, Contract No. NAS 5-10343.

SECTION 12

THE NIMBUS IV CATALOG

The Nimbus IV Catalog will be published monthly, providing a relatively current source of information required for obtaining Nimbus IV data. The Catalog will be divided into 4 main Sections described below.

12.1 Section 1 - Summary of Operations

Section 1 will contain significant highlights of the satellite operation during the period of the catalog including any required post-launch changes in experimental description as contained in preceding sections of this Guide. Performance of the various sensory systems and the spacecraft will be described, particularly when significant deviations from normal operations have been experienced.

12.2 Section 2 - Orbital Elements and Daily Sensors "On" Table

Section 2 will give the Nimbus IV satellite orbital elements valid for the catalog period. This section will also have a Daily Sensors "On" Table tabulating the times the experiments were on for the period of the catalog. The table will include ascending and descending nodes times and longitudes.

To assist the user in determining the sensor coverage on the earth, the first volume will include a Subsatellite Tracks Overlay Transparency with its accompanying World Map. The Subsatellite Tracks Overlay contains 14 correctly spaced tracks with time annotations ending at the approximate day/night transitions.

12.3 Section 3 - IDCS Montages

This section depicts the data from the Image Dissector Camera System (IDCS). The pictorial montage presentation facilitates perusal and search of the IDCS data for preliminary research and also enables the user to determine his specific IDCS film data requirements.

The montages represent the daytime television pictures obtained for each day (UT) and are arranged in chronological order in a world montage format. Complete daylight orbital coverage is obtained with 15 consecutive pictures.

Successive orbits, displaced about 26 degrees westward in longitude at the equator provide adjacent pictorial data, with increasing overlap from the equator towards the poles.

A transparent IDCS grid overlay (Location Guide) will be provided as an insert to the Nimbus IV Catalog for approximate location and orientation. The montages will be reduced to approximately 6" × 7" from the original montage size of 22" × 32". This reduction, required for convenient catalog dimensions, still permits recognition of major cloud and land features.

12.4 Section 4 - THIR Montages

This section pictorially documents the data from the Temperature Humidity Infrared Radiometer (THIR) experiment.

The montages represent the 11.5 micron channel and the 6.7 micron channel data obtained for each day (UT) and are arranged in chronological order in a world montage format. Key latitudes can be read from the superimposed grids. Grid points are identified where each swath crosses 60°N, 30°N, EQUATOR, 30°S and 60°S.

THIR transparent grid overlays (Location Guide), one for daytime montages and another for nighttime montages, will be provided as inserts to the Nimbus IV Catalog for general orientation with the latitude and longitude of the data presented.

A THIR Time Scale will also be included as insert to the Nimbus IV Catalog for measuring time on the data strips in the daytime or nighttime montages.

APPENDIX A

ABBREVIATIONS

AFCRL	Air Force Cambridge Research Laboratory
APT	Automatic Picture Transmission
ATS	Applications Technology Satellite
AVCS	Advanced Vidicon Camera System
A/D	Analog to Digital
AWS	Air Weather Service
BCD	Binary Coded Decimal
BIP	Balloon Interrogation Package
bps	bits per second
BUV	Backscatter Ultraviolet Spectrometer
CDA	Command Data Acquisition
DAF	Data Acquisition Facility
DEMOD	Demodulator
DRID	Direct Readout Image Dissector
DRIR	Direct Readout Infrared Radiometer
ESSA	Environmental Science Services Administration
FWS	Filter Wedge Spectrometer
GACS	Ground Acquisition and Command Station
GMT	Greenwich Mean Time
GSFC	Goddard Space Flight Center
HAX	HRIR APT Switching
HDRSS	High Data Rate Storage System
HRIR	High Resolution Infrared Radiometer
Hz	Hertz (cycles per second)
IDCS	Image Dissector Camera System
IFOV	Instantaneous Field of View
IMCC	Image Motion Compensation and Calibration (a subsystem of IRIS)
IRIS	Infrared Interferometer Spectrometer
IRLS	Interrogation Recording and Location System
ISE	Integration Support Equipment (Platforms)
LABS	Laboratory for Atmospheric and Biological Sciences
MSL	Meteorological Satellite Laboratory
MUSE	Monitor of Ultraviolet Solar Energy
NDUC	Nimbus Data Utilization Center
NASA	National Aeronautics and Space Administration
NASCOM	NASA Communications
NAVOCEANO	Naval Oceanographic Office
NCAR	National Center for Atmospheric Research
NDHS	Nimbus Data Handling System

NER	Noise Equivalent Radiance
NESC	National Environmental Satellite Center
NMC	National Meteorological Center
NMRT	Nimbus Meteorological Radiation Tape
NRL	Naval Research Laboratory
NSSDC	National Space Science Data Center
NTCC	Nimbus Technical Control Center
NWRC	National Weather Records Center
ONR	Office of Naval Research
PCM	Pulse Code Modulation
PLOT	Position Location through Orbital Tracking
rpm	revolutions per minute
RTTS	Real Time Transmission System
SCR	Selective Chopper Radiometer
SDT	Sensory Data Tape
SIRS	Satellite Infrared Spectrometer
STADAN	Station Data Acquisition Network
T&DS	Tracking and Data Systems
THIR	Temperature Humidity Infrared Radiometer
UT	Universal Time
VIP	Versatile Information Processor
WMSAD	World Map Predicts and Station Acquisition Data
XMTR	Transmitter